

DISSERTATION

A DRUG ELUTING, OSSEOINTEGRATIVE PHOSPHOLIPID COATING FOR  
ORTHOPEDIC IMPLANTS

Submitted by

David A. Prawel

Graduate Degree Program in Bioengineering

In partial fulfillment of the requirements

For the Degree of Doctor of Philosophy

Colorado State University

Fort Collins, Colorado

Spring 2011

Doctoral Committee:

Advisor: Susan P. James

Co-Advisor: Ketul C. Popat

Matt J. Kipper

Stewart D. Ryan

## ABSTRACT

### A DRUG ELUTING, OSSEOINTEGRATIVE PHOSPHOLIPID COATING FOR ORTHOPEDIC IMPLANTS

Millions of implant surgeries are performed each year. Titanium is commonly used for implantable metallic devices, especially total hip and knee replacements. However, titanium implants are far from perfect. Although the absolute failure rate is not particularly high, the case-by-case direct and human cost of each device implant failure is tremendous. Cementless titanium implant devices, although preferred by surgeons, frequently fail due to loosening of the device, often as a result of poor integration of naturally forming bone with the metallic implant, and by infection.

Phospholipids are naturally occurring substances that are shown to enhance integration of new bone with implants, and to help reduce inflammation, a common precursor to infection. In addition, numerous studies have shown phospholipids to be effective drug delivery agents. To date, dip and drip coating techniques for applying phospholipid coatings have been used on titanium. Both coating techniques are easy to perform, but result in coatings too thick and non-conformal for *in vivo* use.

Electro-spraying (E-spray) is a method of atomizing a liquid by means of electrical forces. E-spraying provides the advantage of being able to create coatings with relatively

high efficiencies because the electrical charge difference “carries” the liquid source material, which also provides good control of coating morphology, especially on rough and intricately shaped surfaces. Other advantages of this technique are low cost and easy setup.

In our work, the E-spraying technique was successfully adapted to apply thin, conformal, consistent coatings of 1,2-dioleoyl-*sn*-glycero-3-phospho-L-serine (DOPS) to small, flat, commercially pure titanium plates. DOPS coatings were E-sprayed, then loaded with gentamicin sulfate (GS), a popular antibiotic used in treatment of osteomyelitis. An elution study was completed to assess drug delivery capabilities of the coatings. This work demonstrated that elution profile could be modified by changing E-spray parameters.

Rat marrow stromal cells were harvested, and seeded onto the test coatings. Mesenchymal stem cells (MSCs) were selected from the general cell population, successfully cultured and differentiated into osteoblasts. Cytotoxicity of the coatings, along with cell viability, cell differentiation, biomineralization activity, cell morphology and early osseogenesis markers were evaluated at multiple time points in dual multi-week studies.

DOPS coatings were found to be non-cytotoxic, and cell viability and biomineralization were higher on DOPS-coated surfaces and gentamicin-loaded coatings than on plain titanium samples. At the two week time point, excessive delamination of the coatings occurred in the cell growth environment. Research was undertaken to identify and test techniques to enhance coating retention.

Surface chemistry was modified by passivation and pretreatment with calcium-chloride, and cholesterol was added to the DOPS E-spray. A repeated elution study demonstrated that elution profile could be modified as a result of changes in coating chemistry.

An additional MSC cell study was completed to reconfirm the effects of enhanced coating chemistry on the cytotoxicity, cell viability and biomineralization. Cell morphology was re-evaluated at all time points via SEM imaging. Hydroxyapatite formation was confirmed. Preliminary osseogenesis biomarkers were also measured, showing deposition of osteocalcin and osteopontin, important protein precursors to normal bone growth, on enhanced coatings.

This work demonstrates the viability of electro-sprayed DOPS coatings on titanium orthopedic implant material, and the enhanced osseogenic characteristics of these coatings. We also demonstrated that DOPS coatings can carry and release an antibiotic over time at clinically relevant dosages, and that this release profile can be engineered by modifications to E-spray process parameters, surface chemistry and E-sprayed material formulation.

## TABLE OF CONTENTS

1	Motivation & Long Term Goal .....	1
1.1	Implant Rates .....	1
1.2	Implant Failure.....	1
1.2.1	Infection .....	1
1.2.2	Other Causes of Implant Failure .....	3
1.3	Costs & Needed Improvements .....	3
1.4	Long Term Research Goals .....	4
2	Background .....	5
2.1	Biom mineralization & Biochemistry .....	5
2.1.1	Phospholipids in Osseogenesis .....	6
2.1.2	Calcium.....	7
2.1.3	Cholesterol.....	8
2.2	Implant Materials.....	10
2.2.1	Titanium Implants.....	10
2.2.2	Bone Cements & Fillers.....	14
2.2.3	Surface Roughness.....	15
2.3	Implant Coatings.....	15
2.3.1	Calcium, Calcium Phosphates & Hydroxyapatite.....	16
2.3.2	Phospholipid coatings .....	18
2.3.3	Phospholipid Coating Techniques .....	20
2.3.4	Electro-spraying.....	21
2.4	Infection.....	27
2.4.1	Pathogens .....	27
2.4.2	Biofilm Formation .....	28
2.4.3	Standard of Care .....	29
2.4.4	Antibiotics.....	29
2.4.5	Drug delivery .....	34
2.4.6	Phospholipids in Drug Delivery.....	36
2.4.7	Elution.....	37
3	Research Overview, Specific Aims & Hypotheses .....	39
3.1	Specific Aims & Hypotheses .....	41

<b>3.1.1</b>	<b><i>Specific Aim 1: Electro-Spraying DOPS on Titanium</i></b> .....	41
<b>3.1.2</b>	<b><i>Specific Aim 2: Elute Gentamicin from E-sprayed DOPS Coatings</i></b> .....	41
<b>3.1.3</b>	<b><i>Specific Aim 3: Test Effects of E-Sprayed DOPS Coatings on Cells</i></b> .....	42
4	Electro-sprayed deposition of phosphatidylserine (DOPS) coatings on flat CP Ti surfaces.	43
4.1	Experimental Approach .....	43
4.2	Preparation of Titanium Samples.....	44
4.2.1	Fabrication .....	44
4.2.2	Surface Preparation.....	45
4.3	Calculating Electric Field, Current Density & Current.....	46
4.4	Electro-spraying Phospholipid.....	47
4.4.1	Process Development.....	47
4.4.2	Parameter Discovery .....	51
4.5	SEM Characterization .....	58
4.6	Results and Discussion .....	58
4.6.1	E-sprayed DSPC Coatings .....	60
4.6.2	E-sprayed DOPS Coatings.....	71
4.6.3	E-spraying 3D Objects .....	87
4.7	Conclusions.....	91
4.8	Limitations .....	92
4.9	Future Work.....	93
5	Enhancing Coating Retention.....	95
5.1	Purpose.....	95
5.2	Experimental Approach .....	95
5.3	Experimental Design.....	96
5.4	Experimental Methods .....	97
5.4.1	Sample Fabrication & Preparation.....	97
5.4.2	Applying Calcium to Titanium Samples.....	98
5.4.3	Adding Cholesterol to DOPS.....	98
5.4.4	Simulated Cell Study .....	99
5.4.5	Qualitative Photographic Evaluation .....	99
5.4.6	Qualitative Evaluation by Stereo Microscope.....	99
5.4.7	SEM Method.....	100
5.4.8	Statistical Analysis.....	100

5.5	Results.....	101
5.5.1	Control and Baseline Samples .....	101
5.5.2	Simulated Cell Study .....	109
5.6	Discussion.....	117
5.6.1	Effect of Calcium.....	117
5.6.2	Effect of Pretreatment & Passivation.....	119
5.6.3	Effects of Cholesterol.....	121
5.6.4	Effect of Gentamicin.....	123
5.7	Conclusions.....	124
5.8	Limitations.....	125
5.9	Future Work.....	126
6	Controlled Elution of Gentamicin Sulfate from E-sprayed DOPS coatings .....	128
6.1	Purpose.....	128
6.2	Experimental Approach .....	128
6.2.1	Experimental Plan.....	129
6.3	Performing the Elution.....	130
6.3.1	Preparing Gentamicin Loads.....	130
6.3.2	Preparing DOPS-Gentamicin Elution Test Samples.....	130
6.3.3	About the GS Assay.....	135
6.3.4	Performing the Elution.....	136
6.3.5	Performing the GS Assay.....	137
6.3.6	SEM Method.....	138
6.3.7	Statistical Analysis.....	138
6.4	Results and Discussion .....	138
6.4.1	GS Coating Thickness.....	138
6.4.2	Test Elution Performance vs. E-Spray Voltage .....	139
6.4.3	Test Elution Performance with and without Calcium Pretreatment and Cholesterol in Coating.....	141
6.4.4	On the Total Sink Methodology.....	144
6.4.5	Modeling Elution Kinetics.....	145
6.5	Discussion.....	145
6.6	Conclusions.....	148
6.7	Limitations.....	148

6.8	Future Work.....	150
7	Cytotoxicity, osteoblast viability, biomineralization and bone matrix production of DOPS-coated Ti surfaces, in vitro.....	152
7.1	Purpose.....	152
7.2	Experimental Approach .....	153
7.2.1	Preliminary Cell Study.....	154
7.2.2	Follow-up Cell Study.....	155
7.3	Experimental Methods .....	156
7.3.1	Harvest and Differentiate MSCs .....	156
7.4	MSC Response to Test and Control Surfaces .....	158
7.4.1	Cytotoxicity: cell survival, adhesion, viability & morphology.....	158
7.4.2	Osseogenic Differentiation, Mineralization and Matrix Production.....	160
7.5	Null Assay Tests .....	165
7.5.1	Calcium and Total Protein with media but no cells .....	165
7.5.2	Calcium with no media .....	166
7.6	Non-Specific Fluorescence (NSF) Test .....	166
7.7	Statistical Analysis.....	166
7.8	Results and Discussion .....	167
7.8.1	Preliminary Cell Study Results.....	167
7.8.2	Follow-up Cell Study Results.....	187
7.9	General Discussion .....	215
7.9.1	On Calcium/Phosphate in Our Coatings .....	217
7.9.2	About Low Cell Numbers in Follow-up Study.....	224
7.10	Conclusions.....	231
7.11	Limitations.....	232
7.12	Future Work.....	232
8	Summary Conclusions .....	235
9	Acknowledgements .....	237
10	Appendix A. Detailed Protocols for Electro-Spraying.....	239
10.1	Electro-Spraying Protocol.....	239
10.2	Titanium Cleaning & Surface Preparation Protocol .....	240
10.3	Mixing PL Protocol.....	241
10.4	Calcification of Ti surfaces.....	242

11	Appendix B. Detailed Protocols for Elution Study .....	244
11.1	Elution Protocol .....	244
11.2	Gentamicin Sulfate Loading Protocol.....	245
11.3	OPA Assay Protocol .....	245
11.4	Mixing GS Standards.....	246
11.5	Mixing OPA Reagent.....	247
12	Appendix C. Detailed Protocols for Cell Study .....	248
12.1	ALP Assay (for BioAssay Quantichrom ALP Kit).....	248
12.2	BCA Assay for Total Protein (for Pierce Protein Assay Kit) .....	249
12.3	Calcium Assay (for BioAssay Quantichrom Calcium Kit).....	250
12.4	Calcium Assay (for Pointe Calcium Kit) .....	251
12.5	Cell Lysis using Triton-X or Cell-Lytic with SDS .....	252
12.6	Counting Cells .....	253
12.7	Fixing Cells Protocol (e.g. for SEM).....	254
12.8	Using the Flourescent Microscope at VTH.....	255
12.9	Live/Dead Cell Imaging Protocol (using Molecular Probes Live/Dead Cell Imaging Kit) 255	
12.10	Live/Dead Cell and Nuclear Imaging Protocol (using bulk Calcein-AM).....	256
12.11	Making Cell Culture Media .....	258
12.12	MSC Differentiation (to Osteoblasts) Media Change.....	259
12.13	MSC Harvest Protocol (rat) .....	260
12.14	MTT Assay Protocol.....	261
12.15	Cell Staining and Immunofluorescence Protocol.....	262
12.16	Seeding Cells .....	264
12.17	Cell Splitting/Freezing Protocols .....	265
13	References .....	268

# **1 Motivation & Long Term Goal**

## **1.1 Implant Rates**

Many millions of medical devices are implanted in human patients worldwide each year, including both original surgeries and revisions due to injury or disease. This year, more than 4.4 million people will have at least one internal fixation device and more than 1.3 million people will have an artificial joint. [1] Approximately 500,000 total hip and knee replacements were performed in the United States in 2004. [2] The number of hip fractures is expected to more than triple worldwide from 1.66 million in 1990 to 6.26 million in 2050, including an expected increase from 414,000 to 972,000 cases per year over the next 50 years in the European Union. [3] Furthermore, it is expected that osteoarthritis cases will contribute approximately 193,000 hip replacements and an equal number of knee replacements in the US, and about 50,000 in the United Kingdom. ([http://www.abdn.ac.uk/orthopaedics/res\\_bone.shtml](http://www.abdn.ac.uk/orthopaedics/res_bone.shtml)) These numbers will only increase as the average age of the worldwide population increases. The working lifespan of total knee and hip replacements is about 12 to 15 years [4] (<http://www.gatech.edu/newsroom/release.html?id=1964>). This is particularly important because, in 2004 in the US, approximately 40% of orthopedic devices were introduced into patients between 45 and 64 years of age.

## **1.2 Implant Failure**

### **1.2.1 Infection**

There are many causes of implant failure. Infection is one of the most serious. Infection rates resulting from surgical implantation of orthopedic devices occurs in 0.5%-

6% of cases [3], despite adherence to strict antiseptic operative procedures and the use of prophylactic antibiotics. Infection resulting specifically from primary joint replacement ranges from 1% to 3% [5] and from 1.3% to 11% in total hip replacement, while bacterial or fungal bone infections resulting from fractures are still higher, between 10% and 50%. [3] This incidence is much higher in trauma cases involving exposed bone, vascular injury and contamination. Infection rates upwards of 20% have been reported for cranioplasty with acrylic plates. [6] In one particular treatment method, Kummoona [7] reported restorative failure in 10 of 24 patients due to deep-seated infection of the underlying tissue or allergic reaction to the osteomesh. Foreign body reactions and infections can be especially common in craniofacial restorative interventions.

Chronic osteomyelitis often results from pathogens introduced from the skin into bony tissues during traumatic events, orthopedic surgeries repairing fracture or joint replacements (1-13% of cases), by oncological orthopedic surgeries (0-33% of cases), or any orthopedic surgery for patients suffering from diabetes (up to 13 % of surgical cases). [8]

Acute infection or chronic osteomyelitis develops in as many as 5% to 33% of open fractures. [9] It is estimated that 100,000 to 200,000 fracture fixation devices became infected in the United States in 2001. [3]

Revision surgeries due to infection are also common. A study of thirty-four patients with infected endoprostheses found that 26% of patients experienced re-infection, and 17% of the patients required amputation of the infected limb. [8]

### ***1.2.2 Other Causes of Implant Failure***

---

Implant loosening for aseptic reasons is also common, often caused by loosening as a result of poor binding of the mineral phase of the bone to the metal surface and the presence of non-mineralized tissue at the bone-implant interface. [10, 11] Roughly a third of total joint replacements fail due to particulate wear debris, poor apposition and osseointegration, resulting in loosening of the device. In a large study in the UK, 10% of patients required revision surgery. Of these 60% were caused by aseptic loosening. [4] Small amounts of collagen and proteoglycan often form between the nascent bone and the implant surface, impeding direct contact. [12] To further complicate matters, an inflammatory response is usually triggered, resulting in development of fibrous tissue encapsulation between the bone and the implant. [13] The natural tendency for surface dynamics to shift from bone attachment to fibrous encapsulation is governed by surface chemistry, strain and micro-geometry. [14-16]

### ***1.3 Costs & Needed Improvements***

The costs of failed implants come from many sources, as discussed above. Infections alone, as they relate to orthopedic devices, result in billions of dollars in health care costs annually in the United States, and are three times higher worldwide. The direct medical cost per patient (i.e. surcharge to all patients) for occurrence of *Staphylococcus aureus*-associated osteomyelitis alone runs up to \$35,000 in the United States. [3] The overall annual costs of infections relating to orthopedic implant in the United States range between 150 and 200 million USD [17, 18] and about three times that worldwide.

This tremendous direct and human cost associated with orthopedic device failure and related infection motivates the need for improvements in the useful life of implant

devices, with particular focus on reducing risk of infection and optimizing the interface between biomaterials and bony tissues, while minimizing inflammation.

#### ***1.4 Long Term Research Goals***

The fundamental goal of this research is to develop an antibiotic-eluting, phospholipid coating for metallic implants, which is non-cytotoxic, enhances the growth and proliferation of osteoblasts, prevents and fights local infection, and enhances mineralization of bone precursor minerals. If successful, in the long term, this research could yield the first cementless implant alternative which can fight infection locally, and has the potential to provide a platform for future osseogenic and therapeutic coatings that could enable variable, controllable elution profiles, carrying various or multiple bioactive agents, in numerous potential applications, which could be applicable in the surgical ward, custom-designed for each patient.

## **2 Background**

### **2.1 Biomineralization & Biochemistry**

Mineralization of new vertebrate bone occurs in the extracellular matrices of tissues. The characteristic pattern of mineralization in appositional bone is generally a radial-shaped spherulitic deposit composed of numerous individual mineral crystallites of various lengths about a central point referred to as the nucleation center. Bone mineralization occurs in these nucleation centers where mesenchymal cells proliferate around a rich capillary network and where a network of collagen fibrils forms in an amorphous matrix of organic matrix-crystal nucleation, contained with membrane-bound matrix vesicles. [19]

Matrix vesicles are composed of cell membrane fragments with amphiphilic phospholipid bilayer membranes, similar to cells. They contain matrix-processing enzymes, calcium binding phospholipids [20], calcium-phosphate nucleating sites, and alkaline phosphatases. [21, 22] They also contain calcium channels which facilitate the influx of calcium ions from the surrounding environment into the phosphate-rich interior. [23] Intracellular calcium activation and bony growth is dependent on extracellular calcium stores. [24] These matrix vesicles are synthesized and secreted by osteoblasts. [11, 25-28] In this way, osteoblasts control the rate of bone mineralization by regulating the release of these matrix vesicles.

The vesicle interior contains saturating concentrations of calcium and phosphate. The calcium-binding properties of the negatively charged phospholipids, in the presence of such high concentrations of calcium and phosphate, bind calcium ions and catalyze the precipitation of calcium phosphate [29], trigger the formation of an amorphous mineral

phase where crystals aggregate, disrupt the vesicle, and merge with other nucleation centers, thus initiating and regulating bone formation. [22, 30] Through this process, the phospholipid bilayer of these matrix vesicles is thought to provide the primary nucleation site for bone. [11, 26, 27]

Most osseointegration occurs within 8-12 weeks following surgery. [31] Mature bone develops in 4 weeks, with initial bone integration beginning in as early as 4 days.

Maximum bone in-growth is seen in about 6 weeks. [15]

### ***2.1.1 Phospholipids in Osseogenesis***

---

Phospholipids (PL) are included under a broad category of compounds called lipids, which include not only the true fats and oils but also substances which are chemically or biologically related. Other lipids include fats and oils, waxes, cerebrosides, sterols and carotenoids. They are all generally insoluble in water. Lipids are minor components of mineralized tissues. Their amounts vary from only 0.2% to approximately 2%, depending on the type of tissue. [32] About half of these are non-polar lipids such as free cholesterol and its esters, and triacylglycerol.

Phospholipids occur in every animal cell, with particularly high concentrations found in eggs, brain, liver, kidney and bone marrow. They also occur in large quantities in muscle, particularly cardiac and skeletal muscle but also smooth muscle. It has been shown that the phospholipid content of an organ or tissue is proportional to its functional activity; more active tissues contain higher phospholipid content. Phospholipids in bone and cartilage account for only 20-30% of total lipids; the majority of these are neutral phospholipids such as phosphatidylcholine, phosphatidylethanolamine, and/or

sphingomyelin. Only 10% of the phospholipids in these tissues are acidic phospholipids such as phosphatidylserine or phosphatidylinositol. [32]

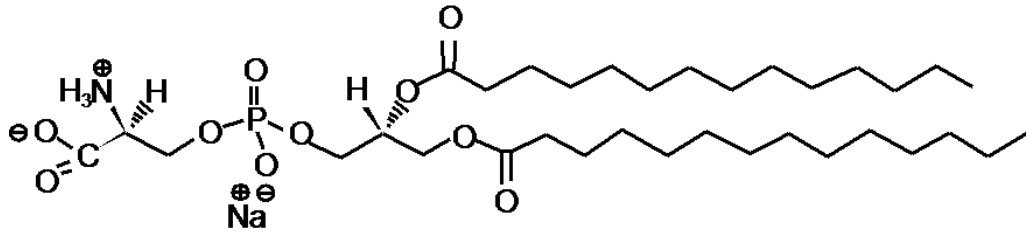


Figure 2-1: molecular structure of phosphatidylserine

Phosphatidylserine (PS) plays a very active role in osseogenesis. It is thought to provide the primary binding sites of the calcium phosphate. [22, 33] Acidic phospholipids may also control the rate of mineral development by electrostatic interactions between their polar head groups and the mineral surface. [27] The specific phosphatidylserine 1,2-dioleoyl-*sn*-glycero-3-phospho-L-serine (“DOPS”)(C<sub>42</sub>H<sub>77</sub>NO<sub>10</sub>PNa) appears to be most effective at enhancing osseointegration and matrix mineralization. [22, 33, 34] As amphiphilic compounds, the hydrophobic end of PS may also play an indirect role in preventing bacterial adhesion [35], as hydrophobic materials are known to participate in controlling which and how much protein adsorption occurs on the materials.

### **2.1.2 Calcium**

---

Calcium also plays an important role in many biological processes, ranging from regulation of numerous cellular functions such as stimulus-contraction coupling, protoplasmic motility, intercellular interaction, and interaction with proteins embedded in the lipid bilayer. Particularly pertaining to osseogenesis, phospholipids (PL), especially phosphatidylserine (PS), have a high affinity for binding calcium as the initial step in the biomineralization process. [36] PS binds cations at physiological pH due to its anionic

character. [37] The role of PS in the process of linking to matrix vesicle membranes and inducing formation of hydroxyapatite in early osseogenesis is also well known [22, 38, 39] and the specific interactions of calcium with PS are well documented.

IR analysis revealed that the calcium ion induces crystallization and immobilization of PS acyl chains crystalline state [40, 41], leading to a crosslinking effect [42] caused by a phase transition from the liquid-crystalline to the gel state. [40] IR analysis also reveals that  $\text{Ca}^{2+}$  ionically binds to the phosphate ester ( $\text{PO}_2^-$ ) group of PS and causes it to dehydrate. [37, 41, 43, 44]

Various phases of calcium-phosphate deposition involve phospholipids. [45] It has been suggested that a complex which forms between calcium, inorganic phosphate and phospholipid may be an essential prerequisite for inducing the deposition of calcium phosphate. [46] The chemical composition of calcium-phospholipid-phosphate complexes is a function of pH, solution composition, the nature of the phospholipid, and the method of isolation. At neutral pH, the most stable calcium-phosphatidylserine configuration occurs when the  $\text{COO}^-$  or  $\text{PO}_4^-$  of every second phosphatidylserine interacts with  $\text{NH}_3^+$  in neighboring PS-Ca-PS groups. [47]

### ***2.1.3 Cholesterol***

---

Cholesterol is one of the most important building blocks of living cell membranes and plays an important role in the cell membrane biology and biochemistry. It has high affinity for the cell membrane, where it plays a key role in controlling the rigidity of the fluid membrane [48], thus reducing passive permeability of the plasma membrane to protons (positive hydrogen ions) and sodium ions and increasing the mechanical

durability of the lipid bilayers. It increases the stability of phospholipids [49] and regulates membrane fluidity over the range of physiological temperatures. [50]

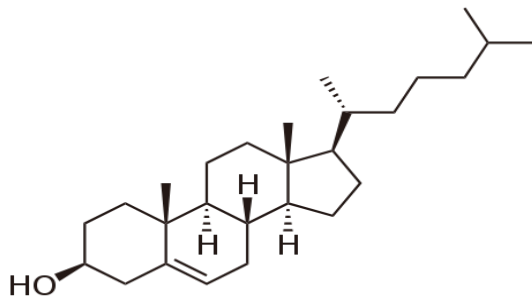


Figure 2-2: Chemical structure of cholesterol

Plasma membranes are composed of numerous patchworks of protein-lipid structures, referred to as membrane domains, whose boundaries and internal makeup are defined by the nature of lipids and proteins they contain. [51] The organization and function of lipid bilayers in membranes is dependent in part on the organization and interaction between phospholipids and constituent proteins in the membrane. [52] Cholesterol in membranes increases the organizational complexity of the lipids and proteins found in the membrane, and either increases or decreases the lateral mobility of the phospholipids in the membrane, depending upon the phospholipid microenvironment. [53-55] Ferraro *et al* [56] reported that cholesterol-rich plasma membrane lipid/protein micro-domains participate in the mechano-transduction process in human fetal osteoblasts. A key role of cholesterol is in the assembly and function of lipid rafts, which act to segregate and concentrate membrane proteins. [57, 58] Lipid rafts are involved in sorting and distributing lipids and proteins to the cell surface, where they play an important role in signal transduction and in generating cell surface polarity.

Interactions between cholesterol, calcium and phosphatidylserine (particularly DOPS), are also important factors modulating many cellular processes that are calcium-

regulated. [59, 60] For example, cholesterol alters the phase behavior of DOPS in the presence of  $\text{Ca}^{2+}$ , which affects cell membrane behavior, and regulates  $\text{Ca}^{2+}$ -induced membrane fusion. [44] FTIR analysis has shown that cholesterol disturbs the acyl chain packing of DOPS [44] but does not appear to affect the hydration or the mobility of the carboxylate group. [41] It also enhances the dehydration and immobilization of the  $\text{Ca}^{2+}$ -bound phosphate group in DOPS. Cholesterol modulates fusion of membranes induced by calcium [44] and alters the  $\text{Ca}^{2+}$  binding mode of phospholipid mono-layers.

## ***2.2 Implant Materials***

An ideal biomaterial for bone integration should increase the mineralization rate of new bone formation, while reducing inflammation to levels below which would inhibit tissue regeneration. [26] Poor performance of a biomaterial is often caused by insufficient apposition or integration of the implant with surrounding tissue, and infection. [61] A careful balance must be engineered between the longevity of the biomaterial and the integration of natural bone.

### ***2.2.1 Titanium Implants***

Titanium sees broad clinical use in orthopedic, dental and craniofacial applications. Titanium fixation devices are also the most common choice for endoprostheses. Commercially pure (CP) Ti, and alloys such as Ti-6Al-4V (and to a lesser extent Ti-6Al-7Nb) have been widely studied and found to be highly suitable for a broad variety of surgical device implantation applications. The success of Ti in these applications is due to its light weight, high strength, low modulus of elasticity, low corrosion resistance and excellent bio- and cytocompatibility [25, 62, 63], all of which can be further improved through numerous surface modifications. [64-66] CP Ti has better corrosion resistance

and biocompatibility than Ti alloys [67, 68], but lower strength, especially in fatigue. CP Ti is more common than Ti alloys in dentistry, but Ti alloys have become much more common in orthopedics due to strength requirements. [69]

Pure titanium immediately reacts with oxygen when exposed to air, naturally forming a surface oxide layer which is an important factor in bone healing and remodeling on titanium. This oxide is typically 2-6 nm in thickness, which increases during prolonged exposure and method of preparation. [68, 70] Oxide coatings on implants retrieved from human tissue are sometimes two to three times thicker. [67, 68] The oxide layer consists primarily of titanium dioxide ( $\text{TiO}_2$ ), but titanium oxide (TiO) and other oxides ( $\text{Ti}_2\text{O}_3$ ) are also present, along with a complex contamination layer consisting mainly of hydrocarbons. Titanium dioxide has physical and chemical characteristics that differ from metallic titanium, which are more closely related to ceramics than to metals. [25, 62, 63, 71, 72]

Ti surfaces are often modified by “pickling” and “passivation” procedures, which increase surface roughness and provide a relatively consistent titanium oxide surface. [68, 73] This also provides a more chemically active surface upon which biomaterials and tissues can more easily interact.

All Ti and Ti alloys develop oxide layers, which differ due to variations in crystallinity of the underlying metal and segregation of alloy components. [69] These subtle differences can also result in modified cell response among the various titanium compositions. The particular composition of the specific Ti alloy used does not have a significant effect on cell interaction. [25, 74] Osteoblast proliferation was reported to be higher on Ti-6Al-4V than on CP Ti. Higher ALPase activity was reported on CP Ti than

Ti-6Al-4V. Higher osteocalcin and collagen production were reported on CP Ti than on Ti-6Al-4V. [69] However, relatively higher risk exposure may exist with Ti-6Al-4V due to known cytotoxicity of vanadium and a possible relationship between aluminum and Alzheimer-type dementia. [75]

Due to the presence of the oxide layer, the fundamental reaction between a tissue and an implant is a reaction with titanium oxide at the implant surface, not with elemental titanium. Titanium oxide surfaces have a net negative charge at the pH values encountered in animal tissues, the pK being 4.0. These surfaces readily bind cations such as  $\text{Ca}^{2+}$ , particularly polyvalent cations. This binding of cations is based on electrostatic interactions between the cations and  $\text{O}^-$  ions linked to the titanium implant surface. The oxide layer is highly polar and attracts water and water-soluble molecules in general. [40, 41]

Calcium is directly involved in bonding between titanium oxide and PS molecules. Calcium ions are attracted to the highly polar [76] titanium oxide surface by electrostatic interactions with the oxygen ions and de-protonated  $-\text{OH}$  groups [77] present there. Calcium deposits have been observed in direct contact with titanium oxide surfaces. [78] In this study, plastic rods were sputter-coated with commercially pure titanium and implanted in rabbit tibia. After three months, the implants were removed, along with a 3 mm collar of surrounding bone, then fixed and sectioned. Bone was found (by transmission electron microscopy) to be in close apposition to the titanium, and no fibrous tissue was found between bone and titanium around the circumference of the implants. Collagen filaments were found in a three dimensional lattice surrounding the implant, and cellular processes from osteocytes were occasionally observed approaching

the titanium, always separated from it by a 200-400 Å wide proteoglycan coat. Calcium deposits were sometimes seen in direct attachment (30-50 Å resolution) with the titanium. It is believed the surface characteristics of titanium change from an anionic to a cationic state by the adsorption of calcium to the surface, which subsequently increases the adsorption of acidic macromolecules like proteins and phospholipids. [76] Thus, liposomes containing more PS adhere more strongly to titanium oxide in the presence of  $\text{Ca}^{2+}$  than liposomes with less PS. [27, 79]

Bone healing around titanium implants is characterized by a gradual mineralization process, directed from surrounding tissue toward the implant. True osseointegration is the formation of a tight bone-implant interface. [80] Bone develops in very close apposition to Ti and Ti alloys. [81, 82] Much of this integration of an implant with bone takes place at the interface between tissue and implant. [83-85] Biological and biochemical reactions at this interface, along with surface roughness, are fundamentally responsible for events leading to in-growth and integration of an implant into its host bone. [70, 78, 80, 86] The process of bony in-growth is characterized by two components: the response of the host to the implant and the behavior of the material in the host. Thus, chemical properties, surface characteristics and viscoelastic properties of an implant surface are particularly significant in anchoring implants, as they clearly have an influence on fast and permanent in-growth of implants into the bone. [87] Direct interaction between bone matrix, bone cells and the implant material are essential prerequisites to the formation of the bone at the implant interface. [88] In particular, the adhesion of osteoblasts to the Ti surface plays a critical role in bone formation processes. Most osseointegration occurs within 8-12 weeks following surgery. [31] Mature bone

develops in 4 weeks, with initial bone integration beginning in as early as 4 days. Maximum bone in-growth is seen in about 6 weeks. [15]

### ***2.2.2 Bone Cements & Fillers***

---

Acrylic bone cements are often used in initial device implantation, and additionally to fill voids and spaces that occur due to the naturally imperfect match between the implant and the tissue. Unfortunately, cemented implants are prone to long-term loosening due to cement failure and an invasion of fibrous tissue into these surgical voids. Cemented implants also fail due to wear and debris ingress at the cement/bone interface, and require a longer, more complex surgical implantation. These factors lead surgeons to prefer cementless, press-fit implants for many of their patients.

Cementless total hip arthroplasty is more common for younger patients who are likely to place a higher demand on their prostheses than elderly recipients. Long-term survival of uncemented hip components is dependent on biological fixation. To achieve biological fixation of uncemented or press fit implants, close apposition of bone to the implant surface and initial mechanical stability are required. Time of recovery is also an important success factor, especially for younger patients.

Long-term success of cementless or press-fit implant devices depends on:

1. a highly adherent, mechanically stable, biological fixation at the device-bone interface;
2. close apposition between the implant device and the implantation site [23, 89-91];
3. a low foreign body/immune response;

4. material properties of the biomaterials, such as viscoelastic properties of an implant surface, as discussed in the following sections.

### ***2.2.3 Surface Roughness***

---

Osteoblastic activity, adhesion and proliferation, and the mineralization of early bone are directly affected by surface roughness, topography and microstructure. [92-95] Adhesion strength of fibroblasts and osteoblasts on various polymeric materials and titanium was reported to increase with increased surface roughness. [69, 70, 96-98] Osteoblasts produce significantly more osteocalcin, prostaglandin E2 and TGF- $\beta$  on rough titanium surfaces than on smooth surfaces. [69, 93] Furthermore, with increasing roughness of the surface, osteoblastic cells showed increasing differentiation and decreasing cell proliferation. [69] Titanium surfaces with an average surface roughness ranging from 22 to 28  $\mu\text{m}$  exhibited significantly higher bone/implant index than smooth surfaces. [99]

## ***2.3 Implant Coatings***

Coatings and coating techniques that provide adherent, mechanically stable, biological fixation and close apposition between bone and an implant can improve osseointegration of an implant device, leading to longer service life for implanted devices, greater long-term surgical success rates and better quality of life for patients.

Although titanium exhibits excellent bio- and cytocompatibility, osteoblasts have difficulty adhering to the surface of titanium implants commonly employed in orthopedic and dental applications. [10, 100] When an implant is introduced, an inflammatory response is triggered as a result of both the implant and the surgical procedure. As a consequence of this inflammatory response, a fibrotic capsule is sometimes formed

between the bone and the implant, leading to loosening of the device, often with extremely costly consequences.

One such improvement was achieved in the mid-90s by coating the surface of a hip (femoral) implant stem with sintered titanium beads, creating a porous surface which, upon implantation, became interpenetrated by growing bone. [101] However, the sintered beads proved prone to detachment from the implant under biomechanical stresses and, ultimately, to the lack of chemical bonding between the metal and the bone mineral phase. [10, 100] More recent improvements make use of various porous coatings to enhance osseointegration of the implant and the strength of the bone–implant interface, while reducing risk of infection and foreign body reaction, all (ideally) resulting in prolonged implant lifespan. [90, 102, 103]

### ***2.3.1 Calcium, Calcium Phosphates & Hydroxyapatite***

---

Implantation of calcium ions on titanium surfaces has been shown to promote osseointegration *in vivo*. [104, 105] Calcium phosphate coatings have been shown to promote early bone apposition at the surface of cementless orthopedic prostheses [106, 107, 108] It is believed that following implantation, the calcium-phosphate coating dissolves, releasing ions into the peri-implant region, increasing the saturation of body fluids and thus precipitating a biological apatite on to the implant. This apatite layer serves as a substrate for osseogenic cells producing a mineralized extracellular matrix discussed earlier. [14]

Hydroxyapatite ( $\text{Ca}_5(\text{PO}_4)_3\text{OH}$ ) is the mineral constituent in living bone and has been widely acknowledged to encourage osseointegration. [14-16, 23, 65, 75, 89-91, 102, 103] Better bone integration would necessarily lead to improvements in implant fixation.

Hydroxyapatite exhibits a surface dominated by negatively charged oxygen that can attract cations such as calcium. Subsequently, anionic macromolecules such as glycosaminoglycans, which bind to calcium, interact electrostatically with the hydroxyapatite surface. [76] Commercially produced hydroxyapatite is very similar in chemical and crystal structure to bone and is shown to provide a good interface between bone tissue and the implant. As such, it is the material most often used to functionalize the surface of metal implants. [12]

Commercial hydroxyapatite-coated femoral hip stems have shown good success as initial and revision total hip replacement implants in patients over a wide age range. [4] However, hydroxyapatite coatings are far from perfect. In some applications, the coatings have been shown to adhere poorly to titanium. [21, 109, 110] The relatively high crystallinity (85%) of these ceramic coatings can make them brittle under biomechanical stresses and prone to a slow particulate degradation. [111]

Plasma-sprayed hydroxyapatite coatings applied to titanium implants show promise in improving the quality of bone apposition and the biomechanical fixation of prostheses. [14, 85] However, variations in crystallinity between hydroxyapatite and the bone mineral phase often lead to a mismatch between mechanical properties, and consequent delamination of the hydroxyapatite coating. [111, 112] Furthermore, plasma-sprayed hydroxyapatite-coated implants exhibited a higher infection susceptibility compared to uncoated titanium implants in an infection model in rabbits. [113] A possible explanation for this higher infection susceptibility could be the higher surface roughness of the HA-coated implants, making it easier for the bacteria to attach. [114, 115] Therefore, the

advantages potentially derived from the presence of hydroxyapatite may be lower than otherwise reported.

Other biomimetic approaches have been considered to modify the metallic implant surface with other bioactive substances that attempt to accelerate the rate of new bone formation on the implant surface as a means to develop better integration of the implant with growing bone. [116] For example, stimulating calcium-phosphate crystal nucleation may accelerate osteoblast adhesion and proliferation. [108, 117] It is also hypothesized that this would help to reduce the risk of fibrous tissue formation, thereby reducing the risk of biofilm formation (see section 2.4.2 below) and implant loosening. [101, 118] The deployment of phospholipid coatings on metal implants is one of these techniques that is showing promising results.

### ***2.3.2 Phospholipid coatings***

---

Numerous studies have shown that phospholipid coatings can be used to produce bioactive orthopedic materials which are capable of encouraging, even accelerating, osseointegration and matrix mineralization, while reducing inflammatory response. [23, 26, 27, 30, 33, 119, 120] Faster osseointegration and reduced inflammatory response could result in faster weight-bearing and less chance for infection, all potentially leading to faster recovery for patients.

Coating titanium with negatively charged phospholipids may induce hydroxyapatite crystal nucleation. [26, 32, 121] It has been suggested that a complex which forms between calcium, inorganic phosphate and phospholipid may be an essential prerequisite for inducing the deposition of calcium phosphate. [46] Coatings consisting of calcium-phospholipid-phosphate complexes are shown to encourage osseointegration and matrix

mineralization in environments rich in calcium and other minerals, such as simulated body fluid. [26, 30, 119-123]

The chemical composition of the calcium-phospholipid-phosphate complexes is a function of pH, solution composition, the nature of the phospholipid, and the method of isolation. At neutral pH, the most stable calcium-phosphatidylserine configuration occurs when the  $\text{COO}^-$  or  $\text{PO}_4^-$  of every second phosphatidylserine interacts with  $\text{NH}_3^+$  in neighboring PS-Ca-PS groups. [47]

Among the various phospholipids studied, a consistent pattern has appeared in which the synthetic phosphatidylserine DOPS appears to be most effective at enhancing osseointegration and matrix mineralization. [22, 33, 34] This may be related to the finding that calcium binding capacity correlates directly with the degree of negative charge associated with the lipid head group. [124] DOPS has a fairly high (compared to other phospholipids) net negative charge of -1 at pH 7.4. Phosphatidylserine-based coatings are also shown to increase the rate of bone in-growth, and the apposition of new bone, on a titanium surface, more than bare titanium [21] alone. This effect was greater with phosphatidylserine than with other phospholipids. After only 8 weeks, newly-formed trabecular bone in-growth had invaded almost completely a porous Ti test implant, establishing a direct contact with its surface in most of the areas analyzed. This bone apposition to the implant surface was completely consolidated after 26 weeks. Furthermore, phosphatidylserine-based coatings do not appear to elicit any adverse fibrous reaction. [21] Phospholipid coatings motivate faster deposition of bone precursor minerals while providing good substrate properties for osteoblast adhesion. [119, 120] This suggests that the calcium binding-phospholipids may gradually drive the in-growth

of new bone tissue towards the implant surface. [11] Possible clinical benefits of phosphatidylserine-based coatings may be significant, as accelerated bone in-growth and reduced risk of fibrous tissue invasion may lead to earlier weight-bearing, and faster recovery for implant patients.

A key consideration in the development of phospholipid coatings is their effect on the inflammatory response at the implant surface. Macrophages adhere rapidly to biomaterial surfaces after implantation and may fuse, forming multinucleated giant cells around the foreign body, which release molecules that contribute to cell activation and inflammation. Negatively charged phospholipid-coatings could potentially alleviate these events, thus improving the osseointegration of the implant by reducing the normal inflammatory response. [124] A naturally occurring stearyl-arachidonoyl form of phosphatidylserine (SAPS) was recently shown to inhibit the pro-inflammatory effects of toll-like receptor agonists. [125] Toll-like receptors are proteins that recognize certain molecules derived from invading microbes and activate immune cell responses. Phosphatidylserine has also been implicated as an important ligand for apoptotic cell recognition and clearance. [126]

### ***2.3.3 Phospholipid Coating Techniques***

---

Dip and drip coating are common techniques for applying phospholipids to titanium, particularly in studies of cell-related phenomenon. Dip coating [21, 74] is performed by dipping a titanium sample in a bath of one or more phospholipids dissolved in a solvent. The advantage of dip coating is that it is easy to perform and enables mixture and application of a variety of coating baths which might be less amenable to other coating techniques. The most important disadvantage is that it is difficult to control or quantify

the amount of phospholipid material actually deposited on the titanium surface without destructive testing.

Drip coating [23, 26] entails dripping solutions containing one or more phospholipids onto titanium test samples. The advantages of drip coating are: (1) one can directly measure the specific amount of material applied to the test surface; (2) it is an easy process to perform, and; (3) it enables mixture and application of various coatings to the test samples. The main disadvantage is that the drip process creates thick, discontinuous, non-adherent coatings which often form 3-dimensional gels in simulated body fluid, resulting in instability under mechanical stresses. [11, 23, 42] In addition, drip coatings are difficult to control on 3D objects. Numerous other coating techniques have emerged, but these are limited by complex processing requirements, toxic chemicals used in the process, poor control of coating texture, composition, and adhesion, and long reaction times. [127]

### ***2.3.4 Electro-spraying***

---

Electrohydrodynamic atomization (electrospraying or E-spraying) is a versatile method of creating thin, adherent coatings by atomizing a liquid by means of electrical forces. [128, 129] The technique has been in use for more than 100 years but only recently has it seen application in biomedical sciences. [130-133] E-spraying has been used to apply coatings consisting of many dozens of materials. A good review of many of the materials used and coatings created is found in. [128, 134]

E-spraying can create thin coatings with high efficiencies [135] because the charged liquid source material is carried by the electrical field rather than being pressurized or carried on another liquid, as in typical pressure-based spraying techniques based on

atomization of a liquid. [133] This is especially advantageous for more costly coating materials, and it enables good control. The term “efficiency” in this usage means that most or all of the material sprayed becomes part of the coating on the target. This is especially advantageous for more costly coating materials, and it enables good control of coating uniformity and morphology, especially on rough and intricately shaped surfaces. [136] E-spray also provides relatively easy control of product stoichiometry and morphology. [136] Other advantages of the E-spray technique are low cost and easy setup. E-spraying is often referred to as “electrohydrodynamic atomization” because electric field is the primary atomization force acting on a liquid that is moving in the electric field. E-spraying is distinctly different from mechanical atomization, such as in paint spraying, because the electric field is the primary force causing atomization and particle acceleration, rather than pressure.

In E-spraying, a liquid is “pushed” into a capillary at a low flow rate (e.g. by a pump). A droplet is formed at the tip of the capillary. A strong electric field is applied to the droplet, inducing electrical stresses in the surface of the droplet. A balance exists between the surface tension and viscoelastic forces of the source material inducing a capillary pressure (directed into the needle) which maintains a hemispherical shape of a droplet of material in the needle tip, and an electrostatic pressure (directed out of the needle) induced by the electric field, which deforms the source material into a conical meniscus referred to as cone-jet or Taylor Cone mode. [129, 137, 138] At the apex of the cone, a liquid jet with high charge density appears and under the right conditions, the jet breaks into small, highly-charged droplets. [43, 129, 136, 139] The formation of these droplets is the result of capillary breakup of the jet by surface tension. [140-143]

Materials with relatively high viscosity are ejected from the electric field-driven jet as very fine threads (a. k. a. “E-spinning”), while relatively low-viscosity materials at low concentrations will break up under the influence of the electric field into numerous smaller droplets [141, 144] which appear as an almost indiscernible mist leaving the tip of the needle (a. k. a. electro-spraying or E-spraying). As the material is carried to the target, evaporation of a droplet takes place, causing the droplet to decrease in size and hence the charge density of its surface increases. This increase in charge density due to Coulomb interaction (repulsion) overcomes the surface tension of the droplet and hence causes the droplet split into yet smaller droplets. [141, 145-147] Thus the source liquid is atomized by Coulombic interaction of charges on particles in solution. This interaction accelerates the liquid through the field, transferring mass from the capillary to a grounded target where the droplets are deposited and, given appropriate conditions, a coating forms on the target. Thus the E-sprayed material is “carried” by the current to the target, following electric field lines which intersect normal to the target surface. [148]

A thorough review on electrospraying and its different modes is provided by [129]. Comprehensive mathematical treatment of the physical and mass transfer underpinnings of E-spraying is given by [128, 139, 149-152].

Numerous E-spraying process parameters affect the creation of the surface on the target material [152-154], including:

1. concentration of the source liquid
2. syringe pump rate
3. size (surface area) of target material
4. distance from source to target

5. voltage potential
6. E-spray time (delivering a known amount of source liquid into the electric field at the pump rate)
7. physical properties of the source liquid (surface tension, viscosity, density and electrical conductivity)
8. needle diameter

In addition, because our application of E-spraying is targeted at creating coatings that would be used in elution and cell growth studies, additional characteristics such as chemical composition of source material were also important considerations.

#### ***2.3.4.1 About Morphological Change and E-spray Parameters***

As discussed in the previous section, the electro-spraying process operates within a balance between the viscosity of the material sprayed, the electric field strength (induced by voltage and distance) and surface tension of the material. It is widely reported that significant changes in coating morphology can be caused by changes in E-spray process parameters. [133, 153-156]

Various combinations of these process parameters produce different surface morphologies at nano- and micro-scales. Many researchers used a strategy of varying material viscosity, voltage, E-spray distance or flow rate, one at a time, while keeping the other parameters constant, as a means of creating desired surface morphology and chemical properties. For example, Kumbar and colleagues [133, 153] – one of the first studies to use E-spraying to coat biomedical implants with low coating material concentrations similar to our work – varied E-spray process parameters such as coating material, concentration and applied voltage (which they determined to be the most

important parameters) to study the effects of process parameters on E-sprayed poly(lactide-co-glycolide) and poly(ethylene glycol) coatings on thin metallic slabs. In this study, they qualitatively characterized morphologies of coated surfaces by scanning electron microscopy (SEM). Maintaining voltage (30 kV), needle gauge (21 gauge), and flow rate (4 ml/hr) constant while increasing coating material concentration resulted in denser coatings with different grain sizes and shapes on the target. The concentration range could be selected to develop individual structures and complexes of structures on the target. Low concentrations resulted in very low surface coverage with irregular grain structures. Slightly higher concentrations resulted in highly porous structures that appeared irregular and flat, while the highest concentrations tested resulted in denser coatings with flat architecture. For all concentrations studied, the polymer grains appeared spherical in shape. Similarly, increasing the E-spray voltage resulted in denser coating deposition, holding other parameters constant. The lowest voltages tested resulted in poor coverage of the target. Increasing voltage resulted in increased polymer deposition on the target, and a denser packing of the coated surface. The highest voltages tested resulted in yet greater coverage and multilayered coatings with individual particle deposition. Varying time produced similar changes in target coatings, other parameters held constant. Increase in E-spray time resulted in an increase in coating thickness as well as increased porosity and uniformity in surface morphology of the coated surface. The longest times tested resulted in thick coatings with reduced porosity.

Similarly, Buchko et. al. [156] and Uematsu et al. [154] produced different films of nanomorphologies and macromorphologies by varying process parameters such as

concentration, applied voltage, working distance, and exposure time while holding others constant. They also evaluated their results qualitatively using SEM.

To summarize the findings, lowering material concentration decreases viscosity, which results in formation of particles, spheres and other microtopological features on the surface. [133] The development of such features in the coating is caused by increased surface tension of the sprayed material, as a result of an increase in surface area per unit mass of the projected droplets (more numerous, smaller particles are formed). [153] This is brought about by increasing the electric field strength. Higher electric field strength increases field current [128], which increases mass flow rate from the needle to the target, all other parameters held constant. [141] Therefore, holding other parameters constant and increasing field strength (and therefore current) will move more material from the needle to the target. This higher mass flow rate increases the number of charged particles in the E-spray jet [128, 129], which increases both electrostatic and Coulombic forces. Higher Coulombic force induces a stretching force on droplets in the jet similar to increasing surface tension, resulting in greater repulsion between adjacent droplets. [157] This repulsive force causes formation of particles and spherical shapes on the surface, and a relatively rougher coating texture. A greater number of spheres, particles and other features formed on the surface results in a relatively rougher coating texture.

Increasing pump rate can yield a similar effect by placing more material into the electric field, other parameters held constant.

## **2.4 Infection**

### **2.4.1 Pathogens**

The most common pathogens found in orthopedic infections are coagulase-negative *staphylococci* [158](25% superficially and 30.1% in deep infection), particularly methicillin-susceptible *Staphylococcus aureus* (17.2% superficially and 13.2% in deep infection). [5] The predominant pathogen responsible for chronic bacterial osteomyelitis is *Staphylococcus aureus*, followed by *Pseudomonas* and *Enterobacteriaceae*. [3, 159] *Staphylococcus aureus*, the most prevalent species isolated from inpatient specimens, accounts for 80%-90% of cases of pyogenic osteomyelitis. Chronic osteomyelitis associated with orthopedic implants and about 90% of pin tract infections are caused by coagulase-negative *staphylococci* such as *Staphylococcus epidermidis*.

Once the pathogens enter the body, their ability to cause pathology is dependent upon their ability to attach to host tissues, their ability to resist attacks by host immune systems, and their ability to damage host tissues. *Staphylococcus aureus* adheres to bone by expressing receptors for components of bone matrix. [3] When a bone becomes infected, the soft, inner part (bone marrow) often swells. As the swollen tissue presses against the rigid outer wall of the bone, the blood vessels in the bone marrow may become compressed, reducing blood supply to the bone. Without an adequate blood supply, parts of the bone may die. The infection can also spread outward from the bone to form collections of pus (abscesses) in adjacent soft tissues, such as the muscle. This phenomenon drastically reduces the patient's recovery process after implant surgery. [160, 161]

### ***2.4.2 Biofilm Formation***

---

Bacteria adhere to an inert or living surface and form microcolonies. A major factor contributing to the development of periprosthetic infection and osteomyelitis is adherence of bacteria to the implant surface. [162-164] Numerous factors are implicated in the ability of pathogens to adhere to titanium implants, and osseointegration thereof [165], including surface texture and surface ion composition. [66] Bacterial adhesion is a two-phase process: an initial, instantaneous, reversible physical phase, followed by a time-dependent, irreversible cellular/molecular phase. [164] Bacteria that cannot adhere quickly to the surfaces are rapidly killed by the immune system. Once they become attached, pathogens can reorganize and mature into specialized communities referred to as biofilms. The formation of biofilms is based on the activation of genes required for the synthesis of extracellular polysaccharide [166] with which they produce a protective coating called a glycocalyx. This provides protection against systemic antibiotics and the host's own immune system. [167, 168] Especially in revision surgeries, debris that remains in the wound often includes clumps of biofilm that contain causative organisms. [169] Pathogens organized such that they are in direct contact with the biomaterial surface can ultimately link the entire biofilm to the biomaterial surface, further enhancing biofilm formation. [35, 170]

Biofilms grow slowly, in one or more locations, and biofilm infections are often slow to produce visible symptoms. Sessile bacterial cells release antigens and stimulate the production of antibodies, but the antibodies are not effective in killing bacteria within biofilms and may cause immune complex damage to surrounding tissues. [171] Even in individuals with excellent cellular and humoral immune reactions, biofilm infections are rarely resolved by the host immune system. Antibiotic therapy typically reverses the

symptoms caused by planktonic cells released from the biofilm, but fails to kill the biofilm.

### ***2.4.3 Standard of Care***

---

The current standard of care for chronic orthopedic infection is prophylactic parenteral antibiotic therapy, debridement, irrigation, reduction and fixation (in fractures), and/or two stage revision. [9, 158, 172] Debridement, reduction, fixation and revision surgery are very time consuming and costly procedures, not only in direct cost, but measured more so in cost to patient quality of life. Following debridement, autologous bone or synthetic grafts or fillers such as antibiotic-impregnated polymethylmethacrylate pellets are used. [173] Most synthetic osseous defect fillers are considered to be osseoconductive. [174] Autograft fillers are the most popular but have shown relatively inadequate performance compared with ideal antibiotic incorporation and elution requirements for osteomyelitis treatment. [175]

### ***2.4.4 Antibiotics***

---

A wide variety of antibiotics are used to treat osteomyelitis and other infections common in orthopedic surgery. Of these, the aminoglycoside antibiotics such as streptomycin, tobramycin and gentamicin exhibit bactericidal activity against a wide variety of microorganisms. As a class, they are considered the most effective antimicrobial agents available against methicillin-resistant pathogens common in orthopedic interventions, such as *Staphylococcus aureus* (MRSA), and *Staph. epidermidis*, and are also generally effective against Gram-negative bacteria such as *Enterobacteriaceae*. [176, 177]

Some aminoglycosides, such as gentamicin, are bactericidal, meaning they kill on contact with appropriate concentrations. Some antibiotics exhibit a bacteriostatic effect, which simply inhibits further growth of susceptible bacteria, leaving final eradication to the host's immune system.

As a class of antibiotics, they exhibit “concentration dependent killing,” meaning their bactericidal effects increase as the concentration increases. However, there are exceptions. Gentamicin is a time-dependent killer. [169] At the concentrations delivered by antibiotic-loaded bone cements, aminoglycosides exhibit concentration-dependent killing of Gram-negative organisms but time-dependent killing of Gram-positive organisms. [169]

Aminoglycosides generally kill by penetrating the outer cell wall and binding with the cytoplasmic membrane. [178] The subsequent loss of permeability control for small ( $K^+$ ) and large molecules (nucleotides, proteins, e.g.  $\beta$ -galactodase) creates the potential lethal event. [179] Aminoglycosides also exhibit a “post-antibiotic effect,” in which the suppression of bacterial growth continues after the antibiotic concentration falls below the bacterial MIC, as discussed below. This post-antibiotic effect can be pathogen specific, as well as drug specific. The post-antibiotic effect of aminoglycosides is less than two hours for most Gram-positive organisms and two to seven hours for Gram-negative organisms. [180] Aminoglycosides are soluble in water and heat-stable at body temperature.

Aminoglycoside antibiotics are powerful against their targeted pathogens, i.e. they have very low minimum inhibitory concentrations (MICs) compared to other antibiotics. MIC is a measure of growth inhibition by a drug against a particular organism at a

specific drug concentration. It provides a means to compare the relative effectiveness of anti-microbial agents. MIC is an *in vitro* measure of the lowest concentration that will inhibit bacterial growth over 18 to 24 hours of exposure to a constant concentration of the antimicrobial agent. [169] Specific bacteria generally are considered susceptible to an antimicrobial agent when serum levels above the MIC of the agent for that bacterium can be reliably achieved using normal doses. MIC values are useful, but bactericidal activity *in vivo* is unpredictable due to host reactions, so recommendations vary widely. One  $\mu\text{g/ml}$  of aminoglycoside is a common MIC for most *Staph. aureus* strains under both aerobic and anaerobic conditions. [181-183] The National Committee for Clinical Laboratory Standards (NCCLS) suggested susceptibility breakpoint for gentamicin against the most common pathogens involved in surgical wound infections is  $\leq 4 \mu\text{g/ml}$  [168] and the minimum MIC for GS against *Staph. aureus* is  $4 \mu\text{g/ml}$ . [184] Although many factors contribute to determination of exactly what plasma concentration of GS is toxic, careful drug monitoring is strongly recommended with an upper limit of 10–12  $\mu\text{g/ml}$  and a lower limit of approximately 2-4  $\mu\text{g/ml}$  against *Staph. aureus*. [180] It has been reported that persistent low levels of antibiotics, below the MIC values, cause the development of resistant bacteria in only a few weeks. [185, 186] Resistance is usually avoided as long as antibiotic concentrations remain several times above established MIC. [187, 188]

Parenteral antibiotic therapy, particularly with gentamicin, presents some important disadvantages limiting their use, including high risks of renal and oto-vestibular toxicity, poor availability and penetration into ischemic or necrotic tissues, patient discomfort, and high cost of treatment, due mostly to required hospitalization to monitor drug levels and

effects. [9, 189, 190] Numerous pathogens contributing to chronic osteomyelitis produce biofilms (see above), further limiting the availability of antibiotic [159, 191] at the implant site, thereby further decreasing effectiveness of parenteral drug administration. Approximately 30 to 60 min after intramuscular injection, peak concentrations in plasma of approximately 2 to 4  $\mu\text{g/ml}$  are reached. The therapeutic level ranges from 4 to 12  $\mu\text{g/ml}$ . [180] Gentamicin dosages administered parenterally are limited by the maximum safe serum concentration of approximately 10  $\mu\text{g/ml}$ , which is further restricted by low transfer of antibiotic from the blood to the infected site. [168, 192] For example, administration of various antibiotics over a wide range of dosages resulted in virtually undetectable amounts of antibiotic in femoral neck and distal femoral sites. [193, 194] When administered to mammals, the major portion is excreted in the urine by glomerular filtration. After intramuscular administration, peak serum concentrations usually occur between 30 and 60 minutes and serum levels are measurable for six to eight hours. [181] Further limiting parenteral efficacy, gentamicin is absorbed from the small intestine, and then travels through the portal vein to the liver, where it is inactivated. Therefore, it can only be given intravenously, intramuscularly or topically.

Detrimental effects on cultured osseogenic cells have been reported as a result of administration of certain antibiotics and antiseptic agents. Tobramycin, for example, has been shown to significantly decrease cell growth at concentrations of 400  $\mu\text{g/ml}$  and above. [195] Cefazolin had a detrimental effect on cell proliferation at concentrations of 200  $\mu\text{g/ml}$  and above. [196] Vancomycin has been reported to be safer with little effect at concentrations of 1000  $\mu\text{g/ml}$  and less. [196] For comparison, quinolone antibiotics such as ciprofloxacin inhibit cell growth at much lower concentrations (20  $\mu\text{g/ml}$ ). [197]

Inhibitory effects of gentamicin appear to be slightly higher than tobramycin. [198] Alkaline phosphatase activity and <sup>3</sup>H-thymidine incorporation were significantly decreased at gentamicin concentrations of 100 µg/ml and above [199] (refer to the *Cell Study* section for further discussion on this study), while total DNA was significantly decreased at 700 µg/ml and above.

#### 2.4.4.1 Gentamicin

Gentamicin is one of the most commonly used antibiotics in orthopedics. [1, 194, 200] It was approved by the FDA in 1966. Like other aminoglycoside antibiotics, gentamicin is chemically stable in biological systems. It is commonly used as a sulfate salt (gentamicin sulfate). Gentamicin sulfate is highly soluble in water (>1 g/ml) but relatively insoluble in organic solvents (0.678 mg/ml in chloroform, 0.2 mg/ml in methanol, 0.04 mg/ml in acetone). [181]

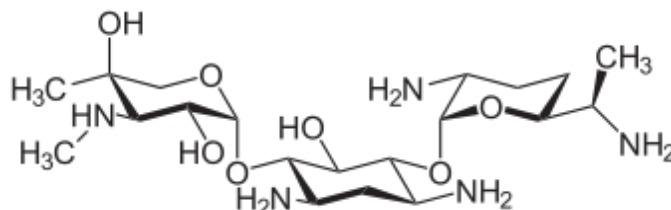


Figure 2-3: molecular structure of gentamicin

Gentamicin works by binding the 30S and 50S subunit of the bacterial ribosome, interrupting protein synthesis. [179] It is heat-stable at body temperature, and remains active even after autoclaving, making it particularly useful in microbiological growth studies.

Gentamicin is not a single chemical compound. Rather, it is a mixture of three major components commonly referred to as gentamicin C1, C1a, and C2, along with a number of minor components. The major components differ in the degree of methylation in the 2-

amino-hexose ring. There is a wide variation in the component ratio between different pharmaceutical gentamicin preparations. [201, 202]

Gentamicin is very persistent in the body. Significant levels of gentamicin were found in bone cement and joint fluid during revision surgeries up to 10 years after initial implant insertion. [183] Sufficient levels of gentamicin were found to inhibit or prevent growth of sensitive pathogens.

#### ***2.4.5 Drug delivery***

---

Low MIC requirements, risk of systemic toxicity, narrow therapeutic range and difficulty managing peak serum levels in parenteral/intravenous treatment are specifically the reasons why aminoglycosides are preferred in local implantable devices. The challenges with parenteral antimicrobial treatment have made local antibiotic therapy a very popular adjunct to systemic antibiotic delivery, for both prophylaxis and existing infections. Local delivery of antibiotics offers the capability of delivering relatively high concentration of antibiotic to the site of trauma, without the disadvantages of systemic toxicity, while improving dead space management, enabling earlier primary wound closure and providing more complete eradication of infections.

A successful drug delivery system achieves a therapeutic concentration of drug at a specific (desired) anatomic location for a length of time suitable to allow the drug to have a desired effect, without causing adverse side effects or excessive local concentrations.

Over the years, many antibiotics have been assessed *in vitro* for their suitability for local delivery. In general, the aminoglycosides, including gentamicin and tobramycin are considered good choices. Gentamicin is considered an excellent choice for use as a locally delivered antibiotic. It is also chemically and heat stable, making it suitable for

manufacture with/in implant devices. It has a broad-spectrum activity against the types of bacteria that cause orthopedic implant infections. McClaren [169] reported time-kill data *in vivo* show a 99.9% reduction of a critical *Staph.* load within less than 2 hours for gentamicin and less than 16 hours for vancomycin, with the concentration of both drugs below 20 µg/ml. As discussed above it is not metabolized but is safely eliminated almost entirely from the kidneys by glomerular filtration. And, gentamicin is bactericidal, killing susceptible bacteria if exposed to sufficient concentrations and not depending on the host's immune system for continued killing. [168]

Numerous studies have shown successful loading and elution of antibiotics from bone cements. [9, 194, 200, 203-205] Characteristics of good antibiotics for local delivery in bone cement are: [194, 206]

1. broad antibacterial spectrum, including Gram-positive and Gram-negative pathogens
2. sufficient bactericidal activity
3. high specific antibacterial potency (low MIC required)
4. low rate of primary resistant pathogens
5. minimal development of resistance during therapy
6. low protein binding
7. low sensitizing potential
8. water soluble
9. long release time
10. chemical and thermal stability at body temperature
11. minimal/no effect on biomineralization and osteogenesis

12. biodegradable

13. low risk of other potential side effects

One of the main risks of local delivery of some antibiotics from some delivery vehicles is the potential for antibiotic to maintain a measureable presence in the host system for a very long time. As mentioned earlier, resistance can develop, and low levels of toxicity can occur, from prolonged low-level exposure. In patients with an infected total hip replacement in which gentamicin-loaded bone cement was used, 88% harbored at least one staphylococcal strain resistant against gentamicin. [207] Little is known about the actual antibiotic concentration around an implant. Thus, there is a risk that the long time low concentration of gentamicin around an implant may induce antibiotic-resistant strains. [208] Some of the commonly used antibiotic-loaded bone cements release no more than 15% of the antibiotic incorporated. [209] Wahlig [186] reported distinct and very prolonged leaching of antibiotics from bone cements which leads, *in vivo*, to high local antibacterial concentrations of gentamicin after implementation of commercial PMMA bone cement (Palacos®-R, Merck, Darmstadt). Their long-term study showed the leaching of gentamicin from Palacos-R for a period of *five* years, with a continuous release throughout the whole period.

Numerous drug-eluting cemented devices are commercially available. However, a review of the literature reveals that there do not appear be any options available for antibiotic eluting cementless implants.

#### ***2.4.6 Phospholipids in Drug Delivery***

---

Phospholipids are widely used as drug delivery vehicles. Their amphiphilic composition and molecular complexity provides them with a wide range of chemical

bonding options, thus enabling them to carry a variety of therapeutics. The majority of phospholipid-derived drug delivery configurations found in the literature make use of lipid meta-structures such as liposomes, microspheres, micelles, and reverse micelles. Few references were found of drug-eluting phospholipid coatings on titanium and all these involved such phospholipid meta-structures and/or hybridizing or co-polymerizing the phospholipid with other compounds, for example, with phenylboronic acid unit and poly(vinyl alcohol). [210]

#### ***2.4.7 Elution***

---

Numerous studies have studied elution of gentamicin from a wide variety of materials. [1, 9, 178, 189, 194, 200, 203-205, 211-214] Some of these specifically involve gentamicin delivery via phospholipid-derived carriers. [211, 214]

The particular material carrying the gentamicin has a direct effect on the elution profile (initial burst, rate of release, and decay). In most cases, the concentration of gentamicin was shown to be well above the MIC required to manage infection locally (see section 2.4.4 above), after many hours and even days (depending on the eluting matrix). Forster [168] reported a release profile from antimicrobial coated polyurethane sleeves characterized by an initial bolus release with gentamicin concentrations of 83  $\mu\text{g/ml}$  at the two-hour and 54  $\mu\text{g/ml}$  at the two-day elution time points, followed by a sustained release well above the NCCLS MIC of 4  $\mu\text{g/ml}$  up to the 26-week time point at which time it dropped below 4  $\mu\text{g/ml}$ . [184] Some high-dose antibiotic-loaded bone cements are capable of delivering vancomycin and gentamicin at the necessary concentration for activity against biofilm-based bacteria, exceeding 100 times the usually expected MIC. [169] Sampath [189] reports that pharmacokinetic studies of gentamicin-

impregnated acrylic cement in 10 patients undergoing total hip joint arthroplasties indicated that only 5.78% of the total quantity implanted was released over 15 days.

Note, however, that nearly all studies were performed *in vitro*, with some bacterial kill studies done in agar cultures. Local release concentrations above MIC and serum concentrations in an animal model may be misleading, and do not necessarily indicate control of infection. The application of *in vitro* time-kill data to clinical infections is an imprecise process because of the many factors affecting drug targeting, such as *in situ* sink conditions, local drug dosages and tissue densities.

#### **2.4.7.1 Ideal Elution Profile**

Typical elution profiles in gentamicin delivery are characterized by an initial release “burst,” the size of which is proportional to the concentration of gentamicin, followed by a gradual release over 3 to 50 days, depending on the particular delivery vehicle used. An “ideal” elution profile is a complex consideration involving many factors. In general, a high level of antibiotic should initially be released in the first one to two hours to manage any pathogens introduced on the implant or in surgery. [9, 215] Following initial burst release, continued efficacy is supported by the relatively long post-antibiotic effect of aminoglycosides for Gram-negative microbes common in osteomyelitis. Therefore, in an ideal situation, the elution rate should decrease quickly, tapering to lower concentrations, but remaining above MIC for at least 7 to 10 days [185], then continually decreasing after that period to prevent sub-inhibitory concentrations thereafter so as not to induce bacterial resistance.

### **3 Research Overview, Specific Aims & Hypotheses**

In our work, the E-spraying technique was successfully adapted to apply thin, conformal, consistent coatings of 1,2-dioleoyl-*sn*-glycero-3-phospho-L-serine (DOPS) to small, flat, commercially pure titanium plates. DOPS coatings were E-sprayed, then loaded with gentamicin sulfate (GS), a popular antibiotic used in treatment of osteomyelitis. An elution study was completed to assess drug delivery capabilities of the coatings. Rat marrow stromal cells were harvested and seeded onto the test coatings. Mesenchymal stem cells (MSCs) were selected from the general cell population, successfully cultured and differentiated into osteoblasts. Cytotoxicity of the coatings, along with cell viability, cell differentiation, biomineralization activity, cell morphology and early osseogenesis markers were evaluated at multiple time points in dual multi-week studies.

DOPS coatings were found to be non-cytotoxic, and cell viability and biomineralization were higher on DOPS coated surfaces and gentamicin-loaded coatings than on plain titanium samples. At the two-week time point, excessive delamination of the coatings occurred in the cell growth environment. Research was undertaken to identify and test techniques to enhance coating retention.

Surface chemistry was modified by passivation and pretreatment with calcium-chloride, and cholesterol was added to the DOPS E-spray. A repeated elution study showed significant enhancements in overall elution profile, as a result of the new coating chemistry.

An additional MSC cell study was completed to reconfirm the effects of enhanced coating chemistry on the cytotoxicity, cell viability and biomineralization. Cell

morphology was re-evaluated at all time points via SEM imaging. Hydroxyapatite formation was confirmed. Preliminary osseogenesis biomarkers were also measured, showing deposition of osteocalcin and osteopontin, important protein precursors to normal bone growth, on enhanced coatings.

This work demonstrates the viability of electro-sprayed DOPS coatings on titanium orthopedic implant material, and the enhanced osseogenic characteristics of these coatings. We also demonstrated that DOPS coatings can carry and release an antibiotic over time at clinically relevant dosages, and that this release profile can be engineered by modifications to E-spray process parameters, surface chemistry and E-sprayed material formulation.

Each chapter, delineated by main heading below, contains methods, results and discussion, and conclusions sections. Then summary discussion and conclusions for overall research are provided thereafter.

### **3.1 Specific Aims & Hypotheses**

#### **3.1.1 Specific Aim 1: Electro-Spraying DOPS on Titanium**

*Discover process parameters that enable electro-spraying of thin, conformal, consistent phosphatidylserine (DOPS) coatings on flat commercially pure titanium with adequate durability to enable testing in specific aims 2 and 3.*

Hypothesis 1a: E-spraying will produce thin ( $< 10 \mu\text{m}$ ), conformal, consistent DOPS coatings on flat commercially pure titanium.

Hypothesis 1b: DOPS coating morphology can be controlled through changes in E-spray process parameters, such as time, voltage and distance.

Hypothesis 1c: The durability of E-sprayed DOPS coatings in aqueous media can be controlled through changes in sample surface preparation, such as passivation and pretreatment, and the chemical composition of the source material, such as inclusion of additional lipids.

#### **3.1.2 Specific Aim 2: Elute Gentamicin from E-sprayed DOPS Coatings**

*Demonstrate elution of gentamicin sulfate (GS) from DOPS coatings electro-sprayed onto titanium.*

Hypothesis 2a: E-sprayed DOPS coatings can be loaded with clinically relevant amounts of GS, which will elute from the coating over time, and less than 100% of loaded GS will elute in the first two hours in PBS.

Hypothesis 2b: E-sprayed DOPS coatings will elute GS at a faster than ideal rate in total-sink *in vitro* studies, but this rate can be adjusted through changes

in one or more E-spray parameters, coating chemistry, titanium surface composition and/or structure.

### ***3.1.3 Specific Aim 3: Test Effects of E-Sprayed DOPS Coatings on Cells***

*Assess the cytotoxicity, osteoblast viability, biomineralization and bone matrix production of DOPS coated Ti surfaces, in vitro.*

Hypothesis 3a: DOPS-coated Ti surfaces, with and without GS, and untreated Ti surfaces will all exhibit similar cytotoxicity and osteoblast viability up to 7 days after initial culture.

Hypothesis 3b: Osteoblast differentiation, mineralization activity and bone matrix production will be higher on DOPS-coated Ti surfaces without GS than on untreated Ti surfaces, which will be slightly higher than on GS-loaded, DOPS-coated Ti surfaces.

## **4 Electro-sprayed deposition of phosphatidylserine (DOPS) coatings on flat CP Ti surfaces.**

### **4.1 Experimental Approach**

As discussed in *Background*, many factors affect the E-spraying process and the coatings it creates. The objective of this study was to determine values for phosphatidylserine E-spray process parameters (listed in *Background*, section 2.3.4 above) that resulted in thin, conformal, consistent coatings on flat commercially pure titanium (Ti) surfaces which would enable testing of gentamicin elution (refer to *GS Elution Study* chapter 6) from and cell response (refer to *Cell Study* chapter 7) to the coatings.

Numerous studies have used E-spraying to create coatings on many implant or scaffold materials. [128, 134] By varying physical properties of the E-sprayed material and the E-spray system, various modes of E-spraying have resulted in a wide variety of surface morphologies. [132, 134, 153, 154] Many of these studies were focused on the application of E-spraying rather than modeling the phenomenon. For example, Kumbar and colleagues [153] – the first study to use E-spraying to coat biomedical implants with low polymer concentration as discussed in *Background* section 2.3.4 above, Kumbar and colleagues [133] – the first study to use E-spraying to coat biomedical implants with low material concentrations, similar to our work – varied E-spray process parameters such as coating material, concentration and applied voltage to study the effects of E-spray process parameters. In this study, they qualitatively characterized morphologies of coated surfaces by scanning electron microscopy (SEM). Similarly, Buchko et. al. [156] and Uematsu et al. [154] produced different films of nanomorphologies and

macromorphologies by varying process parameters such as concentration, applied voltage, working distance, and exposure time while holding others constant. They also evaluated their results qualitatively using SEM.

In our E-spray study, we follow the same approach used by these and other researchers. E-spray process parameters were discovered using phosphatidylcholine and these parameters were then subsequently used as initial parameters for creating phosphatidylserine coatings on the same titanium substrate material. Samples were E-sprayed and promising coatings were subjectively examined under SEM. Tests were performed on these samples in physiological saline to evaluate approximate erosion resistance and degree of potential dissolution as a preliminary trial before subjecting the coatings to subsequent elution and cell response testing. Elution of gentamicin was tested on promising coatings (refer to *Elution Study* chapter 6) and cellular response to coatings was evaluated (refer to *Cell Study* chapter 7).

All references to voltage are in direct current (DC).

## ***4.2 Preparation of Titanium Samples***

### ***4.2.1 Fabrication***

Titanium samples were fabricated as either 0.5 cm by 0.5 cm or 1 cm by 1 cm squares (both nominal) from 0.016 inch commercially pure Ti sheeting (Titanium Joe, [www.titaniumjoe.com](http://www.titaniumjoe.com)). Two sizes (identified below) were used in this study to accommodate particular requirements of each project. Raw material were hand-cut with metal shears, hammered flat if necessary (shearing sometimes caused curling of corners), labeled with a diamond tipped metal scribing pen, and then cleaned and passivated according to procedures described below.

## ***4.2.2 Surface Preparation***

---

Two approaches were used for cleaning Ti samples. During E-spray process development (as described in this chapter), samples were solvent cleaned only, as described in the following section. These coatings easily delaminated during subsequent elution, coating retention enhancement and cell studies, motivating discovery of improvements that would enhance coating retention (see *Enhanced Coating Retention Study* chapter 5). One of these enhancements was to passivate the titanium samples. The passivation process was not used E-spray process development described in this chapter. All test samples used in subsequent elution, coating retention enhancement and cell studies (described in other chapters) were solvent cleaned and passivated, as also described in the following.

### ***4.2.2.1 Solvent Cleaning***

Ti samples were cleaned according to the *Ti Cleaning and Preparation Protocol*, provided in Exhibit A. Briefly, samples were sonicated for 30 minutes in 100 ml acetone to remove organic debris and oils, then rinsed in tap water and sonicated for 15 minutes in 100 ml of 2% Liquinox (stirring vigorously every 5 minutes). Samples were stirred vigorously every 5 minutes to prevent stacking. Samples were then rinsed three times in de-ionized water (DI-water) to remove all Liquinox, sonicated for 15 minutes in 100 ml of DI-water (stirring vigorously every 5 minutes), rinsed once in ethanol and once in acetone, then allowed to dry completely in room air before storage in a dessicator until use. Samples were generally used within one week of manufacture.

#### **4.2.2.2 Passivation**

Passivation was introduced to: (1) better clean the Ti surfaces; (2) standardize uniformity of the base oxide coatings; (3) to increase phospholipid adhesion on the test surfaces.

Following initial solvent cleaning (described in the previous section), samples were “pickled” and passivated, as detailed in the *Ti Cleaning and Preparation Protocol* provided in Exhibit A, which is adapted from the ASTM B600 - *Standard Guide for Descaling and Cleaning Titanium* and other studies. [73] Briefly, samples were bathed in 3.5% HF for 30 seconds to remove the existing titanium oxide layer and then soaked in 35% HNO<sub>3</sub> for 30 min at 50°C to regenerate a new oxide coating. Samples were then bathed in DI-water for 24 h.

Following this chemical treatment, the samples were rinsed twice in DI-water, vacuum dried and used immediately or vacuum sealed in nitrogen and/or stored in a dessicator at room temperature until use.

### **4.3 Calculating Electric Field, Current Density & Current**

The mathematical and physical foundations of E-spraying are complex. For the purposes of our study, we make certain assumptions and experimental decisions to simplify our mathematical treatment, because our objective is focused on the application of E-spraying rather than on modeling the phenomenon. For example, changes in capillary diameter can have a dramatic effect on E-spray performance, requiring extensive mathematical modeling. [216] Because we only used a single capillary diameter in all studies, we did not consider this effect in our model.

The following formulations were used to calculate results for our E-spray testing discussed in results discussed in section 4.6 below. For the purposes of our E-spray application, we calculated electric field strength ( $E$ ) as follows [148]:

*Equation 4-1*

$$E = \frac{F}{D}$$

*where  $F$  is force in the field (volts) and  $D$  is distance (nominal) between capillary and target (cm).*

Spray time is also important, as it constrains the amount of material that can accumulate on the target. As more material builds on the target, the voltage drops due to the natural insulating character of the phospholipid. This decreases current by increasing resistance ( $F=V=IR$ ), which results in “wet” coatings as discussed in section 4.6 below. Therefore, another parameter we refer to as “**coverage**” is calculated  $\text{mg}/\text{cm}^2$  as the spray time multiplied by the grams of phospholipid sprayed per ml of solvent (chloroform), times 1000 to convert grams to milligrams, times the pump rate (ml/hr) divided by 60 to convert hours to minutes, and divided by the target area, as shown in the following equation:

*Equation 4-2*

$$\text{Coverage} = \frac{g}{m} * 1000 * \frac{R}{60A}$$

*where  $g$  is grams of phospholipid,  $m$  is ml of solvent,  $R$  is pump rate (ml/hour) and  $A$  is target area ( $\text{cm}^2$ ).*

## **4.4 Electro-spraying Phospholipid**

### **4.4.1 Process Development**

The initial E-spray technique was developed and preliminary process parameters were discovered using synthetic 1,2-distearoyl-*sn*-glycero-3-phosphocholine (DSPC).

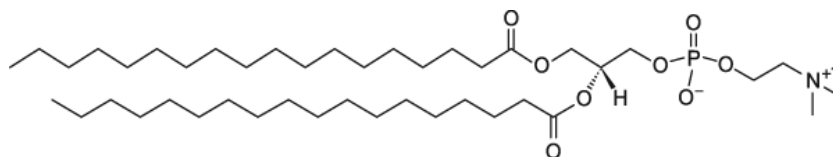


Figure 4-1: molecular structure of DSPC

Our ultimate target phospholipid molecule is synthetic 1,2-dioleoyl-*sn*-glycero-3-phospho-L-serine (DOPS) -  $C_{42}H_{77}NO_{10}PNa$ ). Our choice of DOPS was based primarily on the wealth of prior research done in osseointegration and drug delivery. DSPC was selected as our initial test molecule because it has very similar molecular weight (790.160 g/mol) as DOPS (810.025 g/mol), and similar molecular structure. Both molecules have 18-carbon fatty acid (acyl) chains. DOPS has a single saturated bond on each acyl chain, not found in DSPC, and DOPS is more polar than DSPC.

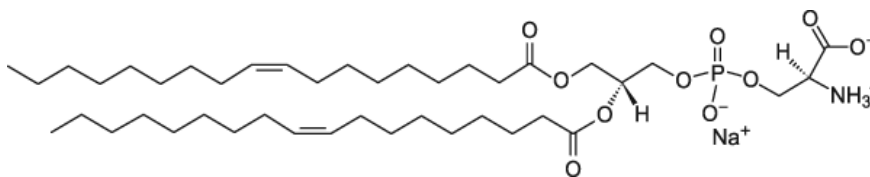


Figure 4-2: molecular structure of DOPS

Samples were E-sprayed according to the *Electro-Spraying Titanium* protocol found in Appendix A. Briefly, phospholipids were first dissolved in chloroform. All storage containers were either glass or polytetrafluoroethylene (PTFE), and plastic caps on mixing bottles were lined with PTFE liners. DSPC was E-sprayed at a variety of concentrations between 2% and 5% w/vol. DOPS was initially E-sprayed at 6% w/vol, which was later reduced to 1.3% as E-spray process parameters were adjusted to produce thin, conformal, consistent coatings.

Figure 4-3 presents a diagram of the E-spray process.

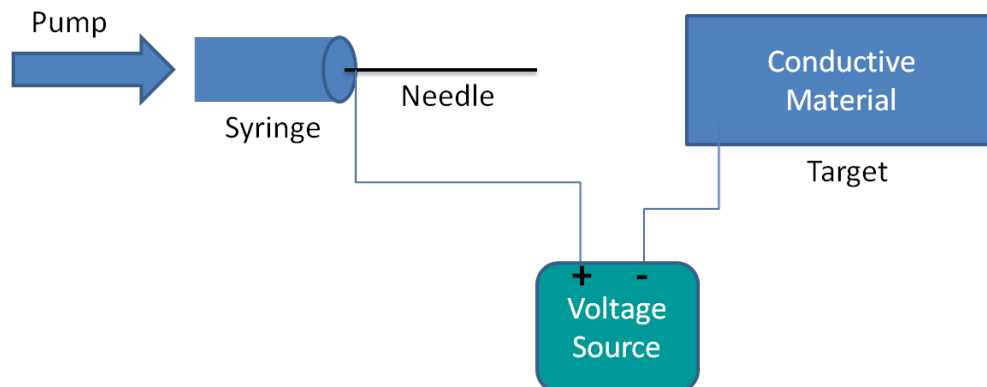


Figure 4-3: Diagram of E-spraying process

A liquid source material is pushed from a syringe (mounted on a syringe pump) at a controlled rate onto a target material under the influence of a high voltage differential between source and target. The target material is mounted at a measured distance from the source, and an electric field is formed over this distance between source and target.

Figure 4-4 shows a photograph of a typical E-spray apparatus setup.

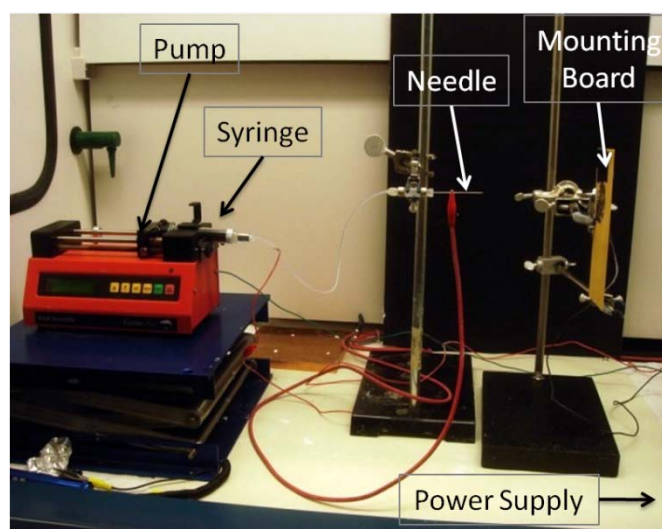
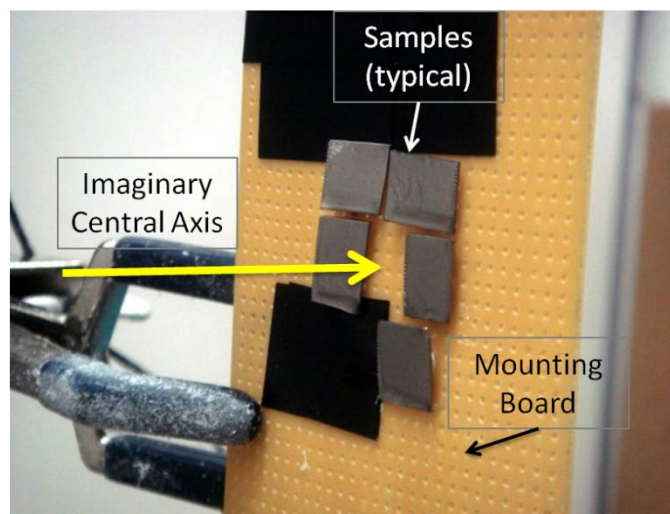


Figure 4-4: typical E-spray setup

In initial technique development, a double-hub syringe tube (12 inch, 20 gauge, Hamilton) connected the syringe (10 cc, glass, air-tight, Hamilton) to the needle (22 gauge, blunt end). Later, the syringe tube was eliminated, opting for direct insertion of

the needle into the syringe. This eliminated approximately 0.2 cc of waste material remaining in the tube after spraying.

Target titanium samples were mounted with removable, residue-free putty (UHU Tac, Basel, Germany) onto an insulated circuit board with copper wires protruding from the back through the board, directly contacting the Ti test samples. The target board was positioned at a measured distance from the needle. The needle was connected to the positive pole of a controlled voltage source, while the copper wire backing the target board (contacting the Ti samples) was connected to negative (ground). The pump, syringe tube, syringe body and mounting hardware were also grounded. The syringe pump calibration was checked every two to three uses. In initial testing samples were arranged in linear configurations on the E-spray board. In later tests, samples were arranged in circular configurations. The target board was positioned such that test samples would lie approximately centered around an imaginary central axis connecting the tip of the needle with the center point of the test samples on the target board, as shown in the following figure.



*Figure 4-5: typical assembly and configuration of titanium samples on E-spray board*

As the syringe pump was activated, source material sprayed from the syringe needle as a very fine, almost indiscernible mist which emerged from the needle in a cone-shaped pattern and became invisible within an inch of the needle, as shown in the following figure. In some cases, black insulating tape was used to mask certain areas from exposure to the E-sprayed solution, for example, conducting wires that were behind the mounting board, which would receive some of the coating if left uncovered.

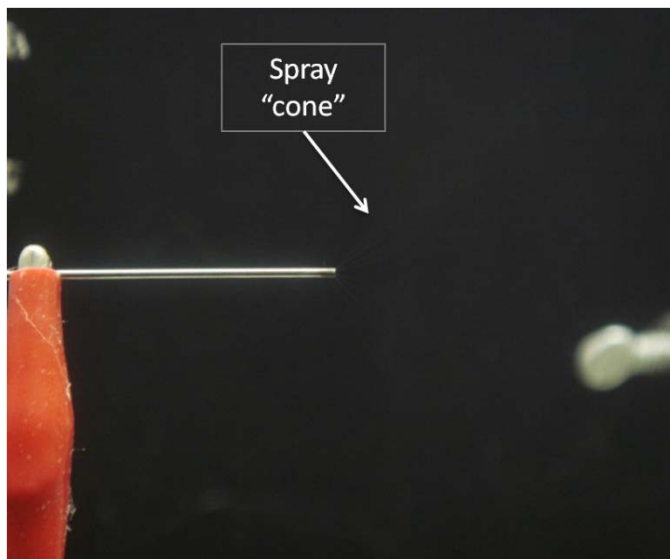


*Figure 4-6: E-spray is indiscernible*

#### **4.4.1.1 Material Storage**

DSPC and DOPS were kept frozen at 4°C.

E-sprayed samples were stored in desiccators until used. Test samples were typically used within one week of manufacture. If stored for longer periods, samples were vacuum sealed in nitrogen and/or stored in a dessicator at room temperature until use.

#### **4.4.2 Parameter Discovery**

---

The ultimate objective of this study was to discover process parameters that would create thin, conformal, consistent phosphatidylserine (DOPS) (Avanti Polar Lipids, Alabaster, AL) coatings on flat commercially pure titanium with adequate durability to

enable testing of gentamicin elution from, and cell response to, the coatings. With this perspective, phosphatidylcholine (DSPC) (Avanti Polar Lipids, Alabaster, AL) was used to discover approximate E-spray process parameters, which were then applied in development of DOPS coatings. More specifically, in our work capillary diameter was held constant while phospholipid concentration, target area, voltage, distance, and spray time were varied, as electric field (E) was calculated from each set of parameters.

#### ***4.4.2.1 DSPC Coatings***

Various tests were completed, as described in the following, to determine E-spraying process parameters that produced coatings to justify further testing with DOPS. Coating success was judged first by visual appearance of the resulting coatings (smoothness, consistency), if any coatings were visible, and then by weight change before and after E-spraying (indicating presence of a coating). Samples were weighed approximately one hour after being E-sprayed, to standardized dry time. Samples judged to be promising (those exhibiting the greatest weight change) were examined with SEM for uniformity of coverage and micro- and nano-morphology. Initial estimations of starting parameters were made based on the literature and discussions with researchers who had electro-spinning experience. All DSPC E-spraying was done on 1 cm square (i.e. 1 cm on each side, nominally) samples. Sample area was measured using a micrometer with a 4 mm measurement tube, measured at the approximate mid-point of each sample. Sample sizes were not precise because samples were fabricated manually. As a result, some samples were smaller than others. Therefore, weight changes were normalized for actual area ( $\text{cm}^2$ ) of each sample, to correct for variations in sample size.

Table 4-1 in Section 4.6.1 below lists the E-spray parameters tested with DSPC, including results and comments.

The following combinations of E-spray process parameters were tested with DSPC:

- DSPC concentrations of 4% and 5% (mass %)
- Pump rates ranging from 7 ml/hr to 11 ml/hr
- Total target sample areas ranging from 1 cm<sup>2</sup> to 5 cm<sup>2</sup>
- Electric field strengths ranging from 0.67 kV/cm to 1.5 kV/cm, developed by:
  - Spray distances ranging from 10 cm to 14 cm
  - Voltages ranging from 8 kV to 18 kV
- Spray times ranging from 3:30 minutes to 25 minutes
- 22 gauge needle diameter

The initial E-spray tests (tests 1 through 5 in Table 4-1) were performed with DSPC concentration held constant at 4% and pump rate held constant at 11 ml/hr, sample areas were 1 cm<sup>2</sup> and 3 cm<sup>2</sup> and electric field strength was varied by changing E-spray distance and voltage.

Following these initial tests at 4% concentration, electric field strength was held constant at 0.67 kV/cm (tests 6 through 8 in Table 4-1), DSPC concentration was increased to 5%, pump rate held constant at 11 ml/hr, sample areas were held constant at 1 cm<sup>2</sup> and E-spray times were varied (8.5, 5, 3 minutes) to evaluate the effect of these changes on coating formation. In tests 9 through 12, DSPC concentration was held constant at 5%, pump rate reduced to 10 ml/hr and held constant, field strength was held constant at 0.83 kV/cm, sample areas were 3 cm<sup>2</sup> and 5 cm<sup>2</sup> and times were again varied (5.5, 6, 7.5, 4.5 minutes). After test 12, samples were arranged in circular configurations.

In tests 13 through 20, DSPC concentration was held constant at 5%, sample areas were 3 cm<sup>2</sup> and 5 cm<sup>2</sup>, distance was held constant at 12 cm and field strengths were varied from 0.67 kV/cm to 1.5 kV/cm by varying voltage only, and times were again varied.

#### 4.4.2.1.1 DSPC Coating Retention Test

Once suitable E-spray parameters for DSPC became evident, tests were performed to assess degradation of the coatings. Samples from a variety of parameter combinations were bathed in PBS on a magnetic stirrer (150 rpm). All samples were first weighed. Samples were bathed in wide glass beakers, no more than 10 in one bath cycle, arranged to prevent contact between samples or with the magnetic stir bar. After 30 minutes, samples were removed from the bath, rinsed in de-ionized water, vacuum dried overnight and weighed. These cycles were repeated until no change in weight was observed, at which time all material was judged to have washed off, which was verified by stereomicroscope (Fisher Scientific Stereomaster).

#### 4.4.2.2 DOPS Coatings

E-spray process parameters discovered in DSPC E-spray testing were used in the initial DOPS testing starting. Parameters for DOPS were discovered in a similar manner, as described in the following. During E-spraying of DOPS, **“ideal” coatings were judged to be those that:**

1. exhibited the most consistent coverage and morphology across the sample surface (evaluated visually, not by SEM);
2. resulted in increased sample weight after E-spraying, normalized for sample area sprayed;

3. exhibited uniformity of coverage and consistency of micro- and nano-morphology (examined with SEM); and
4. appeared (via SEM) to be suitable for cellular adhesion, proliferation and development. This judgment is highly subjective. It has been reported [70, 96] that cell response on various polymeric materials and titanium increased with increased surface roughness, suggesting rougher surfaces would be better for cell growth. However, experience gained through coating retention testing (refer to section 4.6.2.3 below) showed that much of the microtopology erodes relatively quickly, suggesting the roughest coating is not necessarily the best for cell growth. In addition, this judgment was based in part on personal communications with experts in tissue engineering (*ref: Dr. Ketul Popat, School of Biomedical Engineering, Colorado State University, 2010*).

Similar to the approach used in DSPC E-spraying, samples were first judged by visual appearance of the resulting coatings (smoothness, consistency), if any coatings were visible, and weight change. Samples were weighed approximately one hour after being E-sprayed, to standardized dry time. Samples judged to be promising (those exhibiting the greatest weight change) were examined with SEM for uniformity of coverage and micro- and nano-morphology.

Table 4-3 in Section 4.6.2 below lists the E-spray parameters tested with DOPS, including results and comments.

The following combinations of parameters were tested with DOPS:

- DOPS concentrations ranging from 0.6 % to 6% (volume %))
- Pump rates ranging from 10 ml/hr to 20 ml/hr

- Sample square areas ranging from 3 cm<sup>2</sup> to 10 cm<sup>2</sup>
- Electric field strengths ranging from 0.8 kV/cm to 1.67 kV/cm, developed by:
  - Spray distances ranging from 6 cm to 10 cm
  - Voltages ranging from 8 kV to 12 kV
- Spray times from 36 seconds to 9:15 minutes

All test samples were weighed before and after spraying. Any measurable change in weight was considered better than none; “relative” weight change was considered more important than actual, because actual weight changes were often very small and difficult to quantify absolutely within the accuracy limits of the microgram scale used to weigh the samples. Initial DOPS E-spraying was performed on one or more 1 cm square (i.e. 1 cm on each side) samples, but later tests used 0.5 cm square (i.e. 0.5 cm on each side) samples (both nominal measurements).

Sample sizes were not precise because samples were fabricated manually. As a result, some samples were smaller than others. Therefore, weight changes were normalized for actual area (cm<sup>2</sup>) of each sample, to correct for variations in sample size.

The initial E-spray tests (tests 1 and 2 in Table 4-3 below) were performed with process parameters similar to those previously found for DSPC (6% (w/v) DOPS, 10 kV at a distance of 10 cm, electric field of 1 kV/cm, for 3 minutes at a pump rate of 10 ml/hour). These parameters failed to produce prospective coatings, and numerous additional tests ensued, varying parameters as shown in the table, until the first coatings with consistent coverage were produced (test 8). Subsequent tests were performed to improve coatings characteristics and identify parameters for ideal coatings (as defined above in this section). Final tests (16 and 17 in the table) were performed to discover if

cost could be reduced by increasing the number of samples that could be coated with the same amount of DOPS, while maintaining ideal coating characteristics.

#### 4.4.2.2.1 DOPS Coating Retention Test

DOPS coatings were evaluated for coating retention by bathing samples in phosphate buffered saline (PBS) for 45 days, as a simple measure of coating durability. Five 1 cm square (i.e. 1 cm on each side, nominally) DOPS-coated samples were E-sprayed at ideal parameters (as detailed in section 4.6.2.1 below (1.3% (w/v) DOPS, 12 kV at a distance of 8 cm, electric field of 1.5 kV/cm, for 3 minutes at a pump rate of 14 ml/hour) then vacuum dried overnight. Test samples were then placed in a 24-well plate. One ml of PBS was added to each active well and samples were bathed in phosphate buffered saline (PBS) for 45 days in an oscillating shaker at 16 cycles/minute, at room temperature. PBS was changed every 5 to 7 days. Photographs were taken daily for the first 4 days, then approximately every 2 to 4 days for 16 days. After 16 days, samples were observed and changes noted for 45 days. Samples were kept in the oscillating shaker at all times between photographic events and PBS changes.

#### 4.4.2.2.2 DOPS Drip Coating

To compare E-sprayed DOPS coatings with dripped DOPS coatings, 0.15 ml of 1.3% (w/v) DOPS was dripped onto three 1 cm square DOPS E-sprayed samples that were solvent cleaned (not passivated) as described in Section 4.2.2.1 above. Samples were then vacuum dried, observed under SEM and evaluated for coating retention by bathing samples in phosphate buffered saline (PBS) as described in the previous Section.

## 4.5 SEM Characterization

SEM images were taken as needed to confirm visual appearance, consistency, porosity, and topography/morphology. Samples were gold coated with 8 to 15 nm of gold and imaged at 5 kV to 8 kV.

## 4.6 Results and Discussion

E-spraying was able to create smooth, consistent coatings on titanium samples. As discussed below, initial testing focused on discovering parameters that would result in formation of any form of coating (many tests did not form a coating). Based on initial tests, E-spray parameters were adjusted in subsequent testing and ultimately, thin, conformal, consistent coatings were created.

The following SEM image shows the plain titanium control sample, after solvent cleaning (without passivation) with no E-spray coatings.

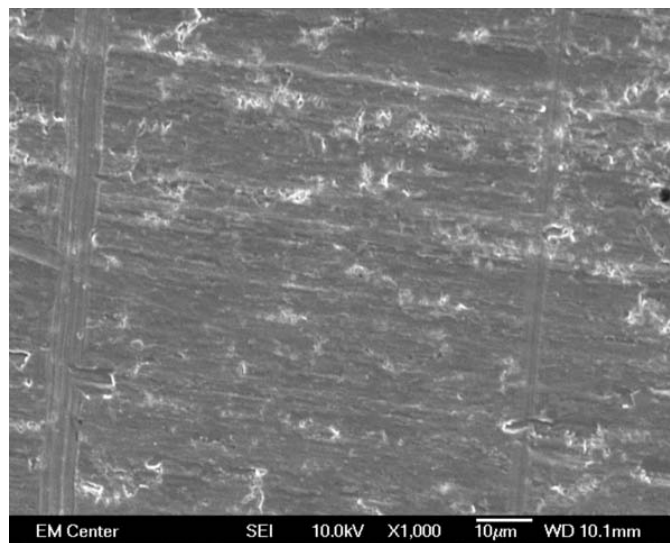


*Figure 4-7: titanium control, solvent cleaned, 1000X original magnification, no treatments*

The quality of DSPC and DOPS coatings was judged differently. Because DSPC was only used to find approximate parameters to use for E-spraying the more expensive

DOPS, evaluation of DSPC coatings was fundamentally based on visual observation of coating consistency and texture, weight change before and after E-spraying, and SEM examination for uniformity of coverage and micro- and nano-morphology. Results and discussion of these evaluations are provided in more detail in section 4.6.1 below. DOPS coatings were also judged using these factors, but weight change was of less importance because actual weight changes were so small (refer to section 4.4.2.2 above). Evaluation of DOPS coatings also included additional consideration for suitability for potential future cell growth (refer to section 4.4.2.2 above). Results and discussion of these evaluations are provided in more detail in section 4.6.2 below.

Some DSPC and DOPS samples dried immediately during spraying, as coatings were powdery white in appearance (refer to comments in Table 4-1 and Table 4-3 below). This is an indication the chloroform solvent in the E-spray solution evaporated completely during material transfer from the needle to the samples. [134, 150] In other tests, coatings appeared wet (shiny), sometimes thick and runny, indicating the chloroform solvent had not yet completely evaporated. Such “wet” coatings (with residual chloroform) were considered non-ideal, although it was not tested whether or not, after drying, these coatings may have performed better in elution and cell response than white, powdery coatings. The best conditions for creation of thin film coatings are when evaporation rate of E-spray solution is equal to deposition rate of solution droplets on the target samples. [134] These coatings appear dry and powdery white in appearance.

On occasion, some samples (DSPC or DOPS), regardless of sample size, exhibited a banded appearance to the coating, notably thicker where the electrode touched the back

of the sample, and thinner or absent further away from this location. It was determined that these cases occurred when samples were not in good conductive contact with the electrode on the E-spray samples mounting board.

#### 4.6.1 E-sprayed DSPC Coatings

Numerous combinations of E-spray parameters were tested for the quality of coating they produced, as judged by factors discussed earlier. The following table provides a summary of E-spray parameters tested for DSPC coatings in chronological order, earliest first to most recent last in the list, along with a key to SEM images provided below (first column of the table). As discussed in section 4.3 above, the column labeled “**Electric Field**” (E) is calculated as the voltage divided by the distance (between needle and target).

Table 4-1 DSPC E-spray Trial Summary

DSPC E-spray Trial Summary										
SEM Image #	Test #	Area		Process Parameters				Calculated Results (E)		Notes:
		(nominal) (cm <sup>2</sup> )	[DSPC] (w/v)	pump rate (ml/hr)	time (min)	distance (cm)	voltage (kV)	Elec-Field (V/cm)	Coverage (mg PL/cm <sup>2</sup> )	
	1	4	4%	12	25	15	10	6.67E+02	100.0	wet, thick, clear, bubbly
	Comment: wet, clear coating, bubbly in appearance, syrupy, visibly dry in a few mins, no weight change									
	2	1	4%	12	7	15	16	1.07E+03	85.4	wet, thick, discontinuous coating
	3	1	4%	12	7	15	16	1.07E+03	85.4	wet, thick, discontinuous coating
	4	1	4%	12	4.5	18	18	1.00E+03	54.9	wet, discontinuous coating
	Comment: no weight change - no PL on samples									
	5	1	5%	12	8.5	15	10	6.67E+02	138.2	wet, viscous, long dry time
	Comment: didn't dry well, still wet after 15 mins; much overspray, very small (.001g) weight change									
	6	1	5%	12	5	15	10	6.67E+02	79.4	wet, cloudy, uneven when dry
	7	1	5%	12	3	15	10	6.67E+02	47.6	uneven, wet, white coating when dry
	Comment: samples dried thick white coating; weight change 0.005 g									
4-8	8	3	5%	10	6	12	10	8.33E+02	25.9	dried thick, white, some overspray
4-9	9	5	5%	10	7.5	12	10	8.33E+02	21.9	thick white, some overspray
	Comment: uneven spray, thinner on upper and lower samples									
4-10	10	3	5%	10	4	12	10	8.33E+02	19.4	white, even coating, slow dry <30 min
	Comment: uneven coating on outer samples - switch to circular sample configuration									
4-11	11	5	5%	10	3.75	12	15	1.25E+03	9.7	shiny, pale white, low weight change
	12	5	5%	10	3.75	12	18	1.50E+03	9.7	shiny, smooth, no weight changes
	13	5	5%	10	6.5	12	15	1.25E+03	16.9	shiny, very small weight changes
	14	5	5%	10	3.5	12	18	1.50E+03	9.1	misty, no weight changes
4-12, 19	15	3	5%	10	4.5	12	10	8.33E+02	19.2	white, even, some overspray
4-13 to 18	16	3	5%	10	4.5	12	8	6.67E+02	19.2	very white, thick, coatings
	17	3	5%	10	4.5	12	12	1.00E+03	19.2	thick, much overspray on board
	Comment: although coatings appear relatively good, all wash off relatively quickly									
	End of study - focus on DOPS									

DSPC E-spray effectiveness was dependent on the particular location of the samples on the E-spray target board relative to the imaginary needle-target central axis (see Figure 4-5 above). Samples arranged in rows/columns (tests 1 through 10 in Table 4-1 above) exhibited inconsistent spray patterns, with those further from the central axis appearing (visually) to receive less coating than those nearer the center point; those farther from the central axis took longer time to exhibit the white powdery appearance typical of coating formation (if a coating formed at all). By Equation 4-1 above, longer distance from the needle to the target at the same voltage, target area and conductivity would result in a lower current carrying charged material to these outer samples. A similar effect can be seen, to a greater extent due to greater distances, in tests shown above as current decreases with increased E-spray distance. Therefore, to maintain consistent electric field (and thus consistent current) between samples, samples were arranged in a circular pattern (see Figure 4-5 above) after test 10.

The conductivity of chloroform is  $2.67E^{-10}$  S/cm [217, 218], which is considered to be low to moderate on an absolute scale relative to  $\sigma$  for distilled water ( $4E^{-8}$  S/cm). [128] Conductivity is directly proportional to E-spray solution concentration, with all other parameters remaining constant. [152, 153] Viscosity does not appear to exert a measurable effect on our results, compared to other parameters such as electric field, sample area and associated current. For example, test 1 above used a 4% concentration, yielding an electric field of  $6.67E^2$ , while tests 5 through 7 used a 5% a concentration, and also produced the same electric field, other parameters (including conductivity) being equal.

There was often overspray on the E-spray target mounting board and other equipment; DSPC residue was found on many objects other than the samples attached to the electrodes. In initial testing, overspray tended to be greater, but was reduced as E-spray parameters were adjusted to develop better coatings. Overspray indicates an overabundance of sprayed material in the electric field -- the current is not high enough to move all the material to the target. This was reduced by increasing electric field strength, decreasing concentration (and therefore viscosity and conductivity), decreasing sample area or E-spray time, or any combination of these parameters. Increasing electric field strength increases the number of charge carriers (charge density) in the electrospray jet [129] [128], requiring a higher current to overcome surface tension between droplets in the jet, all other parameters being equal.

Sample area has a direct effect on E-spray results. An increase in target area would decrease current density, while increasing current. This increase in current would also lead to the effects discussed above.

Coverage increases with increasing E-spray time, with all other parameters held constant. Higher coverage represents a greater amount of DSPC ( $\text{mg}/\text{cm}^2$ ) applied to target samples.

The following table provides weight change results for representative DSPC E-spray samples, with the right-most column showing percentage weight change, normalized for sample area. Test numbers (left-most column) correspond with test numbers in Table 4-1 above.

Table 4-2 Representative DSPC Weight Changes

Representative DSPC E-Spray Weight Changes					
	Average	Average Weights (g)			
Test	area	plain	coated	$\Delta$ weight	normalized
#	mm <sup>2</sup>	g Ti	g Ti+PL	g PL	$\Delta$ %
8	86	0.1936	0.1996	0.0060	3.6%
9	96	0.2155	0.2231	0.0076	3.7%
10	101	0.2279	0.2318	0.0039	1.7%
11	127	0.2850	0.2859	0.0009	0.2%
15	110	0.1931	0.1962	0.0032	1.5%
16	116	0.2038	0.2089	0.0051	2.2%

Weight changes before and after E-spraying DSPC for all “good” (even coverage, dry, powdery white) coatings were generally less than 5%. Samples were weighed approximately one hour after being E-sprayed, to standardized dry time. Some tests that resulted in “wet” coatings had correspondingly large weight increases, for example, 3.6% and 3.7% as seen in tests 8 and 9 in the table. These coatings appeared to be wet, although they were actually dry, with a shiny, glassy surface that made them appear wet. A wet appearance in a coating may be due to excess (heavier) unevaporated chloroform remaining in the coating. [134, 150] Relatively higher weight changes may indicate thicker coatings, which may be non-adherent in body fluid, resulting in instability under mechanical stresses. [11, 23, 42]

As can be seen in Table 4-1, numerous initial tests (tests 1 through 7) produce poor or no coatings. Comments in the table for each test (right-most column of the table) reveal sputtering, wet, viscous, uneven coatings, if any appeared at all. The test samples shown in Figure 4-5 above are representative examples of viscous, wet coatings, with excess E-sprayed material gathering along the bottom edge of the test samples. SEM images below in this section show selected DSPC coatings from tests listed in the table, as indicated in the left-most column of table.

SEM images for DSPC tests mentioned in the text are shown in the following:

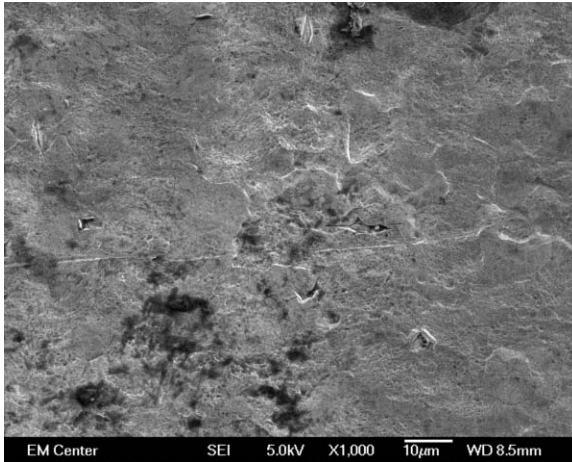


*Figure 4-8: SEM image of DSPC test 8 imaged at 5 kV, 1,000X original magnification. E-field 0.83 kV/cm, voltage 10 kV, E-sprayed for 6 mins.*

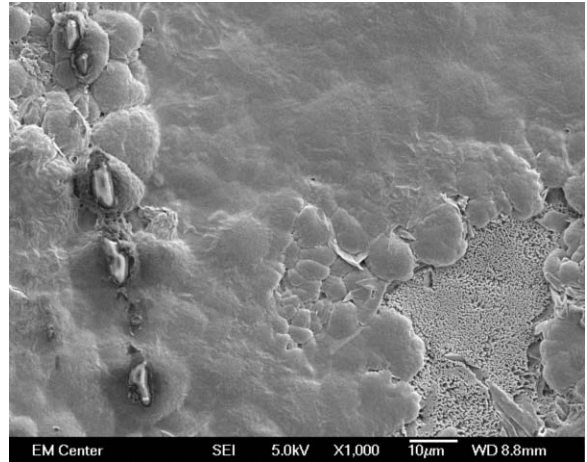


*Figure 4-9: SEM image of DSPC test 9 imaged at 5 kV, 1,000X original magnification. E-field 0.83 kV/cm, voltage 10 kV, E-sprayed for 7.5 mins.*

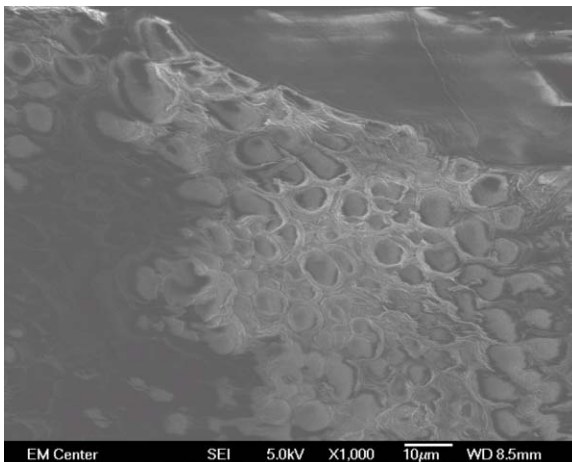


*Figure 4-10: SEM image of DSPC test 10 imaged at 5 kV, 1,000X original magnification. E-field 0.83 kV/cm, voltage 10 kV, E-sprayed for 4 mins.*

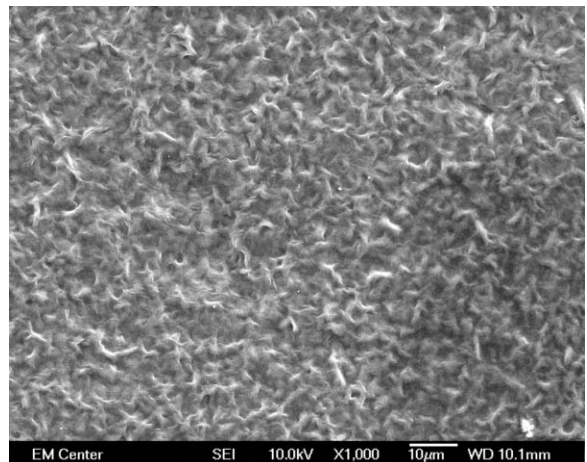


*Figure 4-11: SEM image of DSPC test 11 imaged at 5 kV, 1,000X original magnification. E-field 1.25 kV/cm, voltage 15 kV, E-sprayed for 3.75 mins.*

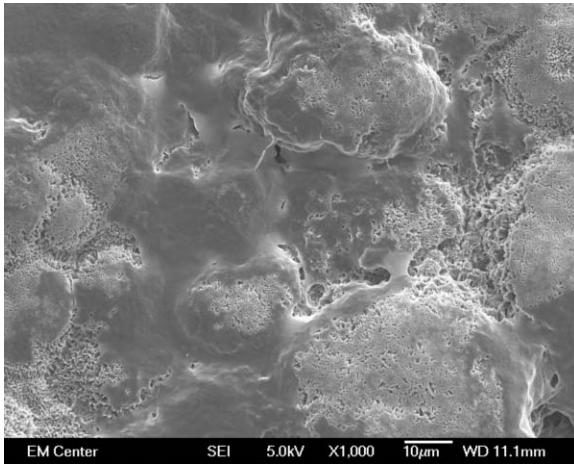


Figure 4-12: SEM image of DSPC test 15 imaged at 5 kV, 1,000X original magnification. E-field 0.83 kV/cm, voltage 10 kV, E-sprayed for 4.5 mins.

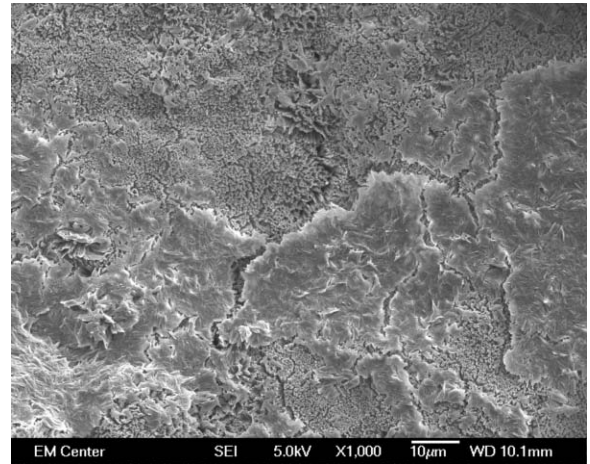


Figure 4-13: SEM image of DSPC test 16 imaged at 5 kV, 1,000X original magnification. E-field 0.67 kV/cm, voltage 8 kV, E-sprayed for 4.5 mins.

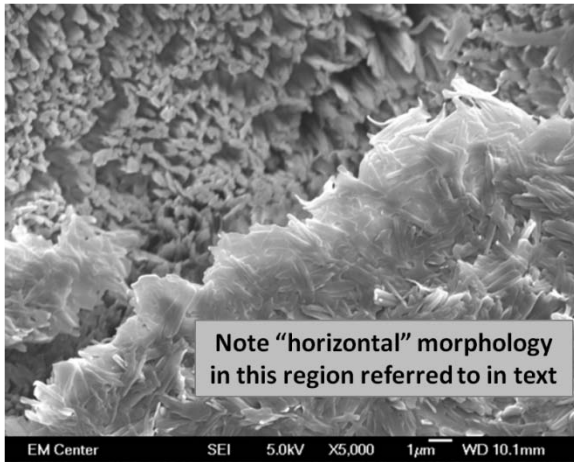


Figure 4-14: SEM image of DSPC test 16 imaged at 5 kV, 5,000X original magnification. E-field 0.67 kV/cm, voltage 8 kV, E-sprayed for 4.5 mins.

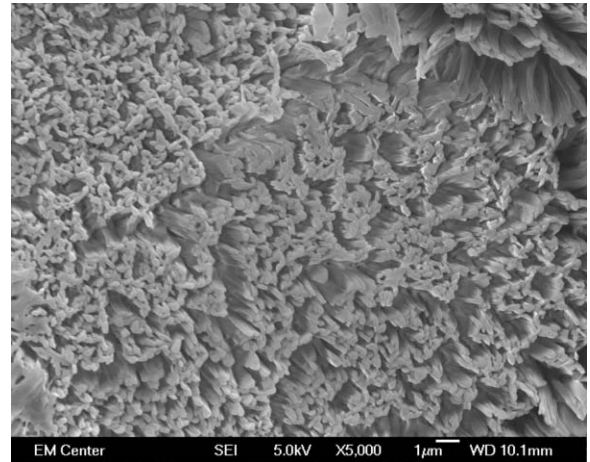


Figure 4-15: SEM image of DSPC test 16 imaged at 5 kV, 5,000X original magnification. E-field 0.67 kV/cm, voltage 8 kV, E-sprayed for 4.5 mins.

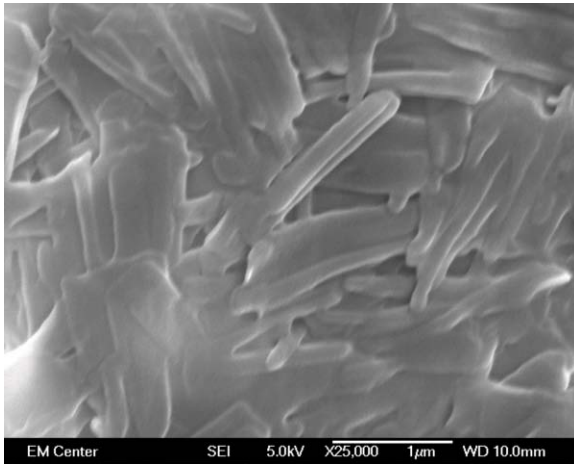


Figure 4-16: SEM image of DSPC test 16 imaged at 5 kV, 25,000X original magnification. E-field 0.67 kV/cm, voltage 8 kV, E-sprayed for 4.5 mins.



Figure 4-17: SEM image of DSPC test 16 imaged at 10 kV, 1,000X original magnification. E-field 0.67 kV/cm, voltage 8 kV, E-sprayed for 4.5 mins.

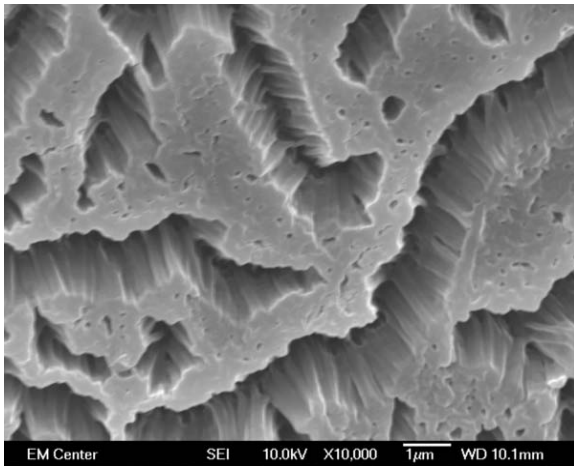


Figure 4-18: SEM image of DSPC test 16 imaged at 10 kV, 10,000X original magnification. E-field 0.67 kV/cm, voltage 8 kV, E-sprayed for 4.5 mins.

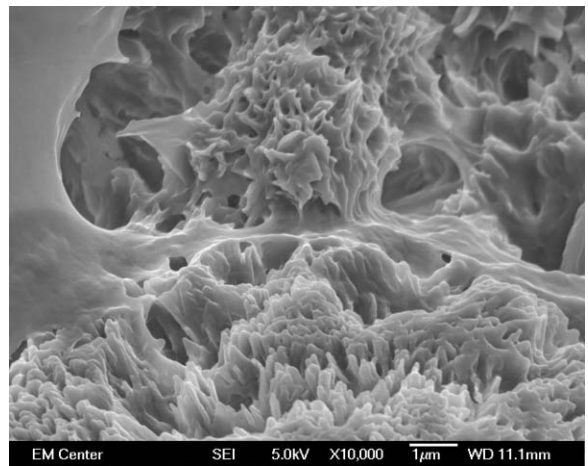


Figure 4-19: SEM image of DSPC test 15 imaged at 5 kV, 10,000X original magnification. E-field 0.83 kV/cm, voltage 10 kV, E-sprayed for 4.5 mins.

The initial test 1 in Table 4-1 above failed to produce a coating. Increasing pump rate, decreasing time and converging field strength at 1 kV/cm led to development of wet, clear coatings that appeared viscous and required 4 minutes to dry (to touch without visual evidence of deformation), but which resulted in no weight increase (tests 2 through 5). Wet, viscous coatings and long dry times are indicative of excess solvent remaining in the E-sprayed material as it lands on the target samples. [134, 150] The lack of weight change suggests that any DSPC which may have landed on the targets was insufficient to

be measurable within the accuracy of our microgram scales. Therefore, DSPC concentration was increased, while field strength and spray time were decreased, as shown in test 5. A coating resulted, which, despite being wet, viscous and requiring a relatively long dry time (15 minutes), yielded a small (0.001 g) weight gain. Holding these parameters constant, increasing field strength (and therefore current), and further reducing spray time, resulted in the first visibly white, yet cloudy, coating (test 8) with a notable weight increase (0.006 g). A stronger electric field delivers more of the charged particles to the target. [128, 129] Holding these settings constant and only increasing spray time resulted in more DSPC entering the electric field (test 8). These parameters produced thick, white coatings with relatively large weight increases (3.6%), normalized for sample area. However, notable overspray was seen, and SEM Figure 4-8 above reveals a relatively rough, uneven, inconsistent coating for test 8 (it is difficult to see at this image size, but some areas of coating appear to be absent, with titanium substrate visible underneath). Test 9 increased time and sample area to evaluate the effect of these parameters on the coatings produced in test 8. Powdery, white coatings were produced (as shown in SEM Figure 4-9 above) but there was also some overspray, and SEM Figure 4-9 reveals an uneven coating. Therefore time and sample area were again reduced to decrease the amount of DSPC material in the electric field (test 10), and a consistent, powdery white coating with relatively moderate weight change (1.7%) was produced (as shown in SEM Figure 4-10 above). Tests 11 through 14 explore the upper and lower limits of the electric field strength, all other parameters held constant. Higher electric fields resulted in very little coating, and very low to zero weight changes (e.g. weight change for test 11 was only 0.2%). Test 15 returns parameters to the last settings that

produced good coatings (test 10), 833 V/cm electric field, 3 cm<sup>2</sup> sample area, and 4.5 minutes spray time (producing coverage of 19.2 mg DOPS/cm<sup>2</sup>). These parameter settings resulted in a weight change (1.5%) very similar to test 10 (1.7%), coupled with SEM Figure 4-12, also notably similar to the SEM image for test 10 (Figure 4-10).

Our ability to revert to earlier parameters and produce similar coatings is indicative of repeatability of E-spraying as a coating technique. Our last two tests explored changes in voltage only, and resulted in relatively comparable weight changes (2.2% for test 16), but relatively inconsistent coating morphology, as shown in SEM Figure 4-13.

It is difficult to visualize, but SEM Figure 4-11 shows that test 11 produced a very thin coating, consistent with a low weight change. SEM Figure 4-13 through Figure 4-18 show various magnifications and the considerable complexity of the coating created in tests 15 and 16. SEM Figure 4-17 shows the inconsistency of the coating in test 16, which otherwise appeared (visually) to be a promising, powdery, white coating. SEM Figure 4-19 shows the coating produced in test 15 at a magnification of 10,000X to show detail of the rough regions of the coating.

Surface morphology of DSPC coatings clearly varied with electric field strength (induced by E-spray voltage and distance), as evidenced in the SEM images. This is consistent with other published reports. [133, 153] For example, Figure 4-8 and Figure 4-9 differ only by 1.5 minutes of spray time and 30 seconds of coverage (minutes/cm<sup>2</sup>), yet exhibit substantially different morphologies. Similarly, Figure 4-12 and Figure 4-13 differ by only 2,000 kV and also exhibit distinctly different morphologies. Effects of E-spray parameters on coating morphology are discussed further in section 2.3.4.1 above.

The most “ideal” coatings for DSPC E-spray were determined by multiple parameters. An electric field of 833 V/cm is consistent for all of the most promising coatings. A slight overspray below a coverage of 19.2 mg DOPS/cm<sup>2</sup> suggests that 4 minutes of E-spray time is ideal. In summary, the ideal E-spray parameters for DSPC E-spray coating are:

- DSPC concentration: 5% (w/v)
- Pump rate: 10 ml/hr
- Spray time: 4 minutes delivering 19.4 mg of DSPC per cm<sup>2</sup> sample area
- Electric field strength: 833 V/cm, developed by:
  - Spray distance: 12 cm
  - Voltage: 10 kV

#### ***4.6.1.1 DSPC Coating Retention Test***

In general, E-sprayed DSPC coatings were not durable, even in a simple PBS rinse. All DSPC-coated samples immediately changed in appearance when placed in PBS. They turned milky white almost immediately, then swelled and developed a spongy texture. They also appeared to begin delaminating immediately. More specifically, they dislocated from the titanium substrate as relatively large, visible flakes. Despite the apparent swelling that occurs, we considered this form of surface degradation to be delamination versus other forms of material degradation, such as dissolution or erosion, because when the material leaves the titanium substrate, it does so as relatively large (in proportion to the total surface) flakes, not small (i.e. microscopic or molecular) fragments. Furthermore, where coating material has delaminated from the titanium substrate, the substrate is clearly visible. There is no visual evidence (i.e. SEM) of any

coating remaining in any form in these regions, indicating that the complete thickness of the coating has wholly dislocated from the substrate. In some cases, whole coatings, the size of the complete sample itself, were seen floating in a well with the sample apparently devoid of any coating. In addition, the bond between DSPC and the titanium oxide surface is probably based on weak secondary interactions. To the contrary, numerous chemical interactions participate in the DSPC bulk coating, many probably motivated by ions in the media, and many probably stronger than the bonding at the DSPC-titanium interface. Therefore, it is reasonable to hypothesize the media (with relatively high ionic strength) invading the interface between the DSPC coating and the titanium substrate, and disassociating the weak bonding there, before the same ions can penetrate the bulk of the DSPC coating itself. In this way, the coating would delaminate *en masse* from the titanium substrate.

After 8 hours, most coating material had delaminated and was suspended in the media, and after 20 hours, all visible coating material had dissociated from nearly all samples. The following Figure 4-20 shows a typical set of samples after 8 hours in PBS. Note that most of the coating material has already delaminated.

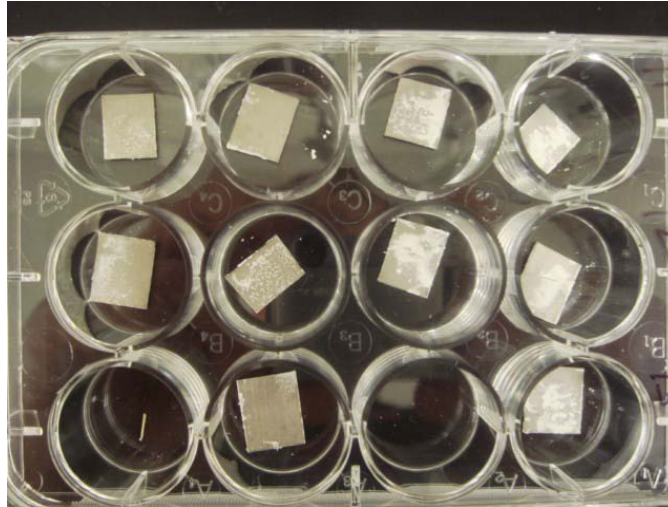


*Figure 4-20: DSPC samples after 8 hours. Most of the coating material has delaminated, as observed during the test.*

Because an initial set of parameters had been discovered, which could be used to initiate DOPS E-spraying, it was decided to cease continued work on E-spray parameter development with DSPC and begin E-spraying DOPS.

#### ***4.6.2 E-sprayed DOPS Coatings***

---

Numerous combinations of E-spray parameters were tested for the quality of coating they produced, as judged by factors discussed in section 4.4.2.2 above.

The following table provides a summary of parameters tested in chronological order, oldest first to newest last, along with comments about results.

Table 4-3 DOPS E-spray Trial Summary

DOPS E-spray Trial Summary										
Process Parameters								Calculated Results		Notes:
SEM	Test	Area	[DOPS]	pump rate	time	distance	voltage	(E)	Coverage	
Image #	#	(cm <sup>2</sup> )	(w/v)	(ml/hr)	(min)	(cm)	(kV)	(V/cm)	(mg PL / cm <sup>2</sup> )	
	1	3	5%	10	3	10	10	1.00E+03	10.0	<i>very thin coating, barely visible</i>
	2	3	5%	12	1	8	12	1.50E+03	4.0	<i>powdery white, uneven coating</i>
	3	3	5%	12	7.25	8	12	1.50E+03	29.0	<i>very thick, white coating, overspray</i>
	4	3	3.6%	12	9.25	8	8	1.00E+03	22.2	<i>very thick, white coating, overspray</i>
	5	3	0.6%	12	3	10	8	8.00E+02	1.1	<i>no visible coating</i>
	6	3	0.6%	12	0.6	10	10	1.00E+03	0.2	<i>no visible coating</i>
	7	3	0.8%	12	3	10	10	1.00E+03	1.1	<i>no visible coating</i>
	8	3	0.8%	12	1.5	10	10	1.00E+03	0.6	<i>no visible coating</i>
4-21	9	3	2.5%	20	2.25	8	8	1.00E+03	6.3	<i>thick coating, liquid on board</i>
4-22	10	3	2.5%	20	2.25	8	10	1.25E+03	6.3	<i>thick coating, but less overspray</i>
4-23	11	3	2.5%	14	4	8	10	1.25E+03	7.8	<i>no overspray, thin coating</i>
4-24	12	3	1.3%	14	3	8	10	1.25E+03	3.2	<i>thick, rough coating</i>
4-25	13	3	1.3%	14	3	8	12	1.50E+03	3.2	<i>powdery, smooth, even, white</i>
4-26	14	3	1.3%	14	3	6	10	1.67E+03	3.2	<i>uneven, spotty coating</i>

E-spraying DOPS created “ideal” coatings using much less material than DSPC, with only a moderately higher electric field. Overspray was much less common in E-spraying DOPS than with DSPC. Few tests produced discernible DOPS spray material on anything except the conductive material at the target. In addition, “wet” coatings were rarely observed, as they were in DSPC E-spraying. DOPS could effectively be E-sprayed at much lower concentrations (and therefore lower viscosities).

The following table provides weight change results, before and after E-spraying, for representative DOPS E-spray samples, with the right-most column showing percentage weight change, normalized for sample area. Test numbers (left-most column) correspond with test numbers in Table 4-3 above.

Table 4-4 Representative DOPS E-spray Weight Changes

Representative DOPS E-Spray Weight Changes					
	Average	Average Weights (g)			
Test	area	plain	coated	$\Delta$ weight	normalized
#	mm <sup>2</sup>	g Ti	g Ti+PL	g PL	$\Delta\%$
9	101	0.1751	0.1774	0.0023	1.3%
10	117	0.2032	0.2051	0.0019	0.8%
11	101	0.1803	0.1818	0.0015	0.8%
12	107	0.1845	0.1856	0.0011	0.6%
13	105	0.1827	0.1833	0.0006	0.3%
14	107	0.1885	0.1890	0.0005	0.3%

Weight changes before and after E-spraying DOPS for all “good” (even coverage, dry, powdery white) coatings were generally less than 1.5%. Larger weight changes corresponded with tests where there was visible overspray (e.g. tests 8 and 9).

The initial test 1 began with parameters similar to those considered “ideal” in DSPC E-spray testing. The electrical conductivity of phosphatidylserine is more than two orders of magnitude higher than phosphatidylcholine (approximately  $4E^{-3}$  versus  $9E^{-5}$  respectively, both equally moderately hydrated at 22°C). [219] We therefore hypothesized that a shorter E-spray distance would be better for DOPS than with DSPC, and reduced our initial trial distance. We also reduced the E-spray time based on similar reasoning – that the DOPS material would be carried more effectively by the current than DSPC, due to its much higher conductivity.

A very thin coating was visible in the initial test. Increasing voltage increases electric field and therefore current, which increases the flow rate of the material mass from the needle to the target, all other parameters held constant. [128, 141] Therefore, keeping concentration (and therefore viscosity and conductivity) and E-spray time constant, pump rate and electric field were increased in test 2 and powdery, white coatings resulted. However, coating coverage was uneven. Therefore, in test 3, spray time was increased to

7.25 minutes to put more material in the electric field. These parameters resulted in very thick, powdery, white coatings, along with some overspray. In test 4, concentration was reduced to 3.6% to reduce the amount of material in the electric field, pump rate was held constant, electric field was reduced slightly and spray time was increased again to 9.25 minutes. Overspray was again evident. This can be reduced by increasing field strength, reducing concentration, sample area or E-spray time, or any combination of these parameters. Therefore, in test 5, time was returned to 3 minutes, the same setting used in test 3. No visible coating was produced. In subsequent tests 6 through 8, pump rate and electric field were held constant while concentration was increased from 0.6% to 0.8% and spray time was varied in an attempt to recreate earlier, more successful coating conditions. No coatings formed at these parameter settings. Therefore, in test 9, concentration and pump rate were increased substantially to place more charged particles in the electric field, while electric field was held constant and spray time was increased. A thick, powdery, white coating was once again produced, as shown in the following SEM Figure 4-21, but some overspray was apparent.

SEM images for DOPS tests mentioned in the text are shown in the following:

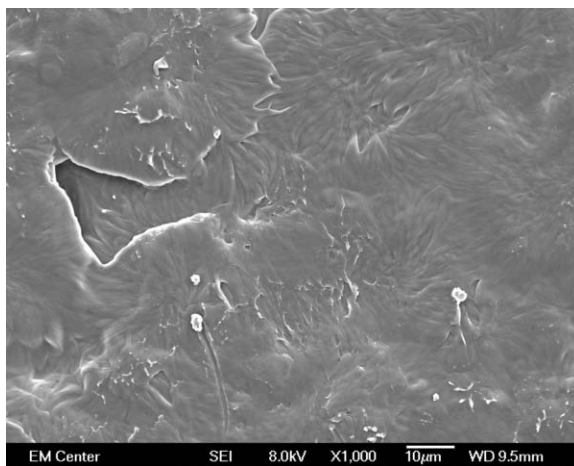
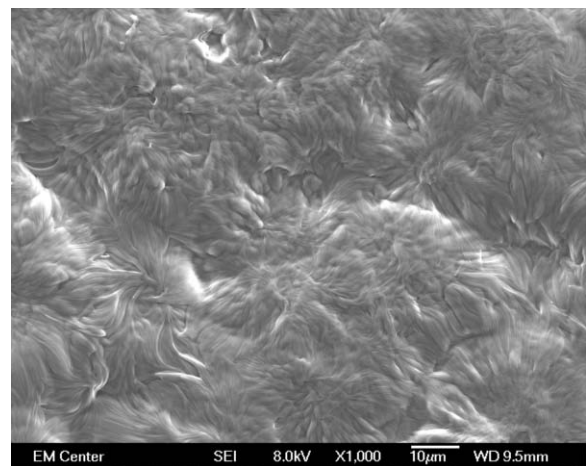


Figure 4-21: SEM image of DOPS test 9 imaged at 8 kV, 1,000X original magnification. E-field 1.0 kV/cm,



voltage 8 kV, concentration 2.5%, E-sprayed for 2.25 mins. at pump rate 20 ml/hr.

Figure 4-22: SEM image of DOPS test 10 imaged at 8 kV, 1,000X original magnification. E-field 1.25

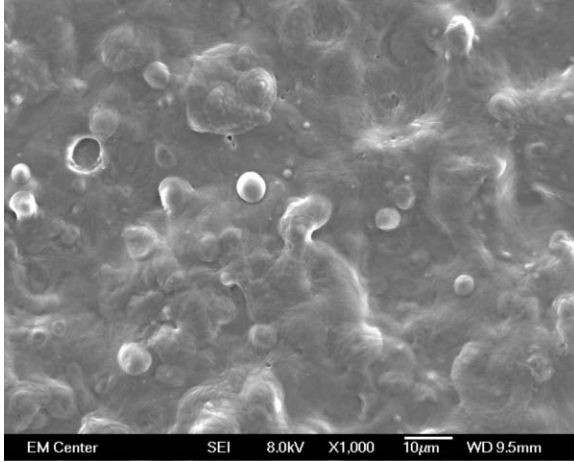


Figure 4-23: SEM image of DOPS test 11 imaged at 8 kV, 1,000X original magnification. E-field 1.25 kV/cm, E-sprayed for 4 mins. at pump rate 14 ml/hr.

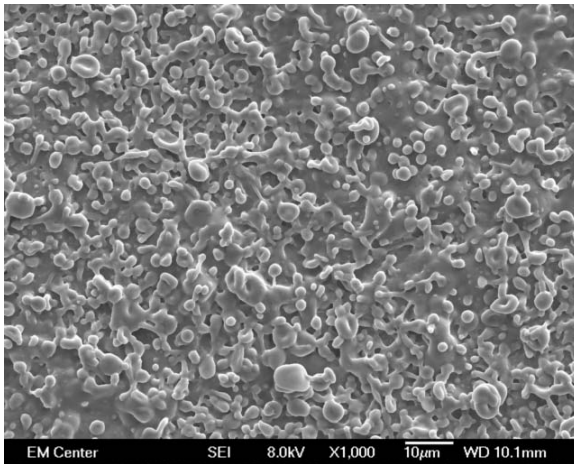


Figure 4-25: SEM image of DOPS test 13 imaged at 8 kV, 1,000X original magnification. E-field 1.5 kV/cm, concentration 1.3%, E-sprayed for 3 mins. at pump rate 14 ml/hr.

kV/cm, voltage 10 kV, E-sprayed for 2.25 mins. at pump rate 20 ml/hr.

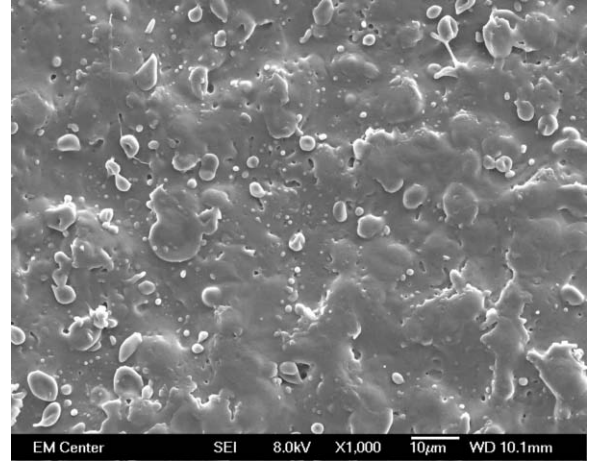


Figure 4-24: SEM image of DOPS test 12 imaged at 8 kV, 1,000X original magnification. E-field 1.25 kV/cm, concentration 1.3%, E-sprayed for 3 mins. at pump rate 14 ml/hr.

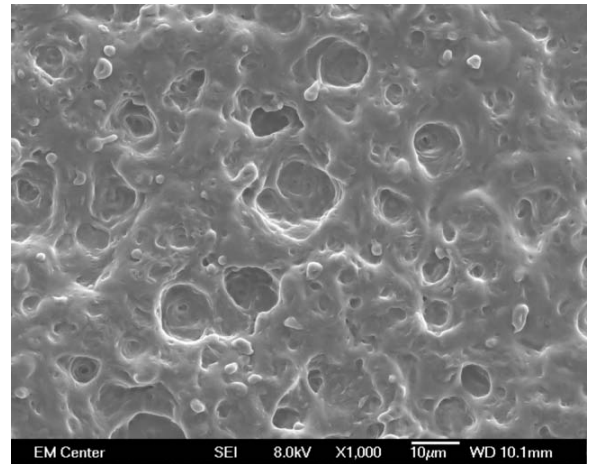
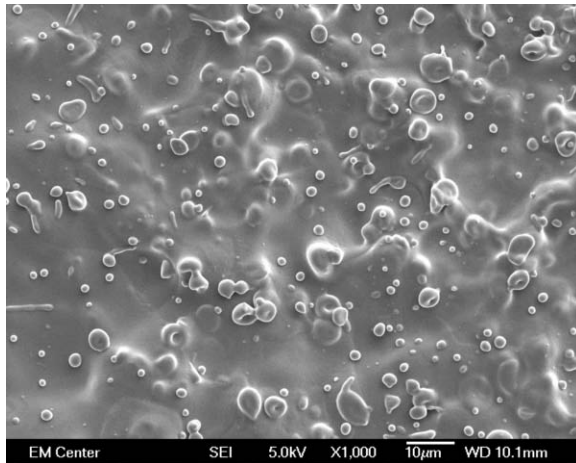
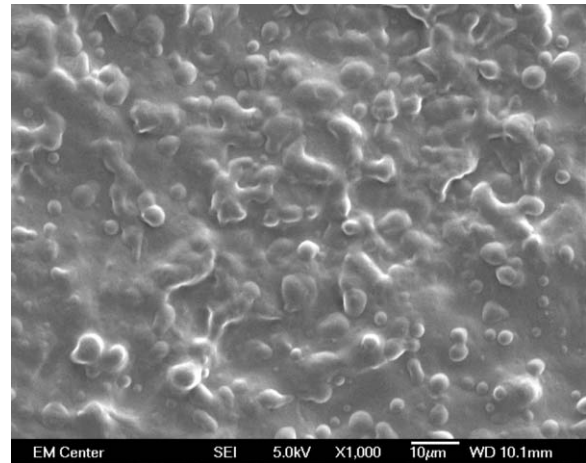


Figure 4-26: SEM image of DOPS test 14 imaged at 8 kV, 1,000X original magnification. E-field 1.67 kV/cm, concentration 1.3%, E-sprayed for 3 mins. at pump rate 14 ml/hr.



*Figure 4-27: SEM image of gentamicin-loaded DOPS test 15 imaged at 5 kV, 1,000X original magnification. E-field 1.5 kV/cm, concentration 1.3%, E-sprayed for 3 mins. at pump rate 14 ml/hr.*



*Figure 4-28: SEM image of gentamicin-loaded DOPS test 16 imaged at 5 kV, 1,000X original magnification. E-field 1.5 kV/cm, concentration 1.3%, E-sprayed for 3 mins. at pump rate 14 ml/hr.*

Test 10 held all parameters constant except for increasing the electric field to 1.25 kV/cm by increasing voltage to 10 kV. A white coating formed, and with less overspray. The coating texture was dense, smooth and featureless, as can be seen in SEM Figure 4-22 above. In test 11 the pump rate was decreased to 14 ml/hr, to put less material in the electric field, and all other parameters were held constant. This adjustment eliminated the overspray and produced a relatively smooth coating that exhibited some spherical features, as seen in SEM Figure 4-23. The development of particles or spherical features in the coating is due to increased surface tension of the sprayed material caused by an increase in surface area per unit mass [133], brought about by increasing the electric field strength, all other parameters held constant. The parameters in test 11 produced the first promising coating but more surface features would be considered an improvement with respect to cell proliferation (refer to section 4.4.2.2 above). Therefore, in test 12, concentration was reduced to 1.3% and time was reduced to 3 minutes, with all other parameters were held constant. Lowering material concentration decreases viscosity, which results in formation of particles and spheres on the surface [133], due to higher

surface tension increasing the surface area per unit mass of the projected particles (refer to section 2.3.4.1 above). A greater number of spheres, particles and other features formed on the surface results in a relatively rougher coating texture, as seen in the test 11 coating in SEM Figure 4-24. Continuing this strategy to develop yet more surfaces features, electric field strength was increased in test 13 by increasing voltage to 12 kV, with all other parameters held constant. The same effect could have been accomplished by reducing E-spray distance, according to Equation 4-1 above, however, the effect of distance may be much less significant in the scale of our experiments, as discussed in section 4.6.3 below.

As referenced earlier but repeated for convenience, increasing field voltage increases field current [128], which increases mass flow rate from the needle to the target, all other parameters held constant. [141] This higher mass flow rate increases the number of charged particles in the E-spray jet [128, 129], which increases both electrostatic and Coulombic forces. Higher Coulombic force induces a stretching force on droplets in the jet similar to increasing surface tension, resulting in greater repulsion between adjacent droplets. [157] This repulsive force causes formation of more particles and spherical shapes. Indeed, as seen in SEM Figure 4-25 substantially more surface features and spheres were present on the coatings created in test 13. This coating is considered the best candidate for cell adherence, proliferation and development (refer to section 4.4.2.2 above). Taking this approach one step further, electric field was again increased to determine if a reasonable upper limit had been reached for the general morphology patterns produced in tests 11 through 13. The coatings produced in test 14 were more

porous and inconsistent than test 13, as seen in SEM Figure 4-26. Therefore it was determined that **test 13 was the best coating for the purposes of this study.**

We showed earlier in DSPC testing that material viscosity exerts no measurable effect on our results, compared to other parameters such as electric field and sample area (see section 4.6.1. above). This is again evident here with DOPS. For example, test 6 above used a 0.6% concentration, while test 7 used a 0.8% concentration, and test 9 used a 2.5% concentration, yet all these tests produced electric fields of  $1E^3$ , other parameters (including conductivity) being equal.

However, when comparing E-spraying of DOPS with E-spraying of DSPC, viscosity likely plays a more important role, as does conductivity. The two metrics are different but closely inter-related. The concentration of DOPS required to create “ideal” coatings is much lower than that for DSPC, other factors being equal. Hence, ideal DOPS coatings can be created at lower viscosity in the same electric field. Indeed, DOPS test 1 and DSPC test 17 employ equal concentrations, in the same electric field, and both create coatings, but the DOPS coating is “very thin, barely visible”, while the DSPC coating is “think, with much overspray on board”. This is most likely an effect of the much higher conductivity of DOPS, compared with DSPC, than due to (much smaller) changes in viscosity. Higher conductivity creates a higher electric field. Therefore a higher current would be required to carry DOPS across the distance than DSPC, because resistance in the circuit is the factor which “carries” the material, and resistance is inversely proportional to current. At the same time, lower viscosity means DOPS E-spray jet separation (to an atomized mist) occurs at a higher electric field strength than with DSPC, due to its much higher conductivity. Indeed, “ideal” DOPS coatings (e.g. DOPS test 13)

were created at higher electric fields (and higher currents) than “ideal” DSPC coatings (e.g. DSPC test 10). Or, in other terms, DOPS E-sprays more efficiently than DSPC, at similar viscosities (concentrations). For example, DOPS test 13 created the “best” coating, but at the same electric field, DSPC tests 12 and 14 created no apparent coating at all. Similarly, DOPS tests 10-12 created good coatings, while, at the same electric field, DSPC tests 11 and 13 failed to produce coatings. Yet, the concentration (and therefore viscosity) of DOPS through these various tests varied only slightly and DSPC not at all.

Therefore, we can conclude that, given the same electric field strength, it takes much less DOPS to create a good coating than DSPC, other factors being equal. The combination of these effects can be thought of as a more “efficient” E-spray physical system for DOPS than for DSPC, enabling development of “ideal” coatings with much less material.

#### ***4.6.2.1 Ideal DOPS E-spray Parameters***

The “ideal” E-spray parameters for DOPS coatings are:

- DOPS concentration: 1.3% (vol%)
- Pump rate: 14 ml/hour
- Electric field strength: 1.5 kV/cm, developed by:
  - Spray distance: 8 cm
  - Voltage: 12 kV
- Spray time: 3 minutes per set of samples delivering 1.2 mg of DOPS per sample, in this case 3 samples producing a coverage of 3.2 mg/cm<sup>2</sup>.

Additional tests were subsequently completed using the parameters developed in test 13, except that the sample area was increased to produce samples for elution testing (refer to *Elution Study* chapter 6 below). Provided coverage is kept constant, additional samples could be E-sprayed using these parameters, and similar coatings would be produced. We E-sprayed up to 20 samples in this way and produced very similar coatings (verified by SEM). These subsequent test samples were loaded with gentamicin in an aqueous solution, to evaluate the effect of this additional compound on coating morphology. Gentamicin is the target antibiotic used in the *Elution Study*, and results of these test are discussed in chapter 6 below. SEM Figure 4-27 above shows the coating produced with gentamicin-loaded DOPS with an increased sample area (from 3 to 4 cm<sup>2</sup>). Interestingly, these changes led to a reduction in the density of surface features, and to appearance of a much smoother, almost glassy, surface upon which the features were attached. All other factors held constant, one would expect that increasing sample area would increase current (consistent with Equation 4-1 above, with  $F=V=IR$ ) and reduce coverage (in this case to 2.4 mg/cm<sup>2</sup>). However, as seen in the SEM image, the opposite effect was found. We hypothesize that as the aqueous solution (containing gentamicin) contacts the DOPS, a smoother surface develops due to an increase in conductivity of DOPS with increased hydration. [219] This would decrease the surface tension of the sprayed droplets, leading to fewer features on the surface, as discussed above. A continuation of this same effect is seen in SEM Figure 4-28 above. In this test, the sprayed area was increased further to 5 cm<sup>2</sup> and the resulting coating contains even fewer surface features.

DOPS E-sprayed coatings exhibit highly consistent surface roughness. The following Figure 4-29 and Figure 4-30 below show atomic force microscopy (AFM) images taken of one representative sample coating from each of tests 13 and 14. Figure 4-29 (test 13) was E-sprayed at 12 kV and 8 cm distance, while Figure 4-30 (test 14) was E-sprayed at 10 kV and 6 cm distance.

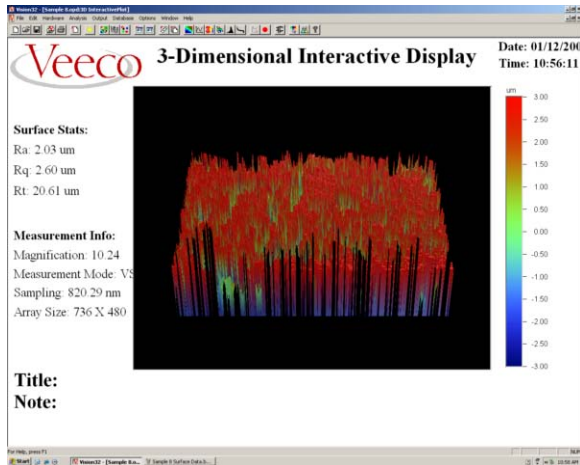


Figure 4-29: AFM image of DOPS coating from test 13, 10X magnification. E-sprayed at 12 kV, 8 cm distance. Color scale bar is  $\pm 3 \mu\text{m}$ .

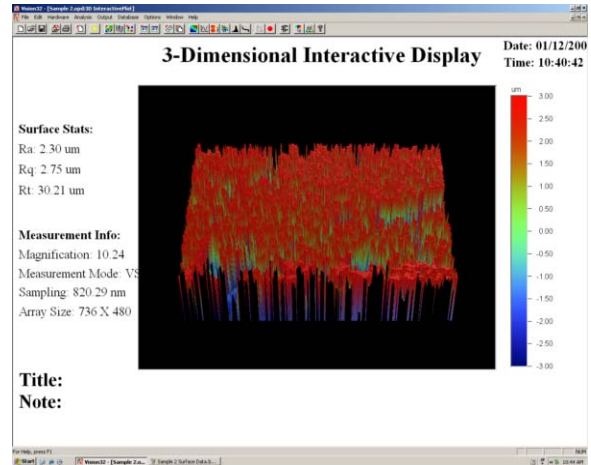


Figure 4-30: AFM image of DOPS coating from test 14, 10X magnification. E-sprayed at 10 kV, 6 cm distance. Color scale bar is  $\pm 3 \mu\text{m}$ .

Both coatings were approximately  $6 \mu\text{m}$  thick and relatively smooth and consistent across both sample surfaces. Test 14 produced a slightly rougher surface morphology than test 13, with an average surface roughness ( $R_a$ ) of 2.3 and a root-mean-square surface roughness ( $R_q$ ) of  $2.75 \mu\text{m}$ , compared to  $2.6 \mu\text{m}$  and  $2.03 \mu\text{m}$ , respectively.

E-spraying DOPS coatings was found to be an easily repeatable process. Figure 4-31 below was taken in July 2009, Figure 4-32 was taken in November 2009 and Figure 4-33 in February 2010. As can be seen, the coatings are quite consistent, despite different spray events and different researchers spraying the coatings.

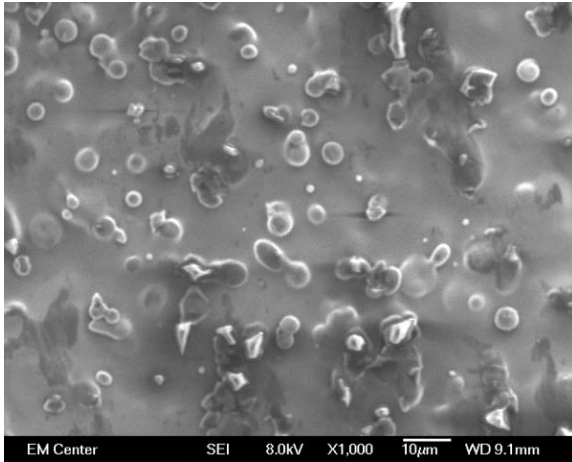


Figure 4-31: SEM image of DOPS coating on Ti at 8 kV, 1,000X magnification. Taken in July 2009.

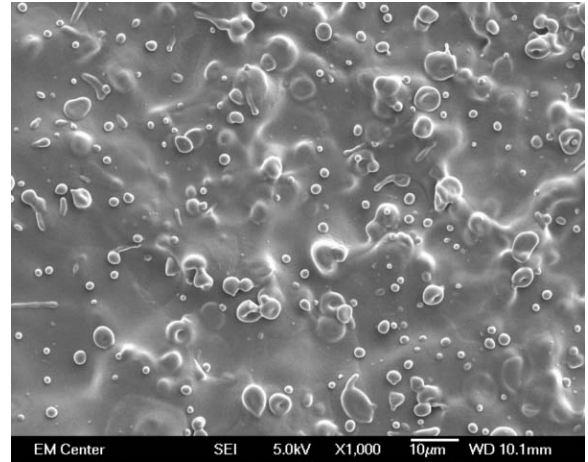


Figure 4-32: SEM image of DOPS coating on Ti at 5 kV, 1,000X magnification. Taken in November 2009.

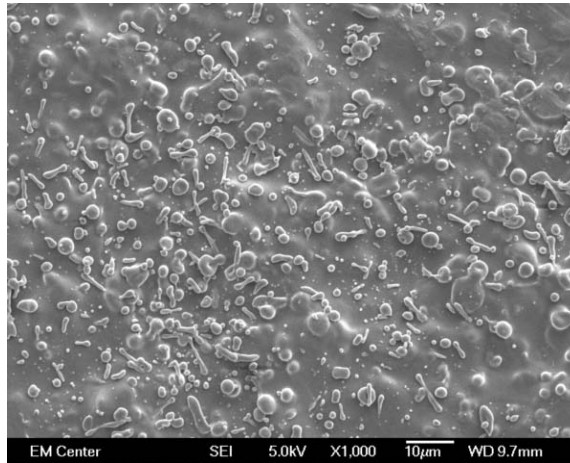


Figure 4-33: SEM image of DOPS coating on Ti at 5 kV, 1,000X magnification. Taken in February 2010.

#### 4.6.2.2 DOPS Coating Thickness

DOPS coatings were determined to be approximately 6 to 8  $\mu\text{m}$  thick, as measured using three methods. First, coating thickness was approximated by measuring the depth of a hole that appeared to penetrate completely through the coating to the titanium substrate. In a moment of scientific serendipity – an opportune scratch found in a typical sample - the thickness could easily be measured by tilting the SEM beam  $20^\circ$  (the maximum possible) relative to the coating. Using this technique, the coating was estimated to be approximately 7  $\mu\text{m}$  to 8  $\mu\text{m}$  thick. Figure 4-34 and Figure 4-35 show

two of a series of SEM images indicating the coatings were somewhat brittle, and delaminate from titanium substrate in small plates. Figure 4-35 shows a magnified portion of this crack that was used to estimate the thickness using the tilted SEM beam as described above.

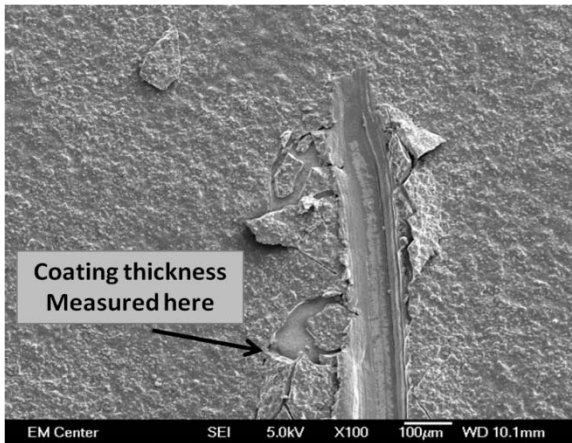


Figure 4-34: SEM image of scratch in DOPS coating on Ti at 5 keV, 100X original magnification. Note coating appears brittle and delaminates from titanium substrate in plates.

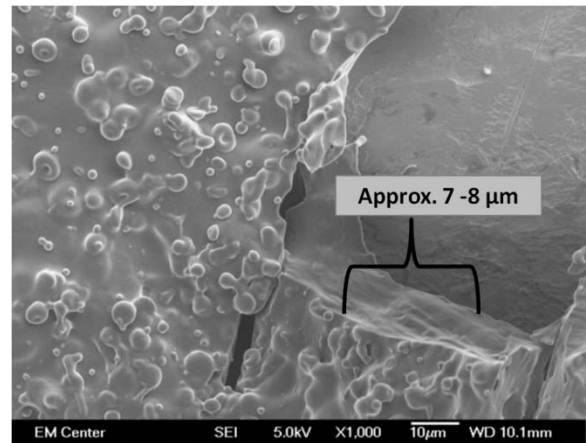


Figure 4-35: SEM image of thickness of DOPS coating on Ti at 5 keV, 1,000X original magnification. Thickness is approx. 7-8 µm along the side wall of the hole shown above.

In addition, AFM images presented in Figure 4-29 and Figure 4-30 above provide accurate confirmation of a 6 µm thickness (n=3, only two shown).

Santin [23] used the drip technique with DOPS and created coatings of approximately 100 µm. They and other researchers [11, 42], reported that coatings of this thickness often form 3-dimensional gels in simulated body fluid, and that these gels were not well adhered to the titanium substrate, resulting in instability under mechanical stresses. They recommend thinner coatings were required to ensure mechanical stability of an implant with these coatings.

#### 4.6.2.3 DOPS Coating Retention Test

DOPS coatings remained intact in PBS for 45 days, exhibiting only minor surface erosion. For each of the 3 samples tested, the majority of any visible erosion occurred

almost immediately, before photographs were taken on day 1. Small areas of the coating appeared to thin, but remained intact, and appeared to swell significantly as they turned whitish in color, within the first few hours of the test. The little degradation that occurred was considered surface erosion because the coating appeared to be slowly degrading from the outside of the coating toward the interior, thinning with time. The coating was not degrading in bulk form, which would be indicated by overall breakdown of the coating structure both inside and out. There was no indication of delamination; no larger-sized flakes were found in the wells. The following figures show minor dissolution of the coating over a period of 16 days.

Figure 4-36 and Figure 4-37 below show images of days 1 and 16 for one of the samples. On day 1, small amounts of erosion had already taken place, but this amount remained relatively constant throughout the remainder of the test. As can be seen in Figure 4-37, these coatings appear to be quite stable; even small features in the coating that were present on day one remained intact by day 16, and in fact 4 days later.

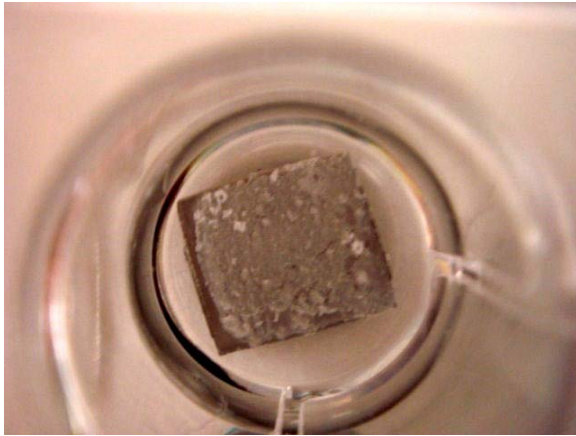


*Figure 4-36: Photograph of DOPS-coated titanium sample showing minor dissolution of coating at day 1.*

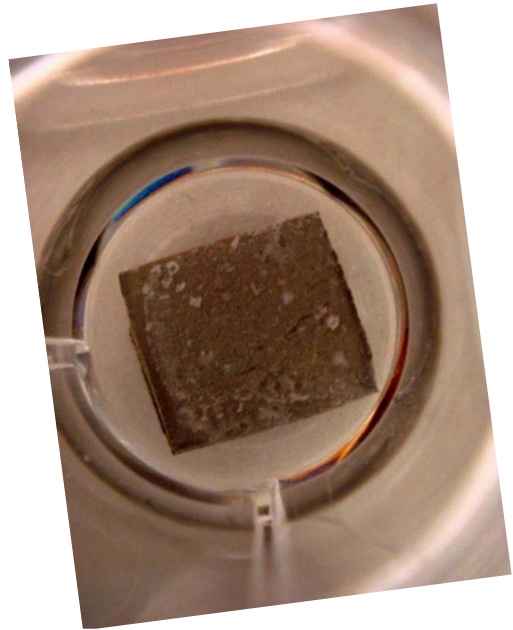


*Figure 4-37: Photograph of DOPS-coated titanium sample showing minor dissolution of coating at day 16. Image rotated to align with image to the left for easier comparison.*

The initial erosion that was observed can also be seen in the following SEM image, taken of a representative sample at the end of day 1. Microtopological change is clearly evident when compared to the same (representative) coating shown in Figure 4-25 above.

The majority of spherical features have eroded and the surface has assumed a very smooth texture, with few remaining features or pockets. This suggests there is a balance to be found between assuming many topological features is better than few. Particularly from a cellular response perspective, it may be advisable to opt for coatings that have some microtopology (as an advantage for cell adherence - refer to section 4.4.2.2 above) but not “too much”, as it washes off, potentially taking the cells with it.

#### **4.6.2.4 Drip Coating DOPS**

DOPS coatings that were produced by drip coating were very inconsistent, and uneven, as shown in the following SEM images.

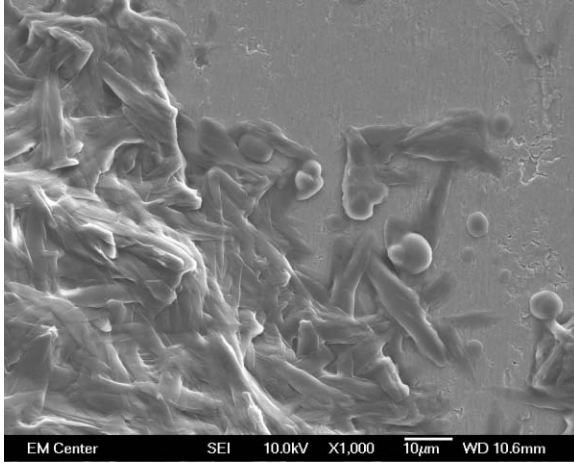


Figure 4-38: SEM image of DSPC drip coating on Ti. Image at 10 keV, 1,000X original magnification.

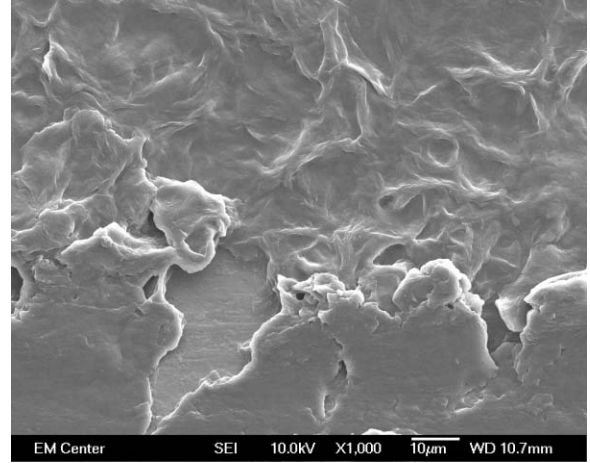


Figure 4-39: SEM image of DSPC drip coating on Ti. Image at 10 keV, 1,000X original magnification

Drip-coated surfaces resulted in greater weight gain than E-sprayed surfaces, as shown in the following table:

Table 4-5 DOPS Drip Coating Results

DOPS Drip Coating Results			
after (g)	before	$\Delta$ weight	$\Delta\%$
0.1844	0.1817	0.0027	1.5%
0.2334	0.2298	0.0036	1.5%
0.1972	0.195	0.0022	1.1%

Drip coated surfaces eroded and delaminated in the initial few hours of erosion testing in a PBS bath, as described in the previous section. This finding suggests that the E-spray process may lend stability to the coatings, perhaps by enhancing alignment of the DOPS polar heads which may improve contact with, and coverage of, the titanium oxide coating. Such increased alignment might also improve packing of DOPS molecules on the surface, thereby enhancing internal secondary and hydrogen bonding within and between the DOPS molecules and available water molecules.

#### 4.6.2.5 Shelf Life

We did not complete a formal study of shelf life, but samples were reserved from very early E-spray tests, and compared (under SEM) with samples from more recent tests.

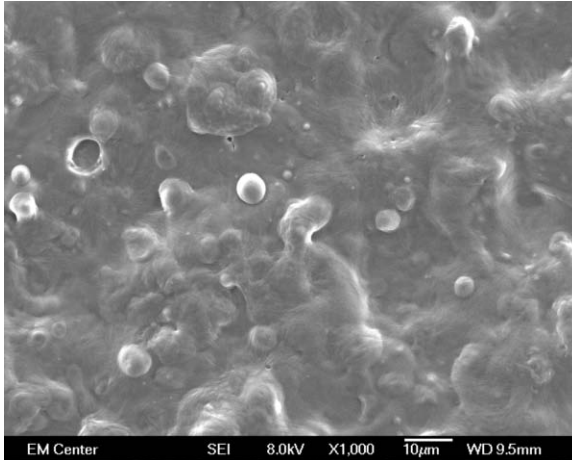


Figure 4-40: SEM image of DOPS drip coating. Image at 8 kV, 1,000X magnification. Taken in September 2009.

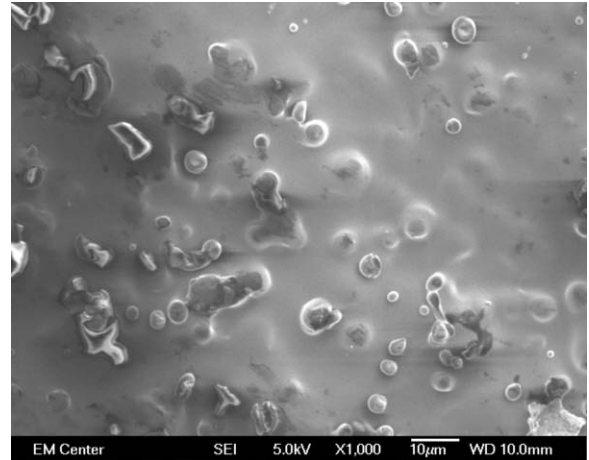


Figure 4-41: SEM image of DOPS drip coating. Image at 8 kV, 1,000X magnification. Taken in February 2010.

Figure 4-40 shows a sample coating from September 2009, and Figure 4-41 is an SEM image of the same coating in February 2010. These samples had been stored in a dessicator during this time. The samples appear quite similar over this 5 month period (only period considered thus far). If the samples were kept dry, the coatings appeared to be relatively stable.

#### 4.6.3 E-spraying 3D Objects

---

One of the most significant and potentially useful characteristics of E-spraying is the ability to consistently coat 3 dimensional objects such as surgical screws and other implant devices. We have shown that a three dimensional object can be coated on all sides in a single E-spray event, from a single spray direction. Figure 4-42 below shows one side of a titanium surgical screw (1.9 mm diameter, 6 mm length, ELI titanium alloy ASTM F136) that was E-sprayed using the ideal parameters discovered earlier (refer to

section 4.6.2.1 above). This image shows the side of the screw that was facing directly at the oncoming spray. Figure 4-43 below shows the “back” side of the same surgical screw – the side which was facing away from the oncoming spray. The two coatings are consistent, showing the E-spray “wrapped” around the screw, completely covering the object. In fact, all surfaces of the screw were examined and found to be similarly coated.

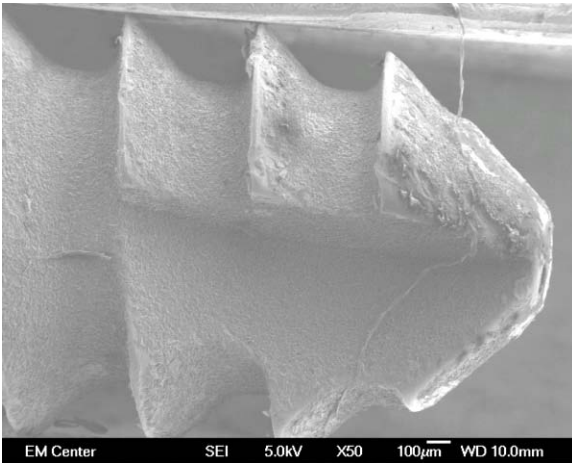


*Figure 4-42: SEM image of DOPS coating on front (facing E-spray) side of a Ti surgical screw. Image at 5 keV, 50X original magnification.*

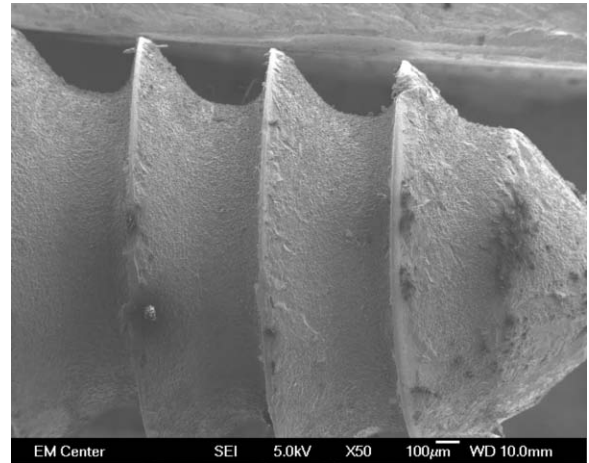


*Figure 4-43: SEM image of DOPS coating on rear (facing away from E-spray) side of a Ti surgical screw. Image at 5 keV, 50X original magnification.*

Figure 4-44 and Figure 4-45 show the same surgical screw at higher magnification, viewed from the front side (facing the E-spray) and away-facing side. Note the consistency of the coatings on both sides of the object.

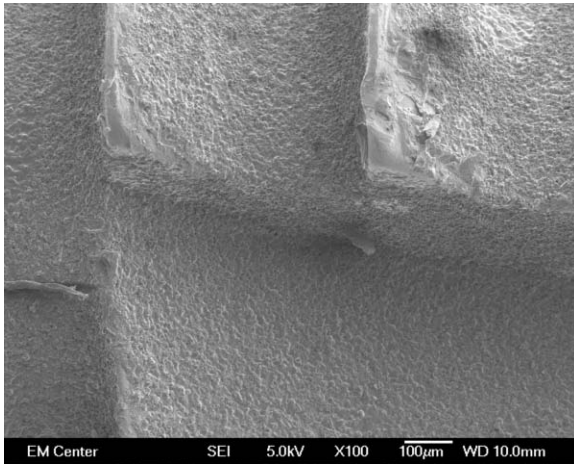


Figure 4-44: SEM image of DOPS coating on front (facing E-spray) side of a Ti surgical screw. Image at 5 keV, 100X original magnification.

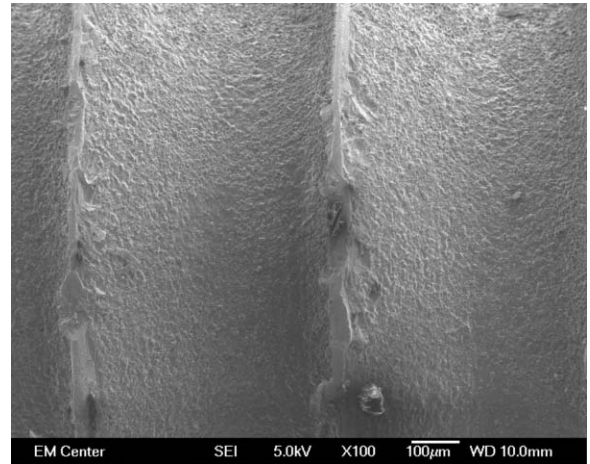


Figure 4-45: SEM image of DOPS coating on rear (facing away from E-spray) side of a Ti surgical screw. Image at 5 keV, 100X original magnification.

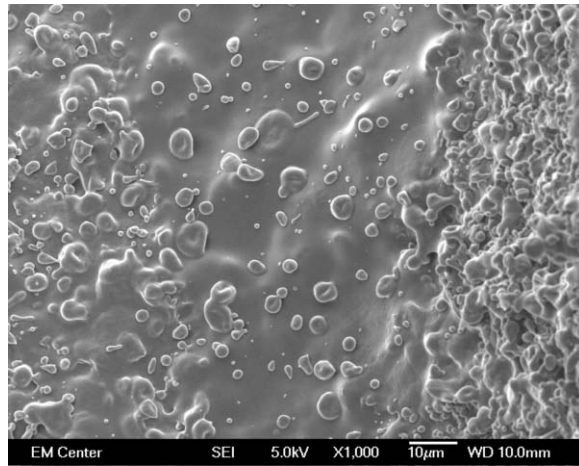


Figure 4-46 and Figure 4-47 show yet higher magnification, again from the front side facing the E-spray and away-facing side. Again, the coatings are quite consistent on both sides of the object, and the coatings are visually very similar to those E-sprayed on flat titanium samples.

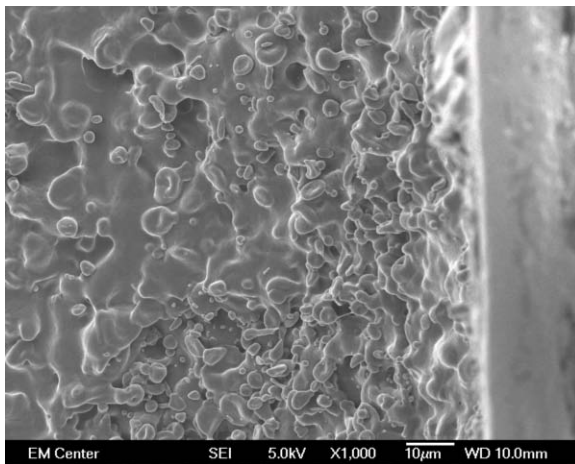


Figure 4-46: SEM image of DOPS coating on front (facing E-spray) side of a Ti surgical screw. Image at 5 keV, 100X original magnification.

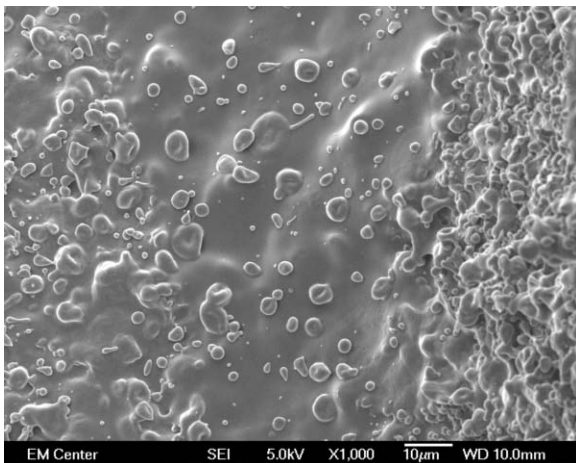


Figure 4-47: SEM image of DOPS coating on rear (facing away from E-spray) side of a Ti surgical screw. Image at 5 keV, 100X original magnification

In E-spraying, charged particles in the E-spray solution are carried in the electric field by a current (refer to *Background*, section 2.3.4 above), following electric field lines which extend to the target, intersecting perpendicular to the target surface [148], providing current is high enough to carry sufficient material to the surface. Because we observe similar coating on all sides of the object, we can hypothesize that the distance parameter in E-spraying may be less important than voltage, within the scale of our experiments. By Equation 4-1 (with  $F=V=IR$ ), current is indirectly proportional to distance. Because electric field (and therefore current) has been shown to exert an effect on our coating morphologies, we can therefore assume, since the morphologies on both sides of the screw were very similar, the current is very similar, despite the shorter electric field lines reaching the front of the screw, than those reach the back.

The consistency of the coating on all exposed conducting area of the object is also worth noting. As with DSPC earlier, we hypothesize that as the E-sprayed material lands on the sample surface, it acts as an insulator to a very small degree, reducing current at the point of impact, thus causing other molecules to seek areas of higher current elsewhere. As more of the sample surface becomes covered, the total phospholipid lipid

thickness increases and reduces the current at that location, causing additional molecules to seek other areas of highest current, and so on, until the coating is “too thick” and the molecules adopt a pattern controlled more by other factors, as yet unknown.

The opportunities for leveraging E-spraying of 3D objects may be quite large. The additional operative cost directly associated with the removal and replacement of infected surgical pins is estimated to be \$1330 per patient, based on 1993 to 1994 data, and these costs have no doubt multiplied to the present. [220] In addition, there is a major therapeutic need for enhancing bony ingrowth on 3D implants, which could be accelerated and strengthened with DOPS coatings.

## ***4.7 Conclusions***

There is a large need for thin, adherent, osseointegrative coatings on orthopedic implants. E-spraying is a suitable method for creating such coatings on titanium. Compared to drip and dip techniques often used in the literature for preparing DOPS coatings, E-sprayed DOPS coatings appear to be more consistent and resistant to degradation. E-spraying consistently produces thinner coatings than common dip or drip coating techniques, which could lead to enhanced mechanical stability of an implant bearing E-sprayed coatings. [23]

Manipulation of the key E-spray process parameters, target surface area, concentration (viscosity), electric field strength (and therefore current) and spray time provide effective, predictable control of coating characteristics such as morphology, porosity and consistency, all of which are important for successful cell growth and adhesion, and therefore to long-term success of orthopedic coatings and the implants upon which the coatings reside. Ideal parameters for E-spraying DOPS coatings are

shown in section 4.6.2.1 above. Coating thickness was measured by atomic force microscope to be approximately 6  $\mu\text{m}$ , as shown in Figure 4-29 and Figure 4-30 above.

SEM reveals similarity in visual appearance (morphology, porosity, consistency) of samples and confirms the repeatability of the E-spray process. Throughout the study, samples were selected (*ad-hoc*) for visual evaluation on SEM. This revealed that coatings were very consistent within groups of samples E-sprayed using the same parameters, and that very consistent coatings can be created repeatedly, using the same E-spray parameters. In fact, the E-spraying production process proved to be highly reproducible over many hundreds of samples created through all aspects of the research described in this dissertation, also verified through SEM imaging. This is a critical success factor for commercial success of an orthopedic technology.

E-spraying was easy to perform and required only a few thousand dollars in equipment investment. Once standardized methodology was developed and experience was gained, coatings could be produced with high consistency and minimal error.

## **4.8 Limitations**

Many materials have been E-sprayed onto many substrates. [128, 134] The only limitation is that the material must be conductive, although otherwise weak conductors have been made temporarily conductive for the purposes of E-spraying coatings. [128]

We measured coating thickness for a few representative samples only. Measuring coating thickness throughout our various tests would have provided additional useful information about the coating characteristics. We did, however, visually evaluate samples from many tests, and determined that coating thickness was, in general, consistent across tests that produced “good” quality coatings. In some coatings, holes

through the coating enabled the titanium substrate to be identified. This enabled visual verification that coating thickness was approximately the same through tests that produced good quality coatings.

We did not measure important characteristics of our E-spray solutions, such as surface tension, viscosity, density, viscosity or conductivity. Although the conductivities and densities of chloroform, DOPS and DSPC independently are available in the literature, measurements of our mixtures would have enabled more detailed calculation of important characteristics of the E-spray tests, such as the current, which would have enabled finer detail in comparison of test results.

We were unable to measure current directly using the available apparatus. Our high-voltage power source displayed current on an analog microampere scale. The highest currents produced in our studies were no more than 1 microampere, not measurable on our meter. Being able to measure current would have enabled us to verify our results empirically.

#### **4.9 *Future Work***

It would be very useful to complete a detailed characterization of our DOPS coatings, on passivated, calcium pretreated samples with and without cholesterol. Discovering characteristics such as stability and durability, thickness, and material properties such as stiffness and viscoelasticity would help to more fully understand our findings.

Shelf life is an important factor for commercialization of any biomedical product. It would therefore be useful to complete a more rigorous study of shelf-life of our DOPS coatings.

It would be useful to E-spray different materials, for example, other phospholipids or combinations of phospholipids. It would also be interesting to spray onto different materials, for example, titanium alloy(s), stainless, cobalt-chrome and various porous forms of all these, and different shapes, for example, 3D lattice structures. These are all popular materials for production of orthopedic implants.

It would also be insightful to attempt E-spraying of other phospholipid conformations, such as liposomes, micelles, and reverse micelles. These structures may provide a broader range of options for controlled drug delivery.

## **5 Enhancing Coating Retention**

### **5.1 Purpose**

The preliminary study was prematurely ended due to excessive coating delamination. The Enhancing Coating Retention study was completed in an attempt to improve the retention of E-sprayed DOPS coatings on titanium.

### **5.2 Experimental Approach**

Adsorption of calcium to the surface of titanium oxide probably changes its surface from an anionic to a cationic state. [76, 221] This subsequently increases adsorption of acidic macromolecules, such as acidic proteins and phospholipids (e.g. DOPS), to bind through Ca-bridging. Therefore it was decided to leverage these characteristics and attempt two approaches to binding calcium onto our titanium surfaces, and then to test the results.

Numerous studies have used calcium-chloride with good success as a means to link various proteins, macromolecules and other compounds to titanium oxide. [76, 119], [79] Calcium plays numerous important roles in the induction of new bone. Thus calcium-chloride was one approach chosen in our study to create opportunities for calcium bridging on the titanium surface. These and other similar studies used calcium-chloride concentration ranging from 1 mM to 2.6 mM. We selected a calcium concentration of 2.25 mM.

Phosphate in many forms plays many roles in phospholipid biochemistry and cell biology. As discussed in *Background*, section 2.1.2 above, the most stable calcium-phosphatidylserine interaction is one in which the  $\text{COO}^-$  or  $\text{PO}_4^-$  of every second phosphatidylserine molecule interacts with  $\text{NH}_3^+$  in neighboring PS-Ca-PS groups. [47]

Furthermore, the addition of inorganic phosphate prior to or in combination with calcium appears to be an absolute requirement for calcium-phospholipid-phosphate complex formation. [47] Therefore, calcium-phosphate was also chosen as an alternative approach in our study to create opportunities for calcium bridging on the titanium surface.

Calcium-phosphate is stable in many forms. For our study,  $\beta$ -tri-calcium phosphate was chosen because it is stable in water, has moderate solubility and has been reported to strengthen ceramics in low concentrations. [222]

This study was designed to test the effects on coating retention of calcium phosphate (specifically,  $\beta$ -tri-calcium phosphate), calcium chloride (anhydrous), and no calcium, with and without cholesterol in the E-spray coating, and with and without gentamicin loading. Samples were put through a complete simulated MSC cell study, as described in the *Cell Study* chapter, including culture media, differentiation media, and all media changes, but without any cells. At 1 and 2 week time points, samples were rinsed and prepared for their respective testing. Samples were observed and photographed at all media changes. Signs of deterioration or degradation of any type were recorded. At each time point, samples were dried and examined with a stereo microscope and graded according to a subjective grading scale (described in section 5.4.6 below). Random samples were also examined through SEM to verify their score given in the subjective grading.

### ***5.3 Experimental Design***

Sample treatments and sample numbers in each treatment group were assigned in a 3x2x2 blocked experimental design, as detailed in the following table.

Table 5-1: Treatments and Sample Counts

<b>Summary Table –Experimental Design</b>					
Treatment	<b>Chol</b>		<b>No Chol</b>		<i>Totals</i>
	Week 1 end point	Week 2 end point	Week 1 end point	Week 2 end point	
<b>CaCl2</b>					
GS	10	10	10	10	40
No GS	10	10	10	10	40
<b>CaPO4</b>					
GS	10	10	10	10	40
No GS	10	10	10	10	40
<b>No Calcium</b>					
GS	10	10	10	10	40
No GS	10	10	10	10	40
<i>Totals</i>	<i>60</i>	<i>60</i>	<i>60</i>	<i>60</i>	<i>240</i>

Ten samples were created for each treatment group for a one week end-point, and ten more for a two week end-point (as shown above). All of the samples from each treatment group were used for subjective photographic and stereomicroscopic evaluation (which is non-destructive) at their respective time points. Three of the ten samples from each treatment group were dried and reserved for examination by SEM. The remaining seven samples were dried and stored in a dessicator for future testing.

## **5.4 Experimental Methods**

### **5.4.1 Sample Fabrication & Preparation**

All samples were 25 mm<sup>2</sup> (i.e. nominally 5 mm square) titanium, fabricated, cleaned and passivated as described in the *E-Spray Study* chapter, section 4.2.2 above, according to the *Ti Cleaning and Preparation Protocol*, provided in Exhibit A. Samples were then bathed in prescribed calcium treatments, as described in section 5.4.2 below. Control samples were examined with SEM before and after addition of calcium. Cholesterol

(Alfa-Aesar, CAS 57-88-5) was added to the DOPS (Avanti Polar Lipids, Alabaster, AL) solution as described in section 5.4.3 below, and samples were then E-sprayed (as described in the *E-Spray Study* chapter) with and without cholesterol in the DOPS E-spray solution, and loaded with gentamicin or not, as prescribed in the experimental design outlined in Table 5-1 above. Addition of gentamicin to the samples is described in the *Elution Study* chapter, section 6.3.1 below. Control samples were examined with SEM after E-spraying, prior to start of the simulated cell study.

#### ***5.4.2 Applying Calcium to Titanium Samples***

---

Calcium was incorporated onto the titanium surfaces according to each respective treatment (as specified in Table 5-1 above). Samples were bathed in anhydrous calcium-chloride,  $\beta$ -tri-calcium phosphate, or no calcium, according to the *Calcification of Ti Surfaces Protocol*, provided in Exhibit B. Briefly, calcium from two sources, calcium chloride or  $\beta$ -tri-calcium phosphate, was applied in equal amounts to Ti samples at a 2.25 mM concentration. Calcium chloride or  $\beta$ -tri-calcium phosphate was mixed with de-ionized water and samples were bathed for 24 hours at 37°C in the resulting mixture, stirred constantly at 150 RPM and occasionally manually agitated to minimize inconsistent coatings due to potential stacking of the samples in the beakers.

#### ***5.4.3 Adding Cholesterol to DOPS***

---

For samples requiring cholesterol in the E-spray solution, 1.29 mg/ml of cholesterol (Alfa-Aesar, CAS 57-88-5) was added to the DOPS E-spray solution (in chloroform) to achieve a ratio of 6:1, moles of DOPS to moles of cholesterol. This resulting solution was then E-sprayed onto titanium samples using the technique described in the *E-Spray Study* chapter.

#### ***5.4.4 Simulated Cell Study***

---

After all samples were prepared and vacuum dried for a minimum of 8 hours, they were transferred to 48-well cell culture plates and 0.5 ml of warm cell culture media was introduced into each well. Half the media was changed on day 1 and a full media change occurred on day 4. On day 7, all media was replaced with MSC differentiation media. At the 2-week (post-seeding) time point, all samples designated for testing were removed from the incubator, rinsed twice in de-ionized water, vacuum dried for a minimum of 24 hours, and stored in a dessicator until tested. All methods and protocols of the simulated cell study were performed as described in the *Cell Study* chapter.

#### ***5.4.5 Qualitative Photographic Evaluation***

---

##### ***5.4.5.1 Group 1 – One Week End Point***

On day 4 and again at the week 1 time point, all ten samples of the week 1 end-point treatment group were photographed for qualitative evaluation of coating retention. Photographs were digitally zoomed and enlarged to enable qualitative evaluation of coating quality, thus qualitatively judging coating retention.

##### ***5.4.5.2 Group 2 – Two Week End Point***

On days 4, 7, 9, 11 and at the week 2 time point, all ten samples of the week 2 end-point treatment group were similarly photographed for qualitative evaluation of coating retention.

#### ***5.4.6 Qualitative Evaluation by Stereo Microscope***

---

Coating retention was also qualitatively evaluated on samples prescribed in section 5.3 above, by examination on a stereo microscope (Fisher Scientific Stereomaster) at 40x magnification.

#### **5.4.6.1 Qualitative Scoring System**

A grading scale was applied, wherein a score of 0 was assigned to coatings which appeared to be completely absent, and 5 was assigned to coatings which appeared to be completely intact. Completeness of coatings was thus judged, based on coverage of the titanium sample surface. Coating thickness was not measured in this *Enhancing Coating Retention* study, as it was very difficult to visualize and not feasible to measure given time and cost constraints. Purely visual examination was applied to all samples to judge the quality of the coatings that had been retained following simulated cell study procedures. Thus the relative effectiveness of each treatment with respect to coating retention was judged and compared.

#### **5.4.7 SEM Method**

---

SEM was performed on a JEOL JSM 6500F. Samples were gold coated (~10 nm Au) and stored in a dessicator until examined under SEM (~5-15 kV).

#### **5.4.8 Statistical Analysis**

---

Statistical analysis was performed using SigmaStat version 11.2, the latest version from Systat Software Inc. Significance testing was performed at  $p < 0.05$  unless otherwise indicated. All the results were analyzed using Student's T Tests to two-treatment comparisons and one-way analysis of variance (ANOVA) for multi-treatment comparisons. The Shapiro-Wilk normality test was performed on all treatments, and the Mann-Whitney Rank Sum test was used for multiple comparisons with unequal variance. Dunn's test for rank-ordered significance was applied in comparisons with unequal samples numbers, for example, if a sample was lost to experimental error.

## 5.5 Results

### 5.5.1 Control and Baseline Samples

#### 5.5.1.1 Pre-E-Spray Controls

The following representative SEM images were taken of calcium chloride, calcium phosphate and no calcium control samples (no E-sprayed coatings). These samples were cleaned and passivated and then pretreated with their respective form of calcium, or no calcium (as described in sections 5.4.1 and 5.4.2 above), but not E-sprayed.

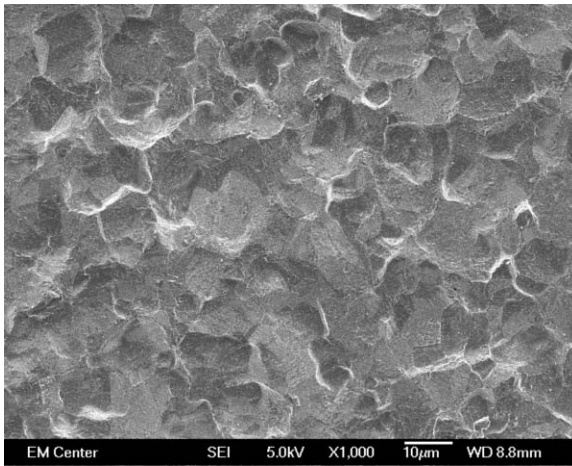


*Figure 5-1: SEM image of passivated titanium with calcium chloride pretreatment, no E-spray, imaged at 5 kV, 1000X.*

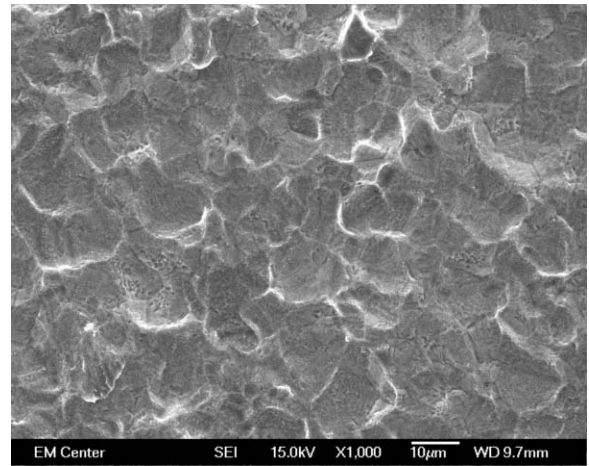


*Figure 5-2: SEM image of passivated titanium with calcium phosphate pretreatment, no E-spray, imaged at 15 kV, 1000X.*

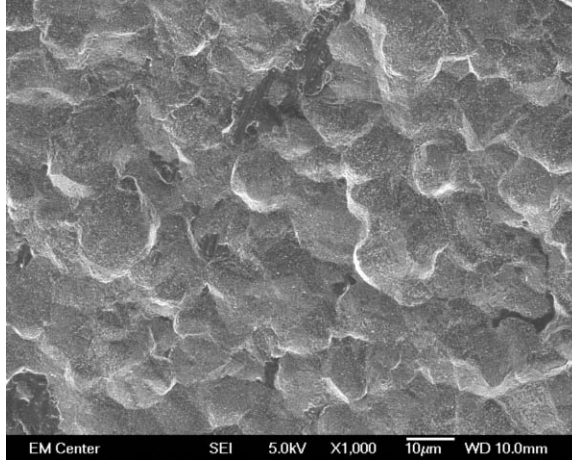


*Figure 5-3: SEM image of passivated titanium with no calcium pretreatment, no E-spray, imaged at 5 kV, 1000X.*

Nothing is notable in these images showing the texture of the passivated titanium surface with various pretreatments. Coatings were not visibly different between samples treated with calcium chloride and calcium phosphate, nor were either calcium chloride or calcium phosphate pretreated samples different from plain passivated (no pretreatment) samples. Passivated samples are, however, visibly different from plain, non-passivated titanium samples, as shown in the following image:

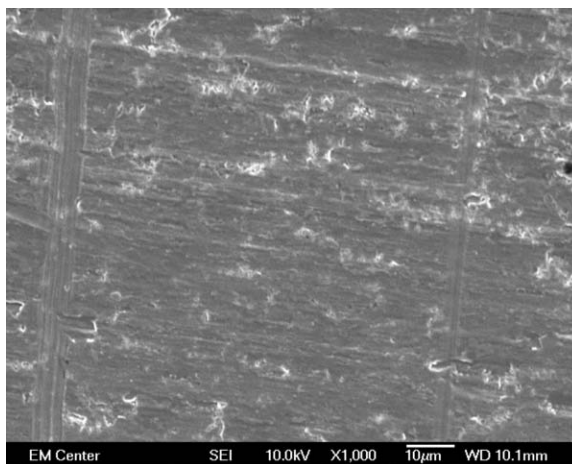


*Figure 5-4: SEM image of un-passivated titanium with no pretreatment, no E-spray, imaged at 10 kV, 1000X.*

XPS characterization confirmed presence of calcium on both calcium pretreated surfaces, and lack of calcium on the samples that were not pretreated with calcium, as shown in the following figures.

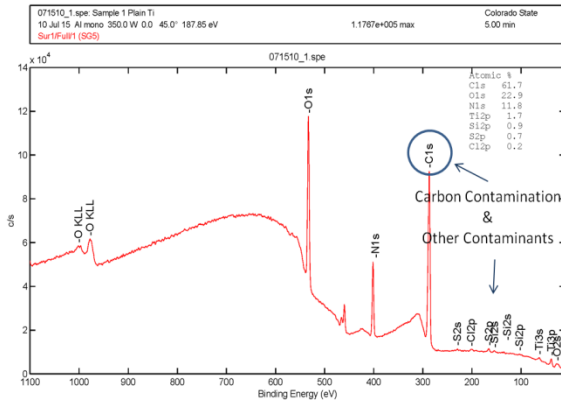


Figure 5-5: XPS spectra of **unpassivated titanium with no pretreatment, no E-spray**. Note numerous contaminants (discussed in 5.6.2 below), but no calcium.

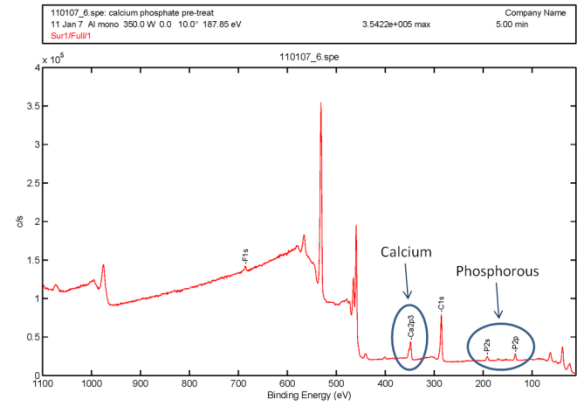


Figure 5-6: XPS spectra of **passivated titanium with calcium phosphate pretreatment, no E-spray**. Spectra confirms presence of calcium and phosphate.

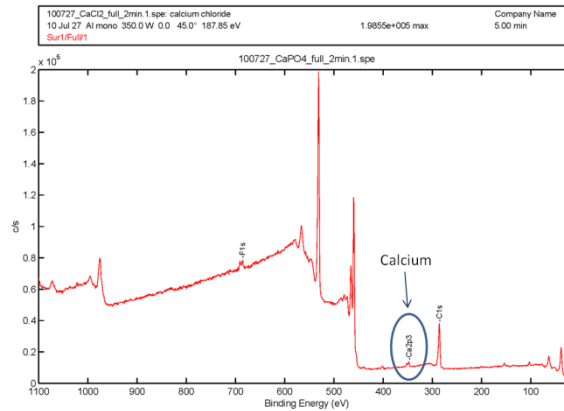


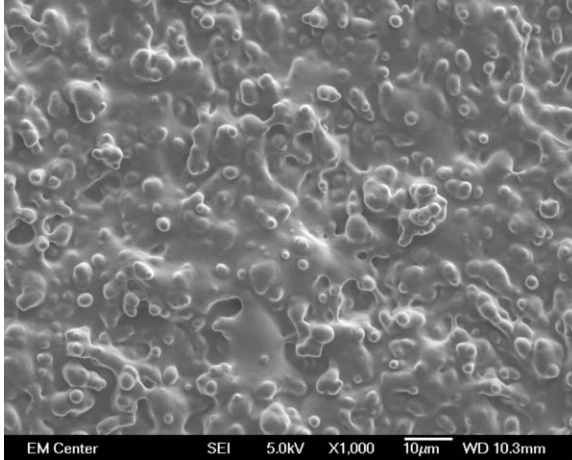
Figure 5-7: XPS spectra of **passivated titanium with calcium chloride pretreatment, no E-spray**. Spectra confirms presence of calcium and no phosphorous or chloride.

Figure 5-7 shows the XPS spectra of passivated titanium with calcium chloride pretreatment, no E-spray, and confirms the presence of calcium, and no residual phosphorous or chloride.

### 5.5.1.2 Before Cell Study Simulation, E-Sprayed DOPS without Cholesterol

#### 5.5.1.2.1 No GS

The following representative SEM images show the effect of calcium pretreatment on **DOPS with no cholesterol and no GS** coatings prior to introduction to cell media.



*Figure 5-8: SEM image of passivated titanium with calcium chloride, DOPS without cholesterol, no GS E-spray, imaged at 5 kV.*

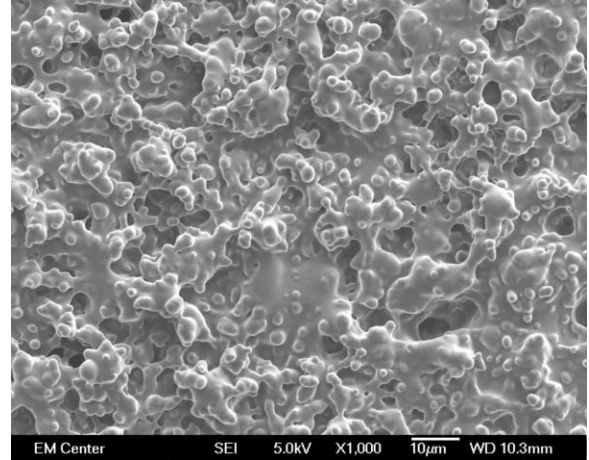


*Figure 5-9: SEM image of passivated titanium with calcium phosphate, DOPS without cholesterol, no GS E-spray, imaged at 5 kV.*

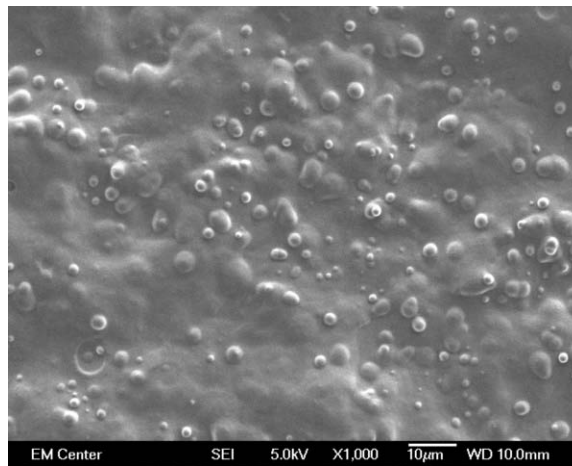


*Figure 5-10: SEM image of passivated titanium with no calcium pretreatment, DOPS without cholesterol, no GS E-spray, imaged at 5 kV.*

Pretreatment with calcium phosphate appears to create a rougher surface topology than pretreatment with calcium chloride, with many more rounded features and pockets. This observation is discussed further in section 5.6.2 below.

However, in E-spray testing (refer to *E-Spray Study* chapter, section 4.6.2.3 above), it was demonstrated that samples exhibiting similar rough topology tended to lose these small surface features very early in coating retention tests. Figure 5-11 below shows a representative coating similar to Figure 5-9 above (calcium phosphate pretreatment, without cholesterol or GS) after a 2 day bath in PBS. Therefore, this rough surface texture is not necessarily viewed as preferable in this instance, as compared to the calcium chloride coating shown in Figure 5-8 above, which is more consistent and has fewer microtopological features.

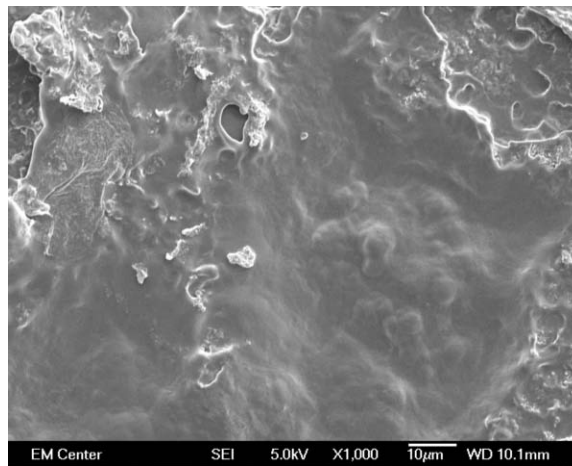


*Figure 5-11: SEM image of DOPS E-spray coating, with calcium phosphate, without cholesterol or GS, after a 2 day wash in PBS, imaged at 5 kV.*

Particularly from a cellular response perspective, it may be advisable to opt for coatings that have some microtopology (as an advantage for cell adherence) but not “too much” as it washed off, potentially taking the cells with it.

#### 5.5.1.2.2 With GS

The following representative SEM images show the effect of calcium pretreatment on **DOPS without cholesterol, with GS** coatings prior to introduction to cell media.

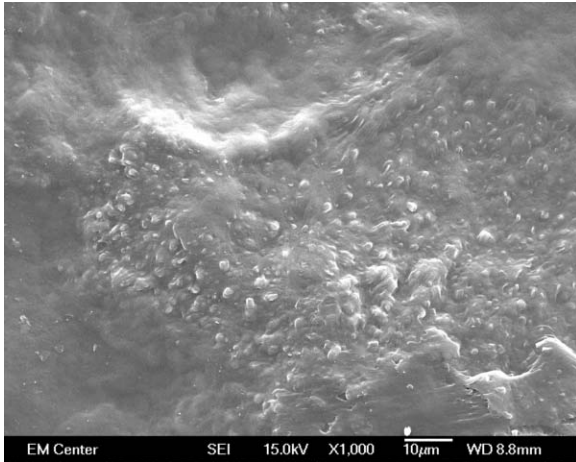


*Figure 5-12: SEM image of passivated titanium with calcium chloride, DOPS without cholesterol with GS E-spray, imaged at 5 kV.*

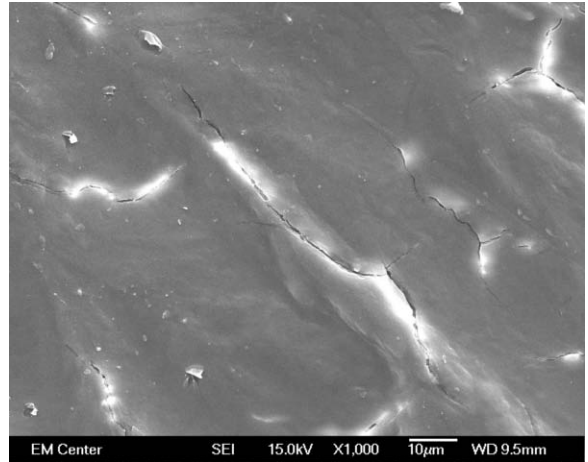


*Figure 5-13: SEM image of passivated titanium with calcium phosphate, DOPS without cholesterol with GS E-spray, imaged at 5 kV.*

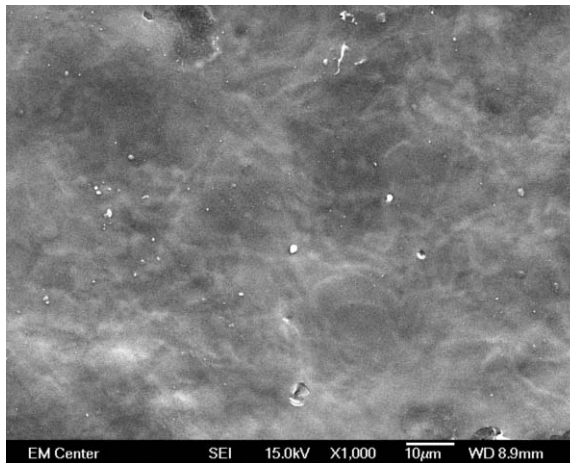


*Figure 5-14: SEM image of passivated titanium with no calcium pretreatment, DOPS without cholesterol, with GS E-spray, imaged at 5 kV.*

These SEM images appear to show that all coatings with GS exhibit a smoother morphology than the same coatings without GS. This is discussed in section 5.6.4 below.

### **5.5.1.3 Before Cell Study Simulation, E-Sprayed DOPS with Cholesterol**

#### **5.5.1.3.1 No GS**

The following representative SEM images show the effect of calcium pretreatment on **DOPS with cholesterol and no GS** coatings prior to introduction to cell media.

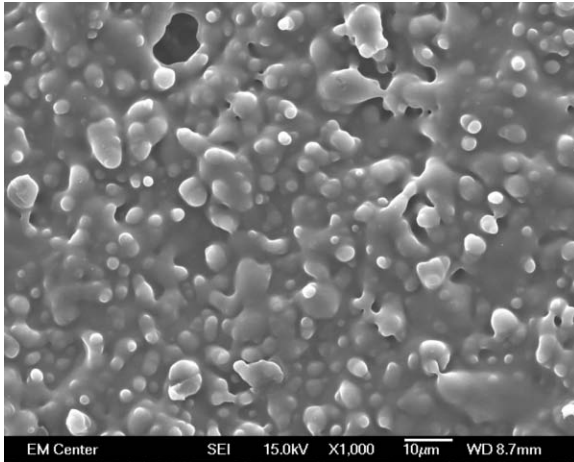


*Figure 5-15: SEM image of passivated titanium with calcium chloride, DOPS with cholesterol, no GS E-spray, imaged at 15 kV.*

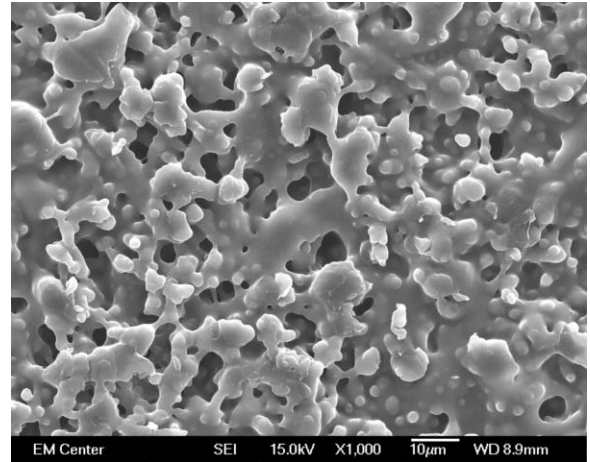


*Figure 5-16: SEM image of passivated titanium with calcium phosphate, DOPS with cholesterol, no GS E-spray, imaged at 15 kV.*

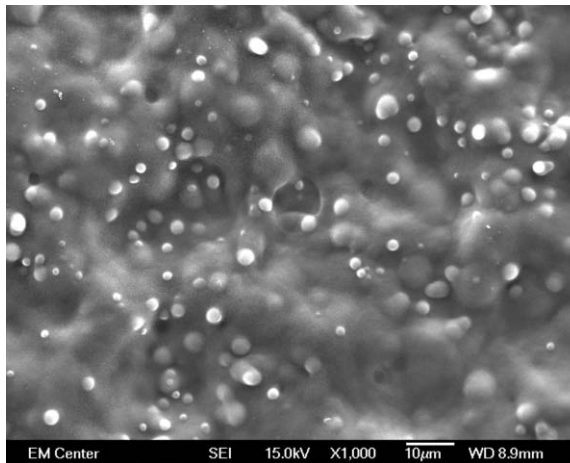


*Figure 5-17: SEM image of passivated titanium with no calcium pretreatment, DOPS with cholesterol, no GS E-spray, imaged at 15 kV.*

Coatings containing DOPS and cholesterol were very different than DOPS without cholesterol. The formation of abundant spherical features is obvious. This observation is discussed further in section 5.6.3 below.

Comparisons between treatments with cholesterol were similar to those without cholesterol. For example, with or without cholesterol, samples pretreated with either form of calcium exhibit a rougher, more featured topology than non-pretreated samples. Also, with or without cholesterol, pretreatment with calcium phosphate appears to create

a rougher surface topology than pretreatment with calcium chloride, with many more rounded features and pockets.

#### 5.5.1.3.2 With GS

The following representative SEM images show the effect of calcium pretreatment on **DOPS with cholesterol and GS** coatings prior to introduction to cell media.

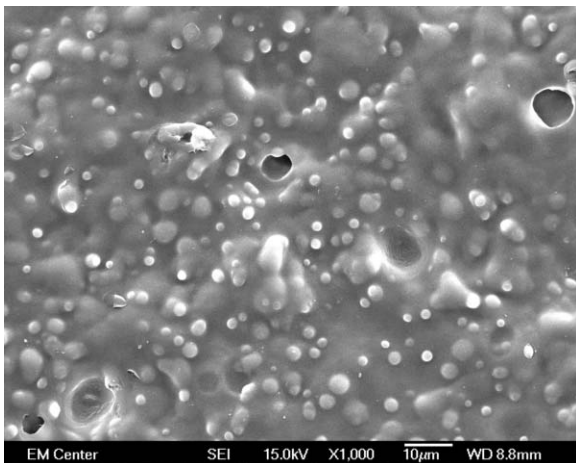


*Figure 5-18: SEM image of passivated titanium with calcium chloride, DOPS with cholesterol and GS E-spray, imaged at 15 kV.*

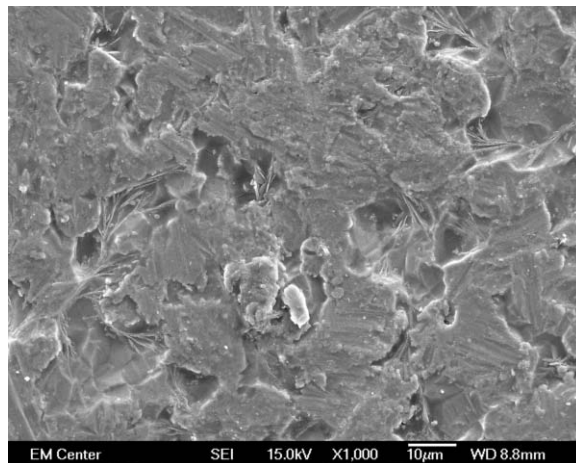


*Figure 5-19: SEM image of passivated titanium with calcium phosphate, DOPS with cholesterol and GS E-spray, imaged at 15 kV.*

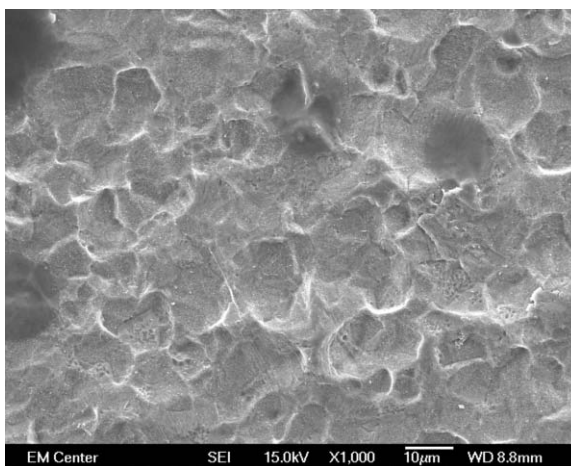


*Figure 5-20: SEM image of passivated titanium with no calcium pretreatment, DOPS with cholesterol and GS E-spray, imaged at 15 kV.*

This series of SEM images is substantially different than the images of samples without cholesterol. Again, coatings containing DOPS and cholesterol were very different than DOPS without cholesterol. Calcium chloride coatings appear more

condensed and, from prior experience, potentially more erosion-resistant. Calcium phosphate images appear more crystallized in texture compared to other treatments. It is unclear what this may mean, and other evidence points to calcium chloride being the preferred coating, so no additional effort is spent on analyzing calcium phosphate coatings.

Samples without cholesterol were similar to past images of DOPS coatings. Because the purpose of this study was to improve the retention of coatings compared with earlier coatings, it was decided that the simulated cell study would be completed with and without cholesterol, in the event it becomes desirable to look back on these samples. And continued work in this study would focus exclusively on coatings containing cholesterol.

### ***5.5.2 Simulated Cell Study***

---

Samples were bathed in cell culture media for two weeks, with half the samples removed at week 1 for assessment of coating retention.

#### ***5.5.2.1 Qualitative Photographic Evaluation***

The following representative photographs show DOPS with cholesterol, calcium chloride pretreated samples with GS (top 3 rows) and without (bottom 3 rows) at the week 1 end-point.

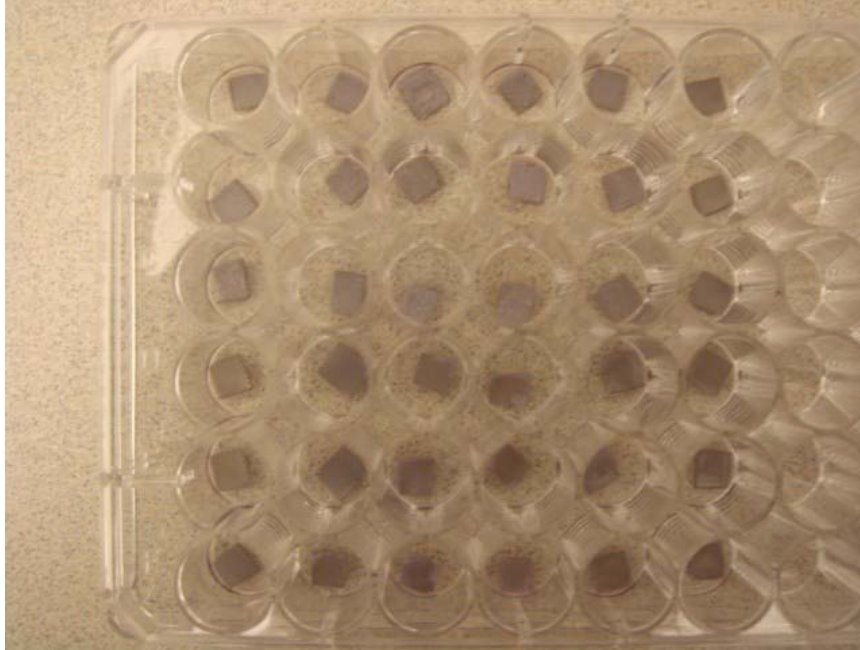


*Figure 5-21: Photograph showing DOPS/cholesterol week 1 end-point. Note near complete retention of coatings in upper 3 rows (containing GS).*

Generally (although highly qualitative), samples with more coating (upper three rows above) appear much lighter in color than samples with less coating (lower three rows). Even with the picture substantially enlarged (digitally on a large, high-resolution display), it is difficult to see that the upper three rows of these samples, which contain GS, were nearly completely intact, while the lower three rows, not containing GS, were less intact (but coatings are still visible upon digital enlargement).

Even though samples without GS were less completely intact, they were substantially more intact than samples with no calcium pretreatment or cholesterol in the E-spray solution (photo not shown).

Similarly, the following representative photograph shows DOPS with cholesterol, calcium chloride pretreated samples with GS (top 3 rows) and without (bottom row) at the week 2 end-point.



*Figure 5-22: Photograph showing DOPS/cholesterol week 2 end-point. Note near complete retention of coatings of coatings in upper 3 rows (containing GS).*

Again, the upper three rows of samples, which contain GS, were nearly completely intact, while the lower row (image was zoomed in as an attempt to better show the intact coatings), not containing GS, is less completely intact.

As in the week 1 end-point photograph, even though coatings without GS were less completely intact, they were substantially more intact than coatings with no calcium pretreatment or cholesterol in the E-spray solution.

Even when enlarged and digitally zoomed, it is essentially impossible to qualitatively judge retention success or failure from these photographs. **Therefore it was determined that this method was not useful in determining surface condition** and a stereomicroscope was used for further qualitative evaluation of coating retention, as described in the following section.

### 5.5.2.2 Qualitative Evaluation by Stereo Microscope

Samples were viewed on a stereomicroscope at the maximum available magnification of 40x and graded on a scale of 0 (no coating retention) to 5 (complete retention). It was sometimes difficult to judge with reasonable certainty if samples had thin or no coatings, especially in flat lighting. Attempts to use colored lighting did not improve the situation. It helped somewhat to use a small spotlight at a high angle of incidence to achieve some amount of reflection on the surface. Samples with coatings were duller in appearance than those with little or no coatings. Scores were then qualified by SEM of selected samples that would represent a full range of coating retention levels. Example SEM images are shown in the following.

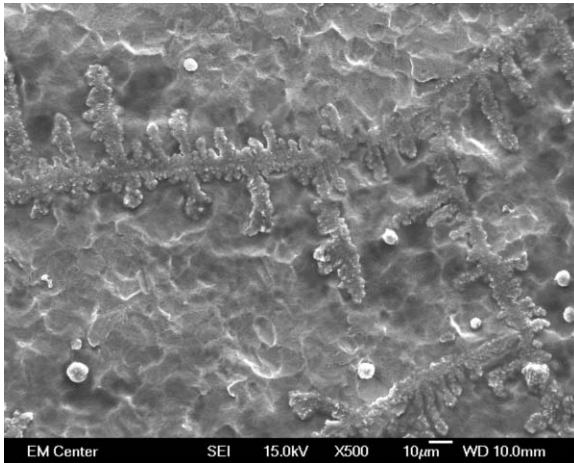


Figure 5-23: SEM image of non-pretreated titanium with DOPS with cholesterol without GS, imaged at 15 kV.

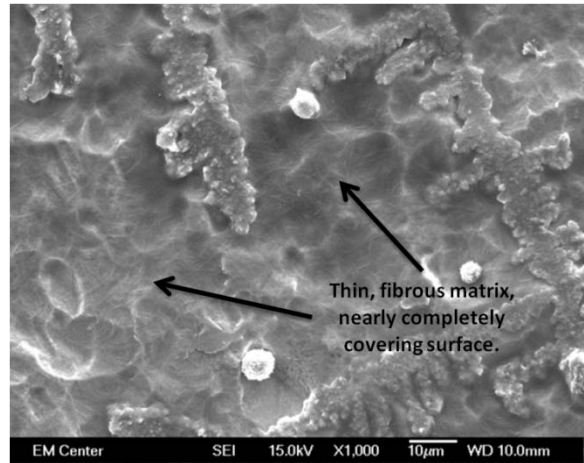


Figure 5-24: SEM image of the image at the left, shown at higher magnification. Note small fibrous matrix covering nearly the entire surface.

These SEM images show a sample with DOPS/cholesterol without GS that was given a score of 3 by stereo microscopic evaluation. In Figure 5-23, a thin (nearly transparent) coating can be seen nearly completely covering the sample, with only occasional small areas where it appeared that titanium substrate was exposed and no coating (fibrous mat) was visible. Thus it was judged that 3 was an appropriate score. Figure 5-24 provides a higher magnification so that the fine fibrous strands of the thin, transparent matrix

coating can more clearly be seen. The dendritic-like structures appear to be common on DOPS/cholesterol coatings that have been hydrated. All cholesterol-containing samples that were examined under SEM in this study exhibited structures similar to these. Further study would be required to ascertain what these structures are and how/why they form.



*Figure 5-25: SEM image of calcium-chloride pretreated titanium with DOPS with cholesterol without GS, imaged at 15 kV.*

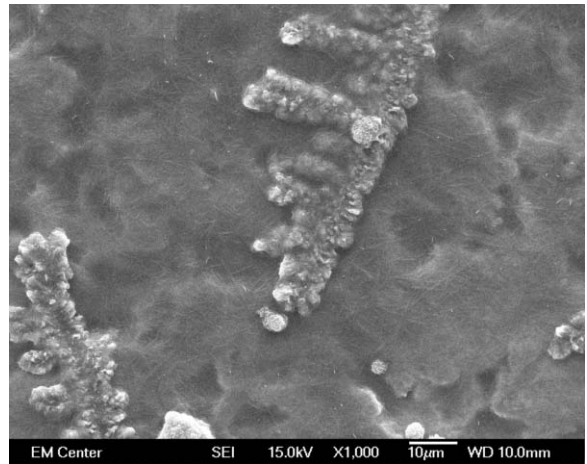


*Figure 5-26: SEM image of calcium-chloride pretreated titanium with DOPS with cholesterol without GS, imaged at 15 kV.*

Figure 5-25 shows a calcium-chloride pretreated sample with cholesterol without GS that was given a score of 3 by stereo microscopic evaluation. Upon examination with SEM, a thin, transparent and tightly adherent coating was seen, again completely covering the sample, and with much more of the dendritic-like structure mentioned above and no gaps (exposing underlying titanium) in the coating could be found. This sample score was corrected to 5. Figure 5-26 provides a higher magnification so that the fine fibrous strands of the thin, tightly adherent coating can more clearly be seen. And again, the typical dendritic-like structures appeared and were quite common all over the surface

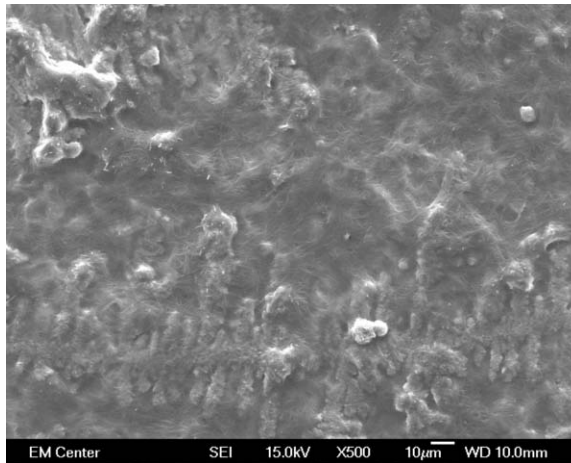


Figure 5-27: SEM image of calcium-phosphate pretreated titanium with **DOPS with cholesterol without GS**, imaged at 15 kV.

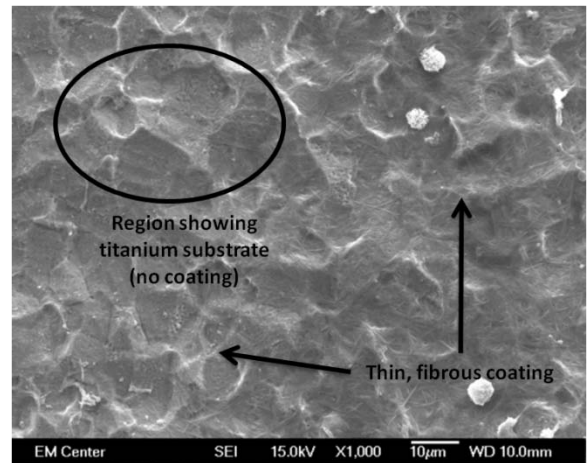


Figure 5-28: SEM image of calcium-phosphate pretreated titanium with **DOPS with cholesterol without GS**, imaged at 15 kV.

Figure 5-27 shows a calcium-phosphate pretreated sample with cholesterol without GS that was given a score of 4 by stereo microscopic evaluation. Upon examination with SEM, small regions could be seen where the underlying titanium was exposed, and fewer of the dendritic-like structures mentioned above were apparent. This sample score was reduced to 3. Figure 5-28 again provides a higher magnification so that the fine fibrous strands of the thin, tightly adherent coating can more clearly be seen, but an area of exposed titanium substrate can also be seen in the upper left quadrant of the image. It is worth noting, as discussed in section 5.8 below, that SEM verification proved helpful, in some cases lowering scores while raising scores in equally as many other cases. This demonstrates relatively even judgment overall of sample scores.

The following charts show coating retention scores, comparing samples by pretreatment, with and without cholesterol and with and without GS. Percentages were obtained by scoring each sample, averaging all scores for each treatments group and converting the average to a 100% scale.

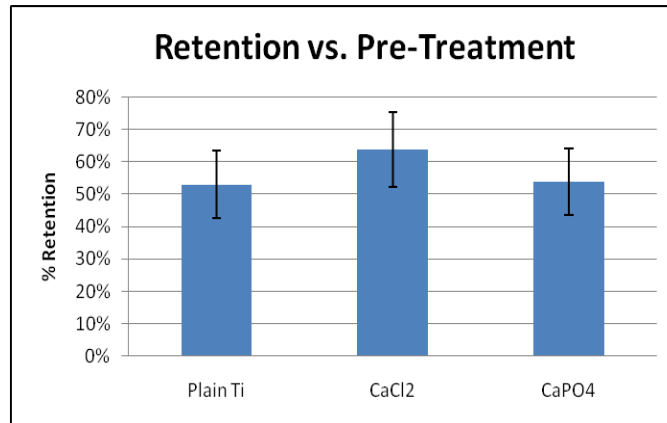


Figure 5-29: Coating retention by pretreatment, with and without cholesterol and with and without GS. Plain Ti is no calcium pretreatment. No significant differences exist.

Although none of the pretreatments result in significant differences, it appears that a calcium chloride pretreatment may provide better coating retention than calcium phosphate or no pretreatment.

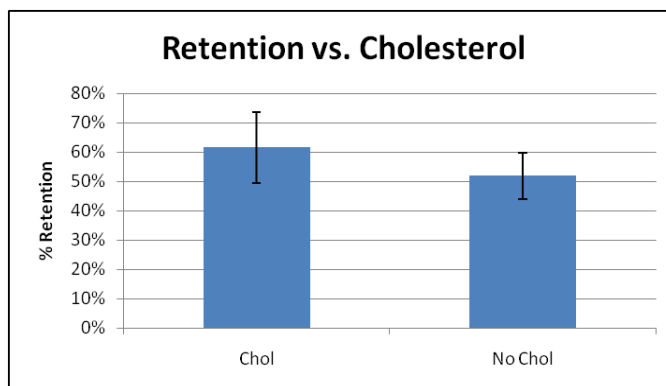
The following figure compares samples by containing GS or not in the coatings, for all pretreatments and with and without cholesterol.



Figure 5-30: Coating retention by GS or no GS, with and without cholesterol and for all pretreatments. With GS is significantly higher than no GS ( $p < 0.05$ ).

GS in coatings produces significantly better ( $p < 0.05$ ) coating retention than no GS in coatings.

The following figure compares samples by cholesterol or no cholesterol in coatings, for all pretreatments and with and without GS in coatings.



*Figure 5-31: Coating retention by cholesterol or no cholesterol, with and without GS and for all pretreatments. No significant differences exist.*

Although coatings with or without cholesterol were not significantly different, it appears that cholesterol in the DOPS E-spray solution may provide better coating retention than without cholesterol.

These indicators support the following observations:

- Calcium chloride pretreatment appears to provide better coating retention than calcium phosphate pretreatment or no calcium pretreatment.
- GS-loaded coatings provide significantly better coating retention than coatings without GS.
- Cholesterol in coatings appears to provide better coating retention than coatings without cholesterol.

To explain these results, it is useful to first discuss calcium and cholesterol biochemistry and their respective interactions with DOPS, and the roles each may play in these coatings.

## 5.6 Discussion

### 5.6.1 Effect of Calcium

As discussed in Background, section 2.1.2 above, Calcium plays an important role in bonding with and between titanium oxide and DOPS molecules. Calcium ions induce crystallization and immobilization of DOPS acyl chains [41, 42], leading to a crosslinking effect. [37, 41, 42, 44] IR analysis also reveals that  $\text{Ca}^{2+}$  ionically binds to the phosphate ester ( $\text{PO}_2^-$ ) group of DOPS [37, 41, 44], where it binds as a bidentate ligand, thereby changing its conformation and causing it to dehydrate. [41, 43, 223]

These interactions provide insights into the enhanced retention of our calcium pretreated surfaces, as the calcium likely interacts with, and binds to, DOPS, more than non-pretreated surfaces. XPS characterization confirmed the presence of calcium on both calcium pretreated surfaces, but notably more calcium on the sample pretreated with calcium-phosphate, and relatively large phosphorous peaks on the calcium-phosphate sample, but no phosphorous on the samples pretreated with calcium chloride, as shown in the following figures.

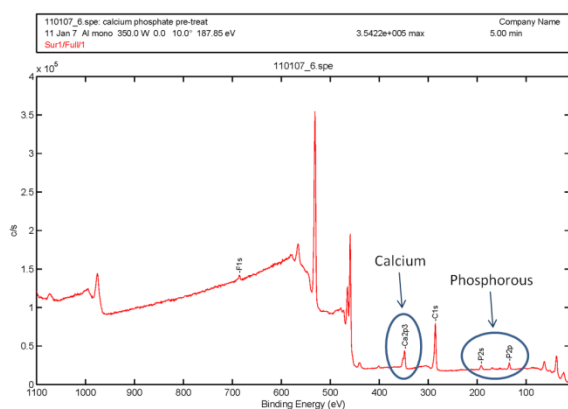


Figure 5-32: XPS spectra of passivated titanium with calcium phosphate pretreatment, no E-spray. Spectra confirms presence of calcium and phosphate.

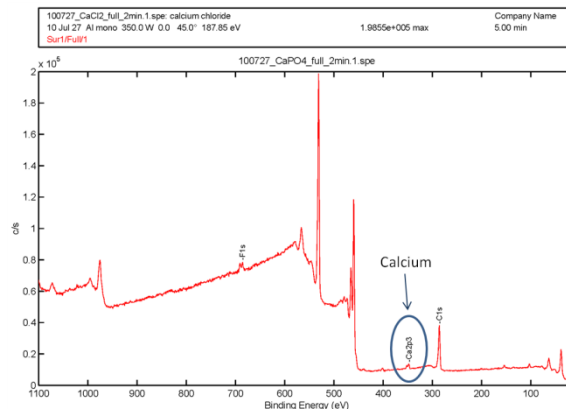


Figure 5-33: XPS spectra of passivated titanium with calcium chloride pretreatment, no E-spray. Spectra confirms presence of calcium and no phosphate or chloride.

We hypothesize that calcium chloride enhances coating retention better than calcium phosphate because anhydrous calcium chloride is more soluble than  $\beta$ -tri-calcium-phosphate, and the calcium-phosphate was not as dissociated, therefore less available to interact with DOPS as was the calcium in calcium-chloride. This would lead to  $\beta$ -tri-calcium-phosphate being less effective in enhancing the binding of DOPS to titanium, as there would be fewer free calcium ions available on the Ti substrate. Furthermore, in general, negatively charged surfaces make good substrates for biomineralization, which often starts with calcium adsorption to the negatively charged surface. Phosphate adsorption does not play a role in biomineralization. [100] This suggests more free calcium ions made available by the dissociation of calcium-chloride compared to calcium-phosphate would provide more such adsorption, enhancing the bonding of the DOPS coatings to the negatively charged surfaces, in a similar fashion.

Calcium-phosphate exhibits a more feature-rich morphology than calcium-chloride when E-sprayed. This morphology may result from processes similar to those described in the previous paragraph. That is, more free calcium may act to stabilize the acyl chains of the DOPS molecules (probably through weak secondary bonds), leading to more consistent orientation of these structures in the DOPS coating, and therefore a smoother, more consistent coating. The most stable calcium-phosphatidylserine configuration occurs when the  $\text{COO}^-$  or  $\text{PO}_4^-$  of every second phosphatidylserine interacts with  $\text{NH}_3^+$  in neighboring PS-Ca-PS complexes. [47] This would result in a more ordered coating structure, which would be visualized as a smoother morphology.

## 5.6.2 Effect of Pretreatment & Passivation

It is also likely that passivation of the titanium surface, which was performed in an effort to enhance coating retention (discussed in 4.2.2 above), also helped improve coating retention, in part because it provides a consistent oxide layer on the Ti surface, and because it removed carbon contamination that is often present on “solvent cleaned” titanium samples. High amounts of carbon contamination are common in titanium oxide layers [68] as a result of air exposure during storage and/or contamination during handling and analytical procedures.

We observed a similar result. The following figures show representative plain titanium test samples before (left) and after (right) the pickling and passivation process, but with no calcium pretreatment.

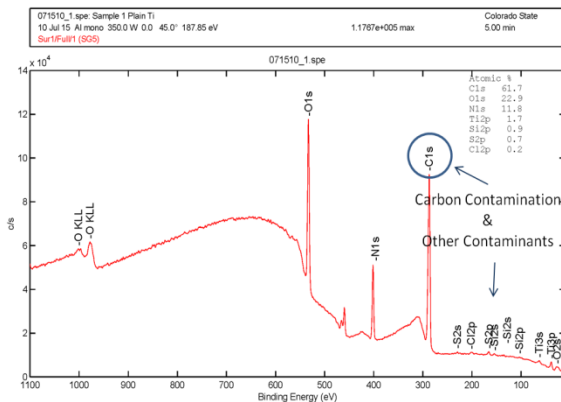


Figure 5-34: XPS spectra of unpassivated titanium with no pretreatment, no E-spray. Note numerous contaminants (discussed in 5.6.2 above), but no calcium.

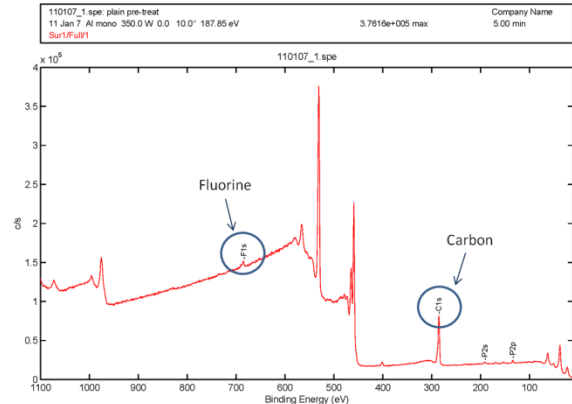


Figure 5-35: XPS spectra of passivated titanium with no pretreatment, no E-spray. Spectra confirms a much smaller carbon peak and a fluorine peak.

The unpassivated, non-pretreated sample contains a large amount of carbon contamination, along with other contaminants. The passivated, non-pretreated spectra confirms the carbon peak has reduced substantially. Of note is the appearance of the fluorine peak identifying residual fluorine from the passivation process.

Passivation also provided a consistent oxide layer on the Ti surfaces, which maximized the number and availability of negatively charged oxygen ions for free calcium ions to bond with, thus maximizing binding sites for phospholipid head groups. This in turn helped to maximize the strength of bonding at this interface and thus the retention of the coating.

SEM images shown in Figure 5-8 through Figure 5-10 above indicate that E-sprayed DOPS coatings on passivated and calcium pretreated samples, without cholesterol or GS, resulted in coatings which were very similar (visually), calcium chloride more so, to the samples from test 13 in the *E-spray Study* (which was selected as the “ideal” coating). Samples used in prior E-spray tests (as in the E-Spray Study) were not passivated. However, in the images above, the coating on non-pretreated titanium appears smoother in texture than E-sprayed coatings with calcium pretreatment. Therefore, it appears that coating morphology on samples with passivation alone is visually distinct from samples that have been passivated and pretreated. This suggests that a process including both passivation and pretreatment does not change our ability to create E-sprayed DOPS coatings very similar to those determined to be “ideal” in previous E-spray testing. The process of passivation alone does appear to change coating characteristics. But, because our subsequent studies used passivation and pretreatment on all samples, additional consideration was not given to this phenomenon. Further study would be required to ascertain the underlying basis of the effect of passivation alone.

### 5.6.3 Effects of Cholesterol

---

We hypothesize numerous reasons that cholesterol in coatings is better for coating retention than no cholesterol, and that the combination of calcium and cholesterol is especially beneficial to coating retention.

The following figure shows the chemical structure of cholesterol.

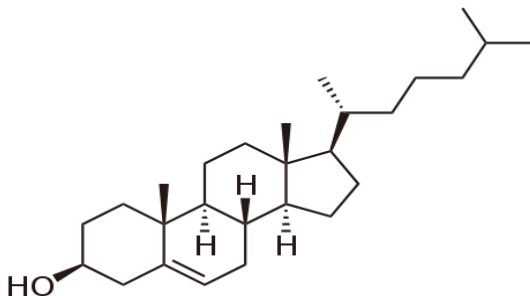


Figure 5-36: Chemical structure of cholesterol

It has high affinity for the cell membrane, where it plays a key role in controlling fluid membrane rigidity [48], thus reducing passive permeability of the plasma membrane and increasing the mechanical durability of lipid bilayers. It increases the stability of phospholipids [49] by increasing the organizational complexity of the proteins and lipids found in the membrane. [54]

Numerous studies have shown that the hydroxyl group on cholesterol interacts with the polar head groups of the membrane phospholipids, particularly with DOPS [41, 44, 223], while the bulky steroid and the hydrocarbon chain are embedded in the membrane, alongside the non-polar fatty acid (acyl) chains of the other lipids. [57, 224] FTIR analysis has shown that cholesterol disturbs the acyl chain packing of DOPS [44] but does not appear to affect the hydration or the mobility of the carboxylate group. [41] In addition, if calcium ( $\text{Ca}^{2+}$ ) is bound to the DOPS phosphate group, cholesterol enhances the dehydration and immobilization of this complex. [44]

These interactions suggest that cholesterol likely plays an important role in enhancing the retention of our E-sprayed DOPS-based coatings. We hypothesize that cholesterol bonds with the DOPS through weak secondary bonds, probably dipole interactions, such as van der Waals interactions, and hydrogen bonding between the –OH group in cholesterol and DOPS acyl chains. Because it has numerous potential binding sites, cholesterol could bond to numerous sites on the DOPS molecule and “bridge” between DOPS molecules through bonds at polar head groups and acyl chains. This effect may be especially potent as calcium bridging (the formation of bidentate ligands with DOPS [43]) between the titanium oxide substrate and the DOPS further immobilizes DOPS molecules.

Coatings containing DOPS and cholesterol exhibit an abundance of spherical features compared with DOPS without cholesterol (refer to Figure 5-15 through Figure 5-17 above). A possible explanation is as follows. Cholesterol probably bonds with DOPS at multiple candidate binding sites. This could reduce the number of potential binding sites available for water molecules, raising the hydrophobicity of the coating. An increase in hydrophobicity would coincide with a thermodynamic propensity toward self-assembly of phospholipid meta-structures, such as micellar and liposomal structures. These may be visible as the spherical features in these SEM images. In addition, cholesterol enhances the dehydration and immobilization of calcium-bound phosphate group in DOPS [44], while disturbing the calcium-induced highly ordered acyl chain packing. Both of these influences would lead to a rougher, less ordered coating.

We hypothesize that this architecture would be stabilized by the presence of gentamicin, which also contains numerous potential binding sites (discussed in the

following section). This hypothesis is further supported by the observation that GS-loaded DOPS coatings were retained for longer and in more complete (un-degraded) condition than DOPS alone or DOPS/cholesterol without GS, as discussed in the *Elution Study* chapter, section 6.5 and Figure 6-11 below, and by the observation that GS-loaded coatings were often smoother than coatings lacking GS.

#### ***5.6.4 Effect of Gentamicin***

---

We hypothesize GS coatings are better than coatings lacking GS because the GS is interacting and bonding with the DOPS at numerous binding sites.

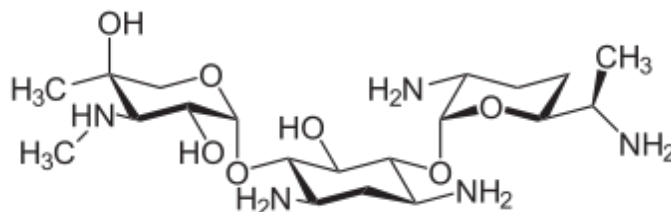


Figure 5-37: molecular structure of gentamicin

As can be seen in Figure 5-37 showing the chemical structure of the GS molecule, there are numerous potential bonding sites on GS, the  $-OH$  and  $-NH_2$  groups being most notable. Similar to hydroxyl group bonding observed in cholesterol [41, 44, 223], the multiple hydroxyl groups on GS probably also interact with the acyl chains of DOPS molecules. These interactions could occur at numerous sites on the DOPS molecule, and could serve to immobilize and stabilize the DOPS, resulting in a smoother surface. Furthermore, each of the multiple hydroxyl groups present on GS may also provide excellent potential binding sites for water molecules, which would lower the hydrophobicity of the coating while immobilizing it, resulting in a smoother coating.

Recall that GS was dripped onto the first (inner) DOPS layer, which was then dried before the second coat of DOPS was applied (as described in the *Elution Study* chapter,

section 6.3.2 below). As suggested in the previous paragraph, it is likely that the aqueous, GS-laden solution penetrated and hydrated the inner DOPS layer and became well established there, likely through multiple bonding configurations. This GS invasion probably immobilizes the DOPS coating, forming a tighter packing of the DOPS molecules, which would be observed as a smoother coating. These bonds between the GS and the DOPS would likely lead to strengthening of the coating, resulting in less coating degradation and better retention. The similarity between calcium pretreated and non-pretreated coatings suggests this GS effect may be greater than any calcium-derived effect that was discussed in section 5.6.1 above.

## ***5.7 Conclusions***

The results of this study support the following conclusions:

- Calcium chloride pretreatment appears to provide better coating retention than either calcium phosphate pretreatment or no calcium pretreatment.
- GS-loaded coatings provide significantly ( $p < 0.05$ ) better coating retention than coatings without GS.
- Cholesterol in coatings appears to provide better coating retention than coatings without cholesterol.

Cholesterol as an additive to a DOPS E-spray solution is an effective means to increase the retention of the DOPS coatings when E-sprayed on passivated titanium samples which were pretreated with calcium-chloride.

The fundamental objective of this study was to reduce the degradation of DOPS-based coatings. Therefore, the most important finding of this study was that no cases of

delamination were observed. In very few cases were any particulates noticed in any of the sample wells during this study, which suggests a slow erosion of the coating.

Throughout our research we have observed that the addition of GS in a coating makes the coatings more resistant to erosion and more adherent to the titanium substrate, but lacked empirical evidence. In this study, we have both empirical and statistical evidence for what has until now only been an observation. Our results find that coatings containing GS exhibit statistically higher coating retention than coatings without GS.

It is also interesting to note that the calcium pretreated, DOPS/cholesterol coatings seemed less brittle and tougher than past DOPS coatings. Fewer fractures were observed in SEM images in general. The coatings were easily tough enough to be handled (with surgical gloves), with no indication of any samples being damaged by such handling. The toughness of these coatings is worthy of future study.

And finally, E-spraying DOPS coatings on calcium pretreated titanium, with or without cholesterol or GS, produces a more feature-rich morphology than non-pretreated samples. Both coatings compare favorably, calcium chloride more so, to the samples from test 13 discussed in section 4.6.2.1 above, which was selected as the “ideal” coating. Moderate topology is preferable for cell adhesion, spreading and normal development (refer to section 4.4.2.2 above), therefore calcium chloride pretreatment is likely to be more suitable for cell growth.

## ***5.8 Limitations***

This study was highly qualitative and subjective. A grading system was informally applied to samples through microscopic inspection. Despite attempts to qualify the scoring assignments through SEM observation, the study could provide better insights if

it were more quantitative. Other analytical techniques, such as lipid stains or immunofluorescence imaging might provide useful additional insights, and would comprise interesting future study. This being said, the study accomplished its objective of significantly reducing the degradation of DOPS-based coatings.

Because this study was based on qualitative assessment of coating quality, it is not surprising that statistical significance is lacking. Despite a relatively high sample size for each treatment group (n=10), there was large variation in the visual appearance of coatings, even at relatively high magnification. It was also difficult to see small, often quite subtle, differences between coatings. SEM verification proved helpful, in some cases lowering scores while raising scores in equally as many other cases. This demonstrates relatively even judgment overall of sample scores.

## **5.9 *Future Work***

We implemented one particular combination of factors to improve coatings retention. Passivation and pretreatment of the titanium surface, in addition to inclusion of cholesterol in the DOPS E-spray solution made a significant difference in coating retention. It would be useful to extend this line of research to test other means of enhancing coating retention. For example, covalent attachment of the DOPS coating to the titanium substrate would reduce variability we observed in testing cellular response to the surfaces due to coating degradation.

Passivation is perhaps the simplest of the surface conditioning techniques. We could extend this approach by testing different surface textures and surface roughness. In addition, it would be interesting to test other techniques for integrating calcium into or onto the metal surface, such as ion implantation or plasma deposition of hydroxyapatite.

It is likely that mixing phospholipids, for example, DOPS with phosphatidylcholine, would also change the coating characteristics to cause changes in coating retention. We could also mix phospholipids with synthetic polymers such as PCL to change coating retention. E-sprayed materials could also be cross-linked to make them more durable. Any combination of these approaches would be fruitful future research.

## **6 *Controlled Elution of Gentamicin Sulfate from E-sprayed DOPS coatings***

### **6.1 *Purpose***

Phospholipid coatings have been electro-sprayed on titanium for the purposes of enhancing bone ingrowth/apposition and delivering antibiotics locally from the implant. This study was designed to approximate the *in vitro* rate of elution of gentamicin sulfate (GS) loaded onto our DOPS coatings, and to determine if that elution rate could be modified by manipulating E-spray parameters and/or coating composition.

As discussed in *Background* section 2.4.7 above previous studies have shown that phosphatidylserine can effectively bind and deliver clinical concentrations of gentamicin. [211, 214] These studies packaged the drug in phospholipid meta-structures such as liposomes and micelles to effectuate localized delivery. We believe ours is the first study to investigate drug delivery from phospholipid coatings directly applied to titanium implant material.

### **6.2 *Experimental Approach***

---

Gentamicin sulfate (Sigma-Aldrich, G1264) was loaded onto titanium samples, sandwiched between two layers of E-sprayed DOPS (refer to *E-spray Study* chapter).

A highly sensitive assay for GS in solution was adapted from the literature. GS elution from E-sprayed DOPS was performed in accordance with the *Elution Protocol* found in Appendix B. Eluents were removed at specific time points and assayed for GS concentration, from which initial loading efficiencies and elution profiles were developed.

This assay can be used to calculate very precise amounts of GS. However, as discussed in section 6.3.3 below, the primary amine group in DOPS can result in inaccuracies. Therefore, because our purpose is to compare different DOPS coating compositions, and not to measure GS amounts, we only used absorbance values from the assay for relative comparisons of elution profiles between samples. Absolute GS amounts were not calculated.

Two main studies are reported here. The first is a preliminary study in which DOPS (Avanti Polar Lipids, Alabaster, AL) coatings applied with three different E-spray voltages were compared for their elution performance. These voltages were selected through a series of tests detailed in the *E-spray Study* chapter. The second study reported here is a follow-up study, in which the elution properties of a new DOPS/GS E-sprayed coating formulation were investigated. In the follow-up study, coatings were E-sprayed on titanium samples that had been pretreated with calcium chloride, using E-spray parameters determined to be “ideal”, as detailed in the *E-spray Study* chapter, section 4.6.2.1 above. In addition, we found in the *Enhancing Coating Retention Study* (see chapter 5) that pretreatment of samples with calcium chloride and the addition of cholesterol to the DOPS coatings would enhance the retention of E-sprayed DOPS coatings.

### **6.2.1 Experimental Plan**

In the preliminary study, one 25 mm<sup>2</sup> square sample (i.e., nominally 5 mm on each side) was prepared for each of three E-sprayed treatments: plain titanium, DOPS and DOPS/GS, for three different E-spray voltages: 10 kV, 12 kV and 14 kV volts, totaling 9 test samples.

An 8-hour elution was performed and results evaluated for elution performance.

In the follow-up study three 25 mm<sup>2</sup> samples (i.e., nominally 5 mm on each side) were prepared for each treatment: plain titanium, DOPS/cholesterol E-sprayed and DOPS/cholesterol with GS E-sprayed. In this study, all E-spray solutions contained a mixture of DOPS and cholesterol, and all samples were pretreated with calcium chloride. Both methods are described in the *Enhancing Coating Retention* chapter 5.

A short three-hour elution was performed to determine if the changes in coating composition had altered elution performance.

## ***6.3 Performing the Elution***

---

### ***6.3.1 Preparing Gentamicin Loads***

GS Loading Solution was created by adding 1.73 ml PBS to 173 mg GS at room temperature, yielding a 100 mg/ml concentration. This mixture easily dissolved into a clear fluid. GS loads were applied to DOPS coated titanium samples by pipetting the quantity of this solution required to achieve desired loading onto samples in microliter increments (e.g., 1  $\mu$ l to load 100  $\mu$ g).

### ***6.3.2 Preparing DOPS-Gentamicin Elution Test Samples***

Titanium samples were E-sprayed with DOPS (Avanti Polar Lipids) using the procedures and ideal settings described in the *E-spray Study* chapter, section 4.6.2.1 above.

To reiterate for convenience, ideal E-spray parameters for DOPS coatings were:

- DOPS concentration: 1.3% (vol%)
- Pump rate: 14 ml/hour
- Electric field strength: 1.5 kV/cm, developed by:

- Spray distance: 8 cm
- Voltage: 12 kV
- Spray time: 3 minutes per set of samples delivering 1.2 mg of DOPS per sample, in this case 3 samples producing a coverage of 3.2 mg/cm<sup>2</sup>.

For each time point, three samples of each treatment were prepared. For example, treatments in the preliminary study were three different E-spray voltages: 10 kV, 12 kV and 14 kV. These values are  $\pm 2$ kV from 12 kV, which was determined to be the best candidate E-spray voltage. All samples were E-sprayed with a single coat of DOPS as described in the *E-spray Study* chapter 4, using ideal parameters listed above, and vacuum dried at room temperature overnight.

GS was then loaded (i.e. dripped by pipette) onto each sample as described below for each specific study (as GS load amounts varied between the preliminary and follow-up studies), and all samples were vacuum dried at room temperature for 24 hours. Then a second DOPS coating was E-sprayed on all samples, using the same E-spray parameters as the first, completely covering the GS layer. Samples were then vacuum dried at room temperature overnight. All samples were stored in a dessicator at room temperature prior to use.

Samples with GS on them were clearly distinguishable from those that did not. The portion of the sample surfaces where the GS was dripped exhibited a dull white color, as can be seen in the following image. In other words, the GS coatings were not uniform across the entire sample, with more drug in the middle and less nearer the edges.



Figure 6-1: Samples on the left above were loaded with GS as described above.

In preparation for the elution study, 2 ml mini-centrifuge tubes were labeled according to their respective time points and placed in tube racks. Immediately prior to commencement of the test, samples were placed in 24-well plates and covered.

### 6.3.2.1 Preliminary Elution Study Preparation

The objective of this study was to compare GS elution performance of DOPS coatings prepared at three different E-spray voltages: 10 kV, 12 kV and 14 kV. DOPS coatings were prepared using “ideal” E-spray parameters listed in the previous section. Titanium samples in the preliminary study were neither passivated nor pretreated with calcium-chloride, and the DOPS E-spray solution did not contain cholesterol. GS was loaded onto DOPS samples in accordance with the *GS Loading Protocol* found in Appendix B. Briefly, 2  $\mu$ l of the GS Loading Solution (at 100 mg/ml - described in section 6.3.1 above) were carefully pipetted (i.e. dripped) onto DOPS samples after the first DOPS coat had been E-sprayed onto unpassivated titanium. Each such application deposits 200  $\mu$ g of GS (2  $\mu$ l of 100 mg/ml) on each sample surface. This amount was

carefully spread for coverage, using the pipette tip to spread the droplet of solution while avoiding contact with the surface. Samples were then dried overnight in a vacuum dryer at room temperature and the process was repeated, resulting in two applications of 200 µg each.

**INITIAL GS LOAD – PRELIMINARY STUDY:** The amount of GS initially loaded onto the samples in the preliminary study is 400 µg, which was applied in 4 µl of GS Loading Solution, on each sample.

Following GS loading, a second DOPS coating was E-sprayed on all samples, using the same “ideal” E-spray parameters as the first (listed in the previous section), completely covering the sample (and covering the GS layer). Samples were then vacuum dried at room temperature overnight. All samples were stored in a dessicator at room temperature prior to use, and all samples were used within one week of production. In early tests, two samples from each test group were imaged on SEM to visually confirm the coating morphology, compared to non-loaded samples. Representative images are provided in Figure 4-27 and Figure 4-28 above (section 4.4.2.2).

After the samples were loaded with GS, E-sprayed and dried, the elution study continued as described beginning with the *Preparing OPA Reagent* section below.

### **6.3.2.2 Follow-up Elution Study Preparation**

In the second or follow-up elution study, the effect of passivating the titanium, pretreating the samples with calcium chloride and adding cholesterol to the E-spray solution were simultaneously tested. These changes from the earlier study were identified as possible candidates for enhancing the retention of the E-sprayed coatings, as discussed in detail in the *Enhancing Coating Retention* chapter 5. The intent of the

calcium pretreatment was to improve retention of the DOPS coating to the titanium surface, while the intent of adding cholesterol to the DOPS E-spray solution was to lengthen the time of drug elution (by affecting the molecular conformation of the DOPS coating and improving adhesion of the coating to the titanium substrate).

In the follow-up study, the GS Loading Solution (at 100 mg/ml - described in section 6.3.1 above) was diluted 5x with additional PBS, resulting in a 20 mg/ml concentration, to enable easier dripping and more even spreading (of larger amounts than earlier) onto the hydrophobic DOPS coating, without requiring extensive manual spreading. Five  $\mu\text{l}$  of this diluted GS Loading Solution were carefully pipetted (i.e. dripped) onto DOPS samples, after the first DOPS coat had been E-sprayed. Each such application deposits 100  $\mu\text{g}$  of GS (5  $\mu\text{l}$  by 20 mg/ml) on each sample surface. Samples were then dried overnight in a vacuum dryer at room temperature and the process was repeated, resulting in two applications of 100  $\mu\text{g}$  each.

**INITIAL GS LOAD – FOLLOW-UP STUDY:** The amount of GS initially loaded onto the samples in the follow-up study is 200  $\mu\text{g}$ , which was applied in 10  $\mu\text{l}$  of GS Loading Solution, on each sample. This GS load was half the load used in the preliminary study. We were concerned that the antibiotic concentration eluted from our samples at an initial GS load of 400  $\mu\text{g}$  (as in the preliminary study) may have been dangerously high for optimum cell growth. Thus the GS load was halved in the follow-up study. The effect of initial loading amount on elution is discussed in section 6.3.4 below.

Following GS loading, a second DOPS coating was E-sprayed on all samples, using the same “ideal” E-spray parameters as the first (listed in section 6.3.2 above), completely covering the sample (and covering the GS layer). Samples were then vacuum

dried at room temperature overnight. All samples were stored in a desiccator at room temperature prior to use. After the samples were loaded with GS, E-sprayed and dried, the elution study continued as described in the following.

### **6.3.3 About the GS Assay**

In order to approximate the GS concentration in a solution, an “OPA” colorimetric assay was performed. OPA reagent was prepared in accordance with the *Making OPA Reagent protocol* found in Appendix B, which was adapted from the original OPA assay proposed by Sampath & Robinson [225] and modified by others. [213] Briefly, an OPA reagent is formulated by mixing o-phthalaldehyde, methanol, 2-mercaptoethanol and sodium borate (in distilled water). In our study, we further modified the published OPA reagent by reducing the borate concentration from 0.5 M to 0.1 M, which successfully removed non-linearities that appeared at high GS concentrations and increased the sensitivity of the assay to low GS concentrations. The reagent was stored in a brown bottle in darkness for 24 hours before use. Then it was used within three days before it begins degrading.

Solutions containing GS were mixed with OPA reagent and iso-propanol (to prevent precipitation of the products formed), in equal proportions, and stored for 30 minutes at room temperature before spectrophotometric analysis. The o-phthalaldehyde reacts with the primary amines in the gentamicin, in the presence of excess sulfhydryl (such as 2-mercaptoethanol) to yield a fluorescent isoindole, the absorbance of which was measured at 332 nm on a spectrophotometer (FLUOstar Omega; BMG Labtech, Durham, NC). This measured absorbance corresponds directly to gentamicin concentration. The OPA assay has a highly linear sensitivity for GS. Cabanillas tested concentrations between 20

and 150 µg/ml. [178, 204] but none lower, and found a GS detection limit of 1.1 µg/ml for the assay in this range. Similarly, Chang *et al* [178] also used the OPA assay at higher concentrations than we used in these studies. Therefore additional testing was performed to verify the efficacy of the OPA assay at lower GS concentrations. After reducing the borate concentration, we consistently and accurately resolved much lower GS concentrations in the range of 2 µg/ml.

Due to inaccuracies potential introduced by the primary amine group in DOPS, we only used absorbance values to enable relative comparison of elution profiles between treatments. We did not complete the full OPA assay to convert absorbance values to actual GS values.

#### ***6.3.4 Performing the Elution***

For all samples, a perfect sink method was used, wherein all solution in any sample well was removed in its entirety and the same amount of GS-free solution replaced at each time point. In a perfect sink condition the concentration of drug in the eluent fluid can be treated as zero right after each solution change so that effusion is not limited by back-diffusion. This is discussed further below.

In the preliminary study, 16 time points were used to measure elution over a period of 8 hours – every 15 minutes for 2 hours, then every 30 minutes for 2 hours, then every 60 minutes for 4 hours. Thus, collection tubes (2 ml micro-centrifuge tubes) totaled  $3 \times 16 \times 3 = 144$ . Higher granularity was chosen in early time points because it was expected that most of the drug would elute in the first few hours, therefore higher time resolution would be required through that time to capture the profile accurately.

In the follow-up study, 9 time points were used to measure elution over a period of 3 hours – every 15 minutes for the first hour, then every 30 minutes for 2 additional hours.

**INITIAL RINSE:** Prior to each elution test, each sample was quickly but gently rinsed (individually in their wells) with 1 ml PBS to remove unbound GS. The full amount of fluid was very gently aspirated and expelled once, and then immediately collected and discarded, leaving only that amount of GS which remained bound to the DOPS coating.

**COLLECTING ELUENTS:** Following initial rinse described above, 1 ml of fresh PBS (at room temperature) was added to each sample, individually in its well. At each subsequent time point, the fluid in the well was very gently aspirated and expelled twice, then the full amount of fluid was collected and transferred in its entirety (i.e. perfect sink condition, discussed further in section 6.4.4 below) into an appropriately labeled 2 ml mini-centrifuge tube corresponding to its time point, and 1 ml of fresh PBS was added to the well. Between times points, samples/well plates were kept in an oscillating agitator cycling at 16 cycles/minute, at room temperature. All sampled eluents were stored at 20°C for no more than a few days until further analysis was performed.

### ***6.3.5 Performing the GS Assay***

The OPA Assay was performed in accordance with the *GS OPA Assay Protocol* found in Appendix B. Briefly, eluents collected as discussed above were split into two parts, with half being stored at 20°C for other potential assays (e.g. ICP). Each remaining 0.5 ml of eluent being tested (representing each time point for each treatment) was mixed with 0.5 ml of the OPA Reagent and 0.5 ml of iso-propanol, totaling 1.5 ml of solution. 200 µl of this solution were plated into 6 wells of each column 96-well plate, one sample per column. This created 6 assay wells per sample, per treatment (N=6). All eluents were

thus plated, and 30 minutes were allowed to pass since the time when the OPA Reagent and iso-propanol were mixed with the eluents. All plates were read on the spectrophotometer at 332 nm. Absorbance values (unitless) were then plotted over time, representing the GS elution profile curves as shown in sections 6.4.2.1 and 6.4.3.1 below.

### **6.3.6 SEM Method**

SEM was performed on a JEOL JSM 6500F. Samples were gold coated (~10 nm Au) and stored in a dessicator until examined under SEM (~5-15 kV).

### **6.3.7 Statistical Analysis**

Statistical analysis was performed using SigmaStat version 11.2, the latest version from Systat Software Inc. Significance testing was performed at  $p < 0.05$  unless otherwise indicated. All the results were analyzed using Student's T Tests to two-treatment comparisons and one-way analysis of variance (ANOVA) for multi-treatment comparisons. The Shapiro-Wilk normality test was performed on all treatments, and the Mann-Whitney Rank Sum test was used for multiple comparisons with unequal variance. Dunn's test for rank-ordered significance was applied in comparisons with unequal samples numbers, for example, if a sample was lost to experimental error.

## **6.4 Results and Discussion**

---

### **6.4.1 GS Coating Thickness**

As discussed previously, GS was dripped onto the first E-sprayed coating of DOPS. For visual verification, SEM images were taken of the GS coating after vacuum drying on samples from the preliminary study (i.e., no passivation, calcium or cholesterol). As seen in Figure 6-2 below, the GS coating has dried and cracked. In a moment of scientific

serendipity, this enabled us to measure the thickness of the GS coatings. As seen in Figure 6-3, GS coatings measured approximately 1  $\mu\text{m}$  in thickness.

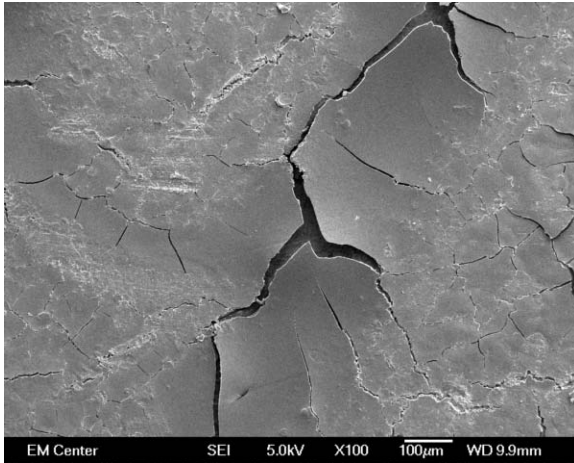


Figure 6-2: SEM image of GS coating on DOPS, after drying, imaged at 5 kV, 100X original magnification. Scale bar is 100  $\mu\text{m}$ .

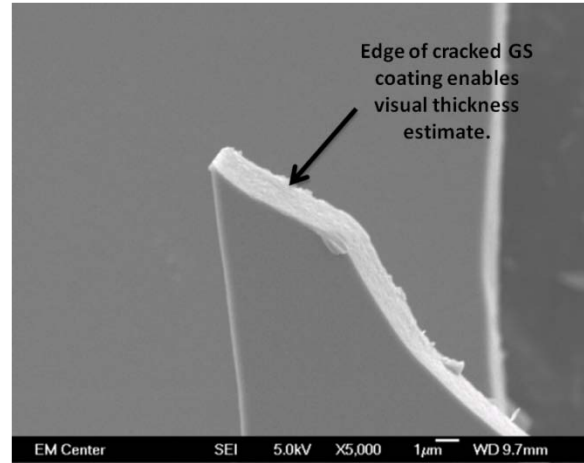


Figure 6-3: SEM image of GS coating on DOPS, after drying, showing thickness of coating. Imaged at 5 kV, 5,000X original magnification. Scale bar is 1  $\mu\text{m}$ .

#### 6.4.2 Test Elution Performance vs. E-Spray Voltage

In the preliminary study, three E-spray voltages were compared for their elution performance. Three 25 mm<sup>2</sup> samples were prepared for each of three E-sprayed treatments: plain titanium, DOPS and DOPS/GS, for three different E-spray voltages: 10 kV, 12 kV and 14 kV volts. Each of the 27 experimental samples was eluted for 8 hours. These voltages were selected through a series of tests detailed in the *E-spray Study chapter*.

##### 6.4.2.1 Elution Results Comparing E-sprayed Voltages

The elution profiles, shown as percentage released, for 10 kV, 12 kV and 14 kV coatings (preliminary study, no passivation, calcium or cholesterol) are shown in the following figures. Higher absorbance values correspond with higher amounts of GS in the eluent solution, meaning that more GS came out of the coating.

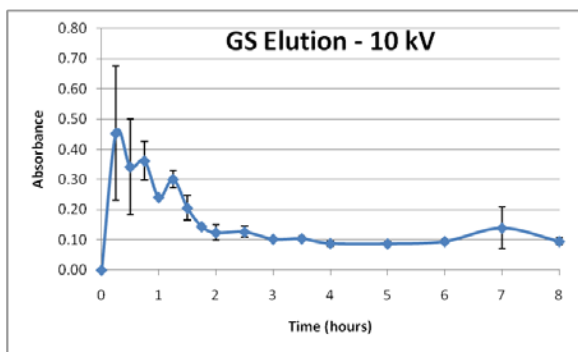


Figure 6-4: GS elution from 10 kV E-sprayed DOPS coatings, preliminary study.

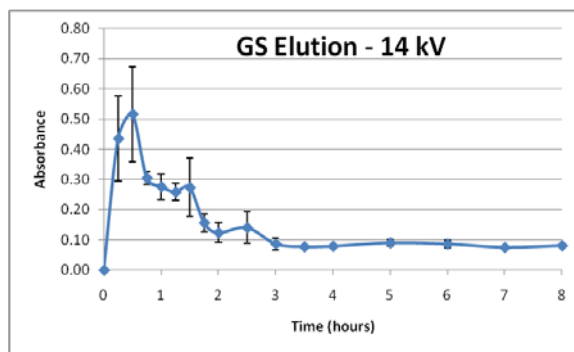


Figure 6-5: GS elution from 14 kV E-sprayed DOPS coatings, preliminary study.

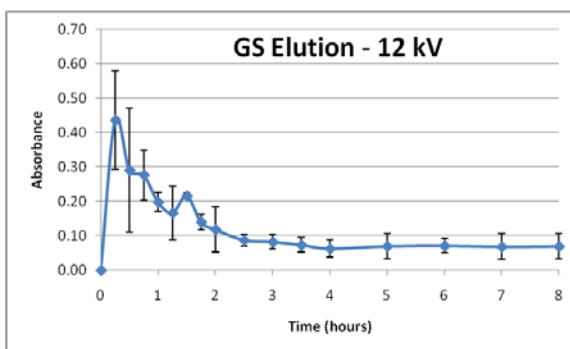


Figure 6-6: GS elution from 12 kV E-sprayed DOPS coatings, preliminary study.

All elution profiles flatten and appear to reach plateaus at later time points. Both 10 kV and 14 kV show higher cumulative absorbance at later time points than results for 12 kV, with 14 kV appearing slightly lower than 14 kV. The 12 kV profile appears to exhibit the lowest plateau, corresponding to the highest amount of GS retained in the coating, suggesting the 12 kV coating appears to hold more drug longer. This also shows that the elution profile can be changed by adjusting the E-spray voltage.

A possible explanation of this improved elution profile is that perhaps the 12 kV coating might have been tougher than the 10kV and 14kV because the 12kV DOPS coatings have an intermediate amount of molecular alignment: too little and the coating breaks away from titanium easily and too much and the coating becomes rigid and brittle.

### **6.4.3 Test Elution Performance with and without Calcium Pretreatment and Cholesterol in Coating**

As a reminder, test samples in this follow-up study were passivated, pretreated with calcium-chloride (i.e. before E-spraying), and E-sprayed with a solution containing both DOPS and cholesterol (mixed). Details of these treatments are provided in the *E-spray Study* chapter. Pretreatment with calcium and the addition of cholesterol were improvements selected through a series of tests detailed in the *Enhancing Coating Retention* chapter.

In this study, new “enhanced” coatings were compared for their elution performance against the original 12 kV coatings from the preliminary study. Test samples (described above) were prepared, passivated and pretreated with calcium-chloride (i.e. before E-spraying), and E-sprayed at 12 kV a solution containing both DOPS and cholesterol to make the inner and outer DOPs layers, with pipetted GS in between. Each of these samples was eluted for only 3 hours. As a result of the preliminary study, it was determined that a shorter time-frame would be sufficient to understand the initial period of the elution, as an early indication of the effect, if any, the enhanced treatments were having on the overall elution performance. Therefore, a shorter (3 hour) elution time-frame was used in the follow-up study.

Despite their general hydrophobic tendency (as discussed in the *E-spray Study* chapter, section 4.6.2.3 above), DOPS coatings have a tendency to swell when hydrated. The swelling begins in just a few minutes, accompanied by a whitish, puffiness in appearance, as shown in Figure 5-1 and Figure 5-2 above. This is probably the effect of hydration of the coatings by the aqueous solvent (PBS). As the solvent enters the coating, the molecular network interacts with the water molecules and expands to a swollen state.

It has been shown that two molecules of water potentially form hydrogen bonds with each of the  $-C=O$  groups in DOPS acyl chains. [44] A thermodynamic swelling force is counteracted by a retraction force from the bonding between the tails of DOPs molecules. A balance is reached as these forces equalize, and the coating appears (by visual observation) to reach a maximum swollen state in approximately 4 to 6 hours where it appears to be many times thicker than the original coating (quantification and characterization is left to future work).

The following images show the eluting samples at 6 and 8 hours. Little if any difference can be seen between these samples. Little difference is seen even after 45 days, as discussed in the *E-spray Study* chapter, section 4.6.2.3 above.

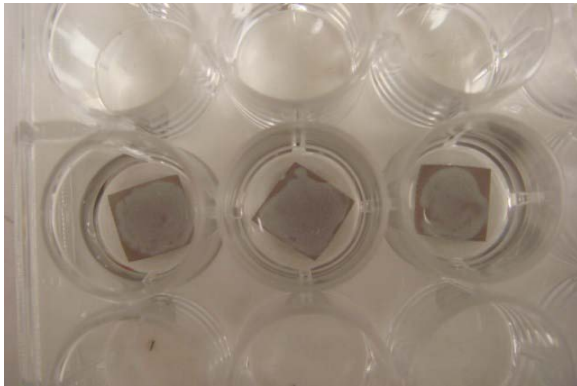


Figure 6-7: Photograph of eluting DOPS/cholesterol test samples after 6 hours

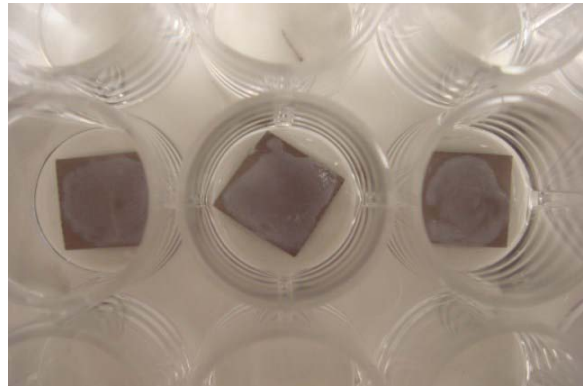


Figure 6-8: Photograph of eluting DOPS/cholesterol test samples after 8 hours

When the aqueous solution containing GS is dripped onto the first DOPS/cholesterol coating, this swelling occurs. Then the coating is vacuum dried and the coating dehydrates, leaving intact the bonds that have likely formed between GS, DOPS and cholesterol. These bonds may provide the foundation for the observed enhancements in coating retention, as discussed in the *Enhanced Coating Retention Study* chapter 5.

### 6.4.3.1 Elution Results Comparing “Enhanced” Coatings with Original Coatings

Elution profiles for “enhanced” test samples E-sprayed at 12 kV (passivated, pretreated with calcium and E-sprayed with DOPS and cholesterol) and the first three hours of our original (preliminary study) 12 kV results are shown in the following figures:

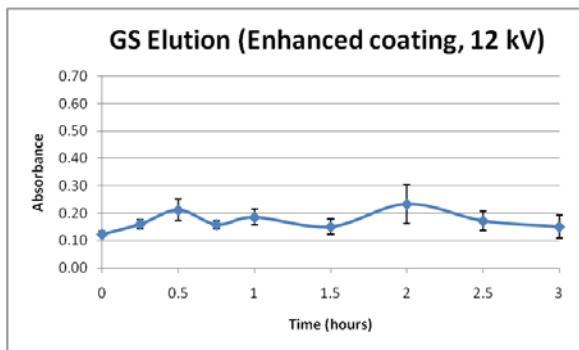


Figure 6-9: GS elution from enhanced coatings -- test samples pretreated with calcium and E-sprayed with DOPS and cholesterol.

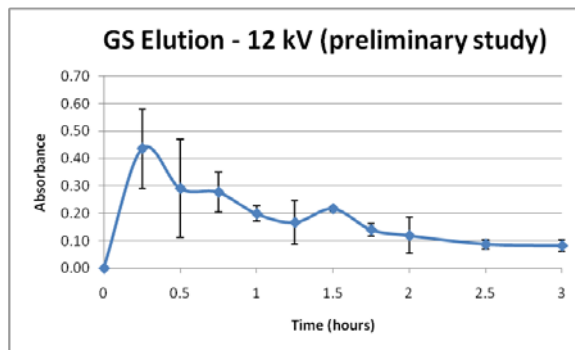


Figure 6-10: Initial three hours of earlier 12 kV E-spray results from original coatings in preliminary study (Figure 6-6 above).

As can be seen, the amount of GS eluting from the coatings after three hours is much less than that for the original elution – absorbance of approximately 0.16 for the enhanced coatings, compared to less than 0.1 for the original coatings. Recall that higher absorbance corresponds to more drug in the eluent, which means it has been released from the coating. The enhanced coatings also do not appear to release a large amount of drug initially, exhibiting a much more consistent release profile. Possible explanations for the apparently improved elution profile of DOPS/cholesterol coatings on calcium pretreated substrate probably involve a combination of better coating retention and slower drug release due to enhanced bonding, both of which are discussed further in the *Enhancing Coating Retention* chapter, section 5.6 above.

#### **6.4.4 On the Total Sink Methodology**

It is worth noting that using the assumption of a perfect sink model has some advantages and disadvantages. In a perfect sink model, all the eluent is withdrawn and replaced with new. So each absorbance read from a particular sample gives the actual GS concentration at that time point, and would not include the initial concentration of GS (which washed off in the initial rinse). On the positive side, this method enables our study to isolate the elution of the drug completely from any mixing effects and other kinetic by-products of a partial sink model. It also greatly simplifies experimental practices and calculations. In a partial sink condition, dissolved drug that eluted from the substrate increases the concentration in the surrounding environment. This increase would reduce the diffusion-based component of the elution, probably not affecting the initial slope, but leading to quicker flattening of the elution profile as the concentration difference between coating and eluent decreases with time. Depending on the amount of drug eluted and the relative drug concentration, solubility of the drug and physical adsorption/desorption of the drug in the coating, these differences often make it very difficult to compare two different systems.

However, a perfect sink model is not without its drawbacks. It appears to oversimplify the actual elution kinetics *in vivo*. Although much about actual *in vivo* elution remains unknown, one thing is clear – it is not a perfect sink. In fact, it has been shown that some *in vivo* applications might best be modeled with non-sink conditions.

[226]

### **6.4.5 Modeling Elution Kinetics**

Mathematical modeling elution profiles can be highly complex. Rigorous modeling of the elution profile of our DOPS coatings is beyond the scope of our work. Excellent reviews of mathematical models are found in Siepmann [227] and Narasimhan. [228]

## **6.5 Discussion**

---

The fundamental driving objective of the elution studies performed in this research is the need for delivery of “high enough” concentrations of anti-microbial drugs to kill potentially biofilm forming (planktonic) and biofilm-based bacteria. As discussed in *Background*, section 2.4.2 above, even just a few bacteria in biofilm are often unresponsive to antimicrobial agents delivered in normal dosages. Parenteral delivery of sufficiently high concentrations of antibiotics is often toxic, fundamentally because locally low perfusion and vascularization prevents concentration of sufficient anti-microbial agents to effectively eradicate the infection. [215] These factors make local delivery the most effective option for preventing and treating osteomyelitis.

While it may seem intuitive to simply load as much antibiotic as possible into a drug-eluting device, these powerful drugs can be highly toxic at even relatively small dosages. On the contrary, long-term, low intensity exposure of these drugs can also create serious complications. Therefore, drug loading and the device’s elution profile must be carefully engineered to balance these too counter-opposing risks.

To accomplish this, it would be essential to calculate the absolute GS concentrations in samples. And to do this, we would need an experimental approach capable of indicating GS concentration without sensitivity to DOPS. We felt this is an acceptable tradeoff, however, because our objective was to determine if there is an effect of E-spray

voltage and “enhanced” coatings on elution profile. Measuring absorbance gives us this evidence, without the need to calculate absolute GS concentration using some other assay or approach.

Our goal was to identify if there is a difference between enhanced and original coatings, and a three hour elution study gave indication that there is a difference. A longer time frame, while desirable for other reasons, was not considered essential to completing this goal. Even a three hour elution identified key differences in the original and enhanced coatings with respect to their elution performance. Further study is required to understand precisely what the longer-term elution profile is and the factors driving it.

It is important to note that tests were performed in a perfect sink protocol, assuming all solution changes at each time point. This is not the case *in vivo*, which in some cases may actually be a non-sink situation. [226] Perfect sink models a worst-case scenario, thus our concentrations will likely be substantially higher *in vivo*, leaving more antibiotic on the target site for longer periods of time.

It is unknown how long these trends will continue, but evidence exists that the coatings containing GS are, for the most part, still completely intact at least seven weeks (longest recorded observation) after initiation of aqueous (cell culture media) bath. The following image shows test samples at the seven week time point. DOPS/GS and DOPS coatings were mostly intact, DOPS/GS more so. Treatments are as indicated, with live cell cultures intact, and media changed biurnally.

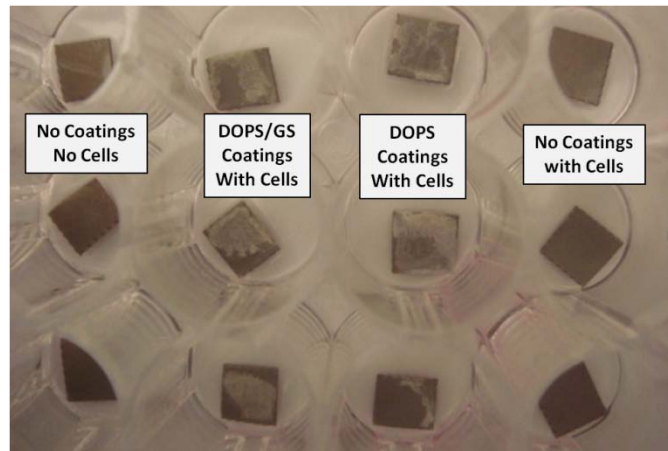


Figure 6-11: Photograph showing test samples at 7 week (post seeding) time point.

This strongly suggests that GS is still present in these coatings, although it is unknown in what state, i.e. if it is available as an anti-microbial agent or chemically bound in the coating in such a way as to render it useless at killing bacteria. Additional strong evidence exists from immunofluorescent imaging reported in 7.8.2.9 below that GS in fact exists in the coatings after three weeks. It would be useful to launch future studies in this regard, to investigate long-term efficacy of DOPS coatings with GS loads.

Anecdotally, in an early test, GS was first dripped onto plain (unsprayed) titanium samples, and then E-sprayed. The coatings delaminated from these samples immediately upon immersion on PBS.

The question of ideal elution profiles is compounded when phospholipids are involved. As discussed in *Background*, section 2.4.7.1 above, deposition of bone precursor minerals begins immediately, with initial bone integration beginning in as early as 4 days. Mature bone develops in 4 weeks. The maximum rate of bone in-growth is reached in about 6 weeks, and most osseointegration occurs within 8-12 weeks following surgery. Phospholipids aid in these osseointegration processes. Therefore, an ideal elution profile would keep antibiotic concentration low to best facilitate bone

mineralization as phospholipid remains available in the coating to support these processes. Hybrids of different types and ratios of phospholipids could be deployed to control these factors.

It is expected that following initial testing of GS loading and elution profiles, release profiles can be modeled such that concentrations required for effective microbe management can be calculated, and coating deposition (and/or multiple coatings) parameters can be tuned to optimize the efficacy of local drug delivery from phospholipid coatings.

Ideally, an additional “burst” of antibiotic could be triggered in three to four weeks, to help manage any potential biofilm formation that may be taking place. This burst should be sudden and strong, but with very quick decay and clearance, so as to not disturb the bone formation and stabilization processes. Such a treatment would probably be adjunct to traditional parenteral biofilm treatment protocols. Multiple coatings could be deployed to effectuate this type of release.

## ***6.6 Conclusions***

---

We demonstrated elution of gentamicin sulfate from DOPS coatings electro-sprayed onto titanium. We found that E-sprayed DOPS coatings can be loaded with GS, and the loaded GS elutes out gradually over the first 8 hours in PBS. We also found that we can modify this elution profile by passivating the titanium surface, and pretreating the surface with calcium-chloride, and then adding cholesterol to the DOPS E-spray solution.

## ***6.7 Limitations***

---

The data collected for the follow-up study resulted from three elutions for each treatment. More conclusive results would be obtained from a higher sample size. In

addition a case might be made for a particular modeling approach with a much larger samples size. Furthermore, a relatively short elution time was used in the preliminary study because of the trial nature of this study. The intention was only to decide which E-spray voltage would be used in future testing, cell study, etc.

The 3 hour time frame in the follow-up study was very short. But our goal was to identify if there is a difference between enhanced and original coatings, not to quantify that difference. Three hours seemed sufficient to accomplish this goal. Although it is quite common in the literature for elutions to be performed with eight-hour time frames, even this is a short time-frame for deriving conclusive evidence about drug delivery efficacy. Future elution studies should be performed for two weeks at a minimum.

In this study, we did not separate out the effects of passivation, calcium pretreatment, and the addition of cholesterol. It would be useful to know the relative effect each or all the factors may be having. Furthermore, we reduced the amount of GS in the second elution test (with calcium pretreatment and cholesterol in the coatings) in order to avoid possible toxic effects on cells. It is possible that the slower elution rate we observed in the follow-up study is in fact due to the reduction in GS, not to the calcium pretreatment and cholesterol. Further study would be required to clarify these effects.

Initial amounts of calcium and cholesterol used in this study were chosen from the literature without advance verification regarding their potential effectivity in our particular study. Fortunately, positive results were achieved. However, even better results could be possible with further study. It is also unknown what the affects of cholesterol actually would be, *vis a vis* their possible impact on the chemistry and

thermodynamics of these coatings and the relationship with drug delivery from the coatings.

In our preliminary study, our control samples (DOPS no GS) were contaminated, making them unusable for testing the effects of the OPA assay on DOPS coated samples with no GS. There is a risk that DOPS alone might be incorrectly measured by the OPA assay, but because the OPA assay is so widely used, we assumed the chances of a reaction to DOPS alone would be very low, so we did not re-create these controls.

## **6.8 Future Work**

It is essential that we test antibiotic elution efficacy of our coatings *in vivo* – all the *in vitro* testing we have done suggests our approach may be an interesting solution for preventing and/or managing orthopedic infection. Such work should start with *in vitro* testing of effective MIC and efficacy of our coatings against various pathogens in the lab (e.g. kill radius testing in petri dish).

Many of the same techniques worth considering for future enhancement of coating retention also apply here to controlling drug-delivery. For example, it would be useful to test variations in coating chemistry, for example, hybridizing the phospholipid layer to include DOPS and other natural lipids, such as phosphatidylcholine, or synthetic polymers such as PLGA would probably afford substantial control over drug-delivery and its range of capabilities.

It would be useful to test various layering approaches, for example, E-spraying multiple layers of material, each with different elution characteristics, or crosslinking the material(s) in the layers. Covalent attachment of phospholipid (DOPS and/or other

candidates) liposomes or micelles to the metal surface, and to each other, would also be an interesting line of study to control elution kinetics and dynamics.

Phospholipids in various configurations have been shown capable of carrying many drugs and other therapeutics. It would be valuable to test the ability of our coatings to carry other therapeutics, such as growth factors, other/mixed antibiotics, angiogenic factors, cancer drugs, etc.

It would be very interesting to test the performance of our coatings in managing other pathological cell types, for example, cancer cells.

## **7 Cytotoxicity, osteoblast viability, biomineralization and bone matrix production of DOPS-coated Ti surfaces, in vitro**

### **7.1 Purpose**

As discussed in *Background*, there are numerous potential advantages of thin, conformal, adherent coatings of phospholipid on titanium (Ti) implant materials. To this end, in this study, phospholipid coatings (specifically DOPS) have been electrosprayed on titanium (see *E-Spray Study* chapter) for the purposes of studying osteoblastic cell response and early biomineralization to the test coatings, and demonstrating elution of antibiotics from the coatings. The study described herein was designed to test the response of osteoblasts and osteoblast progenitors to our E-sprayed coatings and to investigate the ability of our coatings to enhance biomineralization as an indicator of early bone formation. Cytotoxicity of the coatings, along with cell viability, cell differentiation, biomineralization activity, cell morphology and early osseogenesis markers were evaluated at multiple time points.

The role mesenchymal stem cells (MSCs) play in bone formation is believed to be related to their interactions with certain osteoinductive factors present in the intercellular environment, such as bone morphogenic proteins, growth factors and minerals, resulting in their differentiation into osteoblasts.

This study looks at the response of these early bone progenitor cells to DOPS-coated titanium samples. MSCs were selected because they contain a pluripotent population of cells that can differentiate into osteoblasts. [229, 230] Earlier studies have shown that MSCs can successfully be isolated from rat long bones [231, 232] and used to evaluate the effects of various biomaterials on cell development and early bone formation.

## ***7.2 Experimental Approach***

Rat marrow stromal cells were harvested from a single source (i.e. a single rat), counted, seeded and cultured as detailed below. MSCs were selected from the general marrow stromal cell population as they preferentially adhered to our coated Ti samples. Cells were counted and seeded onto 48-well plates as described below. As media changes occurred, MSCs remained preferentially adherent to the various treatments tested. [232]

MSC response was investigated in two phases: a) cell survival, adhesion, viability and morphology up to 7 days after initial culture, and b) osseogenic differentiation, mineralization and matrix production for up to 3 weeks after differentiation media was supplied. On days 1, 4 and 7, fluorescent microscopy imaging of a commercially available live/dead cell stain was used to assess cell survival, adhesion, and spatial organization. On days 1 and 4, a commercially available MTT assay was used to assess viability (mitochondrial activity) of the cells on the test surfaces.

To assess morphology and identify cellular interactions of adhered MSCs to control and test surfaces, cells were fixed, dehydrated, and viewed using scanning electron microscopy (SEM) after 1, 4, and 7 days of culture.

After day 7 MSC culture media was replaced with osteoblast differentiation media. Cell differentiation, mineralization and matrix production were assessed weekly for up to 3 weeks post-differentiation using assays for calcium, alkaline phosphatase and total intracellular protein, and osteocalcin and osteopontin immunofluorescent stains with fluorescent microscopy imaging.

***Two separate cell studies were conducted in this research project.*** For both studies, experimental samples were 25mm<sup>2</sup> squares fabricated from 0.016 inch commercially pure titanium sheeting (Titanium Joe, www.titaniumjoe.com), as described in the *E-Spray Study* chapter. Experimental plans for each study are described in the following.

### ***7.2.1 Preliminary Cell Study***

---

A four week (i.e., 3 weeks post-differentiation) study was conducted to evaluate the response of MSCs to E-sprayed DOPS coatings

1. with two treatments:
  - a. DOPS coatings;
  - b. DOPS coatings with gentamicin;
2. and dual controls:
  - a. tissue culture polystyrene (TCPS); and
  - b. plain (uncoated) titanium.

Test samples were fabricated, solvent cleaned and E-sprayed with DOPS coatings according to procedures detailed in the *E-Spray Study* chapter.

Due to differences in inherent variability of each test performed in this preliminary study, samples sizes for each test varied according to the test, as follows:

- Live cell imaging: n=3
- MTT Assay: n=4
- SEM/EDS: n=3
- Total Protein Assay: n=3
- ALP assay: n=3 (same samples as total protein)

- Calcium assay: n=3

### **7.2.2 Follow-up Cell Study**

---

During the preliminary cell study, coatings exhibited excessive delamination, so an effort was made to remedy this, as described in the *Enhancing Coating Retention* chapter. The result of this coating enhancement work was to pretreat samples with calcium-chloride and add cholesterol to the DOPS E-spray solution. This second follow-up cell study was designed to evaluate the effects of these coating enhancements on the same cell growth metrics tested in the preliminary cell study. Thus a shorter (two week post-differentiation) time-frame was employed.

In this follow-up study, test samples were fabricated, solvent cleaned, passivated, pretreated with calcium-chloride and E-sprayed with DOPS or DOPS/cholesterol coatings according to procedures detailed in the *E-Spray Study* chapter.

This three week (i.e., 2 weeks post-differentiation) follow-up study was conducted to evaluate the response of MSCs to E-sprayed DOPS/cholesterol coatings on titanium pretreated with calcium chloride

1. with two treatments:
  - a. DOPS/cholesterol coatings on calcium-pretreated titanium;
  - b. DOPS/cholesterol coatings with gentamicin on calcium-pretreated titanium;
2. and calcium pretreated titanium as a single negative control (previous data is already available from the preliminary cell study for cell response to plain, unpassivated, uncoated and untreated titanium).

In addition, three samples of each treatment plus Plain Ti control were also exposed to the complete follow-up cell study, including cell culture and differentiation media, but without cells, to test the effects of the calcium pretreatments, along with the media itself (without cells) on calcium assay results.

Sample sizes in this follow-up study were the same as in the preliminary study, except for the addition of the following:

- Osteocalcin n=3
- Osteopontin n=3 (same samples as Osteocalcin)
- Calcium assay with no cells n=3

## **7.3 Experimental Methods**

### **7.3.1 Harvest and Differentiate MSCs**

Rat marrow stromal cells (MSCs) were harvested, counted, and cultured on test samples.

#### **7.3.1.1 Harvesting MSCs**

MSC culture media was made in accordance with a *Making Cell Media Protocol* provided in Appendix C. Briefly, 10% fetal bovine serum (FBS) (Invitrogen) with 1% penicillin/streptomycin (“pen/strep”) (Sigma) was added to  $\alpha$ -MEM acquired through the CSU PMF Freezer Program ([web.research.colostate.edu/pmf/freezer.aspx](http://web.research.colostate.edu/pmf/freezer.aspx)).

Marrow stromal cells were isolated from a single Wistar rat (*Rattus norvegicus*, supplied by Harlan Sprague Dawley) in accordance with a *MSC Harvest Protocol* provided in Appendix C. In brief, limbs were aseptically removed from recently (within one hour) euthanized animals. Femurs, ulnae, and humeri were isolated.

Soft tissue was then removed and bones placed in cold PBS. Working in a sterile biosafety hood, metaphyseal ends were removed to expose the bone marrow cavity. Marrow was repeatedly flushed with culture media ( $\alpha$ -MEM with 10% fetal bovine serum) into a 50 ml conical tube, using 10 ml syringes with 18 and 25 gauge needles. Media containing cells and debris were filtered with a 70 mm nylon filter into a clean tube.

### **7.3.1.2 Counting & Culturing MSCs**

Cells were then counted using a hemocytometer, in accordance with the *Counting Cells Protocol* provided in Appendix C, and seeded onto control and test samples in accordance with a *Seeding Cells Protocol* provided in Appendix C. In the preliminary study, samples were seeded onto 24-well plates at a density of  $1E^6$ /well, while in the follow-up study, samples were seeded onto 48-well plates at a density of  $0.5E^6$ /well. Test samples were slowly warmed to  $37^{\circ}C$  prior to seeding cells.

Cells were cultured in various media described below on test samples for 3 to 4 weeks (depending on the study), with tests (see below) performed on days 1, 4, and 7, and weeks 1, 2 and 3. Test samples and controls were sterilized by exposure to UV light for 30 min. It has been reported elsewhere that UV treatment for even longer periods does not modify the DOPS molecule. [120]

In the preliminary study, an initial half media change occurred on day 4 and all media was changed on day 7. In the follow-up study, half of the media was changed on day 1 and all media was changed on day 4.

### **7.3.1.3 Osseogenic Differentiation**

On day 7, all the media was replaced with an osseogenic differentiation media consisting of  $\alpha$ -MEM supplemented with 10% FBS, dexamethasone ( $10^{-8}$  M), ascorbic

acid (50  $\mu\text{g/ml}$ ), and  $\beta$ -glycerophosphate (8  $\mu\text{M}$ ) (refer to *Making Cell Media Protocol* provided in Appendix C for details on how media was made). Media was changed using differentiation media every 2 days thereafter for the duration of the study, in accordance with a *Changing MSC Differentiation Media Protocol* provided in Appendix C.

## **7.4 MSC Response to Test and Control Surfaces**

MSC response was investigated in two phases:

1. Cytotoxicity: cell survival, adhesion, viability and morphology up to 7 days after initial culture; and
2. Cell differentiation and matrix production for up to 3 weeks after differentiation media was initiated.

### **7.4.1 Cytotoxicity: cell survival, adhesion, viability & morphology**

#### **7.4.1.1 Cell Survival & Adhesion (Live/Dead fluorescence imaging)**

During the initial phase of the cell study, live and dead cellular fluorescence microscopy imaging stains were used to assess cellular activity and response to test surfaces. Commercially available (Invitrogen Molecular Probes) live stain (Calcein-AM) and dead stain (ethidium homodimer-1) (EthD-1) were used to visualize cell viability, population densities, adhesion, and spatial organization. Fluorescence microscopy imaging was performed on all treatments (DOPS-coated Ti surfaces, with and without GS) and controls using a Zeiss Axioplan 2 fluorescence microscope (Carl Zeiss).

The imaging was completed in accordance with the *Live/Dead Imaging Protocol* provided in Appendix C. Briefly, after days 1, 4, and 7 in culture, samples were removed from culture media, rinsed in PBS, then bathed in calcein-AM (3  $\mu\text{M}$  in PBS) and EthD-1 (4  $\mu\text{M}$  in PBS) for 20 to 30 minutes. Samples were then rinsed in PBS and fluorescence

imaged using the following filtration: live stain - excitation at 495 nm, emission at 515 nm (using FITC filtration on the microscope); dead stain - EthD-1 - excitation at 495 nm, emission at 635 (using Texas Red filtration on the microscope). Image-J software ([rsbweb.nih.gov/ij](http://rsbweb.nih.gov/ij)) was used to visualize cell distribution and spatial organization and to quantify approximate cell counts.

#### **7.4.1.2 Cell Viability (MTT Assay)**

MTT assays were performed on days 1 and 4 in culture using a commercially available MTT assay kit (Sigma-Aldrich). The assays were completed on all treatments (DOPS-coated Ti surfaces, with and without GS) and controls.

The assays were completed in accordance with the *MTT Assay Protocol* provided in Appendix C. Briefly, samples were rinsed in PBS warmed to 37°C, to remove non-adherent cells. Remaining cells (which remained adherent) were incubated at 37°C for 3 hours in MTT Reagent (3-[4,5-dimethylthiazol-2-yl]-2,5-diphenyl tetrazolium bromide) prepared in PBS at 10% of culture volume, then mixed such that 10% of the final solution is Triton-X (to lyse cells). This process yields a purple color in wells due to formation of formazan crystals. Samples were then bathed in MTT solvent with gentle agitation for a few minutes until the purple color disappeared. The optical density (absorbance) of the resulting solvent is proportional to mitochondrial activity of the cells on the samples, and was measured with a spectrophotometer (FLUOstar Omega; BMG Labtech, Durham, NC) at a wavelength of 570 nm. Background absorbance at 690 nm was subtracted from the measured absorbance. Blank controls were included in each plate to enable compensation for inter-plate variability. Well plates were kept covered to prevent evaporation, which can affect MTT results.

### **7.4.1.3 Cell Morphology (SEM)**

Qualitative visual characterization of cell morphology, adhesion, and proliferation was performed by examination under SEM (JEOL JSM 6500F) after 1, 4, and 7 days to investigate short-term morphology (and changes in morphology) and weekly to investigate morphology and extracellular matrix production.

Cells were fixed in accordance with the *Fixing Cells Protocol* provided in Appendix C. Briefly, cells were fixed in a solution of 3% glutaraldehyde, 0.1 M sodium cacodylate, and 0.1 M sucrose for 45 minutes. Then samples were soaked in buffer containing 0.1 M sodium cacodylate and 0.1 M sucrose, and then dehydrated by soaking the surfaces in increasing concentrations of ethanol, 10 minutes per cycle. In the preliminary study and days 1, 4 and 7 of the follow-up study, samples were further dehydrated by soaking in hexamethyldisilazane (HMDS) (Sigma). The samples were then dried and stored in a dessicator until examined with SEM (gold coated ~10 nm Au, 5-10 kV). It was observed that HMDS was possibly damaging the coatings by dissolving the lipids (i.e., cholesterol) on the samples, therefore this step was skipped for week 2 of the follow-up study, and replaced by a second ethanol bath. Samples were then vacuum dried overnight and stored in a dessicator until examined with SEM. Refer to *Results and Discussion* below for more details.

### **7.4.2 Osseogenic Differentiation, Mineralization and Matrix Production**

---

Total intracellular protein, calcium and alkaline phosphatase activity levels are indicators of mineralization and extracellular matrix production and were therefore measured to assess osteoinduction and osseointegration potential of these coatings. All

tests were single time point tests performed weekly up to week 3 on all treatments (three weeks in preliminary study, 2 weeks in follow-up study).

#### **7.4.2.1 Total Protein Assay**

The BCA total protein assay was completed in accordance with the *BCA Total Protein Assay Protocol* provided in Appendix C. Briefly, samples were first rinsed in PBS to remove non-adherent cells. Remaining cells (which remained adherent) were lysed, in accordance with the *Cell Lysis Protocol* provided in Appendix C, by shaking in a standard cell lysis reagent (Cell Lytic) (Sigma). A commercially available BCA Protein assay kit (Pierce, Thermo-Scientific) was then used to quantify total protein concentration in the cell lysate. Certain compounds, such as phospholipids, interfere with the color development in the BCA assay, tending to overestimate results. [233] To overcome this interference, 2% sodium dodecyl sulfate (SDS) was added to the reagent as described by Morton. [233]

A standards curve was created using nine graduated concentrations of bovine serum albumin (BSA), according to the vendor-supplied product insert.

A working reagent was produced by mixing two vendor-supplied reagents, one containing sodium carbonate, sodium bicarbonate, bicinchoninic acid and sodium tartrate in sodium hydroxide, mixed 50:1 with the other containing cupric sulfate.

Standards and samples were plated onto one or more 96-well plates, agitated briefly and incubated at 37°C for 30 minutes, then cooled for 20 minutes and read on a plate reader at 562 nm absorbance. Standard curves matched kit specifications. Blank controls were included in each plate to enable compensation for inter-plate variability. The conversion algorithm was checked against standard values to certify correctness. Assays

were performed immediately upon plating, and within ten minutes of each other, because after cooling samples to room temperature, the blanks continue to increase in absorbance at approximately 2.3% every 10 minutes.

Discussion of interpretation of results and advantages/disadvantages of this assay is found in section 7.9 below.

#### **7.4.2.2 Calcium Assay**

Intra- and extracellular calcium were measured using commercially available calcium assay kits. Similar assay kits from different vendors were used in the preliminary study (BioAssay Systems Quantichrome) and in the follow-up study (Pointe Scientific). The procedures for using these kits vary slightly, as detailed in the *Calcium Assay-BioAssay* and *Calcium Assay-Pointe Protocols* provided in Appendix C. The most significant difference is that in the BioAssay Systems kit, calcium concentration is calculated from a standard curve, while in the Pointe Scientific kit it is calculated from the formula:

$$\text{Calcium (mg/dl)} = \text{ABS}_U / \text{ABS}_S \times [\text{STD}]$$

Where  $\text{ABS}_U$  is the Absorbance of the Unknown sample,  $\text{ABS}_S$  is the Absorbance of the Standard and  $[\text{STD}]$  is the calcium concentration of the Standard.

In brief, the procedure used for the calcium assays is as follows. Calcium bearing samples were first bathed in a 6N HCL solution for 2 hours to dissolve calcium into solution. Working reagents were created from reagents supplied in the assay kits, and pipetted into one or more 96-well plates (at 200  $\mu\text{l}$ /well). Standard calibrator solution and HCL were pipetted into the first columns of each plate to provide a standard curve. Standard curves were highly linear, consistent with kit specifications. Blank controls were included in each plate to enable compensation for inter-plate variability. Samples were pipetted into all sample wells, and plates were read at 612 nm absorbance for the

BioAssay Systems kit, and 570 nm absorbance for the Pointe Scientific kit, following short incubation periods. Absorbance values were then converted to respective calcium values. The conversion algorithm was checked against standard values to certify correctness. All data were normalized to total protein content (refer to the previous section) to account for variability in cell populations on each sample.

#### **7.4.2.3 Alkaline Phosphatase Assay**

Cytoplasmic ALP was measured at weekly time points in accordance with the *ALP Assay Protocol* provided in Appendix C, up to week 3 after initiation of differentiation media. Briefly, samples were rinsed in PBS to remove non-adherent cells. Remaining adherent cells were lysed in accordance with the *Cell Lysis Protocol* provided in Appendix C by shaking in a standard cell lysis reagent (Cell Lytic) (Sigma) for 20 minutes at room temperature. A commercially available ALP colorimetric assay kit (BioAssay Systems) was used to quantify ALP concentration in the cell lysate. In the assay reaction, ALP catalyzes the reaction of p-nitrophenolphosphate (p-NPP) into p-nitrophenol and phosphate. The resulting p-nitrophenol in the lysate was measured using a spectrophotometer (yellow filtration at 405 nm). The ALP assay is a kinetic study, therefore the reaction at times 0 and 4 minutes were measured and converted to ALP using a formula provided in the assay kit. Blank controls were included in each plate to enable compensation for inter-plate variability.

Standard calibrator solution and de-ionized water were pipetted into the first columns of each plate to provide a standard curve. Standard curves were highly linear, as expected from kit specifications. Blank controls were included in each plate to enable compensation for inter-plate variability. Samples were pipetted into all sample wells and

plates were read at 405 nm absorbance, following short incubation periods. Absorbance values were then converted to respective ALP values using the standard curve. The conversion algorithm was checked against standard values to certify correctness. All data were normalized to total protein content (see section 7.4.2.1 above) to account for variability in cell populations on each sample.

#### **7.4.2.4 Osteocalcin and Osteopontin Immunofluorescence**

Both osteocalcin (OC) and osteopontin (OP) immunofluorescence microscopy imaging were performed on week 2 of the follow-up cell study. OC/OP tests were not performed in the preliminary cell study due to the relatively high cost of these assays, given the delamination of sample coatings as discussed in section 7.2.2 above and in the *Enhancing Coating Retention* chapter.

OC/OP immunofluorescence imaging was performed in accordance with the *OC-OP Immunofluorescence Protocol* found in Appendix C. Briefly, samples were rinsed in PBS, then fixed in formaldehyde and permeabilized in 1 % Triton-X (Sigma). Test samples were then bathed in 10% blocking serum (bovine serum albumin (BSA)) for 30 minutes to prevent nonspecific binding. After rinsing in PBS, the samples were bathed in a mixture containing both osteocalcin primary antibody (1:50)(V-19 purified goat polyclonal antibody) in 2% blocking serum, and osteopontin primary antibody (1:50)(AKm2A1 purified mouse polyclonal antibody) in 2% blocking serum. Following one hour primary antibody incubation, samples were washed three times with PBS (10 minutes each), bathed again in 10% blocking serum (BSA) for 30 minutes, then rinsed again three times with PBS (10 minutes each). Samples were then bathed for 45 minutes in the dark in FITC-labeled secondary antibody for osteocalcin (donkey, anti-goat IgG)

and Texas Red-labeled secondary antibody for osteopontin (chicken, anti-mouse IgG), both 1:200 in 2% blocking serum. Finally, the samples were rinsed in PBS and imaged on a Zeiss Axioplan 2 fluorescence microscope (Carl Zeiss) using 465–495 nm excitation filtration for OC and 540–580 nm for OP. Image-J software ([rsbweb.nih.gov/ij](http://rsbweb.nih.gov/ij)) was used to visualize cell distribution and spatial organization and to quantify approximate cell counts.

## **7.5 Null Assay Tests**

### **7.5.1 Calcium and Total Protein with media but no cells**

Tests were performed to determine whether the BCA Protein Assay or the Calcium Assay used in this study (described in sections 7.4.2.1 and 7.4.2.2 above) measured any significant amounts of protein or calcium, respectively, from samples containing DOPS and DOPS with gentamicin, in the absence of cells. A complete two week in vitro culture study, with weekly time points, including media changes in both culture media and differentiation media, as described above, was performed on samples from both groups, but with no cells seeded onto the samples.

ALP was not measured because this assay measures specifically the conversion of p-nitrophenolphosphate to p-nitrophenol and phosphate, catalyzed by ALP. Since there were no cells, there could not be ALP.

The same commercially available BCA Protein (Pierce, Thermo-Scientific) and Calcium (Pointe Scientific) assay kits were used to quantify total intracellular protein concentration and calcium, respectively, as described in sections 7.4.2.1 and 7.4.2.2 above.

### **7.5.2 Calcium with no media**

---

Because the test samples used in the follow-up study were pretreated with calcium prior to E-spraying, tests were performed to determine the amount of calcium resulting from this pretreatment, exclusive of any influence from cell media. For this testing, the same calcium assay reagent kit (Pointe Scientific) used in the follow-up cell study was again used.

Three samples from each treatment (plain titanium, DOPS, DOPS with GS) were placed in a well plate, 0.5 ml PBS was added to each well, and samples were assayed using the calcium assay described in section 7.4.2.2 above.

## **7.6 Non-Specific Fluorescence (NSF) Test**

Some substances are known to cause spontaneous, non-specific fluorescence (NSF), sometimes autofluorescence, of the calcein and ethidium-homodimer-1 stains used in this project. Some of the fluorescent images developed in this study exhibited this behavior. Therefore a test was performed to determine which of the compounds used in this study might play a role in NSF.

Three samples from each treatment (plain titanium, DOPS, DOPS with GS) were stained with calcein and ethidium-homodimer-1 and examined by fluorescent microscopy imaging. These samples were not seeded with cells.

## **7.7 Statistical Analysis**

Statistical analysis was performed using SigmaStat version 11.2, the latest version from Systat Software Inc. Significance testing was performed at  $p < 0.05$  unless otherwise indicated. All the results were analyzed using Student's T-tests to two-treatment comparisons and one-way analysis of variance (ANOVA) for multi-treatment

comparisons. The Shapiro-Wilk normality test was performed on all treatments, and the Mann-Whitney Rank Sum test was used on all comparisons with unequal variance.

Dunn's test for rank-ordered significance was applied to adjust for multiple comparisons with unequal sample numbers, for example, if a sample was lost to experimental error.

## ***7.8 Results and Discussion***

### ***7.8.1 Preliminary Cell Study Results***

---

#### ***7.8.1.1 General Observations***

Details of all experiments are provided in the following sections, but some initial general observations can be made. In general, if a coating remained on a sample, cells that populated that coating appeared to proliferate and adhere to the coating normally through the time the coating remained intact, e.g. up to day seven (post-seeding) they deposited extensive networks of ECM-like material (evidence provided below) and grew substantial filopodia which often extended well into the coating substrate. Filopodia are extensions on the leading edge of migrating cells that form focal adhesions to the substrate. This indicates the cells were healthy and adhering to the coating and a positive response in general to the DOPS coating not seen in other coatings.

Thereafter, if the coating survived into the differentiation phase (post day 7), the cells appeared to participate in the mineralization and matrix production processes, as would be expected of osteoblasts, e.g. increases in intracellular calcium levels, presence of osteocalcin and osteopontin. These tests are described in detail in the following sections.

Coatings appeared to soften and appear whitish and “puffy” in the initial 4 hours, an indication of swelling of the coating. Some coatings appeared to degrade considerably in the initial 4 to 6 days, many by day 7 (post-seeding); most by day 14. Large flakes of

coating material (relative to the size of the sample surface) were sometimes seen suspended in the media of a particular well. Sometimes whole coatings in a single sheet of comparable size and shape of the sample it came from had disassociated from samples. Despite the apparent swelling that occurs, we consider this surface degradation to be delamination versus other forms of material degradation, such as dissolution or bulk erosion, because when the material leaves the surface, it does so as relatively large (in proportion to the total surface) flakes, not small (or microscopic) particles. Furthermore, where coating material has delaminated from the plain titanium substrate, the substrate is clearly visible. There is no evidence of any coating remaining in any form in these regions, indicating that the complete thickness of the coating has wholly dissociated.

Fewer coatings with DOPS/GS degraded than coatings without GS. On all samples containing GS in their coatings, white-shaded circular regions were clearly visible where the GS was applied to the coatings. These regions were generally present for the entire length of the study.

#### **7.8.1.2 Cell Adhesion, Proliferation & Organization (Preliminary Study)**

Cell adhesion and proliferation are important measures of cellular contact and interaction, which play critical roles in early stage bone development. Strong attachment to the substrate is one of the primary factors in successful spreading and differentiation of MSCs. Cellular adhesion and proliferation were investigated on the three test treatments by live cell imaging and SEM, and confirmed by evaluating cell viability.

As discussed in section 7.4.1.1 above, calcein-AM stain was used to stain live cells, and occasionally ethidium homodimer-1 (EthD-1) was also used to evaluate relative cell death. Cells with intact cell membranes are able to use nonspecific cytosolic esterases to

convert non-fluorescent calcein-AM into bright green-fluorescent calcein. EthD-1 enters cells with damaged membranes and binds to nucleic acids, thereby producing a bright red fluorescence in dead cells. EthD-1 is excluded by the intact plasma membrane of live cells.

The following images show day 1 (post-seeding), live-stained (calcein) cells for each treatment (all 10x original magnification). EthD-1 stained images are not shown as they were only used to evaluate relative cell death, which was not seen.

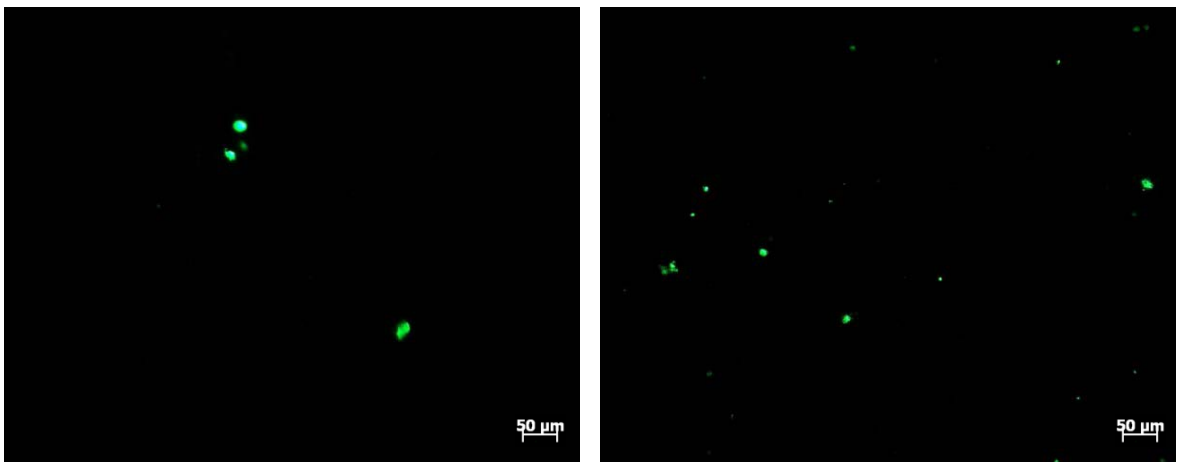


*Figure 7-1 & 7-2: Calcein (live) stain images of cells on **plain titanium** (no coating), day 1 post-seeding, 10x original magnification.*

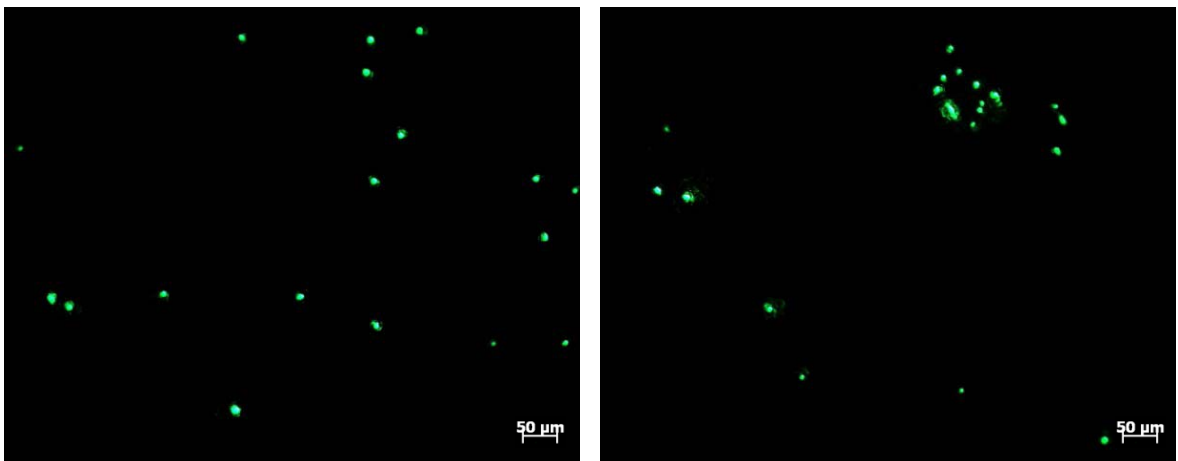


*Figure 7-3 & 7-4: Calcein (live) stain images of cells on **DOPS coating**, day 1 post-seeding, 10x original magnification.*

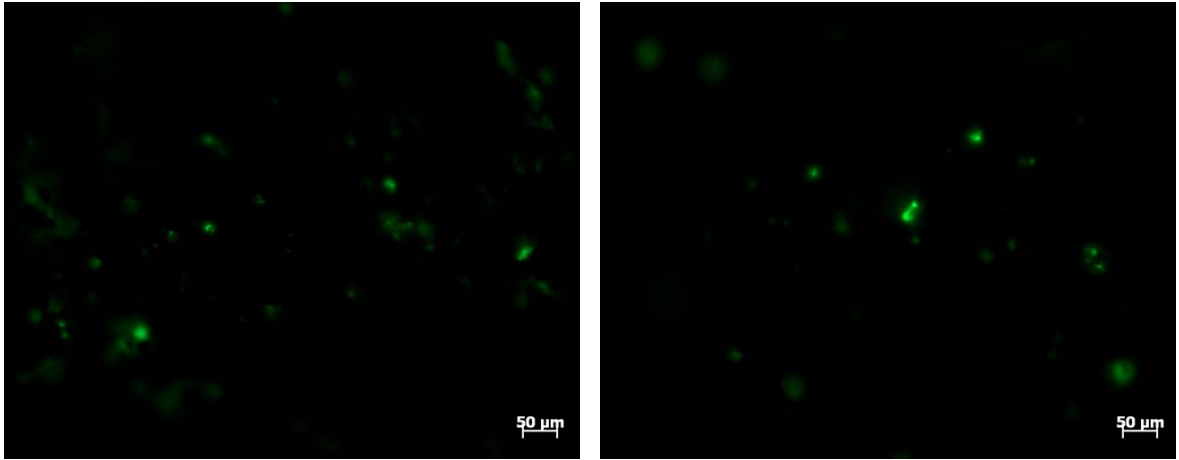


Figure 7-5 & 7-6: Calcein (live) stain images of cells on **DOPS with gentamicin**, day 1 post-seeding, 10x original magnification.

The following images show day 4 (post-seeding), live-stained (calcein) cells for each treatment (all 10x original magnification).

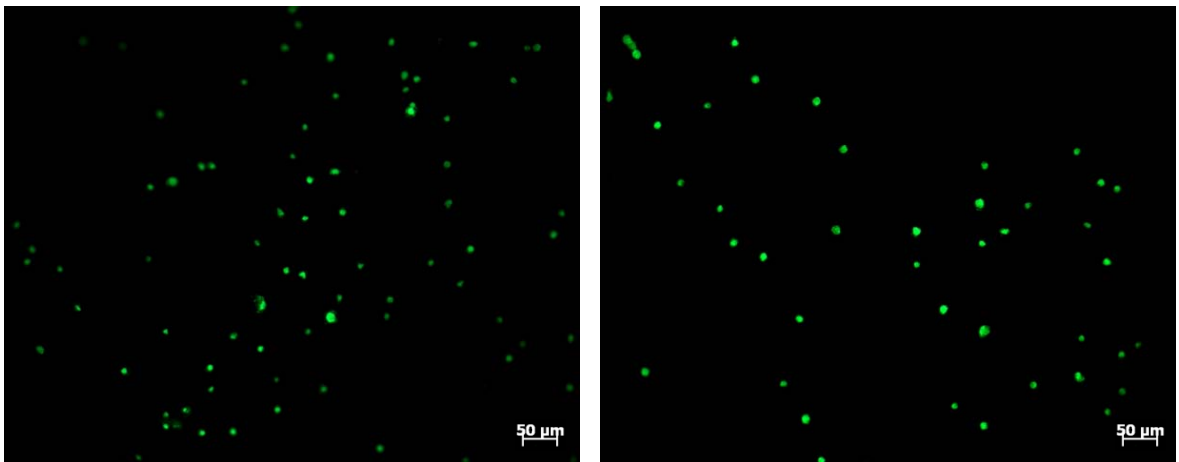


Figure 7-7 & 7-8: Calcein (live) stain images of cells on **plain titanium** (no coating), day 4 post-seeding, 10x original magnification.

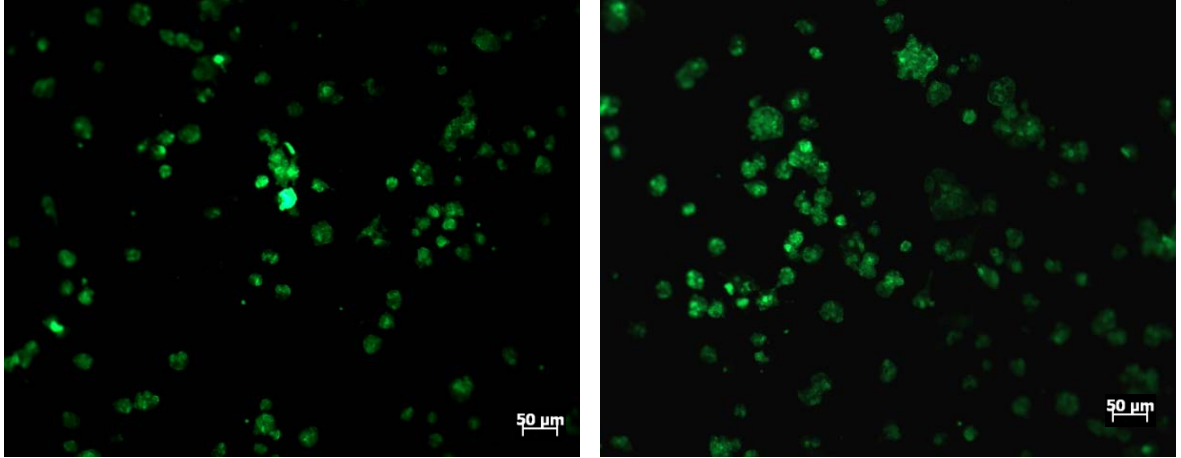


Figure 7-9 & 7-10: Calcein (live) stain images of cells on **DOPS coating**, day 4 post-seeding, 10x original magnification.

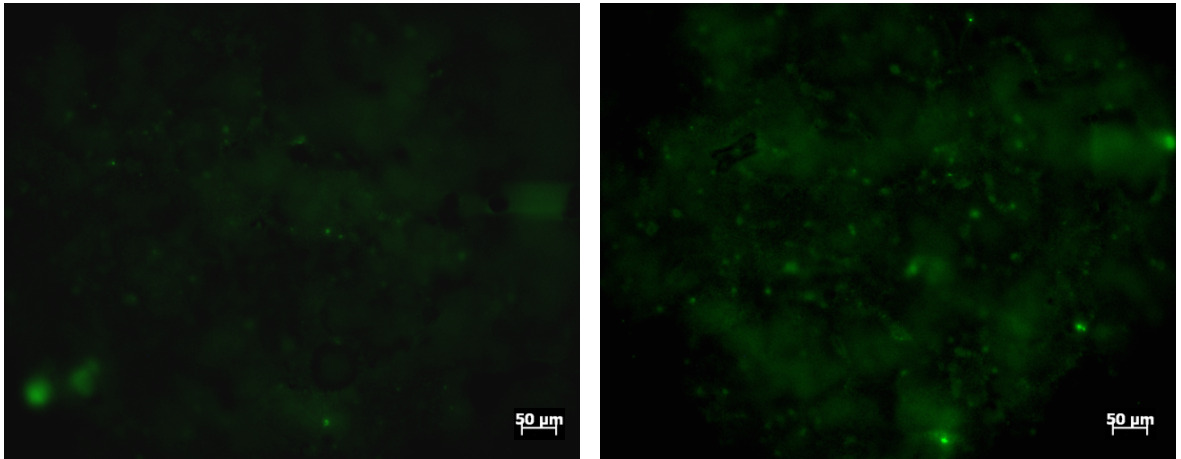


Figure 7-11 & Figure 7-12: Calcein (live) stain images of cells on **DOPS with gentamicin**, day 4 post-seeding, 10x original magnification. Note significant NSF makes it very difficult to discern cells.

The following images show day 7 (post-seeding), live-stained (calcein) cells for each treatment (all 10x original magnification).

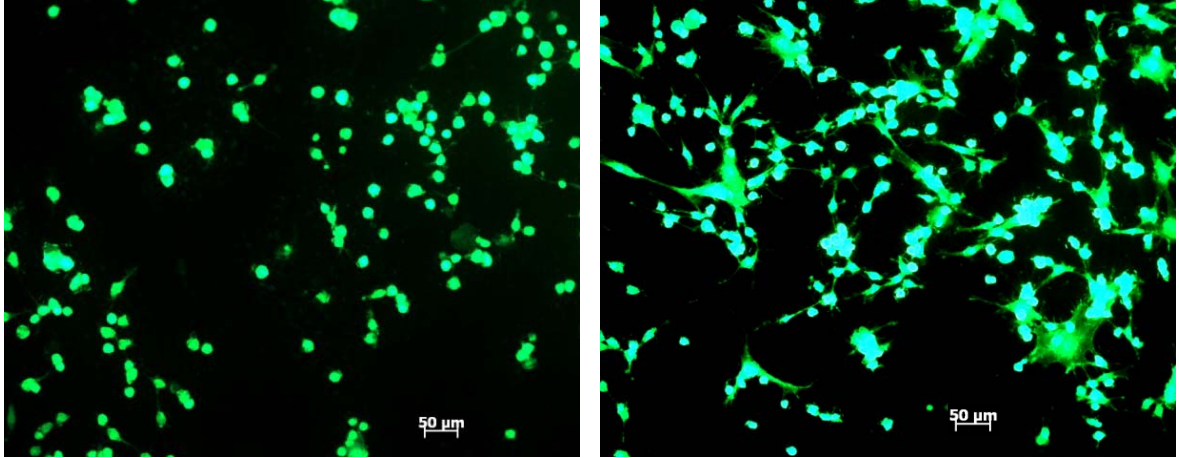


Figure 7-13 & 7-14: Calcein (live) stain images of cells on **plain titanium** (no coating), day 7 post-seeding, 10x original magnification.

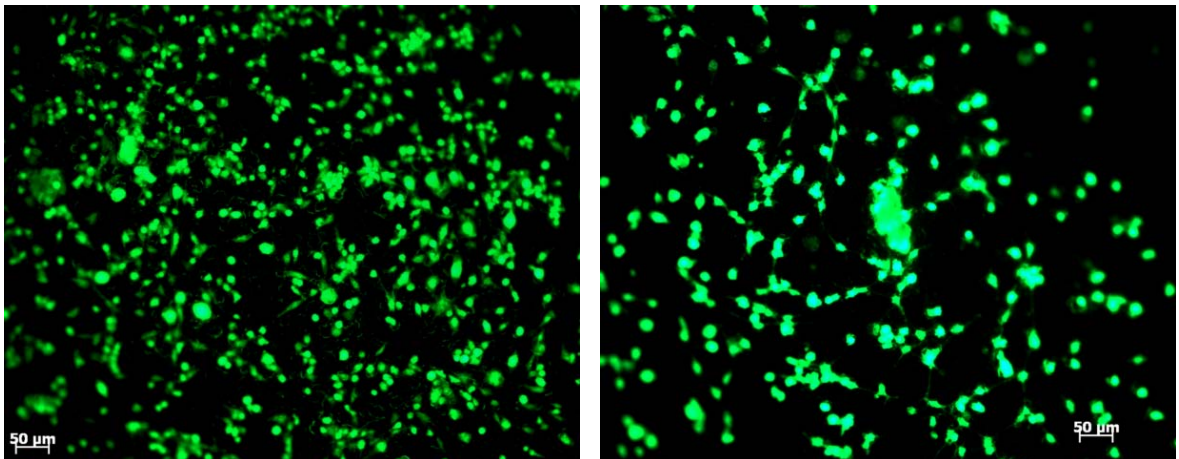


Figure 7-15 & 7-16: Calcein (live) stain images of cells on **DOPS coating**, day 7 post-seeding, 10x original magnification.

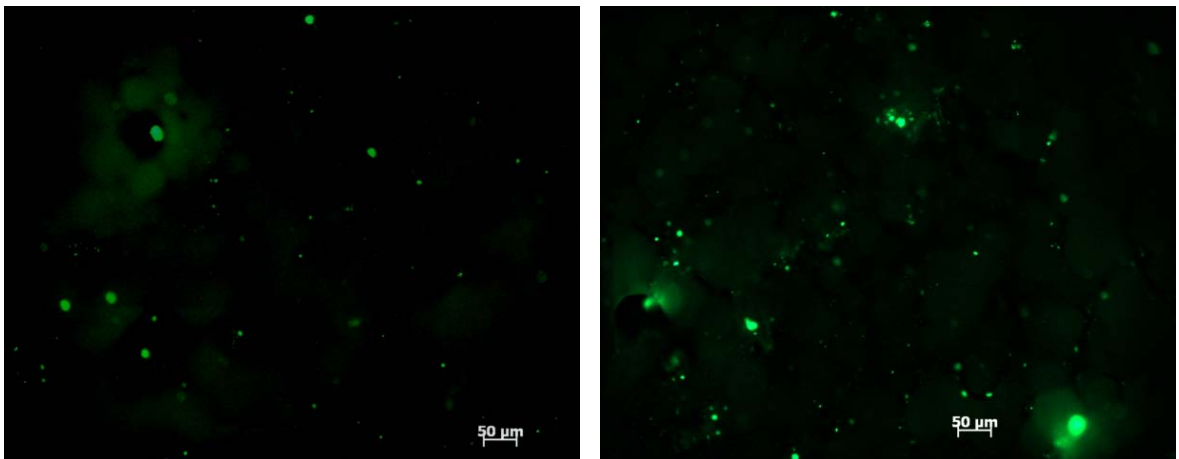


Figure 7-17 & 7-18: Calcein (live) stain images of cells on **DOPS with gentamicin**, day 7 post-seeding, 10x original magnification. Note significant NSF makes it difficult to discern cells.

Cells on day 1 appear normal for this time point. Cell morphology is compact and spherical, typical of cells at this early stage of adhesion. Population densities are sparse. Little indication of adhesion is visible, as would be expected. And there is no indication of aggregation of cells at this early time point.

NSF makes it very difficult to discern cells in DOPS/GS images. Figures showing coatings with GS present were filtered to various extents using the Image-J software ([rsbweb.nih.gov/ij](http://rsbweb.nih.gov/ij)) to reduce the masking effects of NSF that are discussed in more detail in section 7.8.2.3 below.

Starting on day 4, spreading, aggregation and cellular filopodia become visible on DOPS coatings. On day 7, significant spreading and aggregation are now apparent in cells on Plain Ti. More cells were visible on DOPS coated surfaces, also with clearly visible spreading and aggregation. Filopodia were clearly visible on both Plain Ti and DOPS coated surfaces, indicating cells on these coatings were maturing, proliferating and adhering to the substrate. Cells on DOPS coatings with gentamicin show no indication of aggregation, nor were they showing signs of filopodial extensions which would suggest attachment to the substrate. This suggests cells on DOPS/GS were not as healthy as those on Plain Ti or DOPS coated surfaces.

### **7.8.1.3 Cell Viability (Preliminary Study)**

MTT is a commercial colorimetric assay that assesses the short-term viability of the cells by measuring the activity of mitochondrial dehydrogenase, which reduces the MTT reagent to purple formazan crystals, producing a purple color. [234] This transformation only occurs when reductase enzymes are metabolically active, i.e. in cells that are alive

and productive, and is useful to determine cytotoxicity of chemical and other agents which may cause cell toxicity and related metabolic dysfunction.

MTT shows levels of metabolic activity and how the cell are proliferating, but does not show how the cells may or may not be adhering or organizing themselves. Thus it is useful to perform MTT in combination with live cell fluorescence microscopy imaging.

Mitochondrial dehydrogenases of viable cells cleave the tetrazolium ring of the MTT compound, yielding purple MTT formazan crystals. Formazan crystals were then dissolved in MTT solvent. The optical density (absorbance) of the resulting solvent is proportional to mitochondrial activity of the cells on the samples.

Figure 7-19 below shows MTT results for days 1 and 4 of the study. On day one, none of the differences were significant ( $p < 0.05$ ). This is typical of the first day after seeding in a MSC cell study. Although not significantly higher, the data shows a slight tendency for these cells to prefer DOPS and DOPS/GS over Plain Ti surfaces.

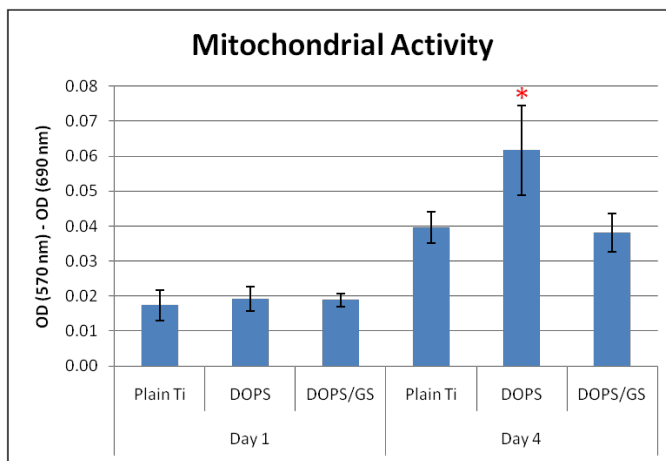


*Figure 7-19: Mitochondrial activity, day 4 in culture, cell viability on DOPS surfaces is significantly greater than on Plain Ti or DOPS/GS ( $p < 0.05$ )*

On day 4, cell viability on DOPS surfaces is significantly greater ( $p < 0.05$ ) than on Plain Ti or DOPS/GS, consistent with other published reports. [23, 26, 235]

The increasing variances seen on day 4 may be an early indication of the as-yet unknown erosion/delamination of coating that was about to become a challenge for this study, as discussed in the following section.

#### **7.8.1.4 Qualitative Cell Morphology (Preliminary Study)**

SEM is a powerful tool for associating observations and potential changes in cell morphology with bone biology and chemistry. The following SEM images were taken at day 7 (post-seeding) and all weekly time points to visualize the morphological changes that took place in the cells on all test samples.

For SEM images of control samples, Plain Ti, DOPS, and DOPS/GS, refer to the *E-Spray Study* chapter.

The following images show day 7 (post-seeding) SEM images for all treatments.

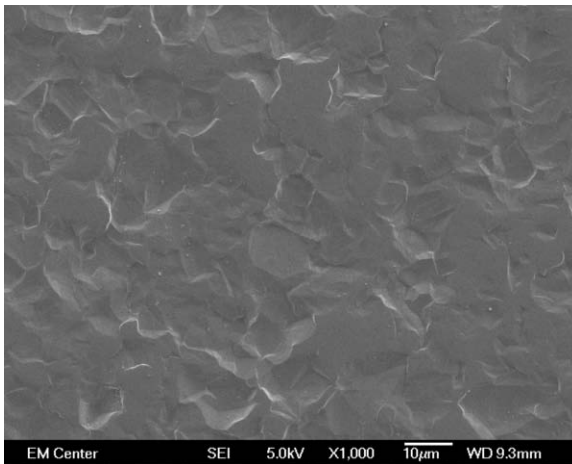


*Figure 7-20: SEM image of Plain Ti day 7, imaged at 5 kV, 1000X original magnification. No cells are visible.*

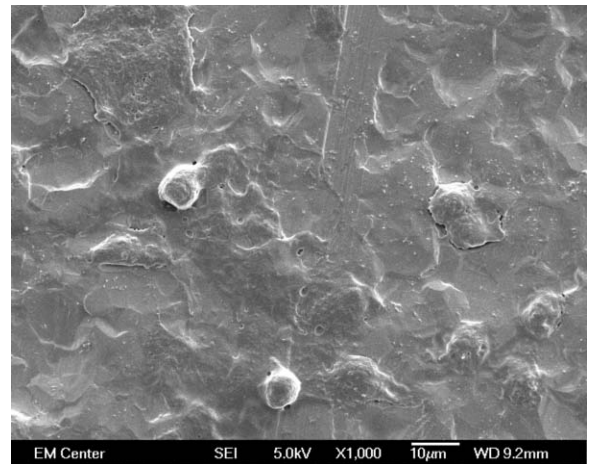


*Figure 7-21: SEM image of DOPS day 7, imaged at 5 kV, 1000X original magnification. Absence of cells may indicate coating has degraded*

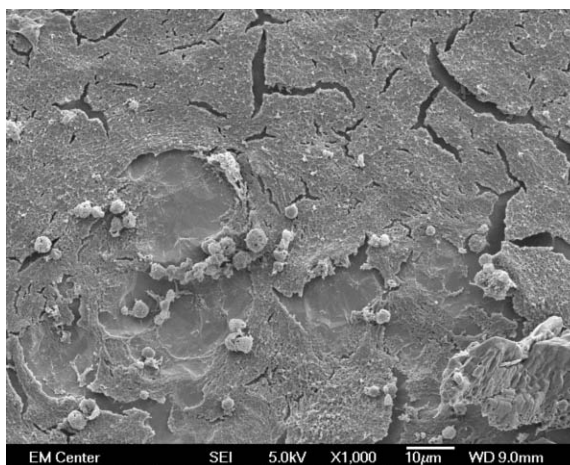
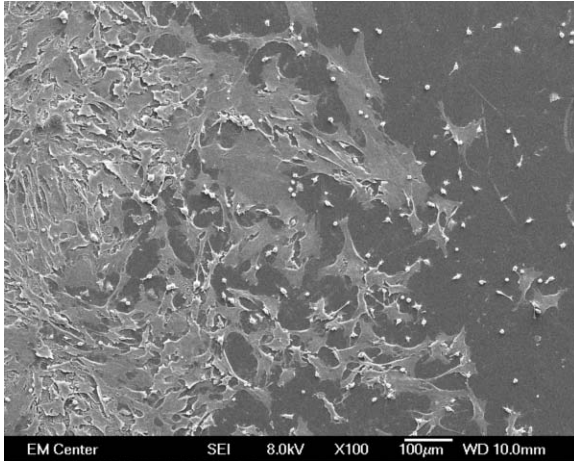


Figure 7-22: SEM image of *DOPS/GS* day 7, imaged at 5 kV, 1000X original magnification.

In these images of day 7 (i.e. 7 days after cells were seeded) samples, it can be seen that there were no cells present on the Plain Ti (Figure 7-20) or DOPS-coated (Figure 7-21) samples. The DOPS coating has nearly completely degraded and plain titanium substrate is visible in many areas. There were three samples dedicated to SEM for each time point. Because most coatings began delaminating and degrading at day 7, many of these samples did not show cells. Indeed there were little or no coatings on any of the day 7 DOPS samples. To the contrary, the DOPS/GS coating (Figure 7-22) appears to be relatively more intact, as discussed in the *E-Spray Study* chapter. The GS SEM image shows a substantial amount of extra-cellular matrix (ECM) and notable cell presence, but cells have a compact morphology, suggesting they were not spreading and adhering to the GS coating as they normally should. This is an early indication that these cells do not prefer the GS coating. Cells were clustering around topographic features, which is typical spreading behavior for MSCs. Without normal spreading, migration and adherence, cellular communication falters and normal development, differentiation and participation in biomineralization and osseogenic processes are unlikely to proceed.

The following images show week 1 (2 weeks post-seeding, one week post-differentiation, i.e. one week after differentiation to osteoblasts began) SEM images for all treatments.



*Figure 7-23: SEM image of TCPS week 1, imaged at 8 kV, 100X original magnification. Significant cell proliferation is visible.*

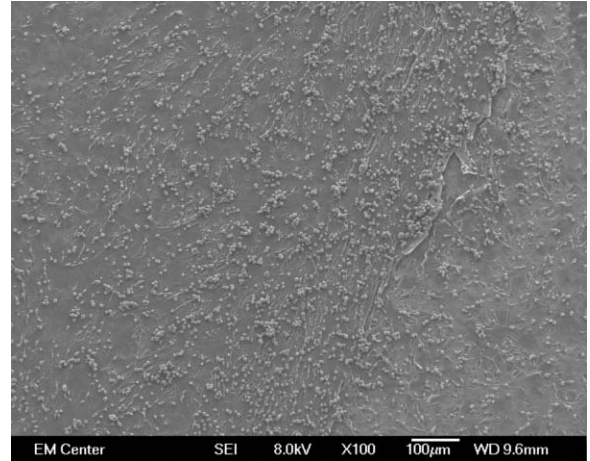


*Figure 7-24: SEM image of Plain Ti week 1, imaged at 8 kV, 100X original magnification. Dense proliferation of cells is visible.*

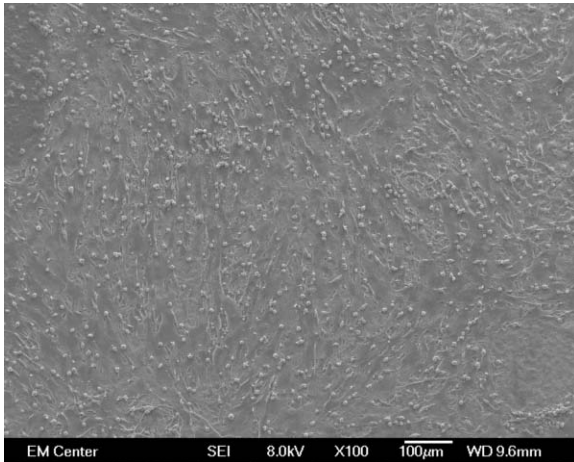


*Figure 7-25: SEM image of DOPS week 1, imaged at 8 kV, 100X original magnification. Significant cell proliferation is visible, broadly across sample surface.*

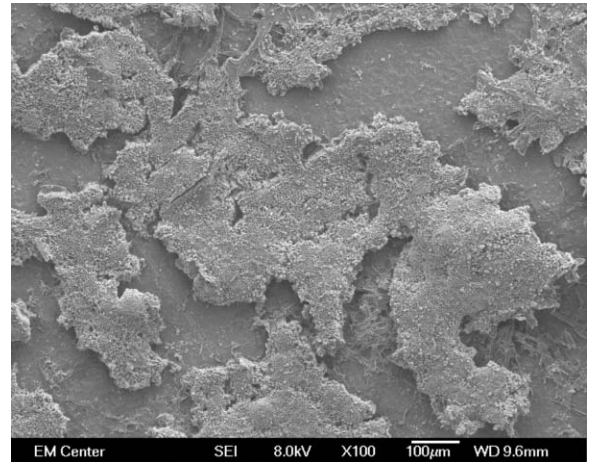


*Figure 7-26: SEM image of GS week 1, imaged at 8 kV, 100X original magnification. Degradation of coating is visible, but dense proliferation of cells, moreso on coating that remains.*

These images show significant cell growth when the coatings remain intact. Cells on the DOPS coating (Figure 7-25) appear to be spreading more than cells on either of the Plain Ti (Figure 7-24) or GS coatings (Figure 7-26), indicating normal development,

differentiation and participation in biomineralization and osseogenic processes. The following images provide higher magnification for better cell characterization.

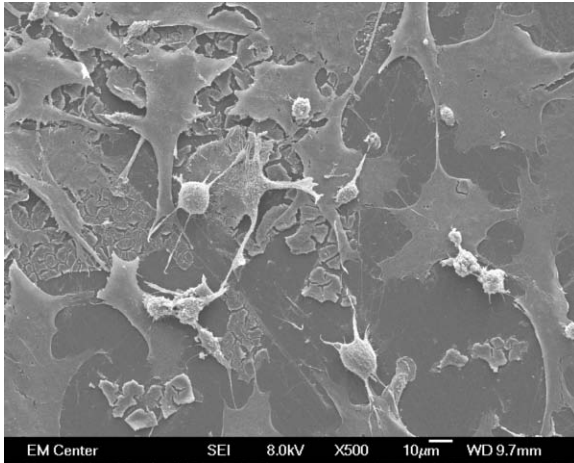


*Figure 7-27: SEM image of **TCPS week 1**, imaged at 8 kV, 500X original magnification. Filopodia are clearly visible - cells are adhering and migrating.*

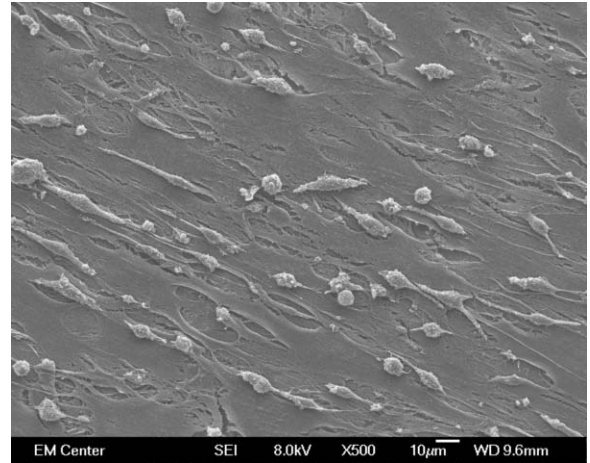


*Figure 7-28: SEM image of **Plain Ti week 1**, imaged at 8 kV, 500X original magnification.*

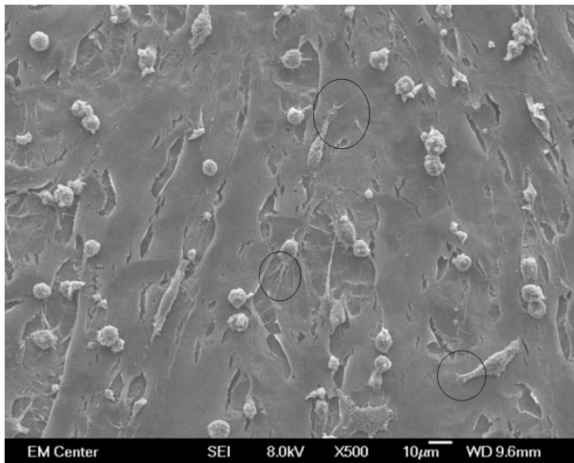


*Figure 7-29: SEM image of **DOPS week 1**, imaged at 8 kV, 500X original magnification. Filopodia are visible (circled) – cells are adhering and migrating.*

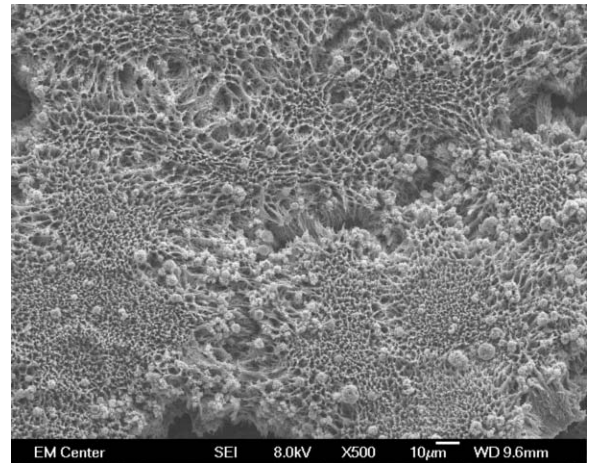


*Figure 7-30: SEM image of **GS week 1**, imaged at 8 kV, 500X original magnification. GS coating has very different morphology.*

In these 500x images, it can be seen on all samples that cells appear to be spreading and adhering normally. At these higher magnifications, extensive networks of filopodia can be seen woven into the ECM on the Plain Ti sample (Figure 7-28), and on the DOPS coatings, as circled in Figure 7-29. Filopodia extend sometimes many times the length of the cell, deeply into the coating and in many places appear to be completely integrated into the coating. The cells on DOPS and Plain Ti samples have larger, longer filopodia,

and the ECM network is extensive and intricately laced over the entire coating. Conversely, cells on GS exhibit a rounded morphology (Figure 7-30), with few visible extensions and little visible ECM, suggesting these cells were neither adhering nor interacting normally. Cells on DOPS, Plain Ti and TCPS coatings exhibit indications of spreading, migration, aggregation and interaction, behaviors prerequisite to enhanced differentiation on a long-term scale. It appears these activities were slightly more prevalent on DOPS coatings than Plain Ti and approximately the same as on TCPS.

The following images show week 2 (3 weeks post-seeding, two weeks post-differentiation) SEM images for all treatments (TCPS images are left out due to similarity to other coatings).

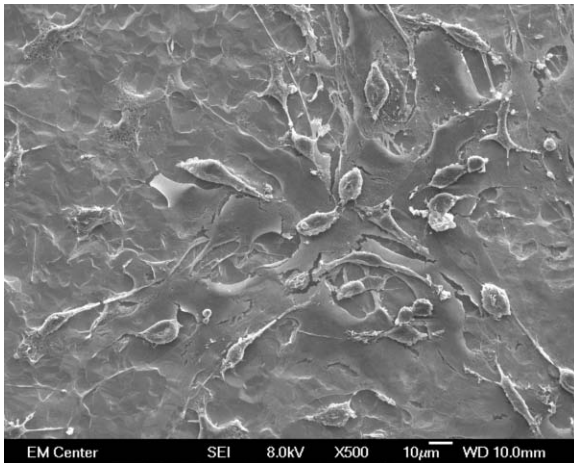


*Figure 7-31: SEM image of Plain Ti week 2, imaged at 8 kV, 500X original magnification. Few cells can be seen.*

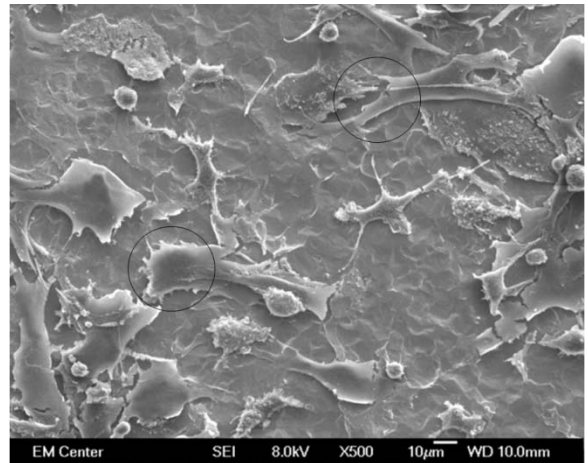


*Figure 7-32: SEM image of DOPS week 2, imaged at 8 kV, 500X original magnification. Coating has apparently delaminated, some ECM but few cells remain.*

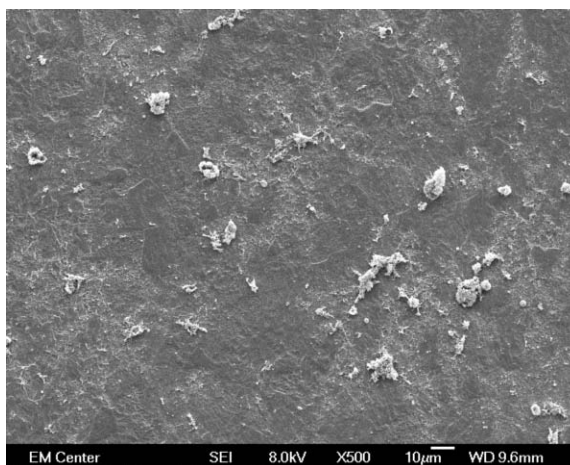


*Figure 7-33: SEM image of DOPS/GS week 2, imaged at 8 kV, 500X original magnification. Coating has apparently delaminated, no cells remain.*

Week 2 (three weeks post-seeding, 2 weeks post-differentiation) reveal thin coatings on Plain Ti and DOPS (Figure 7-31 and Figure 7-32). The titanium substrate is now clearly the predominant visible surface. This is possibly due to erosion, or the coatings were in the process of delaminating. ECM is clearly visible, particularly in the DOPS coatings (refer to circular indications in Figure 7-32 above), as are filopodia, although to a lesser extent than previous (week 1) images. No cells were found on the GS coating (Figure 7-33). This may suggest the GS coating had already delaminated.

The following images show week 3 (4 weeks post-seeding, three weeks post-differentiation) SEM images for all treatments (TCPS images are left out due to similarity to other coatings).

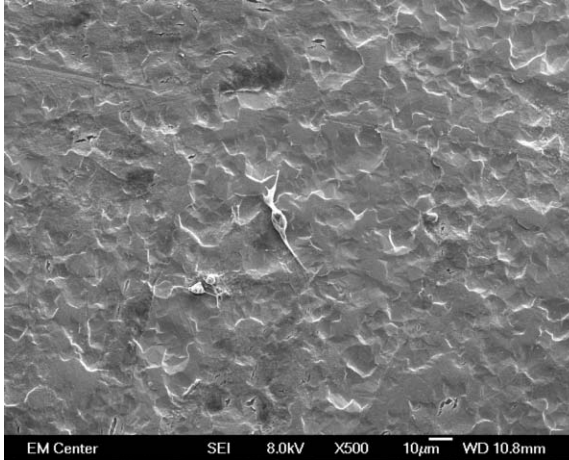


*Figure 7-34: SEM image of Plain Ti week 3, imaged at 8 kV, 500X original magnification. A single cell has re-adhered.*

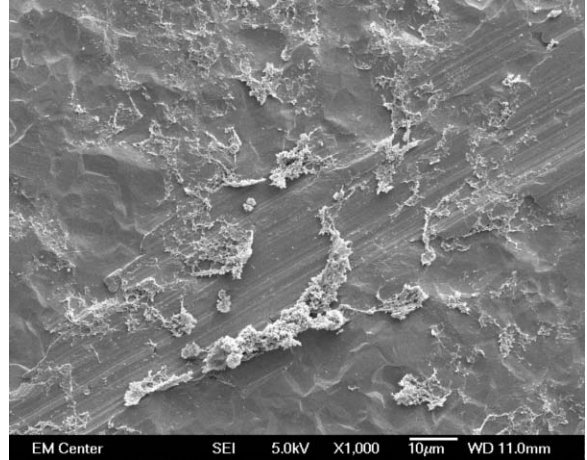


*Figure 7-35: SEM image of DOPS week 3, imaged at 8 kV, 1000X original magnification. Coating has delaminated. No cells are visible.*

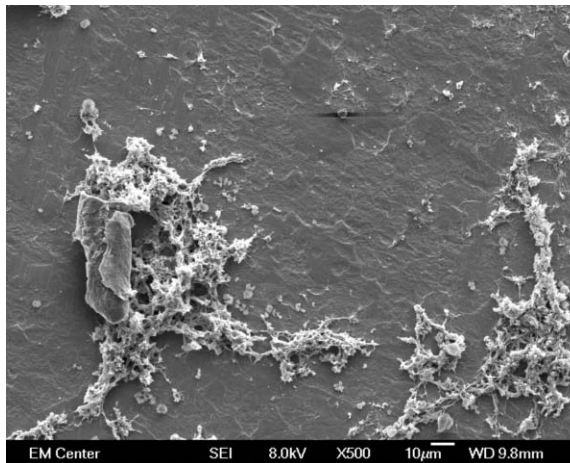


*Figure 7-36: SEM image of DOPS/GS day 7, imaged at 8 kV, 500X original magnification. Remainder of DOPS/GS coating is visible.*

By week 3 (four weeks post-seeding, 3 weeks post-differentiation) all coatings have delaminated or otherwise completely degraded. The only remaining clue of cells is the single cell in the Plain Ti image (Figure 7-34), the remainder of material that appears to be a once extensive carpet of ECM in the DOPS image (Figure 7-35), and the remainder of what appears to be the GS coating infrastructure in the GS image (Figure 7-36).

The lack of cells is likely due to coating erosion or delamination or some other unknown cause. It is possible the fixation process used to prepare samples for SEM (section 7.4.1.3 above) may have damaged the coatings. Coatings from day 1 appear

normal, but all others appear to have been eroded, delaminated or damaged.

Alternatively, it is possible but unlikely that some of the samples could have been reaching or exceeding ideal confluence. This seems to be validated by the day 7 and week 1 SEM images. If this is indeed the case, cell-cell interactions could be hampered and cells would not grow as well. Differentiation would then be affected as the cells would potentially not be as healthy as would be ideal, as they shift their energy from proliferation to bone production. However, it would be expected that some cells would be present if this was the outcome.

These SEM images over time appear to validate the live stain images presented earlier – cell growth was higher on DOPS samples than on Plain Ti or GS.

#### **7.8.1.5 Total Protein Content (Preliminary Study)**

Total intracellular protein content found in osteoblasts growing on the test surfaces is an important indicator of healthy growth and normal response to the surfaces. It is also used to normalize the following ALP and calcium results (described below) to total protein to determine ALP and calcium activity per cell (technically, per total protein). This helps determine, for example, whether observed cellular activity results from more cells producing less ALP/Ca, or fewer cells producing the same or more ALP/Ca.

The BCA (bicinchoninic acid) assay [236] is widely used for measuring total intracellular protein. This assay utilizes the sodium salt of bicinchoninic acid, a highly specific chromophore for copper, to generate a colored complex between peptide bonds in the protein and copper atoms, when the protein is placed in an alkaline environment containing  $\text{Cu}^{2+}$ .

Our use of this assay and interpretation of results is discussed further in section 7.9 below. The following Figure 7-37 shows the measured total intracellular protein for all weeks.

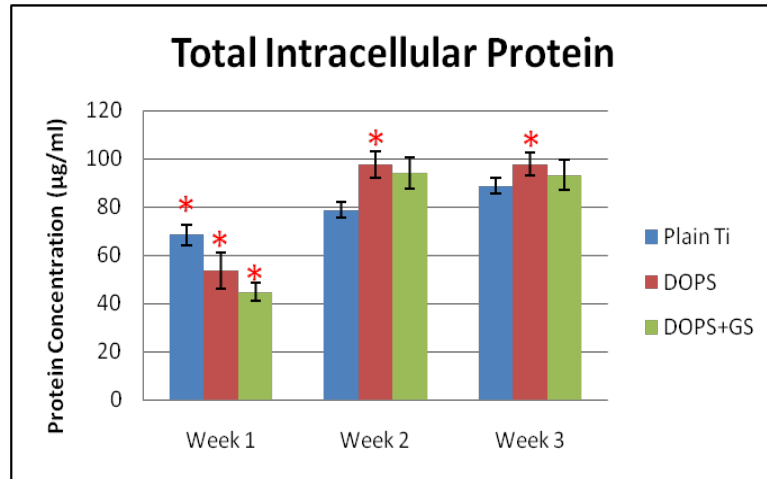


Figure 7-37: Total Protein, all weeks, all values significantly different ( $p < 0.05$ ) week 1, Plain vs DOPS and Plain vs GS significantly different week 2, and Plain vs DOPS significantly different week 3.

In week 1, all treatments elicit a significantly different ( $p < 0.05$  unless otherwise specified) amount of intracellular protein. In week 2, Plain Ti and DOPS samples were significantly different, as were Plain Ti and GS samples. In week 3, Plain Ti and DOPS were significantly different.

These results correlate well with the previously presented live cell staining and SEM imaging results. Cells proliferated better on DOPS coatings than on Plain Ti or GS coatings. Week 3 results would likely have been higher if many of the coatings had not delaminated.

#### 7.8.1.6 Osseogenic Differentiation (Preliminary Study)

Alkaline phosphatase (ALP) is an enzyme responsible for removing phosphate groups from many types of molecules. It catalyzes the hydrolysis of phosphate esters, which is an important step for hydroxyapatite formation, a precursor to normal bone formation.

ALP is found throughout the mammalian body, but is especially concentrated in liver and

bone, where it is produced by healthy osteoblasts, making it an effective osteoblast viability marker. [237] ALP plays a key role in development of matrix vesicles in the process of bone mineralization by regulating the development of hydroxyapatite crystals on ECM. [238] The following chart presents total ALP for all treatments for all weeks.

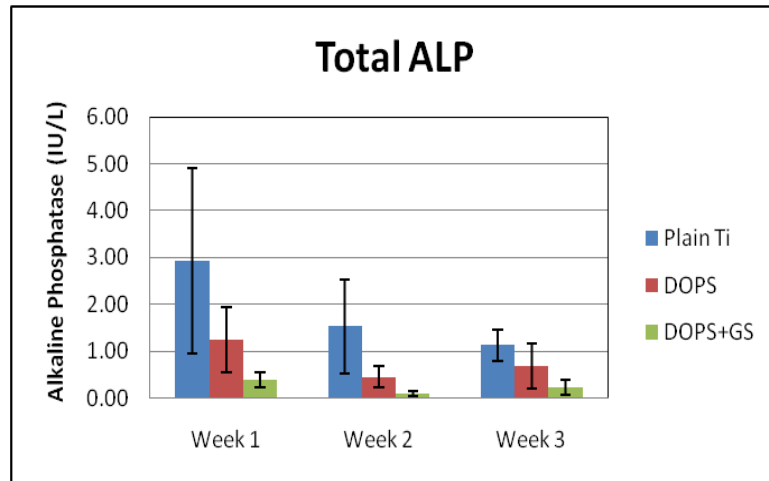


Figure 7-38: Total ALP, all weeks

There were no significant differences ( $p < 0.05$ ) in total ALP among the treatments, due to high variance among samples. The following chart presents total ALP normalized for total intracellular protein, for all treatments for all weeks.

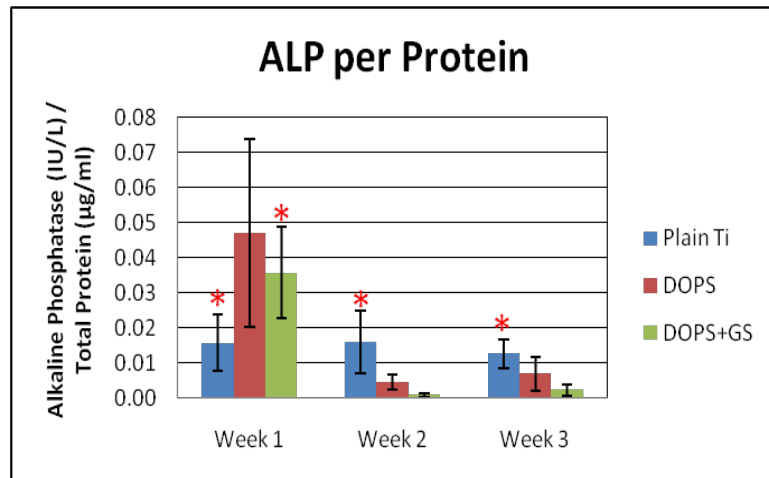


Figure 7-39: ALP per total intracellular protein, all weeks

In week 1, Plain Ti is significantly different ( $p < 0.05$ ) from DOPS/GS and DOPS is significantly different from DOPS/GS. In weeks 2 and 3, all treatments were significantly different from all other treatments in a given week.

As discussed in section 7.4.2.3 above, ALP values were normalized for total intracellular protein to account for variations in cell populations between both samples and treatments. Two factors play a role in the decreasing ALP values seen in our study. Fluctuations in ALP are a natural occurrence resulting from its role as an early transient biomarker for the onset of the differentiation process, which points to elevated values in earlier time points and lower values in later time points. [239] By week 3, ALP is typically down-regulated as osteoblasts mature.

The ALP assay used was not expected to indicate the presence of phospholipid coatings, despite the presence of the phosphate groups in phospholipids, because ALP catalyzes the pNPP reaction discussed in section 7.4.2.3 above. However, for extra precaution, additional tests were performed on additional samples with the same treatments, but with no cells.

ALP levels fluctuate with the age of the cell, with levels generally higher during the initial period of active osteoinduction and then decreasing with time. In addition, as discussed elsewhere, these coatings were delaminating. Fewer coated samples translates into fewer samples at week 1 from which measurements were taken. The coatings degraded more in the later weeks of the study than in the earlier time points, at the same time when ALP might normally be decreasing. This could further decrease the ALP measured in later time points.

### 7.8.1.7 Mineralization (Preliminary Study)

Normal, healthy biomineralization is indicated by production and adherence of matrix vesicles containing calcium. As discussed in *Background*, presence of calcium indicates the formation of matrix vesicles, which act as primary nucleation sites for future hydroxyapatite formation on an implant surface. Therefore, it is useful to evaluate intra- and extracellular calcium in order to assess biomineralization activity of cells.

The calcium assay kits used in the preliminary study (BioAssay Systems Quantichrome) detects calcium deposition by osseogenic cells through the interaction of calcium with suitable chromogenic agents. The BioAssay kit uses a phenolsulphonophthalein dye to form a stable blue colored complex specifically in the presence of free calcium. [240] The intensity of the color, measured at 612 nm, is directly proportional to the calcium concentration in the sample. The minimum accuracy of this assay is reported by the vendor to be  $\pm 0.08$  mg/dl calcium. The following chart presents total calcium for all treatments for all weeks.

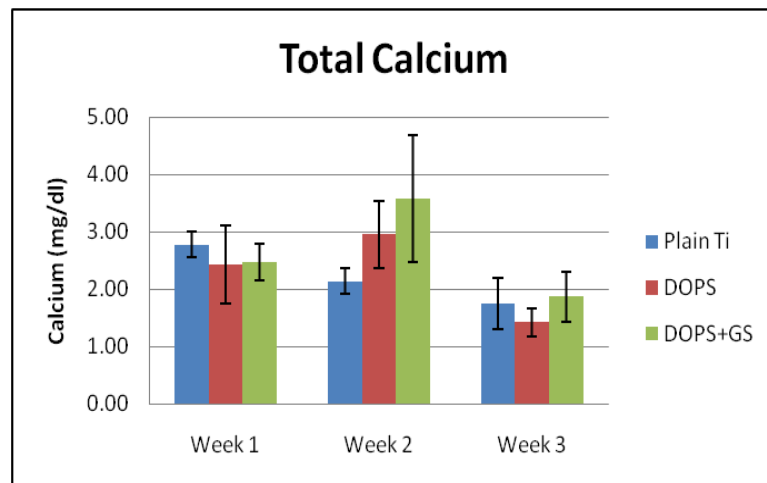


Figure 7-40: Total Calcium. All weeks.

There were no significant differences ( $p < 0.05$ ) in total calcium among the treatments, due to high variance among samples. The following chart presents total calcium normalized for total intracellular protein, for all treatments for all weeks.

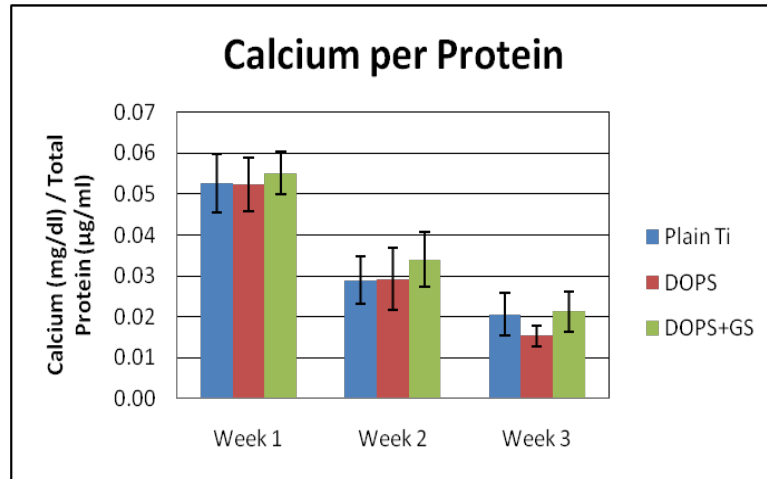


Figure 7-41: Calcium per total intracellular protein. All weeks.

In all weeks, none of the normalized treatments were significantly different ( $p < 0.05$ ). Again, there is high variance among samples. As discussed in section 7.4.2.2 above, calcium values were normalized for total intracellular protein content, to account for variations in cell populations between samples and between treatments. All other indicators of cell viability, proliferation and adhesion discussed earlier point to normal cellular processes at work. It therefore follows that these calcium levels might have been higher, had the coatings been better retained on the samples, and/or if cells had been seeded at higher levels on the samples (discussed in section 7.9.2 below). Calcium levels would also have increased through time if the coatings had been better retained on the samples.

### **7.8.2 Follow-up Cell Study Results**

---

Recall that in the preliminary cell study, many coatings were delaminating between days 7 and 14 (post-seeding), with most absent by day 21. Therefore, an effort was made

to improve the retention of coatings by considering chemical and physical changes that could be made to the coatings and the titanium surface. The results of this study led to the inclusion of calcium on the surface of the titanium to improve the strength of the interaction between DOPS and titanium, and the inclusion of cholesterol in the DOPS coatings to decrease the rate of penetration of media into the coatings. This study took place between the preliminary and follow-up cell studies, and is discussed in detail in the *Enhancing Coating Retention* chapter.

### **7.8.2.1 General Observations**

Coatings did not appear to delaminate as much as they did in the preliminary study. Rather, they appeared to slowly erode and dissolve, after the first week. Many coatings were more than 50% intact at the end of the three-week study, especially gentamicin coatings. Nearly all gentamicin-loaded coatings were almost fully intact at the end of the study. Detailed discussion of these results is found in the *Enhancing Coating Retention* chapter, section 5.6 above.

Coatings appeared to soften and appear whitish and “puffy” in the initial 4 hours, as in the preliminary cell study, an indication of swelling of the coating. However, the onset of swelling was delayed in comparison, only notable after the first day. DOPS coatings degraded the most. This is discussed further in section 7.8.1.1 above.

It is also interesting to note that samples containing cholesterol actually floated in media when placed flat in the well and media was added. Throughout the follow-up study, it was often necessary to physically push the samples into the media to get them to the bottom of the wells. This was not observed with DOPS coatings that did not contain cholesterol, such as used in the preliminary study. This may indicate that coatings

containing cholesterol were more hydrophobic than coatings without cholesterol. Furthermore, coatings containing cholesterol were more difficult to load with GS than those without cholesterol. This was the primary reason for reducing the concentration of GS in the follow-up study (so that we could apply more liquid, enabling it to be spread more easily on the sample), as discussed in section 6.3.1 above. This observation may provide further potential evidence of higher hydrophobicity of cholesterol-containing coatings.

### **7.8.2.2 Cell Adhesion and Organization (Follow-up Study)**

The following images show day 4 (post-seeding), live-stained (calcein) cells for each treatment (all 10x original magnification).

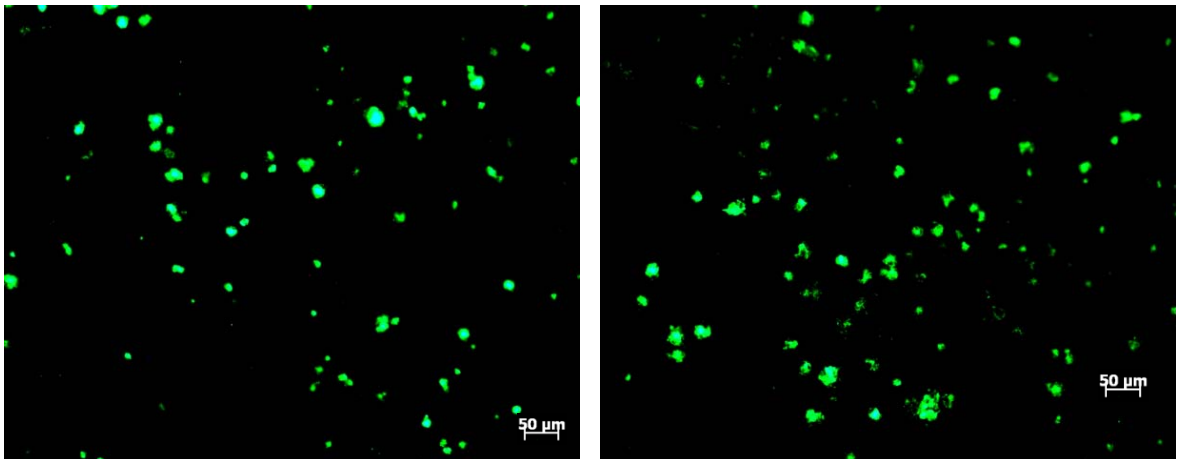


Figure 7-42 & 7-43: Calcein (live) stain images of cells on *plain titanium* (no coating), day 4 post-seeding, 10x original magnification.

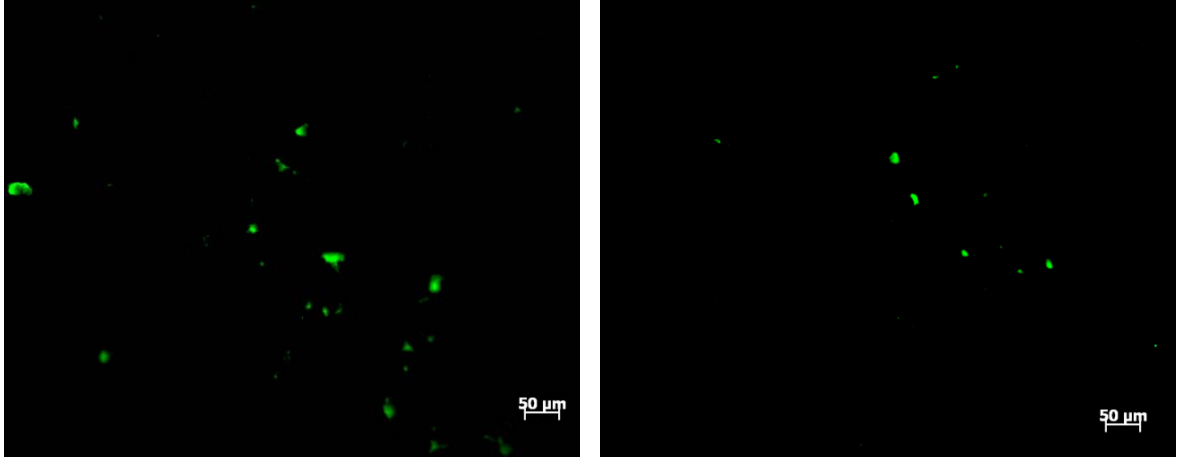


Figure 7-44 & 7-45: Calcein (live) stain images of cells on **DOPS coating**, day 4 post-seeding, 10x original magnification.

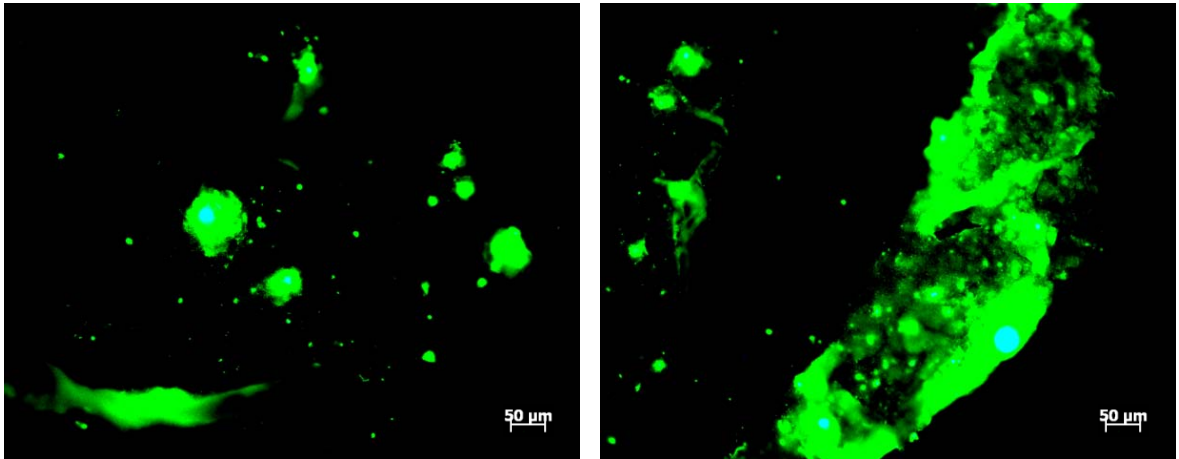


Figure 7-46 & 7-47: Calcein (live) stain images of cells on **DOPS with gentamicin**, day 4 post-seeding, 10x original magnification.

Figure 7-46 and 4-45 are exemplary of a common problem with live stain imaging with cholesterol and/or GS. One or both of these compounds appear to cause calcein stain (also EthD-1 and DAPI nuclear stain) to fluorescence, sometimes making it difficult to accurately identify cells. This issue is discussed in more detail in section 7.8.2.3 below.

Non-specific fluorescence notwithstanding, cell numbers, spreading and proliferation appear to be lower on DOPS coatings than on Plain Ti and DOPS/GS on day 4. This finding is discussed in section 7.9.2 below.

Figure 4-48 also provides a good example of a coating that had partially degenerated. There are notably more cells, although difficult to see in this image size, in the non-specific fluoresced region of the image than in the black area. There appear to be many cells on the remaining coating.

The following images show day 7 (post-seeding), live-stained (calcein) cells for each treatment (all 10x original magnification).

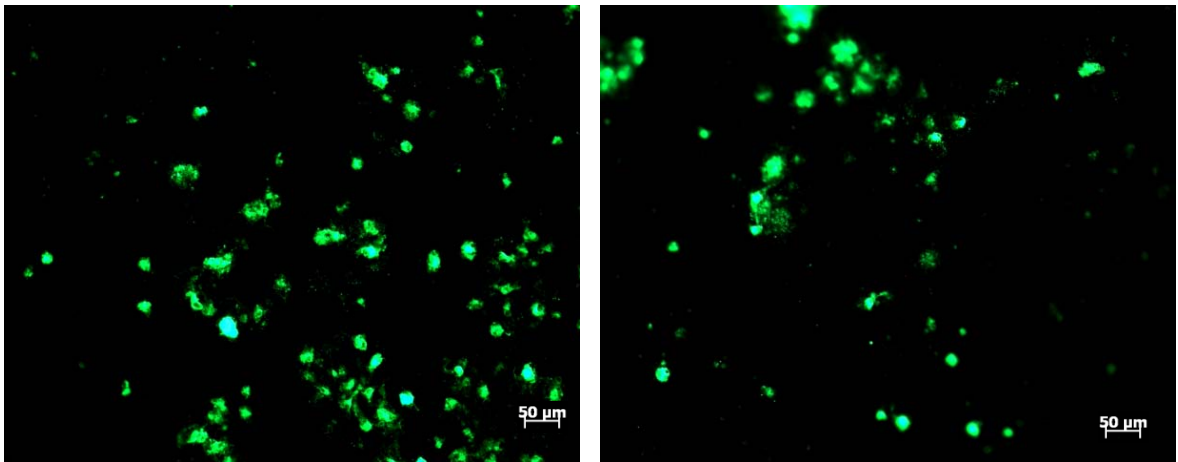


Figure 7-48 & 7-49: Calcein (live) stain images of cells on **plain titanium** (no coating), day 7 post-seeding, 10x original magnification.

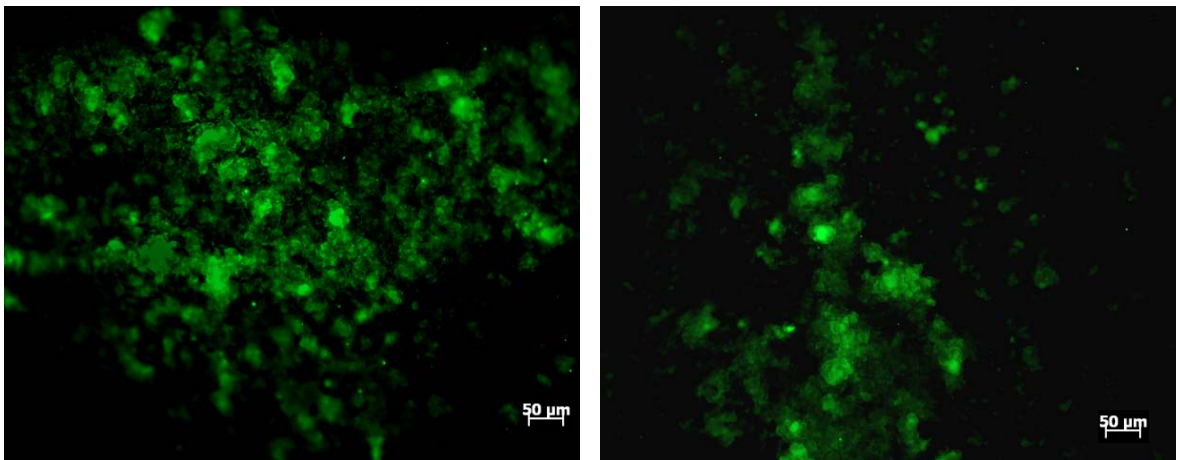


Figure 7-50 & 7-51: Calcein (live) stain images of cells on **DOPS coating**, day 7 post-seeding, 10x original magnification.

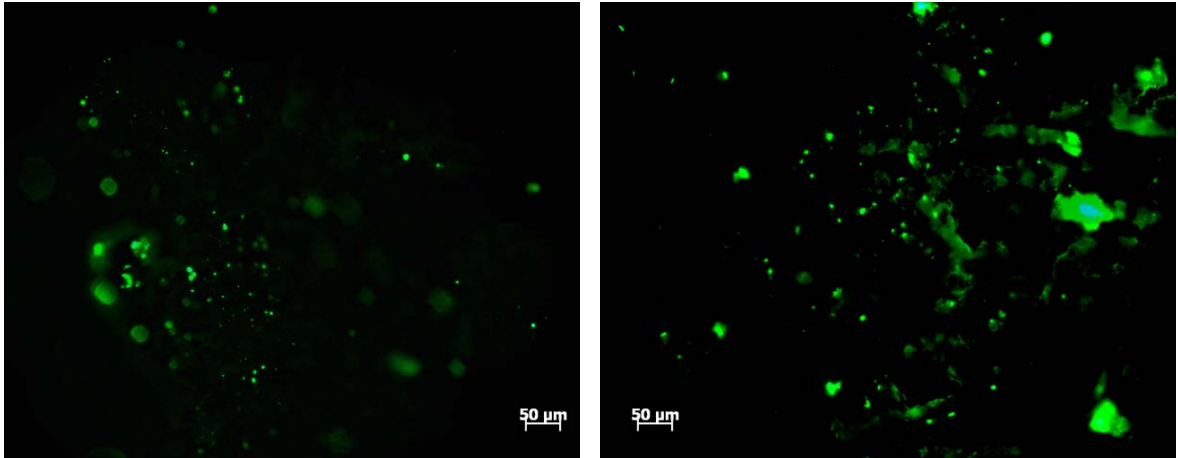


Figure 7-52 & 7-53: Calcein (live) stain images of cells on **DOPS with gentamicin**, day 7 post-seeding, 10x original magnification.

Some figures, particularly those that contained GS, were filtered to various extents using the Image-J software to reduce the masking effects of non-specific fluorescence that are discussed in more detail below.

Taking into account any non-specific fluorescence masking effect, cell numbers, spreading and proliferation appear to be similar on Plain Ti, DOPS and DOPS/GS coatings on day 7. This finding is discussed in section 7.9.2 below.

### **7.8.2.3 Non-Specific Fluorescence Testing**

It is difficult to identify the source of non-specific fluorescence (NSF) in our studies, because of distortions introduced by scattering and absorption caused by various compounds used in our studies. The results of our NSF test with calcein and ethidium homodimer-1 (EthD-1) stains are discussed in the following sections.

#### **7.8.2.3.1 Calcein - DOPS/No cholesterol, with and without GS**

Figure 7-3 through Figure 7-11 above (section 7.8.1.2 above) show day 1 through day 7 calcein stain on DOPS with no cholesterol and no GS. Slight NSF is visible on day 1 GS images, which progressively increases with time.

#### 7.8.2.3.2 Calcein – DOPS with cholesterol, with and without GS

Figure 7-42, Figure 7-44, and Figure 7-46 above (section 7.8.2.2 above) show day 4 calcein on DOPS with cholesterol, Plain Ti, DOPS and DOPS/GS respectively. There is no substantial NSF (a small amount was filtered with Image-J software) but it is becoming apparent in coatings containing GS by day 4.

By day 7, NSF is very visible on samples containing GS, but not on Plain Ti. This can readily be seen in Figure 7-50 (DOPS) and Figure 7-52 (DOPS/GS) above, both of which were filtered with Image-J software, but still unable to remove the NSF effects entirely.

To summarize findings, calcein fluoresces mildly with only DOPS (no GS) in the coatings. This does not appear on day 1, only very occasionally and slightly on day 4, and more so but still only slightly on day 7. Calcein fluoresces moderately with GS (no cholesterol) in the presence of DOPS, strongly when cholesterol appears in the coating and very strongly when cholesterol and GS both appear in the coating. EthD-1 fluoresces in all coatings, more so if GS is present, in which case nothing but fluorescence (red) is visible. DAPI nuclear stain was also tested and found to fluoresce heavily in the presence of GS and cholesterol, more so when both are present (no images provided).

NSF appears to be compounded when both cholesterol and GS are present on a sample, starting at day 4 time points. Numerous natural materials exhibit NSF, due to structural or biochemical changes in the tissue. Some of this fluorescence is “intrinsic” in nature. For example, lipids are widely reported to be active in autofluorescence. Cholesterol has been implicated in various forms of lipid-related fluorescence, such as skin autofluorescence. [241, 242] Furthermore, it is also possible that some component of the coating is degrading with time and resulting degradation components cause more

NSF than in non-degraded coating. For example, phospholipids are prone to oxidation. [49] Oxidized low-density lipoprotein (LDL) particles have been shown to exhibit a strong autofluorescence, which emanates from lipid-rich cells, cholesterol-rich LDL particles [241, 243] and lipid droplets, which are rich in CH<sub>2</sub> groups. [244] In addition, GS may unbind from DOPS as the coating degrades, thereby becoming available to bind the stain and possibly inducing additional autofluorescence, oxidation-driven or otherwise.

Although samples used in our NSF testing were not seeded with cells, our normal test samples were. NSF was also apparent in many situations in our cell study. Collagen is widely known to be one of the major spontaneous fluorophores in normal tissue. [242, 244-246] Elastin fibrils also exhibit a strong autofluorescence signal. [242, 244] It is likely that our cells were expressing proteins such as collagen or other substances that, by themselves [244-246] or together with cholesterol and/or GS, elicit an NSF reaction, which increases as more of these proteins are expressed. Indeed, in our study, NSF did appear to increase over time, consistent with similar reports, for example, that autofluorescence of collagen has been shown to increase over time. [246] Furthermore, hydrophobic surfaces adsorb more proteins than hydrophilic surfaces. [35] Cholesterol appears to make our surfaces more hydrophobic (see section 7.8.2.1 above), thus we would expect greater NSF with cholesterol in our coatings.

#### **7.8.2.4 Cell Viability (Follow-up Study)**

Results from the measurement of MTT in sample coatings, as an indicator of early cell viability, are shown in Figure 7-54 and Figure 7-55 below.

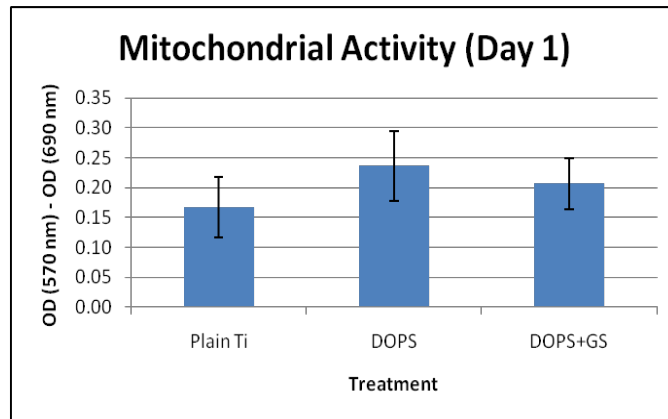


Figure 7-54: Mitochondrial activity, day 1 post-seeding, no significant differences ( $p < 0.05$ )

On day 1, none of the differences were significant ( $p < 0.05$ ), which is typical of the first day after seeding in an MSC cell study. Although not significantly higher, the data show a tendency for these cells to prefer DOPS and DOPS/GS over Plain Ti surfaces.

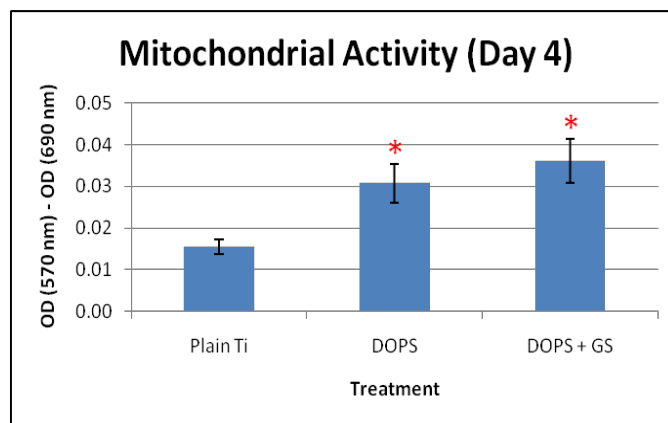


Figure 7-55: Mitochondrial activity, day 4 post-seeding, DOPS and DOPS/GS significantly greater than Plain Ti ( $p < 0.05$ )

The tendency for rat bone marrow-derived MSCs to prefer growth on a DOPS substrate is well documented. [23, 119] Consistent with these prior reports, cells in our study seeded on DOPS and DOPS/GS surfaces exhibited a significant ( $p < 0.05$ ) preference for and high viability on these coatings, as measured by the MTT assay. Cell viability on DOPS and DOPS/GS surfaces is significantly ( $p < 0.05$ ) greater than on Plain Ti, after four days of culture. These results are difficult to correlate accurately with the

live fluorescence microscopy images above due to NSF discussed earlier. But live-cell staining does appear to correlate with these MTT findings, that is, overall cell numbers decreased from day 4 to day 7. It is notable that the amount of MTT measured overall is much lower on day 4 than on day 1. This seems to support the findings in the live stain imaging that fewer cells were seen on day 4 for DOPS and DOPS/GS coatings, despite the challenges of NSF as noted. Discussion of this finding is found in section 7.9.2 below. SEM imaging cannot confirm these numbers, due to apparent damaging effects of SEM fixation on our coatings in this follow-up study. Discussion of this finding is found in section 7.9.2 below.

#### **7.8.2.5 *Qualitative Cell Morphology (Follow-up Study)***

SEM images were taken at all time points to visualize the morphological changes that may have taken place in the cells on the test samples.

Day 4 (post-seeding) images follow:

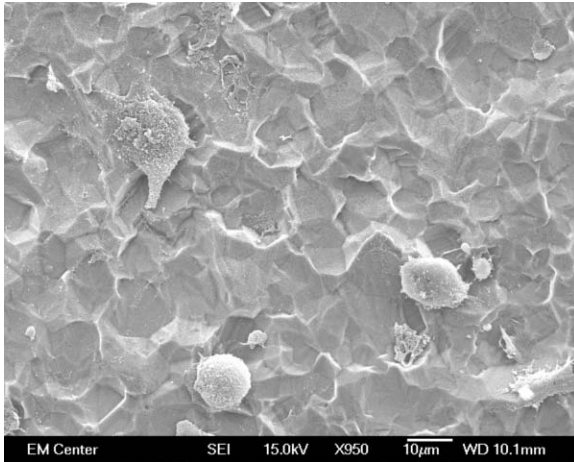


*Figure 7-56: SEM image of Plain Ti day 4, imaged at 15 kV, 1000X original magnification. A few cells are adhering and spreading.*

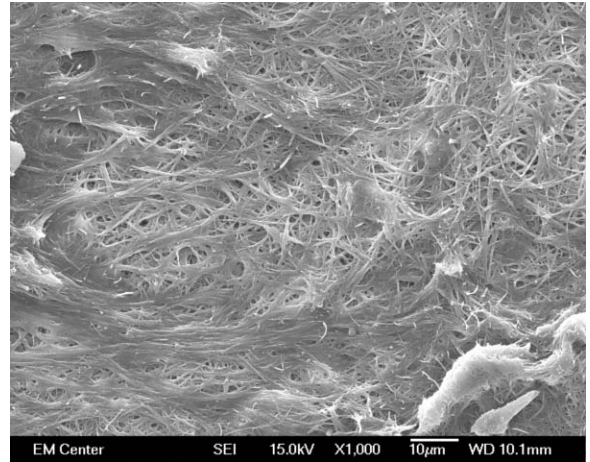


*Figure 7-57: SEM image of DOPS day 4, imaged at 15 kV, 1000X original magnification. Absence of cells hypothesized in text.*

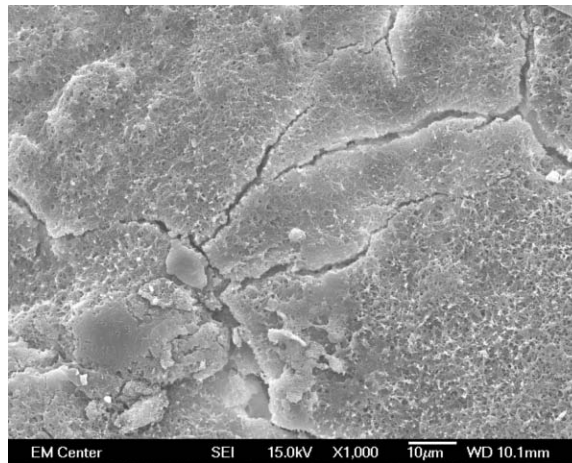


*Figure 7-58: SEM image of DOPS/GS day 4, imaged at 15 kV, 1000X original magnification. Thick coating, but absence of cells is notable.*

Day 7 (post-seeding) images follow:

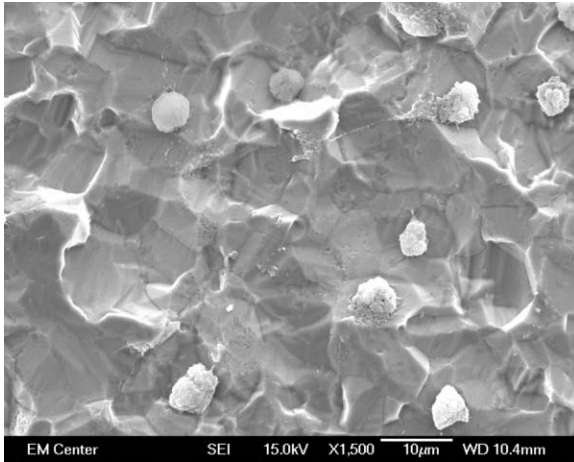


*Figure 7-59: SEM image of Plain Ti day 7, imaged at 15 kV, 1000X original magnification. Cells appear to be proliferating normally.*

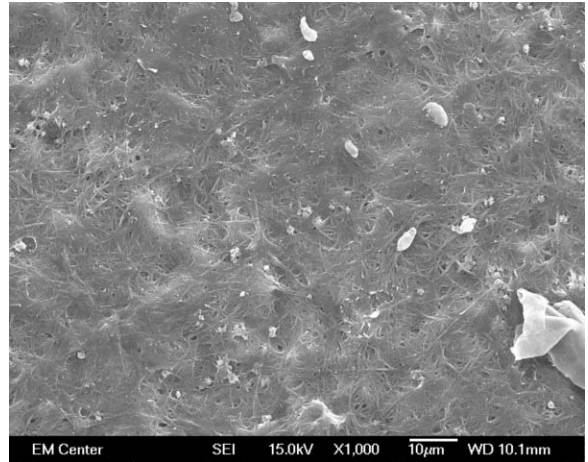


*Figure 7-60: SEM image of DOPS day 7, imaged at 15 kV, 1000X original magnification. Absence of cells hypothesized in text.*

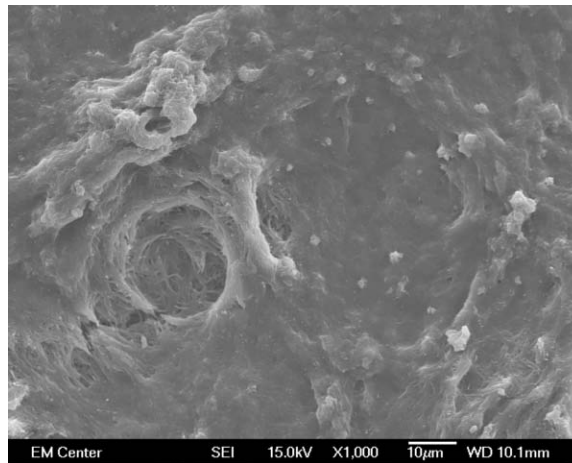


*Figure 7-61: SEM image of DOPS/GS day 7, imaged at 15 kV, 1000X original magnification. Few if any indicators of cells - hypothesized in text.*

Few if any cells were found on the DOPS or DOPS/GS coatings in either days 4 or 7. These results do not correlate well with the MTT nor the live fluorescence microscopy imaging, where low but notable populations of cells were found on both DOPS and DOPS/GS coatings. Possible causes are discussed in section 7.9.2 below.

Week 1 (2 weeks post-seeding) images follow:

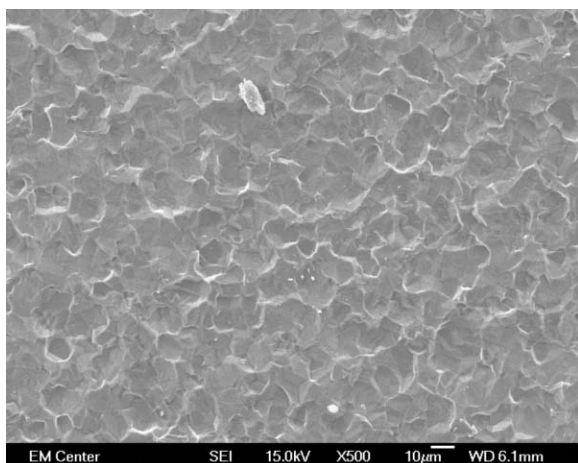


*Figure 7-62: SEM image of Plain Ti week 1, imaged at 15 kV, 500X original magnification. Few cells are visible.*

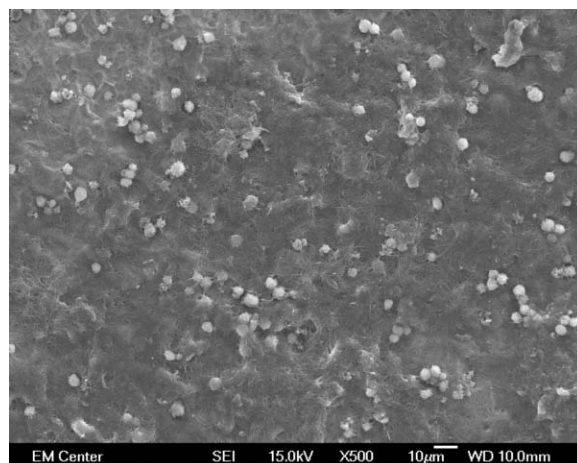


*Figure 7-63: SEM image of DOPS week 1, imaged at 15 kV, 500X original magnification. No cells are visible*

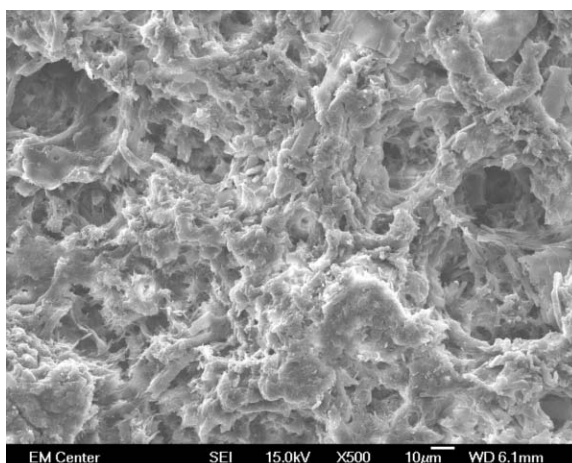


*Figure 7-64: SEM image of DOPS/GS week 1, imaged at 15 kV, 500X original magnification. Thick coating remains, but no indication of cells.*

Figure 7-63 above (and magnified in Figure 7-67 below) shows a thick layer of fibrous mat-like material, closely adherent to the Ti surface (which is discussed further in section 7.9.2 below), with numerous small spherical objects, discussed in section 7.9.1 below. As reported earlier, the GS coatings typically remain relatively intact, as can again be seen in Figure 7-64 above. However, there is no sign of cells on the GS sample and perhaps on the DOPS samples, depending on what the spherical objects are. There are no apparent ECM or cell fragments visible, even at higher magnifications. Possible causes are discussed in section 7.9.2 below.

It is also interesting to note that coatings appearing to be nearly intact were visible (direct observation) on all samples prior to the fixation step done in preparation for SEM. In fact, Figure 7-65 below shows samples at the 7-week time point, some of which still have near completely intact coatings. However, further study would be required to ascertain if these visible coatings were, in fact, already degraded. If the first coating layer was missing, and the cells were attached there, this would explain the lack of cells on our samples. SEM imaging, for example, in the *Enhancing Coating Retention* chapter and in Figure 7-60 above, is inconclusive, as we do not know from SEM images the extent to which the coatings may or may not be degraded. Indeed, SEM does reveal that some coatings were completely missing on some samples, while others retained a very thin, elaborate mesh-work of fibrous coating and still others possessed a thick, dense fiber network.

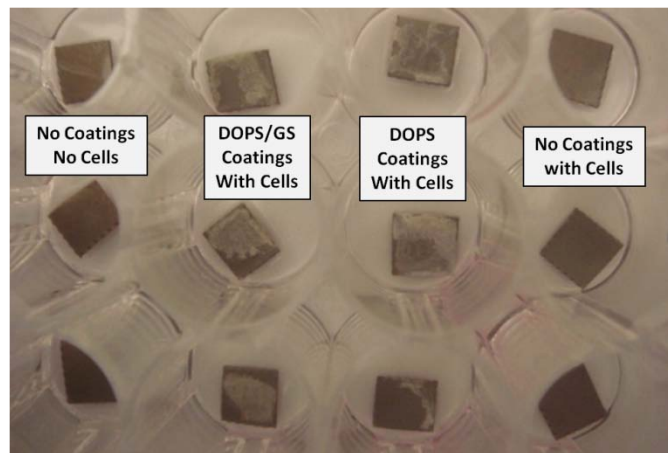
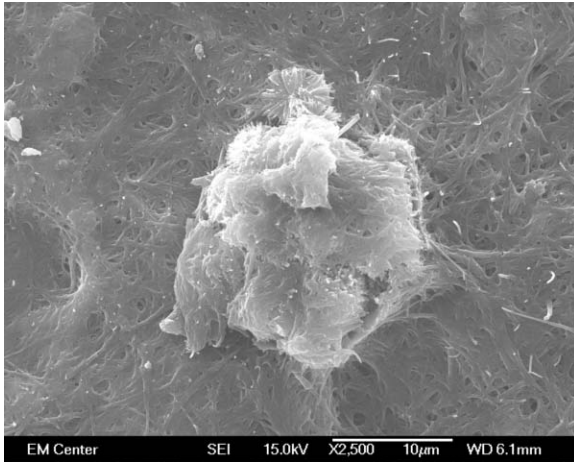
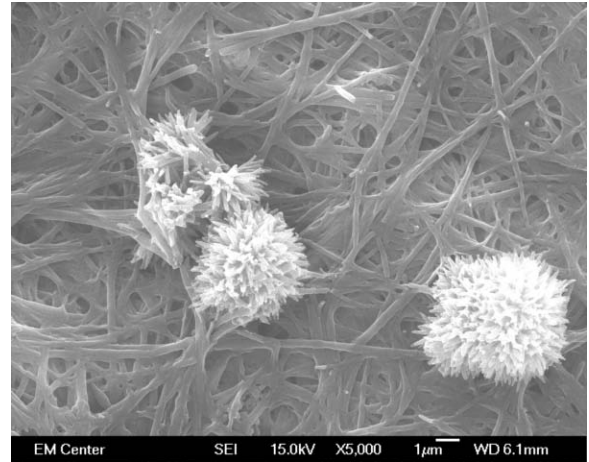


Figure 7-65: Photograph showing test samples at 7 week (post seeding) time point.

Of further interest are the small objects seen in the DOPS Figure 7-63 above. Higher magnification images of such representative objects are shown in the following images.



*Figure 7-66: SEM image at 15 kV, 2500X original magnification. Object is well established into the underlying matrix.*



*Figure 7-67: SEM image at 15 kV, 5000X original magnification. Scale bar is 1 µm. Small objects on rich matrix are discussed in the text.*

The object in the image on the left above is firmly embedded in the underlying matrix material. It is possible this is the remains of a cell or other object that was embedded deeply enough in the coating to not be removed by degradation. The underlying matrix is clearly attached upwards throughout the periphery of the object. Whatever may have become of the coating, the object was exposed, but it remained attached to what remained of the underpinning matrix. The objects in the image on the right are different, and are discussed in more detail in section 7.9.1 below. The underlying matrix in both images is very similar, the right being magnified twice as much as on the left. It may be what remains of the thick “normal” matrix seen in other images, for example Figure 7-69, Figure 7-89 and Figure 7-90 below following some catastrophic degradation event such as delamination. It is interesting to note that in the preliminary study, in which samples were not pretreated with calcium, no such thin matrix was apparent following delamination. It is possible their presence in calcium pretreated samples provides visual evidence that calcium pretreatment does indeed form a relatively strong bond with the DOPS coatings.

Week 2 (3 weeks post-seeding) images follow:

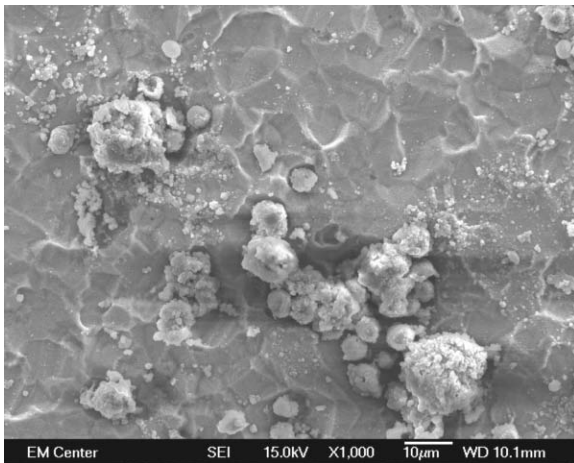


*Figure 7-68: SEM image of **Plain Ti week 2**, imaged at 15kV, 1000X original magnification. Many spherical objects similar to other treatments, unlikely cells.*

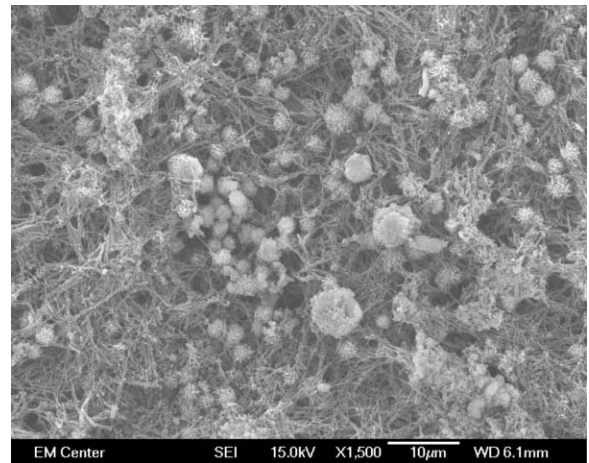


*Figure 7-69: SEM image of **DOPS week 2**, imaged at 15 kV, 1500X original magnification. Rich rope-like matrix and spherical structures.*



*Figure 7-70: SEM image of **DOP/GS week 1**, imaged at 15 kV, 1000X original magnification. Thick coating remains, with two distinct materials.*

The Plain Ti image (Figure 7-68 above) has numerous small objects, very similar to those seen on the DOPS coating. These are discussed in section 7.9.1 below. There are no visible indications of cells on the Plain Ti sample.

The DOPS image (Figure 7-69 above) is quite notable. As can be seen, a dense, rope-like network of material completely covers the sample. This is very different from DOPS samples in SEM from earlier time points in this study or in the preliminary study. The DOPS coating with cholesterol (Figure 7-69 above) appears to be an ideal scaffold for

cell growth. An ideal scaffold for growth of cells should be highly porous with sufficient pore connectivity to ensure permeability for oxygen, sufficient nutrient transport towards the cells and removal of waste products. This accurately describes the DOPS coatings, at least as seen in these images.

The DOPS image also suggests that the likely cause of degradation of DOPS coatings is a form of bulk erosion (or perhaps bio-erosion) or dissolution, not delamination. Unlike the preliminary study when coatings were delaminating (detaching in full, intact slabs), these coatings maintain a distinct rope-like morphology through multiple time-points. Of those coatings that exhibit signs of degradation, the effect appears to be on a micron scale in which the coatings transform from a dense morphology and appearance at time zero (see for example, Figure 5-15 and Figure 5-18 above), to a coating consisting mainly of this thick, rope-like matrix. This suggests bulk erosion is not a significant factor. Although it is not possible to determine with any certainty the composition of these rope-like structures within the scope of work reported herein, it is possible this structure remains as a result of erosion of the DOPS coating that has taken place. It is possible the coatings erode and/or rearrange in media, leaving behind this thick, rope-like matrix.

In addition, this matrix is heavily populated with the various objects discussed throughout this results section, particularly the white objects approximately five to ten microns in diameter, which are also common in Figure 7-63 and Figure 7-67 above. These objects are discussed in section 7.9.1 below. One would expect these structures to be disturbed or absent if there was significant bulk erosion or dissolution of the coating.

The GS image (Figure 7-70 above), as in week 1 images, also shows the remains of a very dense coating, also completely devoid of any indication of cells. The puffy substance noted in the center of the image has a very different texture than the rest of the matrix. This material could be the remains of calcium/phosphate mineralization deposited by cells that once populated these coatings, a topic which is discussed in section 7.9.1 below.

### 7.8.2.6 Total Protein (Follow-up Study)

Total intracellular protein content was measured at week 1 and week 2 (post-differentiation), as shown in the following figures.

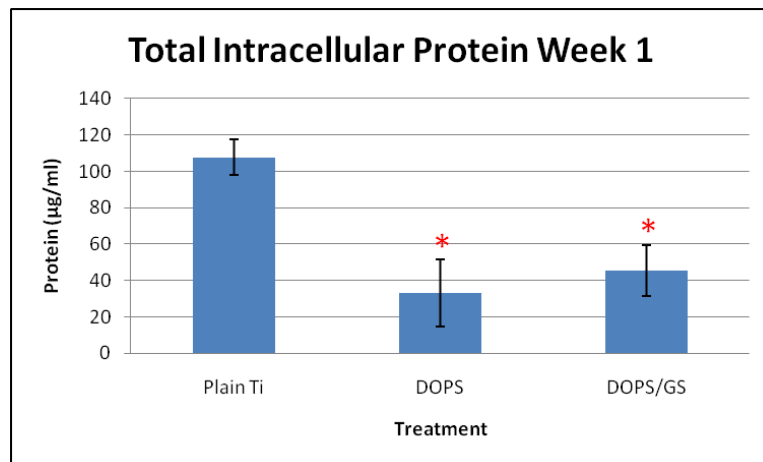


Figure 7-71: Total Intracellular Protein, week 1 post-differentiation, Plain Ti and DOPS, and Plain Ti and GS significantly different ( $p < 0.05$ )

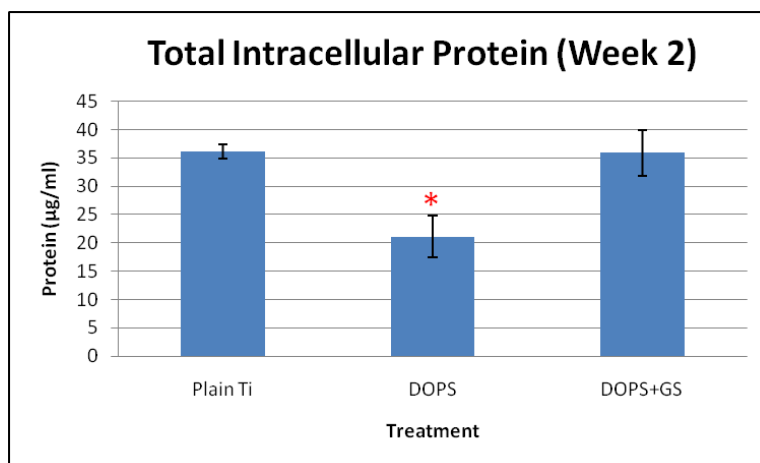


Figure 7-72: Total Intracellular Protein, week 2 post-differentiation, Plain Ti and DOPS/GS, and DOPS and DOPS/GS significantly different ( $p < 0.05$ )

Total intracellular protein content decreased from week 1 to week 2. Fewer cells indicated in live fluorescence microscopy imaging, MTT and SEM all support lower actual cell counts, which is correlated with lower total intracellular protein. The decrease in total protein seen in this study is likely also related to factors discussed in section 7.9.2 below.

### 7.8.2.7 Osseogenic Differentiation (Follow-up Study)

The results for week 1 and week 2 ALP assays are presented in the following figures.

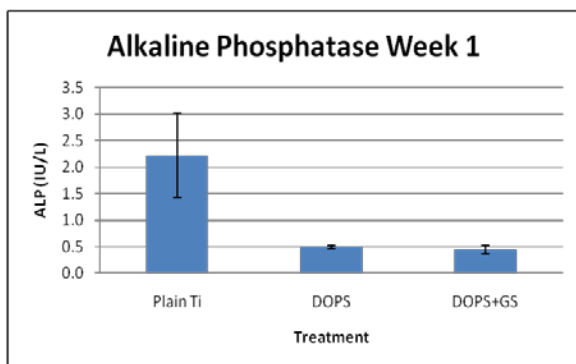


Figure 7-73: Alkaline Phosphatase, week 1 post-differentiation, No significant differences ( $p < 0.05$ )

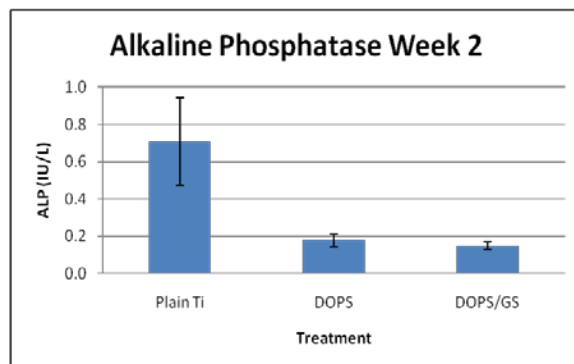


Figure 7-74: Alkaline Phosphatase, week 2 post-differentiation, No significant differences ( $p < 0.05$ )

There were no significant differences ( $p < 0.05$ ) among the treatments in Alkaline Phosphatase, due to high variance among samples.

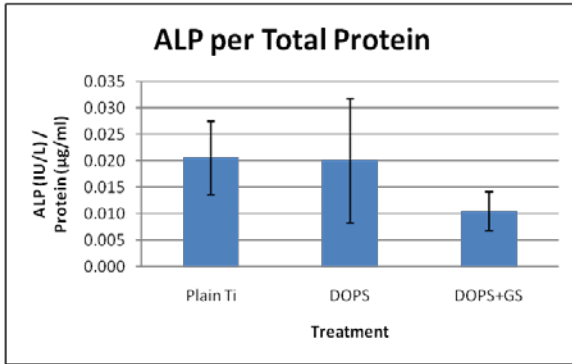


Figure 7-75: ALP per Total Protein, week 1 post-differentiation, No significant differences ( $p < 0.05$ )

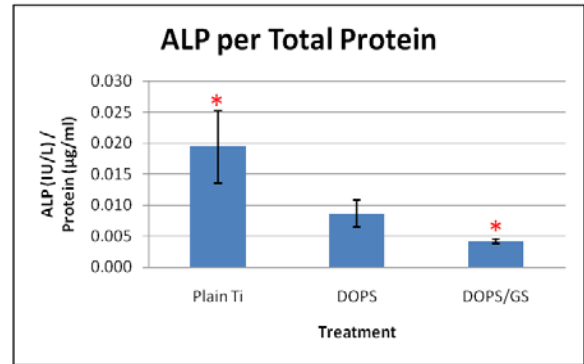


Figure 7-76: ALP per Total Protein, week 2 post-differentiation, Plain Ti and DOPS/GS, and DOPS and DOPS/GS are significantly different ( $p < 0.05$ )

When normalized for total protein, Plain Ti and DOPS/GS, and DOPS and DOPS/GS were significantly different ( $p < 0.05$ ). Plain Ti and DOPS were not significantly different due to high variance among samples.

The decrease from week 1 to week 2 may be explained by the typical rise and fall pattern often seen in ALP measurements, as discussed in section 7.8.1.6 above. Other evidence from this study, for example, cell morphology (SEM), calcium and osteocalcin (below), suggest there were actually many cells in these coatings. In addition to this evidence, ALP plays an important role in hydroxyapatite formation on matrix proteins. There is a good possibility that the small vesicles on the rope-like fibers in DOPS SEM images of week 2 samples (Figure 7-89 below) are matrix vesicles. In addition, strong evidence (from EDS) suggests the presence of hydroxyapatite in the coatings, as discussed in section 7.9.1 below. It is highly likely that cells were responsible for both of these factors, providing strong evidence that ALP must have been normal.

It is possible that GS in the coating may be affecting ALP production. Isefuku [199] reported that ALP activity and 3H-thymidine incorporation were significantly decreased

at gentamicin concentrations of 100  $\mu\text{g/ml}$  and above, while total DNA was significantly decreased at 700  $\mu\text{g/ml}$  and above. This study was completed on “human osteoblast-like cells”. In this study, exposure to gentamicin in media took place for only 1 to 4 days, after which it was removed and samples rinsed. No study was found that looked at similar effects of gentamicin over time frames longer than 4 days, nor the ability of bone cells or tissues to recover from exposure to these drugs over a longer time frame. This study specifically considered levels of 100  $\mu\text{g/ml}$  and above. They measured response at 30  $\mu\text{g/ml}$  and reported no effect, but did not show data. It would be useful to see similar data for a range of GS between 30 and 100  $\mu\text{g/ml}$ . GS loading in our study was 200  $\mu\text{g}$ . A substantial amount of GS elutes out of the coating (refer to *Elution Study* chapter) and is removed with each media change, but 30  $\mu\text{g}$  to 40  $\mu\text{g}$  could remain in the coatings after the first day and 10  $\mu\text{g}$  could remain in the coating after 4 days and thereafter for an undetermined length of time.

#### **7.8.2.8 Mineralization (Follow-up Study)**

The calcium assay kit used in this follow-up study (Pointe Scientific) detects the presence of calcium deposition by osseogenic cells through the interaction of calcium with suitable chromogenic agents. The Pointe Scientific kit uses o-cresolphthalein complexone as a complexing reagent to form a stable purple/red color, which intensity, measured at 570 nm is directly proportional to concentration of free calcium in a sample. [247] The minimum resolution (potential error) of this assay is reported by the vendor to be approximately 2%.

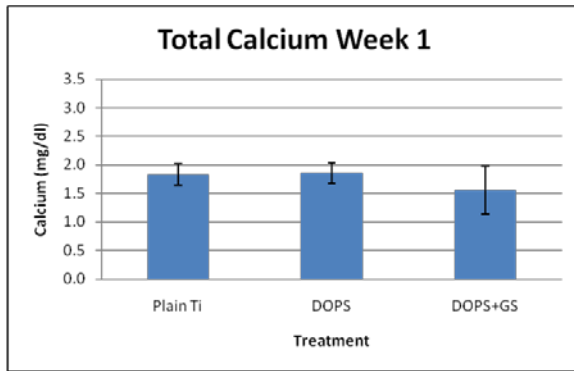


Figure 7-77: Calcium, week 1 post- differentiation, No significant differences ( $p < 0.05$ )

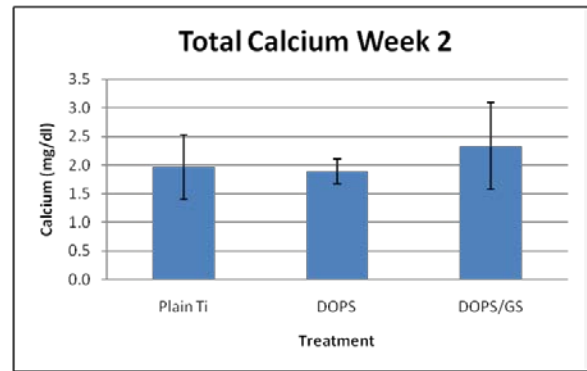


Figure 7-78: Calcium, week 2 post- differentiation, No significant differences ( $p < 0.05$ )

There were no significant differences ( $p < 0.05$ ) among the treatments in total calcium week 1. However, when normalized for total protein, as shown in the following figures, DOPS and DOPS/GS calcium per total protein were significantly higher than Plain Ti.

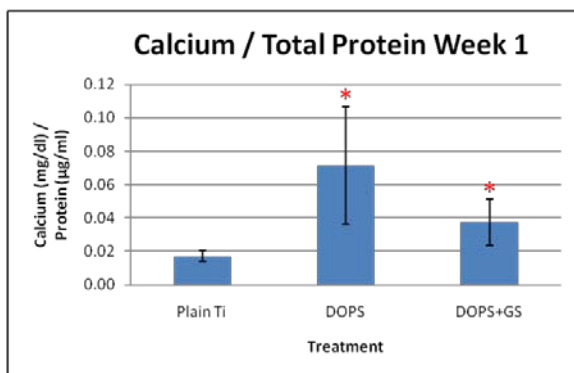


Figure 7-79: Calcium per Total Protein, week 1 post- differentiation, Plain Ti and DOPS, Plain Ti and DOPS/GS significantly different ( $p < 0.05$ )

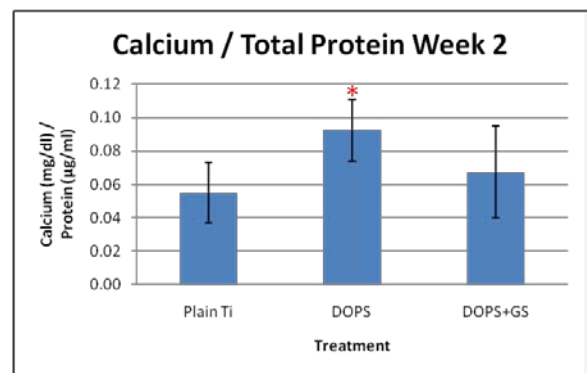


Figure 7-80: Calcium per Total Protein, week 2 post- differentiation, DOPS significantly different from Plain Ti ( $p < 0.05$ )

Total calcium and calcium per total intracellular protein content levels increased from week 1 to week 2. In addition, calcium on DOPS is significantly higher than on Plain Ti or DOPS/GS in both results. Although there were fewer cells present, as indicated in live fluorescence microscopy imaging, protein, MTT and other tests, the cells that were present were apparently producing large amounts of calcium on a per cell basis. This is a positive indicator for healthy bone mineralization.

This relatively high amount of calcium per cell provides strong evidence that the vesicle-like structures seen in the DOPS SEM images above may indeed be matrix

vesicles deposited by the young osteoblasts (discussed further in section 7.9.1 below). The low absolute amount of calcium may be related to experimental process. The protocol for the BioAssay Systems test kit does not specify the correct blank to use for this test. In most tests, HCl was used, but it is possible that de-ionized water was used. Prior experience has shown that DI-water as a blank in this assay will produce abnormally low results (as it shifts the standard curve much higher).

Because this study measured calcium produced by cells on titanium pretreated with calcium, it is important to understand the amount of calcium on the samples and that which might have been produced by the cells. As discussed in *Background*, earlier studies [23, 30, 120] have shown that DOPS will sequester calcium from cell growth media, as it plays a role in early bone formation.

The first such calcium test involved using the Pointe Scientific Calcium Assay on titanium samples that were pretreated with calcium chloride, and completed a 2 week cell study with no cells using both cell culture or cell differentiation media as dictated by the protocol described above. This test measures the amount of calcium on pretreated samples and from the sequestering of calcium by the DOPS.

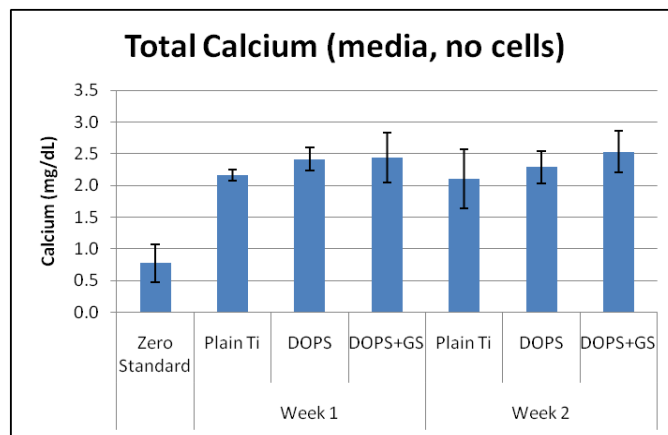


Figure 7-81: test of Pointe Calcium assay on two-week cell study samples with no cells, calcium treated samples. All treatments significantly different ( $p < 0.05$ ) from zero, but none different.

No significant differences were found between any of the treatments, however all were significantly different from the zero standard value (the zero value of the standard curve). The minimal amount of calcium found on the DOPS and DOPS/GS samples follows a pattern confirmed by earlier studies. [23, 30, 119]

An additional test was performed to measure the amount of calcium in samples that were never exposed to cell media. The results, shown in the following figure, show significant differences ( $p < 0.05$ ) between the zero standard value and NoDOPS-Plain Ti (no calcium pretreatment), NoDOPS-Plain Ti (with calcium pretreatment) and DOPS/Cholesterol-NoGS (no calcium pretreatment) values.

These results indicate a very consistent amount of calcium on all samples, which matches expectation from samples that received equivalent calcium pretreatments in calcium-chloride baths.

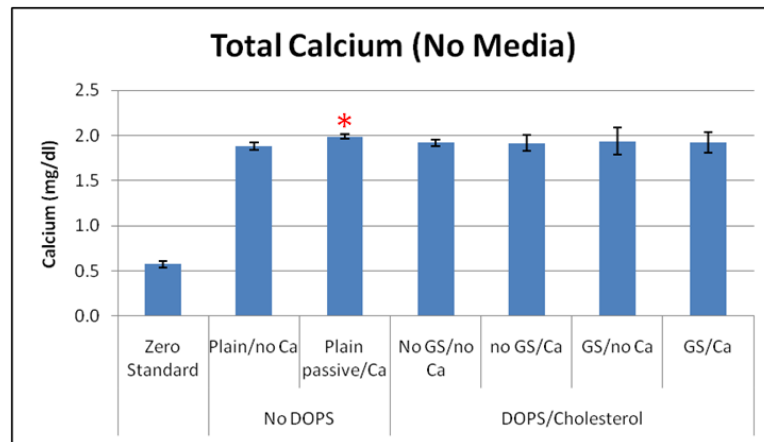


Figure 7-82: calcium in samples that does not come from media. All treatments significantly different ( $p < 0.05$ ) from Zero, Plain/passivated significantly higher than Plain/no Ca and No GS/No Ca.

It is interesting to note that the overall level of calcium in these samples is approximately the same amount (approximately 2 to 2.5 mg/dl) as that measured in the previous test with media and no cells. This suggests that the absolute amount of calcium

sequestered by the DOPS in the coatings, although very small, is entirely responsible for the differences between samples.

DOPS has a primary amine group, which could be visible to the BCA total protein assay and must also be factored out. No protein values were significantly different ( $p < 0.05$ ) from zero (data not shown). This result suggests the primary amine group in DOPS is not visible to the BCA total protein assay. Therefore, protein measurements were not taken in the assays when tested without media.

The tests reported above (media with no cells) show that the amount of calcium in the environment (pretreatment on samples and sequestered by the DOPS coatings) is approximately equal to the amount created by the cells. This result is expected, given the relatively low cell numbers apparent on our test samples. Although the absolute amount of calcium measured is relatively small, the trend is suggestive of normal osteoblastic activity. We believe the trend in this study is more important than the actual amounts of calcium. Furthermore, the presence of matrix vesicles and hydroxyapatite-like material in week 2 DOPS coatings (as discussed in section 7.9.1 below), and the osteocalcin immunofluorescence imaging results presented in the following section also suggest healthy osteoblastic activity.

#### **7.8.2.9 Matrix Production - OC and OP (Follow-up Study)**

Osteocalcin (OC) and osteopontin (OP) are proteins found in extracellular matrix which are uniquely secreted by osteoblasts. Osteocalcin is thought to play a role in mineralization and calcium ion homeostasis. [248] Osteopontin is as an important factor in bone remodeling and cell signaling. [249, 250]

Osteocalcin is the most abundant of the non-collagenous proteins of bone produced by osteoblasts. It is implicated in sequestration of calcium by osteoblasts and production of hydroxyapatite. It promotes adhesion and spreading of osteoclasts, triggering the release of bone sialoprotein, osteopontin (OP) and fibronectin from these cells. Cell spreading is partially dependent upon the synthesis of these proteins.

OP is a multifunctional extracellular protein involved primarily in cell signaling, adhesion, migration, and regulation of mineral deposition. It plays a unique role in adhesion by helping to maintain overall structural integrity of bone and bone/implant systems.

The concentrations of these matrix proteins are biomarkers for the bone formation process, and are indicators of the overall activity of mature osteoblast cells as they may be actively producing bone. [251]

In OC/OP immunofluorescence imaging, cells on test surfaces are immuno-labeled with primary antibodies against osteocalcin and osteopontin and then with secondary antibodies containing fluorescent markers that indicate the presence of the primary antibodies, all in the presence of blocking agents (proteins) which serve the purpose of preventing miscellaneous binding of non-specific proteins to the primary epitopes. These tests are also helpful in determining if cells are integrating with test sample surfaces and producing matrix components, or simply producing precursor minerals for matrix.

OC images of samples from all treatments on week 2 (three weeks post-seeding, two weeks post differentiation) are shown in the following.

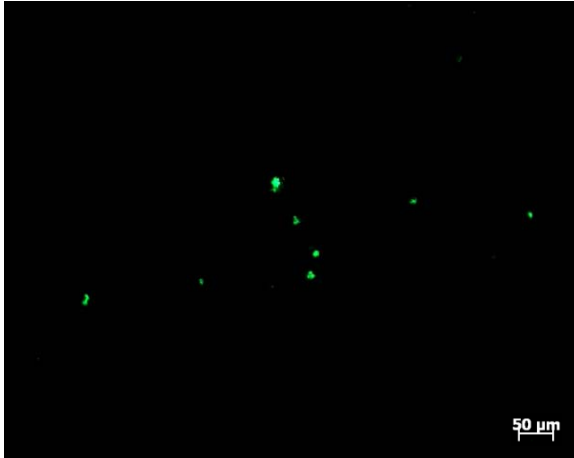


Figure 7-83: OC immunofluorescent stain on **Plain Ti** coating, 10X original magnification.

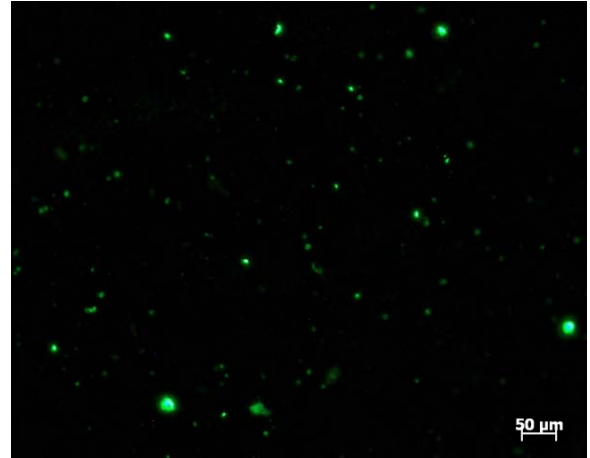


Figure 7-84: OC immunofluorescent stain on **DOPS** coating, 10X original magnification.

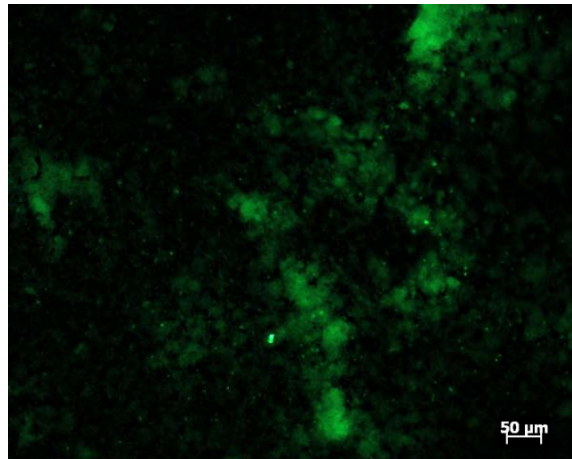


Figure 7-85: OC immunofluorescent stain on **DOPS/GS** coating, 10X original magnification.

Many of the smallest spots in the DOPS/GS image are too small to indicate cells, and are more likely noise in the signal due to non-specific fluorescence (NSF) of the coating. Considering only the larger spots (for example, the spots in the Plain Ti image with no NSF), OC immunofluorescent images above appear to reveal greater production of OC on DOPS coatings than on DOPS/GS and more on DOPS/GS than on Plain Ti. These results compare favorably with other published studies [252], demonstrating a relatively high presence of OC after two weeks of culture. This also correlates well with earlier hypotheses that the spherical objects seen in the SEM images are indeed a form of hydroxyapatite, the calcium phosphate discussed in section 7.9.1 below, and the calcium

assay results that show significant amounts of calcium per total intracellular protein (see Figure 7-80 above).

The cells expressing OC in these images do not appear to be clustering together, which would be more normal for this time point. This may suggest the combination of materials in the coatings might be creating less than ideal environmental conditions for cell cohesion. [98] Further discussion of the possible role of our coating chemistry and possible implications for cell growth is provided in section 7.9.2 below.

OP images of samples from all treatments on week 2 (three weeks post-seeding, two weeks post differentiation) are shown in the following:

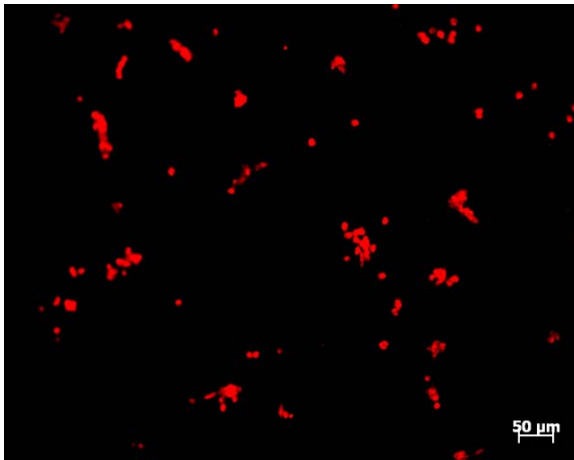


Figure 7-86: OP immunofluorescent stain on **Plain Ti** coating, 10X original magnification.

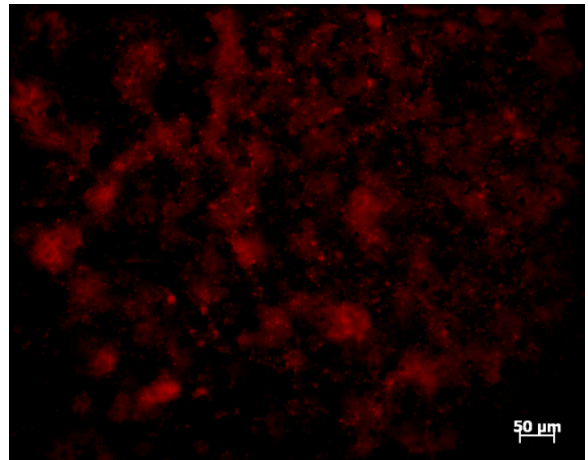


Figure 7-87: OP immunofluorescent stain on **DOPS** coating, 10X original magnification.

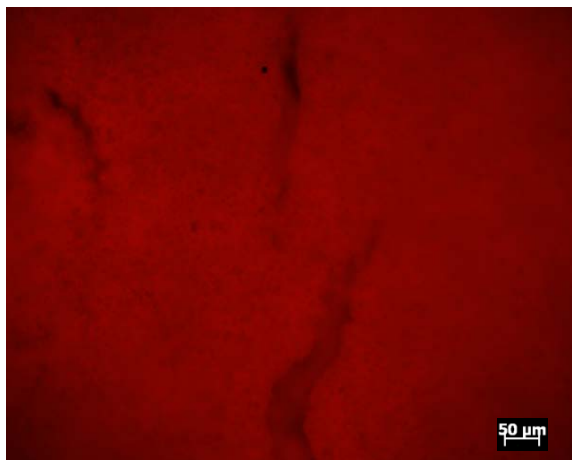


Figure 7-88: OP immunofluorescent stain on **DOPS/GS** coating, 10X original magnification.

As can be seen, the DOPS and DOPS/GS samples exhibit non-specific fluorescence with OC and OP, OP much more than OC. NSF was discussed earlier in section 7.8.2.3 above. Samples with no cells exhibited significant NCF in the presence of cholesterol, and more when GS was also present in the coatings. NSF seen here is likely also due to similar reactions caused by a combination of cholesterol and/or GS, and is more exaggerated in these OC and OP immunofluorescent images. This also indicates the presence of GS in these coatings at week 3 post-seeding.

Despite NSF, OP is clearly abundant, and apparently more abundant than OC. The release of OP by cells is triggered in part by OC, supporting the argument that OC is present in the samples in sufficient quantities to promote mineralization, and that cells were also present on the coatings. This also correlates well with earlier hypotheses that the spherical objects seen in the SEM images are indeed a form of hydroxyapatite discussed in section 7.9.1 below, and the calcium assay results that show significant amounts of calcium per total intracellular protein (see Figure 7-80 above).

## **7.9 General Discussion**

In the preliminary cell study we reported normal, healthy cell growth, with normal metrics and assay results, but the coatings delaminated. The *Enhancing Coating Retention* study found that passivation of the titanium combined with pretreatment of titanium with calcium and addition of cholesterol to the DOPS coatings would enhance coating retention. The *Elution* study showed these coating enhancements also had a positive effect on the elution profile, and therefore the drug delivery potential of these coatings. The follow-up cell study reported herein also supports this finding. Coatings containing DOPS alone appeared thick and dense by SEM evaluation, compared to

coatings in the preliminary cell study, and coatings containing GS exhibited near-complete coating retention past the end-point of the study. Coatings were clearly well-adhered and mostly intact, even out to the 7 week post-seeding time point. And, immunofluorescent imaging provides strong evidence for the presence of GS in the coatings after three weeks.

A positive result in this study would be non-cytotoxicity of the coatings, enhanced cell viability and biomineralization activity, with positive osseogenic indicators, and presence of bone morphogenic proteins. It appears that our initial cell viability and cell numbers were lower than expected, but there is no evidence of cytotoxicity. Live cell fluorescence microscopy and SEM examination showed relatively fewer cells on DOPS coatings, with or without GS, and dead cell staining did not reveal any abnormal indication of cell death. Evidence of biomineralization (calcium) was low on an absolute basis but higher than on control surfaces on a per-cell basis. There was very clear evidence of extensive biomineralization under evaluation by SEM. And there were relatively strong indications of bone morphogenesis markers for calcium production (OC) and for cell migration, signaling and mineralization (OP). The coatings remained intact through week 1 and well through week 2.

However, SEM evaluation in weeks 1 and 2 revealed few if any cells. See section 7.9.2 below for further discussion of this phenomenon.

As discussed in section 7.4.2.1 above, our study used the BCA assay to estimate total intracellular protein as a means to normalize ALP and calcium results, in order to determine ALP and calcium activity per cell (technically, per total intracellular protein). This helps determine, for example, whether observed cellular activity results from more

cells producing less ALP/Ca, or fewer cells producing the same or more ALP/Ca. As also discussed in section 7.4.2.1 above, certain compounds, such as phospholipids, interfere with the color development in the BCA assay, tending to overestimate results. [233] To overcome this interference, 2% sodium dodecyl sulfate (SDS) was added to the reagent as described by Morton. [233] SDS is a detergent that is likely to dissociate some (unknown amount) of the extracellular protein from the matrix, thereby distorting the results of the BCA assay as a measure of intracellular protein. It is unknown if, or to what extent, this possible misrepresentation of intracellular protein may have actually occurred. But it is possible that this effect may have exaggerated our protein results, which were then used to normalize our calcium and ALP measurements. If the protein estimates were incorrectly high, then the normalized calcium and ALP values would be incorrectly low, which is consistent with our findings. However, the decreasing trend observed in total calcium and ALP over time would not be impacted by this possible misrepresentation of total protein.

### ***7.9.1 On Calcium/Phosphate in Our Coatings***

---

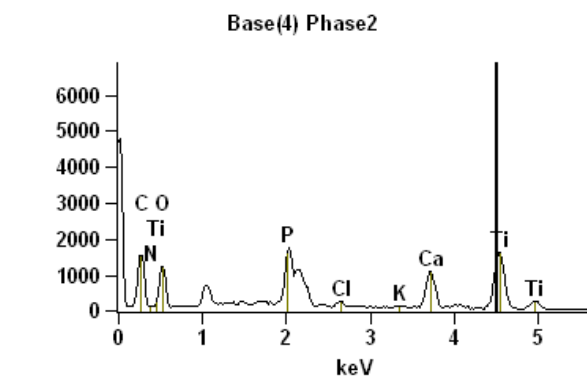
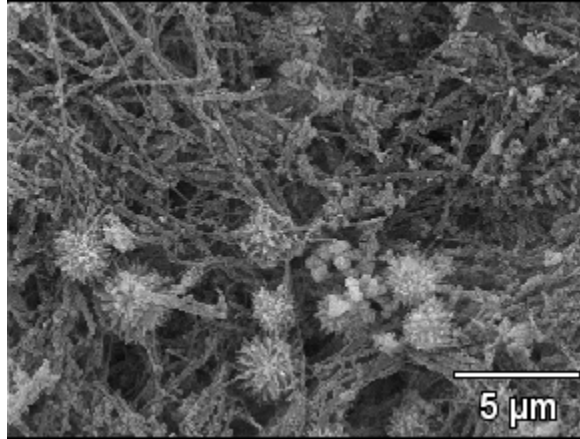
This section discusses evidence of calcium phosphate and hydroxyapatite in our coatings, despite the lack of cells in SEM images.

The spherical, “fuzzy”, white objects in Figure 7-67 above appear to be calcium phosphate spherulites. Spherulites are patterns of mineral deposition often found in the extracellular matrices of a variety of vertebrate tissues. Spherulites are generally three dimensional and radial-shaped, composed of many individual mineral crystals of various lengths oriented about a central point, which is presumed to be the nucleation center from which point the mineralization began. Spherulitic mineral deposition patterns are

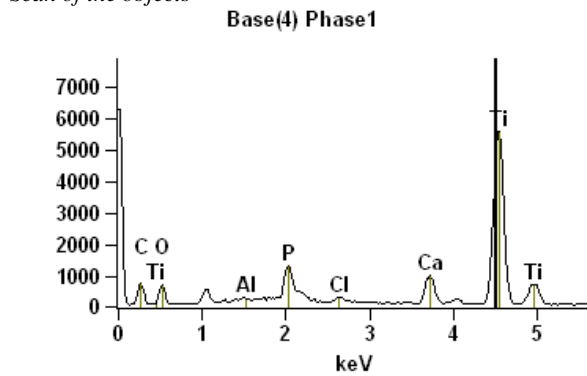
common in appositional bone formation [253] and in tissue assumed to be undergoing the first steps in the process of calcification. [32, 238] Santin [23] reported “needle-shaped crystals” appearing on their DOPS surfaces after only 15 to 30 minutes, with significant mineralization taking place after 7 days. Porter *et. al.* [252] reported calcium-phosphate minerals in the early form of spherulites after 1 week of differentiation on nanowire surfaces. Numerous researchers have reported calcium phosphate minerals in the early form of spherulites in early phases of biomineralization. [252, 254, 255] However, the objects in Figure 7-67 above appear to be slightly larger than other spherulites reported. This may be the result of the cells responding very positively to the DOPS coatings, as reported elsewhere in this study. Spherulitic objects were not seen on acellular samples treated in media.

Further investigation was performed by energy-dispersive X-ray spectroscopy (EDS). EDS is an analytical technique used for evaluating spatial organization and composition of mineralization of materials. It analyzes X-rays emitted by a substance in response to bombardment with charged particles, in our case through the SEM. EDS is used for the elemental characterization of a material, and was thus used to investigate the composition of some of these objects on and in our coatings.

EDS analysis (shown below the image) was performed on the following image.



Scan of the objects



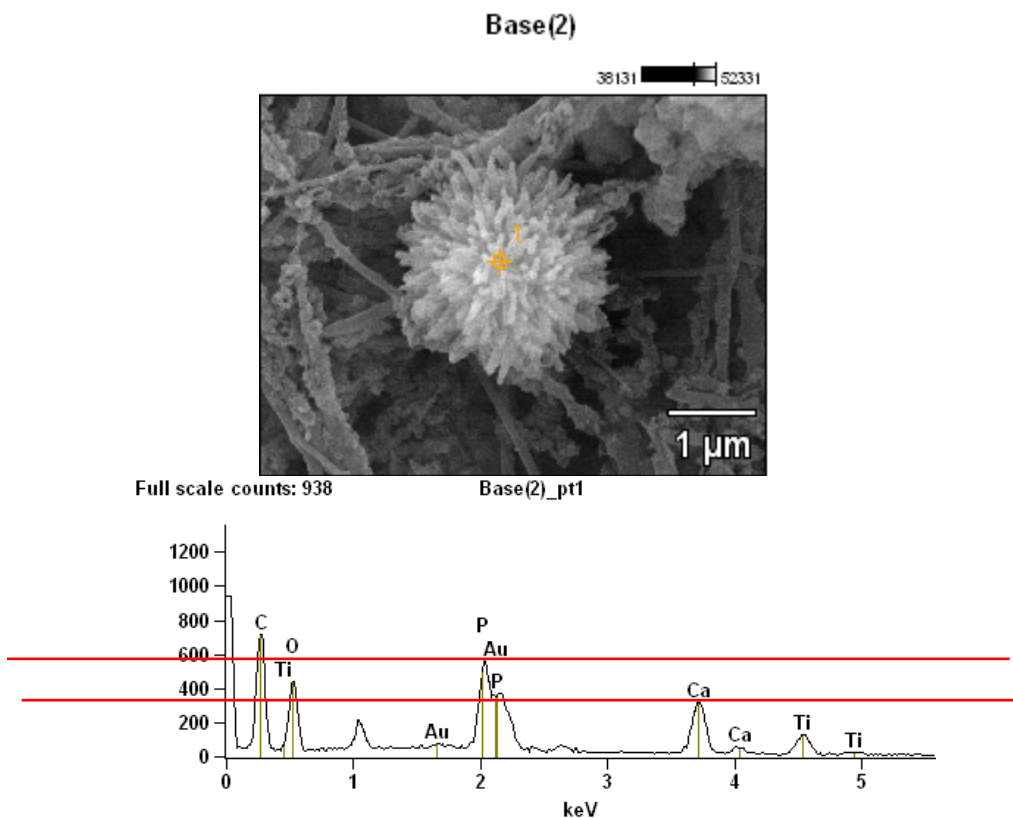
Scan of everything else but the objects

<i>Element Line</i>	<i>Weight %</i>	<i>Weight % Error</i>	<i>Atom %</i>	<i>Atom % Error</i>
<i>P K</i>	3.87	+/- 0.10	2.32	+/- 0.06
<i>Ca K</i>	8.68	+/- 0.14	4.02	+/- 0.07

The objects contain significant amounts of calcium and phosphate. This suggests they may indeed be mineral spherulites. Furthermore, elemental ratio analysis provided in the table above

reveals a Ca:P ratio of 1.73, very close to 1.67, the theoretical stoichiometric Ca:P ratio found in hydroxyapatite. [256] Further studies are required to definitively characterize the precise composition of the calcium and phosphate identified, but it matches well with hydroxyapatite, which also supports our belief that the spherical objects are mineral spherulites. They are larger than typical spherulites, which may be a result of cells which may have been prolific calcium producers. Spherulites were not observed on DOPS/GS coatings.

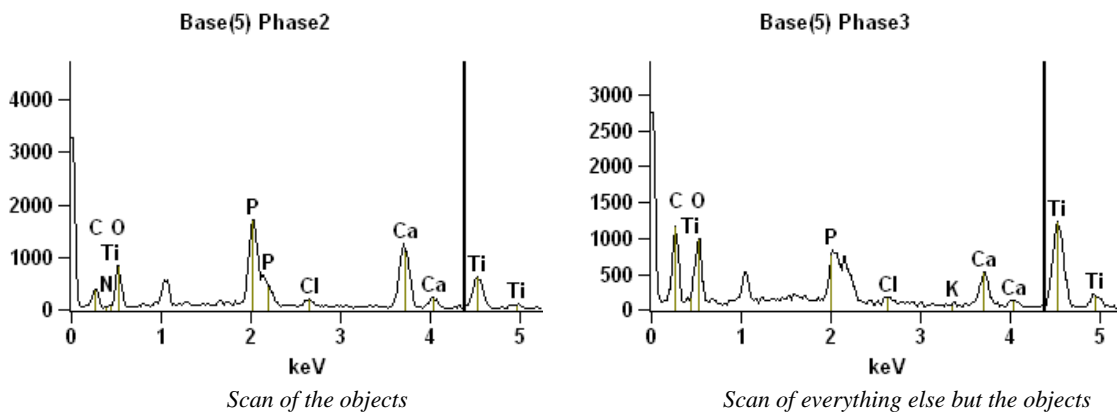
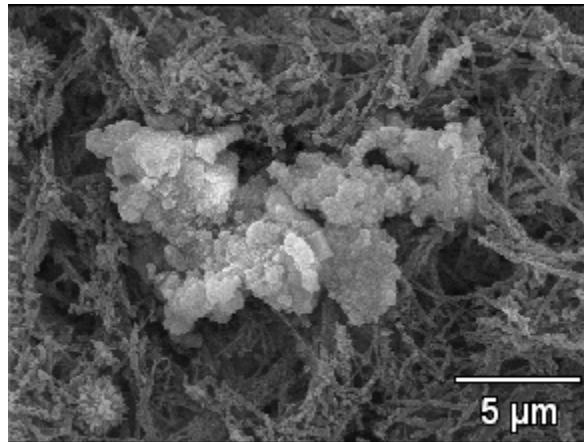
A magnification of the same EDS result is provided in the following image.



Again, it can be seen that these objects are rich in calcium and phosphate. The Ca:P ratio taken from the chart above is approximately 1.63 (590/360 as indicated by horizontal lines in the chart above), again very close to 1.67, the theoretical stoichiometric Ca:P ratio found in hydroxyapatite.

These presumed mineral spherulites were also seen on Plain Ti samples in week 2 (e.g. Figure 7-68 above). It is not unreasonable to expect that osteoblastic cells would develop on Plain Ti samples, as they were on DOPS samples. These cells are indirectly responsible for the initial formation of spherulitic deposits as they deposit the mineral-laden matrix vesicles from which spherulites form, as discussed below.

The additional amorphous “puffy white” structure also found in many of our DOPS and DOPS/GS coatings (e.g. Figure 7-69 and Figure 7-70 above) is analyzed with EDS in the following.



<b>Element Line</b>	<b>Weight %</b>	<b>Weight % Error</b>	<b>Atom %</b>	<b>Atom % Error</b>
<b>P K</b>	10.63	+/- 0.17	7.23	+/- 0.11
<b>Ca K</b>	21.29	+/- 0.25	11.19	+/- 0.13

This structure is also composed of relatively large amounts of calcium and phosphate. The Ca:P ratio in these objects is lower, 1.56 but still close to hydroxyapatite. It may be a less crystallized (amorphous) form, perhaps which has yet to crystallize further.

Both these EDS analyses provide strong evidence that a rich population of osteoblasts were once present on these samples. However, conversely, the reduced presence of calcium phosphate and the apparent absence of hydroxyapatite (or spherulites) in the GS-loaded coatings suggest an inhibitory effect of GS on osseogenesis, as reported elsewhere. [199]

Additional evidence of osseogenic activity is also visible in the DOPS coatings. Closer examination of Figure 7-69 above reveals additional interesting information, as shown in the following image taken at 5,000x original magnification.

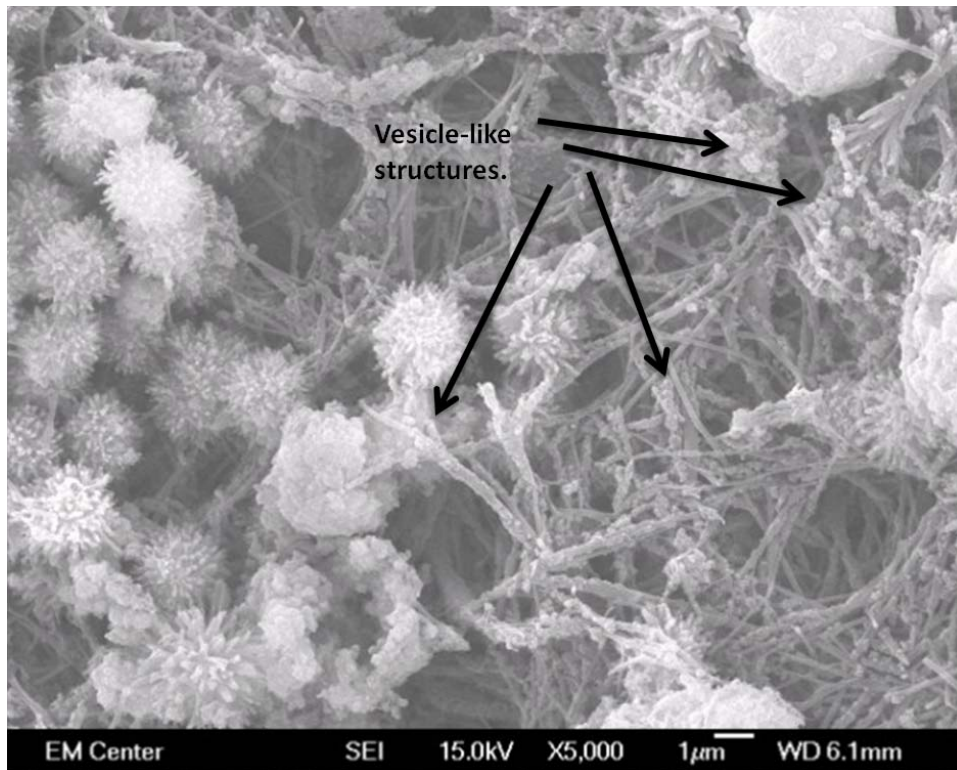


*Figure 7-89: SEM image of DOPS week 2, imaged at 15 keV, 5000X original magnification. Small spherical objects and vesicle-like structures are clearly visible and plentiful.*

The vesicle-like structures are likely matrix vesicles. Matrix vesicles are extracellular, approximately 100 nanometer diameter particles selectively located within the matrix of bone, cartilage, and predentin. A more magnified image of these, the mineral spherulitic objects, and the underlying fibrous matrix follows:

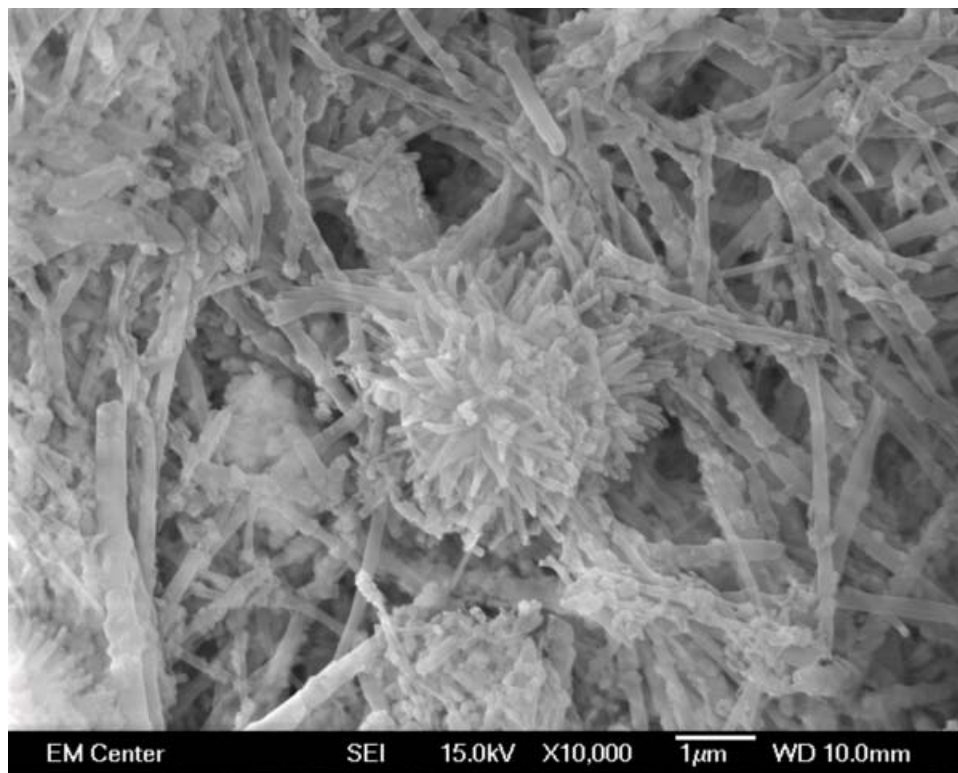


*Figure 7-90: SEM image of DOPS week 2, imaged at 15 keV, 10,000X original magnification. Small spherical objects and vesicle-like structures are clearly visible and plentiful.*

Matrix vesicles incorporate a variety of enzymes, notably alkaline phosphatase [238, 253] and are presumed to be the initial nucleation site of the (abundant) mineralizing spherulites discussed above during the early phase of biomineralization [254, 257]. The spherulites are themselves further evidence that these structures are matrix vesicles. Matrix vesicles form by the budding and pinching off of vesicles from outer regions of chondrocyte, osteoblast, and odontoblast plasma membranes [238], thus providing further evidence of the existence of osteoblasts on our samples. These vesicles were not observed in acellular samples.

Prior studies have observed very similar structures in similar time frames. [252] As with the EDS analysis presented above, the presence of strong evidence of matrix vesicles strongly suggests these coatings were once populated by a rich population of active bone producing cells. Explanations for the notable absence of cells from our SEM images and what might have become of the coatings is provided in the following section.

### ***7.9.2 About Low Cell Numbers in Follow-up Study***

---

In our preliminary study, cells appeared to develop normally, with normal osseogenic tendencies. In the follow-up study, we observed low cell numbers in the early time points, as evidenced by MTT and live cell fluorescence microscopy, and an apparent absence of cells in later weeks, as evidenced by the above SEM images. One would expect to see many cells, given the ample evidence (calcium per total protein, OC/OP, matrix vesicles, spherulites, calcium phosphate-hydroxyapatite) of their existence. One of the most important differences between these studies was the presence of cholesterol in the DOPS coatings in the follow-up study. We can hypothesize four possible reasons for these results: (1) insufficient cell seeding densities and/or early media changes in the follow-up study; (2) presence of cholesterol in the coatings potentially interfering with normal cell adhesion; (3) unsuitable surface roughness for ideal osteoblast adherence to the coatings, and; (4) mechanical degradation of coatings removed cells. These are each discussed in the following sections.

It is also possible that residual chlorine remained in the samples, from unevaporated chloroform. Trace amounts of chloride can be seen in some of the EDS data presented in section 7.9.1 above. It is not found on all samples from any single treatment, nor is it observed in all treatments. Furthermore, chlorine has not been seen in any of our earlier work. We are confident that all chloroform (E-spray solvent) was dried out of the samples by evaporation and

vacuum dryer before being introduced to the cells. Therefore we believe an aftereffect from chlorine is highly unlikely.

Another possible explanation is experimental error in the staining procedure. This is unlikely because the more cells were found in the preliminary study using the same stains, assays and protocols, and performed by the same researcher.

### **7.9.2.1 Low Seeding & Media Changes at Early Time Points**

In the preliminary study, samples were seeded onto 24-well plates at a density of  $1E^6$ /well, while in the follow-up study, samples were seeded onto 48-well plates at a density of  $0.5E^6$ /well. Furthermore, in the preliminary study, an initial half media change occurred on day 4 and all media was changed on day 7. In the follow-up study, half of the media was changed on day 1 and all media was changed on day 4.

It is likely that at least a portion of the apparent decrease in total cell number on days 4 and 7 of the follow-up study could be explained by the half media change that occurred on day one and full change on day 4 in this follow-up study. In the preliminary study, half of the media was changed on day 4 and the first full media change occurred on day 7. Our follow-up study protocol was designed for faster growing cells, such as fibroblasts and was considered suitable to this study. MSC cells are somewhat slower to adhere than are other cell phenotypes, such as fibroblasts. MSCs achieve approximately 90% of their population growth in their first 7 days post-seeding. Thereafter, they only increase approximately 10% in population, as they dedicate more energy to bone production. This means that if something impedes the normal proliferation of MSCs within the first week of a study, it is likely to negatively impact the complete study by reducing all measures of cellular activity (e.g. calcium, ALP in later weeks of study).

If cholesterol plays a role in interfering with osteoblast adhesion on our coatings it is possible that osteoblast growth may be slower on coatings with cholesterol than without. This is discussed in the following section, and might explain why growth is faster on Plain Ti in the follow-up study, and appears to be supported by findings of Kubinova [258] discussed in the following section.

### **7.9.2.2 *Poor Cell Adherence to DOPS/Cholesterol Coatings***

As discussed in sections 2.1.1 and 2.3.2 above, phospholipids play critical roles in osseointegration. Cells are reported to adhere better to phospholipid coated surfaces than non-phospholipid coated surfaces [25, 235] but these studies considered relatively short time frames (less than 72 hours). Bosetti [26] cultured fibroblasts and human osteoblast-like cells on titanium samples pre-mineralized by soaking in simulated body fluid. They reported insignificant differences in cell numbers for DOPS or DOPS/cholesterol drip coatings than for Plain Ti, in a 72 hour window. Unfortunately they did not look further. Satsangi [119] reported approximately equal amounts of total protein in 0, 7 and 14 days, and significantly higher ALP in 14 days with human embryonic palatal mesenchymal stem cells, but did not report any short-term viability or proliferation findings. It is possible that at longer time-frames the cells might have become dislodged.

The presence of cholesterol in the coatings may be creating non-ideal adhesion conditions for cells. Numerous studies have reported compatibility of osteoblasts and fibroblasts with cholesterol containing surfaces. [11, 50, 56, 235, 259] Other studies have used cholesterol in combination with DOPS in other cell growth/drug delivery studies, most commonly in liposome formulations. [29, 49, 54, 260] Additional studies report that other cholesterol-containing polymers [50] were found to create a high-affinity surface for the attachment of osteoblasts or

endothelial cells. [96, 258, 259, 261] None of these studies have reported cytotoxic effect due to the presence of cholesterol. These studies indicate cholesterol can have an effect on osteoblast adhesion for some materials in some conditions, but our study design did not allow us to test the independent affects of cholesterol versus calcium pretreatment and passivation, so we cannot reach any firm conclusion.

Osteoblasts preferentially adhere to hydrophilic surfaces more than hydrophobic surfaces. [98] Therefore, it is also possible that cholesterol is adversely affecting cell adherence by increasing the hydrophobicity of our coatings. Indeed, we observed what appeared to be higher hydrophobicity in our cholesterol coatings than in coatings without cholesterol (refer to section 7.8.2.1 above). Furthermore, as discussed in section 2.1.3 above, cholesterol stiffens cell membranes. It is possible cholesterol also stiffens our coatings, thus helping to improve elution characteristics and coating retention, as discussed in sections 6.5 and 5.6.3 above, respectively. If our coatings containing cholesterol were stiffer, they might have been less suitable for osteoblast adhesion. [98]

Therefore, a most likely explanation is that the cells did not adhere well to the coatings (and thereby to the cholesterol in the coatings), and were removed from culture when media was changed (initially and biurnally through the study). It is also possible that cholesterol is not implicated, but rather some other factor led to the absence of cells in our follow-up study. This question merits further study in future work.

Another possible explanation is that the concentration of cholesterol may have been too high. For our study, the cholesterol concentration was chosen based on a common phosphatidylcholine/phosphatidylserine/cholesterol ratio of 7:2:1 often used in other studies. [11, 29, 60, 235, 260] No studies have been found using only cholesterol and DOPS, without a third

(or more) phospholipid, but these studies are typically targeted at liposomal drug retention, and the phospholipid content schemes and mixtures are relatively diverse and complex. Toxicity to fibroblasts was observed at cholesterol concentrations higher than 10 mg/ml and significant decreases in adhesion were reported at greater than 5 mg/ml of cholesterol. [54] Our coatings contained 0.47 mg of cholesterol per sample, so this is an unlikely effect in our study, but small changes in concentration apparently can have profound effects on cell adhesion and toxicity.

To estimate the amount of cholesterol to use in our study, we applied the following reasoning. Cholesterol has three potential binding sites available for attachment of other compounds, such as DOPS. These include the terminal –OH group and two reactions leading to formation of oxysterols, by oxidation at C5 and C6, creating a triol (double –OH groups), and oxidation of C7, creating an –OH and donating a hydrogen atom. Infrared spectral analysis has confirmed that cholesterol interacts with the phosphate head group of the DOPS molecule while the bulky steroid and hydrocarbon tail of the cholesterol molecule interact with the fatty acid (acyl) chains of the DOPS. [22, 60] Cholesterol is known to bridge between head and tail groups of 2 DOPS molecules in this way. Thus it was determined that cholesterol has the potential to bind 2 DOPS, leaving one site available, thus the minimum amount would be a 3:1 ratio of DOPS to cholesterol. We doubled this ratio in order to avoid all DOPS being bound with cholesterol, leaving some DOPS available to bind with other compounds. Therefore, a 6:1 ratio of DOPS to cholesterol was chosen.

### **7.9.2.3 Unsuitable Surface Roughness**

As discussed in section 2.2.3 above, adhesion strength of fibroblasts and osteoblasts on various polymeric materials and titanium was reported to increase with increased surface roughness [69, 96-98] With increasing roughness of the surface, osteoblastic cells showed

increasing differentiation and decreasing cell proliferation. [69] Titanium surfaces with an average surface roughness ranging from 22 to 28  $\mu\text{m}$  exhibited significantly higher bone/implant index than smoother surfaces. [99] Although these metrics apply to titanium, not DOPS coatings, they may provide a clue to which we can compare our coatings in the same context. As discussed in section 4.6.2.1 above, two of our DOPS coatings exhibited average surface roughness ( $R_a$ ) of 2.3 and 2.6  $\mu\text{m}$ . Although we judged our “ideal” coatings to be of suitable roughness for cell growth, we only judged visually by SEM. It is possible our DOPS coatings were in fact too smooth for effective cellular adhesion. We did not measure surface roughness for DOPS/cholesterol coatings, but they appear, at least from SEM assessment, to be similar in roughness to the DOPS coatings.

#### **7.9.2.4 *Cells Adhered Well but Coating Degradation Removed Cells***

Another possible explanation is that the cells adhered well to the cholesterol in the coatings, but the coating itself was dissolved away, and the cells with it. Recall earlier observation of tiny droplets of a fat-like substance observed floating up from each sample to the surface of the dish while samples were being fixing for SEM. We suspect this was lipid dissolving from the coatings. This was NOT seen in the preliminary cell study. The fact that the thick, rope-like matrix seen in week 2 images is absent in week 1 SEM images strongly suggests our week 1 SEM fixation process was much more aggressive. Before week 2, the process used HMDS, which was eliminated from the process thereafter. SEM images from week 1, for example Figure 7-63 and Figure 7-67 above, show a dense, mat-like matrix apparently well-adhered to the titanium surface, but clearly much thinner than the DOPS coatings that remained in week 2 images, when HMDS was no longer used. Possibly, multiple alcohol baths used to fix samples for SEM in week 2 were also enough to dissolve away some component of the coatings, and with

it, the cells that were adhered to it. Further study is required to determine the effects of SEM fixing on our coatings and possible implications in cell detachment.

It is also possible, but unlikely that the cells migrated below the surface into the matrix of the coating. For human osteoblasts, an ideal dry pore size for growth, migration and matrix formation is approximately 600  $\mu\text{m}$  [88] with a minimum size of approximately 100  $\mu\text{m}$ . [262] It can be seen in SEM images above, particularly Figure 7-89, that the largest pores in our coatings are perhaps 4  $\mu\text{m}$ , but these coatings had been desiccated for SEM imaging. Further study would be required to determine if the hydrated pore size of our coatings would be large enough that cells could migrate beneath our coatings.

Furthermore, if the degradation of the coating was caused by erosion, this would likely have destroyed the spherulites. Thus, it remains unlikely that the coatings eroded. The spherulites were likely bound to the coating matrix by ionic bonds set in place by the cells as they produced the matrix vesicles from which the spherulites developed.

We further hypothesize that the rich rope-like matrix that underlies these objects is the remainder of the DOPS coating after it dissolved or delaminated. This remaining matrix was not observed in the preliminary study, therefore suggesting its presence may result from the calcium pretreatment and/or the presence of cholesterol in the coatings. It is as yet unknown what this material might be, but it appears to be an opportune discovery as potential scaffold structure, warranting further investigation. A magnified image of this potential scaffold material is shown in the following:

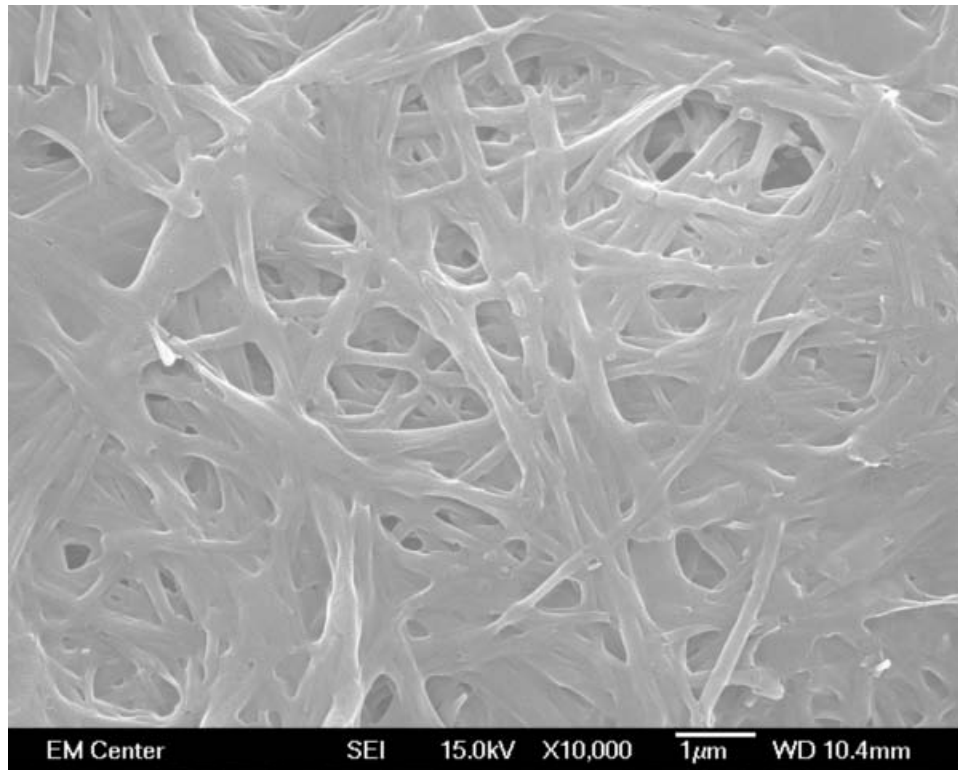


*Figure 7-91: SEM image of potential DOPS-based scaffold material, imaged at 15 keV, 10,000X original magnification.*

## **7.10 Conclusions**

The preliminary cell study successfully confirmed that DOPS coatings are non-cytotoxic, enhance cell viability and biomineralization activity, and exhibit positive osseogenic indicators. The follow-up study, to test the effects of enhanced coatings, yielded low initial cell viability and cell numbers, but no evidence of cytotoxicity. Live cell fluorescence microscopy and SEM examination showed relatively fewer cells on DOPS coatings, with or without GS. Evidence of biomineralization (calcium) was low on a total basis but higher than control surfaces on a per-cell basis. But there was very clear evidence of extensive biomineralization under evaluation by SEM. And there were relatively strong indications of bone morphogenesis markers for calcium production (osteocalcin) and for cell migration, signaling and mineralization (osteopontin). The coatings remained intact through week 1 and week 2. However, SEM evaluation in weeks 1 and 2 revealed very few cells. It is believed that multiple factors played a role in the absence of cells,

including cholesterol having potentially adverse effects on cell adhesion at concentrations used, low cell seeding densities and media changes at early time points. And, we conclude that, of the two protocols used for changing media in earlier time points of our MSC cell studies, the preferred protocol is to change half the media on day 4 and the full media on day 7.

### **7.11 Limitations**

A longer time-frame would have enabled closer scrutiny of the absence of cells in later time points. In addition, marker values measured in this study, such as calcium, ALP and protein values measured on samples, were too low to clearly distinguish trends and significance. For example, absolute calcium was similar to background calcium from the titanium pretreatment and from the media itself.

Higher seeding densities on larger 1 cm<sup>2</sup> samples (rather than 0.5 cm<sup>2</sup>) would increase total area for cell growth, thereby increasing visibility of potential markers (e.g. calcium, ALP, total protein), thereby better enabling detection of trends and patterns in cell growth. And finally, larger numbers of samples would compensate for the inherent variability in the tests used in this study, enabling more statistically significant findings.

Finally, our study design did not account for testing the independent affects of cholesterol versus calcium pretreatment with and without passivation. This should be researched in future work.

### **7.12 Future Work**

Numerous projects could be contemplated to continue investigation of cellular response to DOPS coatings.

Future work should be completed to study the independent affects of cholesterol versus calcium pretreatment with and without passivation. It appears these factors have an effect on

coatings retention and elution, making it especially useful to understand more detailed cause and effect relationships.

Additional cell studies should be conducted to understand the affect of cholesterol on the cellular response to DOPS coatings. Changes in cholesterol concentration would affect many other factors, adherence for example. In these future studies, it may be advisable to use fibroblasts rather than osteoblasts to study factors affecting proliferation and adhesion, as fibroblasts are much more prolific than osteoblasts. Then, it would make sense to revert to osteoblasts to study osseogenic response. Future work should use higher seeding densities, perhaps 2 million cells/well, on larger 1 cm square samples. It should also consider calcium-free media, such as Tris, which would increase the relative amount of calcium measured from cells versus that measured from the media, both via sequestration by the DOPS and independently depositing on the surfaces.

It appears that DOPS may inhibit short-term cell proliferation and viability, but enhance longer term mineralization. We performed only very preliminary investigation of the deposition of calcium from the media on samples, versus sequestration of calcium by DOPS in the coatings. It would be very interesting and useful to consider these effects to help better determine the role DOPS plays in early bone mineralization.

A rich rope-like matrix, underlying spherulites and matrix vesicles developed on the DOPS coating. It is as yet unknown what this material might be, or how it developed, but it appears to be a possible scaffold structure, warranting further investigation. A porous scaffold which can be easily produced from naturally occurring materials, and which is apparently a good target for mineralization and matrix deposition would be a very interesting discovery. One could

determine more about the composition of this structure with immunostains, for example, of collagen in the matrix.

It would be very useful and interesting to conduct *in vivo* experiments to evaluate actual performance of the DOPS coatings in an animal model, and to compare results of *in vitro* tests with *in vivo* performance. Prior to such tests, it may be useful to evaluate the reaction of blood to our coatings *ex vivo*.

Other factors could be considered to better understand cell adherence with respect to our coatings. For example, it would be useful to investigate expression of specific adherence proteins, such as integrins and cadherin, to better understand the absence of cells in our follow-up study. Such a project would start with a simple adhesion study looking at short term cell counts, probably using prolific cells like fibroblasts, with various concentrations of cholesterol and other combinations of coating chemistry.

As we investigate further the effects cholesterol may or may not be having in our coatings, we could also gain additional useful insight by studying expression/presence of laminin in our DOPS layers with the intent of better understanding factors inducing the colonization of our coatings by cells.

It would also be useful to look at osteonectin to better understand calcium binding by cells in our coatings.

Our preliminary and follow-up studies were both performed with cells from a single MSC source. This was due to budgetary limitations. All tests should be duplicated using a second MSC source (rat), budget permitting.

## **8 Summary Conclusions**

E-spraying is a suitable method for creating thin, adherent, osseointegrative coatings on titanium. Compared to drip and dip techniques for creating DOPS coatings, E-sprayed DOPS coatings appear to be more consistent and more durable. Manipulation of the key E-spray process parameters, target surface area, concentration (viscosity), electric field strength (and therefore current) and spray time provide effective, predictable control of coating characteristics such as morphology, porosity and consistency. DOPS coating thickness was measured by atomic force microscope to be approximately 6  $\mu\text{m}$ , as shown in Figure 4-29 and Figure 4-30 above. E-spraying is easy to perform, and repeatable at low cost.

Cholesterol as an additive to a DOPS E-spray solution is an effective means to increase the retention of the DOPS coatings when E-sprayed on passivated titanium samples which were pretreated with calcium-chloride. GS-loaded coatings provide significantly ( $p < 0.05$ ) better coating retention than coatings without GS.

We found that E-sprayed DOPS coatings can be loaded with clinically relevant amounts of GS, and approximately 80% of the loaded GS elutes out in the first 8 hours in PBS. We also found that we can modify this elution profile by passivating the titanium surface, then pretreating the surface with calcium-chloride, and then adding cholesterol to the DOPS E-spray solution.

We confirmed that DOPS coatings are non-cytotoxic, enhance cell viability and biomineralization activity and exhibit positive osseogenic indicators. The follow-up study, to test the effects of enhanced coatings, yielded low initial cell viability and cell numbers, but no evidence of cytotoxicity. There were relatively fewer cells on DOPS coatings, with or without GS. Evidence of biomineralization (calcium) was low on a total basis but higher than control surfaces on a per-cell basis. We found clear evidence of extensive biomineralization of

DOPS/cholesterol coatings. There were relatively strong indications of bone morphogenesis markers for calcium production (osteocalcin) and for cell migration, signaling and mineralization (osteopontin).

## 9 Acknowledgements

We are grateful to the following organizations that provided funding for our work:

- Colorado State University Cancer Supercluster Translational Research Grant Program
- Colorado Bioscience Discovery Evaluation Grant Program

*And a personal note of gratitude...*

Like Cedalion standing on the shoulders of Orion (Nicolas Poussin, 1658), I could not have accomplished this work without the support, kindness and patience of countless mentors, friends, colleagues and family members. I extend my utmost appreciation to Sue James, my friend, mentor, advisor and colleague (in this order). Without Sue's patience and counsel, I would not have finished this work. In fact, I wouldn't have started this work were it not for Sue giving me the opportunity to live my dream in her lab, and extending her kind support as I climbed back into the academic saddle. My thanks also go to my co-advisor, Ketul Popat, who withstood countless knocks on his door, often with what must have seemed the oddest of questions, many no doubt repeated in various forms of confoundedness. Ketul was always there, always rich with advice, and always patiently helpful. I also thank my dear friend and colleague, Barb Smith, for always being there when it seemed the walls were crashing in, always with a smile, and always reminding me that the work is the learning and the learning is the fun, and that is what we're doing here after all. And I thank my other advisors, Matt Kipper and Stewart Ryan, for being there to help me learn how to think, and then pushing me to learn more than I ever imagined I would or dreamed I could. I thank Debbie Crans and her colleagues in chemistry for many good ideas and discussion. And thanks to my friend and colleague Tim Ruckh, also ever patient, helpful and constructive in his criticism. Thanks to Marisha Godek for opening a rusty door, switching on a light and starting a fire, and to Keri Hansen for putting more wood on the fire,

being so patient in my early re-introduction to research, and not putting the fire out. And lastly among my academic friends and colleagues, I sincerely thank my fellow lab rats in the James lab for patient assistance and kindness for a non-traditional student landing in their midst, especially to Hannah Hudson for helping me develop the techniques we have come to depend on and upon which my dissertation is fundamentally based, and to my friends and colleagues Tom Triffo and Derek Carroll for helping me work through some especially challenging and long hours in the lab.

And finally, I could not have stood on the shoulders of these many giants without someone holding my ladder. To my wife I am forever indebted. I have fulfilled a lifelong dream – a really big ticket item in my bucket list. As I changed my life’s path, and indeed her’s along with me, Aleesha, my best friend and soul mate, was always there to nurture, support, advise and propel me forward, sometimes with a kick, but always with the love that has made us best friends for all these three wonderful decades. And to my son Kyle, who must at first have wondered if his Dad was going through a bad life change, but who was always supportive of both Aleesha and I, and for which I am also forever indebted. And lastly, my deepest thanks to my father and mother , who taught me to always wonder, loudly if necessary, question everything, never fear change or failure, and always search for answers and truths in our pursuit of life’s fulfillment. For to follow a life dream is to reach the highest level of fulfillment, and in the end, that’s really all we can ask for in life.

A handwritten signature in blue ink, appearing to read "David Prawel". The signature is fluid and cursive, with a large loop at the end.

... David A. Prawel  
February 28, 2011

## 10 Appendix A. Detailed Protocols for Electro-Spraying

### 10.1 Electro-Spraying Protocol

Feb, 2010

#### Materials and Supplies

- 1010 Gastight Glass Syringe and plunger
- Pipetter Gun and 5mL graduated pipette
- 50mL beaker , 100mL beaker, small vials with Teflon tabbed lids
- Titanium squares
- Teflon sticky tack
- Cotton swabs and kim wipes
- Sufficient chloroform and phospholipid
- well plate(s) to store samples
- sample mounting board
- sufficient copper mounting plates
- Electrospraying apparatus and needle

#### Methods

*\*Always wear gloves*

#### Chemical Set Up

1. Set up clean work space in hood with Kimwipes
2. Clean all glass wear (syringe, beakers, pipette, vials) thoroughly with chloroform before beginning to avoid any possible contamination
3. Rinse needle with chloroform to make sure to remove any remaining solution from previous use, and ensure needle works properly –air dry
4. Weigh and label all titanium samples.
5. Clean the non-labeled side of all titanium samples with chloroform.
6. Clean sample mounting board. Make sure the area where the samples will be attached is free of any old phospholipid and all tape is in place covering any leads you will not be using.
7. Connected needle tube to syringe.
8. Prepare the DOPS/Chloroform solution as required. Keep container closed as much as possible to avoid (rapid) evaporation of the mixture.
9. Carefully transfer the solution to the syringe. Get prepared in advance and work quickly – the solution evaporates very quickly. Attach tube and needle to syringe. Push syringe plunger completely in. Open vial containing chloroform mixture. Draw all solution into Syringe. Minimize air intake.

#### Electro-Spray Apparatus Set up

1. Check the pump rate on pump (\*every third or fourth use you will want to check the pump rate and ensure calibration)
2. Put syringe in place on pump and clamp needle into holder in apparatus
3. Clamp sample mounting board in place
  - a. Align needle such that it points at the center of the ring of samples on the sample mounting board
  - b. Adjust distance from needle tip to sample mounting board
  - c. Recheck alignment, and then distance again.
4. Attach ground wires to syringe and sample mounting board
5. Attach positive pole to needle tip
6. Check that Voltage on power supply is set as required
7. Attach clean titanium squares to copper mounting plate using Teflon tack stuck around the copper, ensuring that they are touching the copper. If there is no connection, no phospholipid will get on the samples. Clean samples again with chloroform on a cotton swab after attaching.
8. Double check samples (make sure they are touching) and clean one last time with chloroform.

9. Double check all connections: that solder board and syringe are grounded and needle is powered
10. Push pump activator manually until you see fluid start to move again in tube, this is to make sure the pump activator is in contact with the syringe plunger
11. Turn on power supply
12. Turn on pump
13. Watch for a spray cone, once you see the spray cone, start the timer and close the door to the apparatus
14. When the prescribed time has run out, turn off the pump and turn off the power supply
15. Remove ground and power wires, and remove sample mounting board
16. Remove samples from the sample mounting board
17. Reweigh samples
18. Clean the sample mounting board

#### Clean Up

1. Push a few mls of chloroform through the syringe, into a waste beaker
2. Clean all glass wear (beakers, pipette, vials) and needle with chloroform
3. Very carefully clean syringe
4. Store needle with E-spraying apparatus
5. Rinse glass wear with lab soap and then rinse in DI water
6. Dry carefully and store
7. Double check that E-spray apparatus is clean and clean up area in hood
8. Do one last check of lab and make sure you have stored everything properly – leave the lab in better shape than you found it

### ***10.2 Titanium Cleaning & Surface Preparation Protocol***

Prawel  
July 2010

Allocate about 2 hours, plus possible overnight rinse, for complete procedure.

#### **Solvent Cleaning**

Purpose:

In this procedure, Ti samples are sonicated in solvents and de-ionized water to remove organic debris and oils.

Notes:

Use glassware on solvents.

Need:

Sonicator  
Acetone

Procedure

1. Sonicate 30 minutes in 100 ml Acetone (stirring vigorously every 5 minutes)
2. Rinse in tap water
3. Sonicate 15 minutes in 100 ml 2% Liquinox (stirring vigorously every 5 minutes)
4. Rinse in Di water until no evidence of soap
5. Sonicate 15 minutes in 100 ml DI water (stirring vigorously every 5 minutes)

6. Rinse once in acetone
7. Air dry and store in dessicator.

### Surface Preparation

Need:

Hydroflouric Acid

Nitric Acid

**Polypropylene**, HDPE or PTFE lab equipment (for handling HF):

Tweezers or forceps

Beaker (>150 ml)

Chloroprene gauntlet gloves (or double nitrile)

Graduated cylinder (10 ml)

Storage bottle for waste solution

Calcium gluconate gel (in case of skin contact with HF)

Note:

In the nitric-hydrofluoric pickling solution, the ratio of nitric acid to hydrofluoric acid is more important than the concentration of either of these two acids. When this ratio is maintained at 10 to 1, hydrogen absorption during pickling is minimized. (from ASTM B600)

Avoid pouring water in acid. It's best to always pour acid into water.

Procedure

Summary: Samples are bathed in 3.5% HF for 30 seconds to remove the existing Ti oxide layer and then soaked in 35% HNO<sub>3</sub> for 30 minutes to regenerate a new oxide coating.

1. Slowly add 50 ml of 70% HNO<sub>3</sub> to 50 ml de-ionized water and warm to 50°C, stirring at 150 RPM.
2. In a **polypropylene beaker**, slowly add 7.3 ml of 48% HF (measured in a **polypropylene** graduated cylinder) to 92.7 ml de-ionized water, at room temperature.
3. Gently bath no more than 50 Ti samples at once in the HF solution for 30 seconds.
4. Pour off the HF solution into another **polypropylene** beaker, and carefully transfer samples to the HNO<sub>3</sub> solution, stirring at 150 RPM, at 50°C. Stir for 30 minutes, manually mixing samples every few minutes to prevent samples from stacking on each other for more than a few minutes.
5. Then, samples are then rinsed briefly in de-ionized water and either soaked in DIH<sub>2</sub>O water at 37°C for 24 hrs or boiled in DIH<sub>2</sub>O water for 1 h.
6. Following this chemical treatment, samples are rinsed with de-ionized water, vacuum dried, and placed in dessicator for relatively immediate (few days) use, or vacuum packed in Nitrogen, and stored at room temperature for future use.

### 10.3 Mixing PL Protocol

Prawel

March 13, 2009

Note, actual amount of PL/chloroform mixture created is always greater than necessary in this protocol, due to loss of small amount of PL on weighing dish, and desire to keep the concentration of PL as desired.

All at room temperature ...

M = desired total mls of PL/chloroform mixture in solution  
[PL] = desired concentration (weight %) of PL/chloroform solution  
 $G_{PL}$  = grams of PL to get desired [PL]

Algorithm...

For M grams (mls) of PL/chloroform mixture,

$$M \times [PL] = G_{PL}$$

$M - G_{PL}$  = grams of chloroform / 1.48 g/ml = ml chloroform to get M ml of solution

$$G_{PL} = [PL] \times (1.48 \times M) / (1 - [PL]) = 0.0526 \times (1.48 \times M)$$

Weigh out PL using Teflon weighing dishes

(grounding hands and weighing dish whenever possible – PL is very electrostatic)

Place PL in small beaker (~50 ml)

Weigh empty weighing dish

Calculate W, the actual weight of PL in beaker (weight with PL – weight without PL)

Calculate amount of chloroform actually needed to get desired [PL]

$$W = 0.0526 \times (1.48 \times M), \text{ solve for } M = 0.0779 \times M$$

So,  $M = W / 0.0779$  in mls

Example:

Desire 2.7 mls of 5% PL/ $\text{CHCl}_3$

$$0.0526 \times (1.48 \times 2.7) = 0.21 \text{ g PL}$$

Weigh out 0.2172 g PL. Weighing dish weighs 0.0112, so actual weight of PL is 0.2060

$$0.206 / 0.0779 = 2.64 \text{ ml } \text{CHCl}_3$$

Measure out this much chloroform and pour into beaker with PL.

Mix with spatula until no PL is visible (few minutes).

Pour mixture into small vial with Teflon-lined lid and close lid (it evaporates quickly).

Draw mixture as need, quickly opening and closing lid on vial.

Store any remaining mixture at  $-20^\circ \text{C}$ .

#### 10.4 Calcification of Ti surfaces

D. Prawel

February 09

##### Overview

Calcium from two sources, calcium chloride and  $\beta$ -tri-calcium phosphate, was applied in equal molar ratios to Ti samples at a 2.25 mM concentration.

##### Definitions

##### Assumptions/Parameters for this Procedure

Samples are cleaned and prepared according to separate Ti Clean & Prep Protocol

##### Supplies/equipment

- Calcium sources (calcium chloride (anhydrous) and  $\beta$ -tri-calcium phosphate)
- 2 hot-plate/stirrers (temperature controlled)

### Preparation

1. Weigh out equal molar ratios of the two calcium sources
  - a.  $\text{CaCl}_2$ 
    - i. 1 mole Ca in  $\text{CaCl}_2$  weighs 109 grams; 2.25 mM = 0.245 mg/ml; 24.5 mg in 100 ml  $\text{DIH}_2\text{O}$
  - b.  $\text{CaPO}_4$ 
    - i. 1 mole Ca in  $\text{CaPO}_4$  weighs 310 grams; 2.25 mM = 0.698 mg/ml; 68.8 mg in 100 ml  $\text{DIH}_2\text{O}$

### Procedure

1. Place calcium sources each in separate 250 ml beakers
2. Add 100 ml  $\text{DIH}_2\text{O}$  to each beaker and set on stirrer at  $37^\circ\text{C}$ , at 150 RPM.
3. Cover each with \_\_\_\_\_ and stir for 24 hours, occasionally mixing (manually) to prevent stacking effects. (note: an easy technique is to puncture a disposable LDPE pipette through the \_\_\_\_\_ cover and use it to jet the samples around as they stir. The pipette can be left in place until the samples are fully treated.
4. Rinse by replacing calcium solution with  $\text{DIH}_2\text{O}$  in each beaker, twice.
5. Vacuum dry and used immediately or vacuum pack in nitrogen and store at room temperature until use.

## 11 Appendix B. Detailed Protocols for Elution Study

### 11.1 Elution Protocol

GS and P Assays from DOPS coated Ti surfaces

D. Prawel

February 09

#### Definitions:

N = number of Ti samples to be eluted

T = number of time points (= 16 for 8 hour study 10 for a 3 hour study)

Z = number of treatments, e.g. 10kV vs 12 kV E-spray voltage

#### Initial Assumptions/Parameters for this Procedure

- 16 elution time points (T)
  - 15 mins for 2 hours
  - 30 mins for 2 hours
  - 60 mins for 4 hours
- 3 Ti samples of DOPS for each treatment, e.g. 10 kV, 12 kV and 14 kV E-spray voltage (N)
  - 3 samples per time point per treatment = 3 x 16 x 3 = 144 samples per treatment
  - Plus controls per time point if necessary, or run control study separately

#### Check supplies/equipment

- 2 ml mini-centrifuge tubes for each T times N times Z (for GS – OPA assay)
- 1.5 ml mini-centrifuge tubes for each T times N times Z (for P – ICP assay if done)
- 24 well plates for all N samples
- mini-cent tube racks or similar method to hold all tubes for full study
- PBS
  - Assays: T x N x Z x 1 ml x 2 (OPA and ICP) – for 1 ml eluents
  - Rinse: N x Z
- OPA Reagent
  - T x N x Z x 0.5 (see separate OAP Assay protocol for component quantities needed) plus enough for standards curve(s) (one per plate)
  - need to prepare 24 hours prior (see separate OAP Assay protocol for mixing instructions)
- Oscillating shaker available for use

#### Preparation

- Label 2 ml and 1.5 ml mini-tubes for rinse and all 15 min time points in advance
- Place mini-tubes in tube rack
- Carefully place samples into wells of 24 well plate(s)
- Turn on oscillating shaker – set at 5 units on dial (approx. 16 cycles per minute)

#### Procedure

- Rinse all samples quickly in 1 ml PBS to remove unbound GS and evaluate the loading efficiency of the drug on the samples.
  - SLOWLY and gently aspirate and expel 1 ml PBS 3 times and transfer the full ml into a 2 ml micro-centrifuge tube (for OPA assay).The loading efficiency will be expressed as percentage of loaded drug after rinsing, according to the following previously published relationship:

$$\eta = \frac{C_0 - C_r}{C_0}$$

where  $\eta$  is loading efficiency,  $C_0$  drug in the original solution,  $C_r$  is the drug in the rinse solution (drugs are in micrograms, not concentration)

7. Time zero: Add 1.0 ml PBS (room temperature) to each Ti sample
8. At each time point:
  - a. Retrieve micro-tube sample rack from refrigerator
  - b. Retrieve well plate from oscillating shaker
  - c. CAREFULLY pipette 0.5 ml into one 2 ml vial (for OPA assay)
  - d. Replace pipette tips at each sample draw
  - e. CAREFULLY replace 1 ml PBS into each Ti sample well
  - f. Place well plate into oscillating shaker
  - g. Close caps on microtubes, check correct labels
  - h. Place microtube racks in refrigerator
  - i. Prepare/label microtubes for next time point
9. Near end of elution study (between 1 hour time points) – prepare second full set of 1.5 ml micro-centrifuge tubes for all eluent samples (for ICP assay if needed)
  - i. Slowly, carefully pipette 0.5 ml from each 2 ml micro-tube into each corresponding 1.5 ml micro-tube (for ICP assay)
  - ii. Dilute each of these samples 100% by adding 0.5 ml PBS, totaling 1 ml in each 1.5 ml micro-cent tube
  - iii. Close caps on micro-tubes, check correct labels
10. At last time point, do not replace PBS into sample wells
11. Place well plate(s) in dessicator
12. Place all microtube racks in refrigerator for later assays

**At end of elution study:**

1. Perform OPA Assay for GS according to separate OPA Assay protocol.
2. Perform ICP Assay for P according to separate ICP Assay protocol.

<b>11.2 <i>Gentamicin Sulfate Loading Protocol</i></b>
--

Prawel  
November, 2009

1. Mix 0.173g GS in 1.73ml PBS at room temperature, yielding a 100mg/ml concentration, then dilute 5x resulting in a 20mg/ml concentration
2. Carefully drip (pipette) 5µl of the above GS mixture onto Ti samples (@ 20mg/ml = 100 µg GS)
  - a. Gently spread for coverage, avoiding contact with surface
3. Dry in vacuum dryer for at least 2 hours.
4. Repeat, starting at step 2 above if higher amounts of GS are desired (each cycle deposits an additional 100µg of GS on each surface).

<b>11.3 <i>OPA Assay Protocol</i></b>
---------------------------------------

Prawel  
December 16, 2009

Supplies Needed:  
Sufficient OPA Reagent (see below)  
Sufficient 96-well plates  
Sufficient Gentamicin Sulfate standards (see below)  
Plate reader that can read at 332 nm  
ADVISORIES:

Mix OPA Reagent at least 24 hours before use.  
OPA Reagent has shelf life of only three days.

Samples must be read after 30 minutes has passed since mixing in the reagents.

#### Protocol

1. **Mix desired quantity of OPA Reagent at least 24 hours prior to planned OPA assay.** (see Mixing OPA Reagent below)
2. Combine equal amounts of eluent being tested with OPA Reagent and iso-propanol.
  - a. If vial containing eluent being tested is large enough, add OPA Reagent and iso-propanol in amounts equal to amount of eluent being tested, into vial containing eluent being tested. For example, in DOPS-GS elution studies, we typically have 0.5 ml of GS eluent in a 1.5 ml vial. In this case, we would **add 0.5 ml of OPA Reagent and 0.5 ml of iso-propanol into the vial containing the 0.5 ml of GS eluent.**
3. Wait at least 30 minutes before reading the plates, to allow the reaction to progress.
4. Carefully (to **avoid dripping or splashing into any adjacent wells**) plate 0.2 ml of each GS standard concentration into the first three wells of each row of a 96-well plate. There are five [GS], so the first three wells of five rows should be occupied. Plate 0.2 ml of plain PBS into the each of the first three wells of the 7<sup>th</sup> row. Leave the 8<sup>th</sup> row blank.
5. Carefully (to **avoid dripping or splashing into any adjacent wells**) plate 0.2 ml of each eluent time point into six wells of each column of the same 96-well plate, starting with column 4 and continuing to the end of the plate.
6. If eluent time point samples remain, start a new plate, repeating step 4 above until all eluent time points are plated. When starting a new plate, **repeat step 3 above for each plate.**
7. Set plate reader to read at 332 nm. Read all plates.
8. Discard samples and clean up.

#### **11.4 Mixing GS Standards**

Combine in a small cap-sealed vial equal amounts of each GS standard concentration (see GS concentrations below) with OPA Reagent and iso-propanol

It is typical to mix at least 100 ml at a time, since the GS standards store virtually unlimited time at 20°C and you don't use very much. Since so little GS powder is used, mix enough to get sufficiently large amount to be able to measure accurately.

##### **GS Concentrations (for DOPS-GS OPA Assay)**

The effective range for the OPA Assay is 20-150 µg/ml GS but we only use 25 to 125 range for our purposes.

First create a 1% w/v mixture of GS in PBS by mixing 40mg GS in 4mL PBS.

Then dilute this stock solution to get final standard concentrations. The final volume of each GS concentration was 20mL. Using  $C_1V_1 = C_2V_2$ ; where  $C_1$  = concentration of stock solution,  $V_1$  = volume of stock solution,  $C_2$  = concentration of final solution, and  $V_2$  = volume of final solution; the following initial volumes are used:

- For 125mics/ml  $V_1 = 0.25\text{ml}$
- For 100mics/ml  $V_1 = 0.2\text{ml}$
- For 75mics/ml  $V_1 = 0.15\text{ml}$
- For 50mics/ml  $V_1 = 0.1\text{ml}$
- For 25mics/ml  $V_1 = 0.05\text{ml}$

### 11.5 *Mixing OPA Reagent*

NOTE: OPA Reagent has shelf life of only three days.

Base Proportions

2.5 g <b>o-phthaldialdehyde</b>
62.5 ml <b>methanol</b>
3 ml <b>mercapoethanol</b>
560 ml <b>borate</b> (1 mM)

(for Borate mixing, see Mixing Borate below)

Typical volume mixed for elution studies

<b>7% of base proportions above</b>
$2.5 \times .07 = 0.175$ g o-phthaldialdehyde
$62.5 \times .07 = 4.375$ ml methanol
$3 \times .07 = 0.21$ ml mercapoethanol
$560 \times .07 = 39.2$ ml borate (1 mM)
<b>Yields <math>4.375 + .21 + 39.2 = 43.785</math> ml OPA Reagent</b>

<b>3% of all</b>
$2.5 \times .03 = 0.075$ g
$62.5 \times .03 = 1.875$ ml
$3 \times .03 = 0.09$ ml
$560 \times .03 = 16.8$ ml
<b><math>1.875 + .09 + 16.8 = 18.765</math> ml</b>

Mixing Borate

1 mM borate consists of 381.37 mg borate in 1 L diH<sub>2</sub>O  
For 200 ml, use 0.0763 g borate

## 12 Appendix C. Detailed Protocols for Cell Study

### 12.1 ALP Assay (for BioAssay Quantichrom ALP Kit)

D. Prawel  
Sept. 2010

ALP assay determines alkaline phosphatase in cell samples. This is a kinetic study so will measure reaction at time 0 and at time 4 minutes and use formula to calculate results. Addition of Working Reagent to samples should be quick and mixing should be brief but thorough. Assays can be executed at room temperature or 37°C.

Need about 2 hours for this study. **Perform concurrent with BCA Total Protein Assay, ON SAME SAMPLES.** Use same lysis solution and match results, sample for sample, i.e. ALP sample 1 result is normalized with results from BCA sample 1 result, etc.

Fresh reconstitution of working reagent is recommended, but working reagent is stable for at least one day when stored in closed container at room temperature.

1. Equilibrate reagents to room temperature. **Thaw pNPP** (should be stored at -20°C) – **about 20 minutes**, and then mini-centrifuge briefly to accumulate reagent in bottom of tube.
2. Prepare **Cell-Lysis solution** and **lyse cells** according to **separate Cell Lysis Protocol**.

**NOTE: THIS SAME SOLUTION IS USED FOR BOTH BCA AND ALP ASSAYS, CONCURRENTLY, I.E. ONE SET OF SAMPLES PRODUCES ONE SET OF LYSATES, FROM WHICH BOTH BCA AND ALP SAMPLES ARE DRAWN.**

3. While cells are lysing, in 50 ml centrifuge tube, **prepare Working Solution**: Will need 150µl of solution per well of 96 well plates to be read in plate reader, plus 10% extra. Include wells for standards and some blank wells as negative plate controls (blank correction).
  - a. For example, for 3 treatments x 6 samples/treatment x 3 wells/sample/treatment = 54 wells x 0.15ml/well = 8.1ml + 10% = **~9ml**. Add 2ml extra for 2 standards x 3 samples per standard (= 6 wells x 0.2ml per well + 10%) = **~11 ml**. These easily fit on one plate with ample wells for blanks.

Can get four treatments maximum (6 x 3 = 18 wells each = 72) per plate plus standards (6 wells) on a single 96-well plate with ample wells remaining for blanks.
  - b. For 11 ml working solution, combine reagents from kit as follows (based on ratio of 200µl Assay Buffer, :
    - i. In 15 ml centrifuge tube, pipette **11ml ALP Assay Buffer** (based on example above)  
*Note: 25 ml pipette tubes do not fit into reagent bottle – use 10ml pipette tubes.*
    - ii. **275µl Mg Acetate** (based on 5µl per 200µl (2.5% of 200) buffer per well, a final 5mM concentration)
    - iii. **110µl pNPP Reagent** (based on 2µl per 200µl (1% of 200) buffer per well, a final 10mM concentration)
4. Plate ALP Calibrator (standard) solution (from kit)
  - a. Pipette 200µl of ALP Calibrator solution into 3 wells of first column of a 96 well plate. These samples provide to high end data point for the (highly linear) standard curve.
  - b. Pipette 200µl of DI-water into next 3 more wells in the first column of the plate. These samples provide to low end (zero) data point of the standard curve.
5. Pipette 50µl of each sample, 3 wells per sample, into the same 96 well plate containing the Calibrator, until all samples are plated.

6. Pipette 150µl of Working Reagent into each sample well. The final reaction volume in the sample wells is 200µl.
7. Tap plate gently to mix.
8. **As soon as possible, measure absorbance at 405 nm** on plate reader, subtracting blanks (protocol available in Ketul's plate reader). Make sure plate reader protocol is set to read 200 µl per well. This represents time 0.
9. **Repeat measurement after 4 minutes.** This repeat run is built into the protocol on the plate reader, unless it was changed. Check that it's set for 2 cycles with a 240 second cycle time.
10. **Refer to kit instructions for formula to calculate final results.**

## 12.2 BCA Assay for Total Protein (for Pierce Protein Assay Kit)

D. Prawel  
Sept. 2010

BCA assay determines amount of total protein in cell samples.

Need about 2 hours for this study. **Perform concurrent with ALP Assay, ON SAME SAMPLES.** Use same lysis solution and match results, sample for sample, i.e. ALP sample 1 result is normalized with results from BCA sample 1 result, etc.

Fresh reconstitution of working reagent is recommended, but working reagent is stable for several days when stored in closed container at room temperature.

1. In 1.5 ml micro-centrifuge tubes, **prepare standard solutions** (dilute Albumin standards from kit) – refer to kit instructions. Use DI-water as diluent.
2. Prepare **Cell-Lysis solution** and **lyse cells** according to **separate Cell Lysis Protocol**.  
**NOTE: THIS SAME SOLUTION IS USED FOR BOTH BCA AND ALP ASSAYS, CONCURRENTLY, I.E. ONE SET OF SAMPLES PRODUCES ONE SET OF LYSATES, FROM WHICH BOTH BCA AND ALP SAMPLES ARE DRAWN.**
3. While cells are lysing, **prepare Working Reagent:** Will need 200µl of reagent per well of 96 well plates to be read in plate reader, plus 10% extra. Include wells for standards and some blank wells as negative plate controls (blank correction). Working Reagent is stable for several days at room temperature in a closed container.
  - a. For example, for 3 treatments x 6 samples/treatment x 3 wells/sample/treatment = 54 wells x 0.2ml/well = 14.4ml + 10% = **~11ml**. Add 6ml extra for 9 standards x 3 samples per standard (= 27 wells x 0.2ml per well+ 10%) = **~17 ml**. Leave some empty wells for blanks. 72 + 27 = 99 will require more than one 96-well plate, and need blanks, so plan no more than **two treatments** (6 x 3 = 18 wells each) **per plate plus standards** (27 wells).  
  
Due to inter-plate variance, need standards on every plate. So need additional 6ml for a second plate. So round up to a total of **24ml Working Reagent needed** for a full test of 3 treatments, 6 samples per treatment, 3 wells/sample/treatment, plus standards.
  - b. For 24ml working reagent, combine reagents from kit as follows:
    - i. In 50 ml centrifuge tube, **mix 23.52 ml Reagent A with 0.48 ml Reagent B** (to achieve a 50:1 ratio)
    - ii. Shake gently until turbidity clears, resulting in a clear, light-green liquid.
4. Plate all solutions
  - a. Pipette 25 µl of each standard solution onto first rows/columns of 96-well plate

- b. Pipette 25  $\mu\text{l}$  of each sample into 3 wells each of the 96 well plate, until all samples plated
- c. Pipette 200  $\mu\text{l}$  of the Working Reagent into each standard and sample well
5. Cover and **agitate for 30 seconds**
6. Incubate for **30 minutes** at 37°C.
7. Cool plate to room temperature (about **20 minutes**). **Perform assay as soon as possible, and read all wells within ten minutes of each other**, because after cooling samples to room temperature, the **blank continues to increase in absorbance at ~2.3% every 10 minutes**.
8. Measure the absorbance of the samples at 562 nm absorbance subtracting blanks (protocol available in Ketul's plate reader). **Make sure plate reader protocol is set to read 225  $\mu\text{l}$  per well.**

### 12.3 Calcium Assay (for BioAssay Quantichrom Calcium Kit)

D. Prawel  
Sept. 2010

To determine intracellular calcium content of unknown cell samples.

This technique uses a plate reader.

Need about 2 hours to complete this study.

Equilibrate reagents to room temperature.

1. Prepare **HCL solution**: HCL comes as 12N (37%) solution, need 50% dilution to achieve 6N. Need enough to put 0.5 ml per well of 48-well cell plates, so for 2 48-well plates, need 24 ml.
2. Move cell plates from incubator into cell hood – one at a time.
3. Aspirate media
4. Move samples to new plate
5. Rinse gently with PBS, replace lid and let sit ~ 5 min, repeat on next plate until all plates rinsed
6. Aspirate PBS from all plates/wells and move plates into chemical hood
7. Add 0.5 ml (for 48-well plate) of 6N HCL into each well (pipette down well walls) (cover with foil)
8. Agitate on plate shaker (at 300) for **2 hours**
9. Sample solutions can be frozen -80°C for later assay. Solutions are stable for \_\_\_\_???
10. Prepare **Working Solution** in 50 ml centrifuge tube: will need 200  $\mu\text{l}$  of reagent per well of 96 well plates to be read in plate reader, plus 10% extra. Include at least 6 wells for standards and some blank wells as negative plate controls (blank correction). **Combine equal parts Reagent A (from kit) with Reagent B (from kit)**.
  - a. For example, for a single 96-well plate, need  $\sim 100 \times 200 \mu\text{l} = 20 \text{ ml} + 10\% = \mathbf{22 \text{ ml}}$ . (Note: can fit standards and 4 treatments + 6 samples per treatment, 3 tests per sample, all on a single 96-well plate, and have 10 wells remaining for blanks.
11. Plate the standard calibrator, zero point and sample wells.
  - a. Pipette 200  $\mu\text{l}$  of Working Reagent into six cells of first column of 96-well plate and into all wells to be tested.
  - b. Pipette 5  $\mu\text{l}$  of **standard calibrator solution** into the first 3 wells of the working reagent in (a). These samples provide to high end data point for the (highly linear) standard curve.

- c. Pipette 5  $\mu$ l of **de-ionized water** into the second 3 wells of the working reagent in (a). These samples provide to low end (zero) data point of the standard curve.
  - d. Pipette 5 $\mu$ l of each sample (containing HCL) into 3 wells each of the 96-well plate, until all samples plated. Use additional well plates, but always include a standard column on all plates.
  - e. Tap lightly to mix. Let stand for at least one minute at room temperature.
12. Incubate 3 minutes at room temperature.
  13. **Measure absorbance at 612 nm** on plate reader, subtracting blanks (protocol available in Ketul's plate reader). And make sure protocol is set to 200  $\mu$ l per well.
  14. Save all sample solutions until test is satisfactorily completed. Samples can be saved for up to one week at 20°C.

#### 12.4 Calcium Assay (for Pointe Calcium Kit)

D. Prawel  
Sept. 2010

To determine intracellular calcium content of unknown cell samples.

This technique uses a plate reader.

Need about 2 hours to complete this study.

Equilibrate reagents to room temperature.

1. Prepare **HCL solution**: HCL comes as 12N (37%) solution, need 50% dilution to achieve 6N. Need enough to put 0.5 ml per well of 48-well cell plates, so for 2 48-well plates, need 24 ml. We will normalize plate reader to HCL as blanks so need additional HCL solution for blanks – 10 ml will suffice.
2. Move cell plates from incubator into cell hood – one at a time.
3. Aspirate media
4. Move samples to new plate
5. Rinse gently with PBS, replace lid and let sit ~ 5 min, repeat on next plate until all plates rinsed
6. Aspirate PBS from all plates/wells and move plates into chemical hood
7. Add 0.5 ml (for 48-well plate) of 6N HCL into each well (pipette down well walls) (cover with foil)
8. Agitate on plate shaker (at 300) for **2 hours**
9. Sample solutions can be stored for later assay. Solutions are stable for 24 hours at room temperature, one week at 2 to 8°C and up to five months at -80°C (protected from evaporation).
10. Prepare **Working Reagent** in 50 ml centrifuge tube. For example, for 3 treatments x 6 samples/treatment x 3 wells/sample/treatment = 72 wells x 0.2ml/well = 14.4ml + 10% = **~16ml**. Add 2ml extra for 2 standards x 3 samples per standard (= 6 wells x 0.2ml per well+ 10%) = **~18 ml**. These easily fit on one plate with ample wells for blanks.

**Combine equal parts Color and Buffer Reagents (from kit) and let stand for 20 minutes at room temperature.** Combined reagent is stable for two weeks refrigerated and one week at room temperature.

Can get four treatments maximum (6 x 3 = 18 wells each = 72) per plate plus standards (6 wells) on a single 96-well plate with ample wells remaining for blanks.

11. Plate the standard calibrator, blanks and sample wells.

- a. Pipette 200  $\mu$ l of Working Reagent into six cells of first column of 96-well plate and into all wells to be tested.
  - b. Pipette 4  $\mu$ l of **standard calibrator solution** into the first 3 wells of the working reagent in (a). These samples provide to high end data point for the (highly linear) standard curve.
  - c. Pipette 4  $\mu$ l of the **HCl solution from above** into the second 3 wells of the working reagent in (a). These samples are used as blank wells.
  - d. Pipette 4 $\mu$ l of each sample (containing HCL) into 3 wells each of the 96-well plate, until all samples plated. Use additional well plates, but always include a standard column on all plates.
  - e. Pipette 6 to 8 additional wells with HCl solution as blanks.
  - f. Tap lightly to mix. Let stand for at least one minute at room temperature.
12. **Measure absorbance at 570 nm** on plate reader, subtracting blanks (protocol available in Ketul's plate reader). And make sure protocol is set to 200  $\mu$ l per well. **Final color is stable for 20 minutes.**
13. Calcium values are calculated as described in the spec sheet that comes with the assay. Unlike the BioAssay Quantichrome Calcium Assay Kit, the Pointe kit does not use a standard curve. Rather, the calibrator solution provides a high-end value for the following equation:
- $$\text{Absorbance of Unknown/Absorbance of Standard} \times \text{Concentration of Std.} = \text{Calcium (mg/dl)}$$
- Example: If the absorbance of unknown = 0.47, absorbance of standard = 0.50, and concentration of standard = 10mg/dl, then:  $0.47/0.50 \times 10 = 9.4\text{mg/dl}$
14. Save all sample solutions until test is satisfactorily completed. Samples can be saved for up to one week at 20°C.

### 12.5 Cell Lysis using Triton-X or Cell-Lytic with SDS

D. Prawel  
Sept. 2010

11. Prepare Cell-Lytic or Triton-X (Lysing Agent) solution.

**NOTE: THIS SAME SOLUTION IS USED FOR BOTH BCA AND ALP ASSAYS, CONCURRENTLY, I.E. ONE SET OF SAMPLES PRODUCES ONE SET OF LYSATES, FROM WHICH BOTH BCA AND ALP SAMPLES ARE DRAWN.**

If **adding sodium dodecyl sulfate (SDS)** (to mask any effect of phospholipids), it comes as 10% solution so dilute as follows:

- a. Estimate amount of lysis solution required for all wells, e.g. for full 48-well plate, need 0.5ml total solution per well plus extra = 24 ml + 10% = ~ 30 ml.
  - b. Need 2% SDS in the lysis solution, so estimate amount of 10% SDS needed to get this. For each 10ml total solution needed, add **02ml of 10% SDS to 8ml** Lysing Agent. So, for 30ml total solution, add **6ml of 10% SDS to 24ml** Lysing Agent.
  - c. Pipette Lysing Agent into 50 ml centrifuge tube.
  - d. Add SDS into Lysing Agent. Aspirate gently to mix (SDS is detergent and will foam).
12. Move cell plates from incubator into cell hood – one plate at a time.
13. Aspirate media. Move samples to new plate.
14. Rinse gently with PBS, replace lid and let sit about 5 min, repeat on next plate until all plates are rinsed.
15. Aspirate PBS from all plates/wells and move plates into chemical hood.

16. Add 0.5 ml (for 48-well plate) of lysis solution into each well - pipette gently down walls
17. Cover and shake for **20 minutes**
18. Sample solutions can be frozen at this point for later assay. ALP is stable for 48 hours at 4°C or two months at -80°C

## 12.6 Counting Cells

D. Prawel  
James Lab  
July, 2010

Need:

1 Epi-tube  
Hemocytometer with cover slip  
Trypan Blue stain

Procedure

1. Pipette 20µl cell solution and 20µl Trypan Blue stain into epi-tube. Gently aspirate to mix.
2. Place cover slip on hemocytometer.
3. Transfer 20µl to slot on each side of a hemocytometer (at outer edge of cover slip).
4. Count cells in cross-hatched area on each side and average the two counts.
5. Total cell count is: Average (from previous step) x 2 (because counted volume has been doubled with trypan blue) x  $E^4$  (volume in one cross-hatched region of hemocytometer) x # mls of solution (media) cells came from  
Example: 100 count from 5ml cell solution is  $200 \times 2 \times E^4 \times 5 = 20 \times E^6$  cells

Note: Trypan Blue is highly toxic. Avoid all skin contact.

Desired goal = more than  $0.5 \times 10^6$  cells/ml

Assuming 1 ml per well in typical study, this determines number of cells needed for study.

Cleanup

Bleach cells, then Liquinox, rinse and alcohol hemocytometer

Carefully wipe dry and put back in its box.

To increase concentration of cells:

Centrifuge cells 5 min at 1000 rpm

Aspirate off media, based on cell count (to achieve higher concentration of cells)

Re-homogenize and count again

## 12.7 Fixing Cells Protocol (e.g. for SEM)

D. Prawel  
James Lab  
April 2010

The cells will be fixed in a solution of 3% glutaraldehyde, 0.1 M sodium cacodylate, and 0.1 M sucrose for 45 min. The surfaces will then be soaked in buffer containing 0.1 M sodium cacodylate and 0.1 M sucrose. The cells will then be dehydrated by soaking the surfaces in increasing concentrations of ethanol (35%, 50%, 70%, and 100%) for 10 min each, and further dehydrated by soaking in hexamethyldisilazane (HMDS) for 10 min. The surfaces will then be dried and stored in a dessicator until examined with SEM.

### **Need:**

2-3 small petri dishes  
glutaraldehyde (3% - in freezer)  
sodium cacodylate (in dessicator)  
sucrose (in chemical cabinet)  
hexamethyldisilazane (HMDS) (in hazardous materials cabinet)  
50ml cent tube  
15ml cent tube

### **Cell Fixing Protocol**

Thaw glutaraldehyde.

Mark bottom of both petri dishes with zones for sample groups, e.g. Plain Ti, TI/DOPS, etc.

Make 20ml of **buffer solution** – start with 19.4ml DI-water in 50 ml centrifuge tube

+ 0.68gm 0.1M sucrose

+ 0.42gm 0.1M sodium cacodylate

Split into two 10ml portions.

Add 0.6ml glutaraldehyde to one of them - this is the **primary fixative**.

*Note: can make larger amounts for multiple uses. Fixative and buffer are stable at room temp.*

Place all samples in small petri dish in fume hood (not cell hood) – keep separated in treatment groups

Rinse twice in PBS. *Note: adding liquids to dishes can disturb and mix samples, so better to transfer samples to new petri and add PBS, twice.*

Put 10 ml primary fixative (above) into other petri dish and transfer samples into it.

Leave in fume hood for **45mins**.

Place buffer in the other dish and move the samples from the fixative into the buffer.

Leave for **at least 15mins, up to 20 hours**. Agitate occasionally.

Move samples out of buffer and dehydrate with ethanol as follows (transferring samples in each step):

35% - 10mins (dilute 70% by half)

50% - 10mins (dilute 100% by half)

70% - 10mins

100% - 10mins

If fixing cells on DOPS or DOPS/GS, replace the following HMDS step with a second 100% ethanol bath for 10 minutes, and then vacuum dry overnight.

If not, place 10ml HMDS in the other dish and move the samples from the ethanol into the HMDS for 10mins. Then move samples out of HMDS into other dish and allow samples to air dry.

Store samples in dessicator for future use.

## 12.8 *Using the Fluorescent Microscope at VTH*

Need:  
Slides  
Samples  
Gloves  
PBS (small amount for wetting slides)  
Pipette (1 ml) with ~6 tips  
Tweezers  
USB drive

Power up in order: turn on switches 1, 2, then 3  
Set Switch A on selector box to KS  
Set switch on right side of scope head to KS

Scope Controls  
Slider controls on upper scope: in -> camera, out -> direct view, mid-way -> both  
Iris toward rear of scope head, right side: F = iris width, I = intensity, middle slider = light

Computer  
Login: administrator, pw: nooil  
Record time on small counter box in book  
Open software: Axiovision Rel 4.6

Clean slide(s) with pink cleaner fluid

SW controls/settings (left to right icons)  
Microscope: use 470 (green)-10X  
AxioCamHR – camera controls (200 ms shutter)  
Live: instant view

“Snap” to take picture, then “Save” to USB drive (or folder then USB)

DO NOT turn bulb (box one) off if you’re switching samples – it resets and you must wait at least 30 minutes to get on again.

## 12.9 *Live/Dead Cell Imaging Protocol (using Molecular Probes Live/Dead Cell Imaging Kit)*

March 2010

### **Summary**

This test uses a commercially available Live/Dead Cell Viability Kit (Molecular Probes) containing Calcein AM (live stain) and Ethidium homodimer-1 (dead stain). Samples will be removed from culture media, rinsed in PBS, then bathed in live/dead stain working solution. Cells with intact cell membranes are able to use nonspecific cytosolic esterases to convert nonfluorescent calcein-AM into bright green-fluorescent calcein. EthD-1 enters cells with damaged membranes and binds to nucleic acids, thereby producing a bright red fluorescence in dead cells. EthD-1 is excluded by the intact plasma membrane of live cells. Surfaces are then imaged using appropriate filters with a (470 nm excitation) fluorescence microscope. Refer to Live Cell spec sheet from supplier for details on test. **The stains photobleach, so keep them in darkness as much as possible.**

### **Need**

Live/dead stain kits sufficient for samples to be tested.  
Aluminum foil pieces for covering calcein vial and well plate(s)  
Sterile PBS – about 2 mls per sample to be tested

15 ml centrifuge tube

### Preparation

1. Remove live and dead stains from freezer and thaw at room temperature (or in bath if necessary). They are light sensitive, so wrap in aluminum foil if left out for more than a few minutes.
2. Calcein AM is sensitive to moisture (it hydrolyzes) so aqueous solutions must be prepared immediately prior to use, and used within one day.

### Procedure

1. Sterilize hood - UV for 10 minutes.
3. Working in the hood, fill a centrifuge tube with **0.5mL sterile PBS per sample to be tested**.
4. Remove foil from stains, if used, and move them into hood after ethanol-ing.
5. Add to the PBS:
  - a. **2  $\mu$ l of EthD-1 per sample to be tested**
  - b.  **$\frac{1}{2}$   $\mu$ l of calcein per sample to be tested**
6. Mix thoroughly - remove from hood, vortex, sterilize, place back in hood.
7. Remove samples from incubator and place in the hood.
8. Aspirate media from each well. Rinse GENTLY with 1 ml sterile PBS in each sample. Aspirate PBS.
9. Turn all lights off and use only red lights from this point on.
10. Add 1mL of Live/dead stain/PBS solution to each well.
11. Cover well plate(s), remove from hood and wrap entirely with aluminum foil to prevent light from photobleaching.
12. Soak samples in Live/dead stain/PBS solution for 45 minutes.
13. Rinse samples in PBS.
14. Use fluorescent microscope to examine.
  - a. 470nm (FITC) excitation for live
  - b. 612nm (Texas Red) for dead

## **12.10 Live/Dead Cell and Nuclear Imaging Protocol (using bulk Calcein-AM)**

D. Prawel  
James Lab  
September 2010

### Summary

This test uses commercially available (Invitrogen Molecular Probes) Calcein AM (live stain), Ethidium homodimer-1 (dead stain) and \_\_\_\_\_ (DAPI) (nuclear stain). Samples will be removed from culture media, rinsed in PBS, then bathed in live/dead/nuclear stain working solution(s). Cells with intact cell membranes are able to use nonspecific cytosolic esterases to convert nonfluorescent calcein-AM into bright green-fluorescent calcein. EthD-1 enters cells with damaged membranes and binds to nucleic acids, thereby producing a bright red fluorescence in dead cells. EthD-1 is excluded by the intact plasma membrane of live cells. DAPI passes through live cell membranes and into nuclei, staining \_\_\_\_\_. Surfaces are then imaged using appropriate filters with a (470-490/520 nm (excitation/emission) for Calcein (FITC), 612nm for EthD-1 (TRITC), 358/461 for DAPI) fluorescence microscope.

**The stains photobleach after contacting cellular material, so keep them in darkness as much as possible after staining cells. Especially DAPI.**

### Need

Live/dead stain reagents sufficient for samples to be tested.  
DAPI stain (Santa Cruz Biotech sc-3598) (blue nuclear stain)  
DMSO (liquid in chemical cabinet)  
Aluminum foil pieces for covering calcein vial and well plate(s)  
Sterile PBS – about 2 mls per sample to be tested  
15 ml centrifuge tube

## Preparation

15. Remove live and dead stains from -20 freezer and **thaw** at room temperature or in bath. Calcein is **light sensitive**, so wrap in aluminum foil if left out for more than a few minutes.
16. Calcein is sensitive to moisture (it hydrolyzes) so aqueous solutions must be prepared immediately prior to use, and used within one day.
17. If using: **Nucleus Stain (DAPI)** arrives from Invitrogen as a powder (10mg). Dissolve all 10 mg of DAPI powder in 2 ml of DI water. This makes a 5 mg/ml stock solution of dihydrochloride and dilactate. On day of use, dilute the stock solution to 300nM in PBS - for 5ml of stain, add 105µl of the stock solution to 5ml PBS (300nM DAPI).

## Procedure (done in the bio-hood)

2. Move stains into bio-hood.
3. Make a Calcein Stock Solution (if not already available).
  - a. Fill a centrifuge tube with **0.5mL PBS per sample to be tested**.
  - b. Reconstitute calcein-AM bulk solution vial by adding 50µl of DMSO.
  - c. Mix thoroughly - remove from hood, vortex, sterilize, place back in hood. Solution is now ready to be used.
4. Make a Live/Dead **Working Solution** with the amount of mixture needed for all test samples.
  - a. For DOPS and DOPS/GS staining, use 3 µl calcein per 1 ml PBS to create a 3 µM solution.
    - i. E.g. for 16 samples: 24 µl Stock Solution in 8 ml PBS yields a 3 µM concentration (see note below)
  - b. **2 µl of EthD-1 per sample to be tested (if using dead stain)**
5. Mix thoroughly - remove from hood, vortex, sterilize, place back in hood.
6. Remove samples from incubator and place in the hood.
7. Aspirate media from each sample well.
8. Rinse samples GENTLY in PBS. Aspirate PBS.
9. Turn all lights off and use only red lights from this point on.
10. Add 0.5 mL of Live/Dead Working Solution to each sample well. **Do not add DAPI stain yet, if using. This should be added at the microscope.** Carefully plan how many samples will be imaged in what order. You only get a half hour of fluorescence with FITC and TRITC, so you may want to add some at the microscope if you're imaging many samples, especially if you're doing DAPI. If you're using DAPI and/or imaging many samples, don't add the stains yet. – do it at the microscope. See Rule of Thumb below.
11. Soak for **20 to 30 minutes**.
12. **Go to microscope.**
13. Aspirate Working Solution from sample wells.
14. **Add the DAPI stain at the microscope and image it in 3 minutes – it expires in about 10 to 15 minutes.** Need to look at the DAPI first due to fast photobleaching, so plan accordingly.

*RULE OF THUMB – you can easily image about four FITC and TRITC samples (after everything is set up), in time before they begin photobleaching. If you're using DAPI, add the FITC to four samples, and DAPI to only the first two of these, then wait 3 minutes and image the DAPI, then image these same two samples with FITC/TRITC. When finished, add the DAPI to the next two already stained with FITC/TRITC, stain the next four with FITC/TRITC, and image the second two of the first group with DAPI (just stained) from 3 to 15 minutes, and then FITC/TRITC. By then the new four FITC will be ready and repeat cycle until all samples are imaged.*

15. Rinse samples GENTLY in PBS.
16. Wrap covered well plate(s) entirely with aluminum foil to prevent photo-bleaching.
17. Use fluorescent microscope to examine.
  - a. 470nm (FITC) excitation for live
  - b. 612nm (Texas Red - TRITC) for dead

Note: Lower Calcein concentrations will photobleach faster than higher concentrations. Depending on time delay between staining and microscopic examination, one can use 2 µM (i.e. 2 µl calcein per 1 ml PBS) to 5 µM concentration, which is quite bright but lasts a relatively long time, so may be better for beginners or when delays are expected. The concentration should be determined based on material type and your cells.

## 12.11 Making Cell Culture Media

Prawel  
April, 2010

### MSC Culture Media

Need:

1 bottle  $\alpha$ -MEM (500 ml) (CSU Freezer Program, Hyclone or Invitrogen, 12571-063)

1 tube (50 ml prepared) FBS (Sigma, F2442)

1 tube (5 ml prepared) Penn/strep (5ml of 100X for 500ml media) (Invitrogen, 15140-148)

*Note: use Penn/Strep/Amphotericin (PSA) if no cells, to prevent fungal growth. It should be added as 100x less than media, so 1 ml media (in a well) would get 10 $\mu$ l PSA.*

Warm all ingredients to 37°C

Pour all ingredients into sterile vacuum filter

Filter media

Cover and store in refrigerator - is stable if refrigerated. (Can also be kept at 37°C for use for ~ 8 hr)

### HfOB Culture Media:

1:1 mixture of F-12 and DMEM (Invitrogen, 21041025)

0.3 mg/ml of G418 sulfate (ATCC, 30-2305)

10% FBS – fetal bovine serum (Sigma)

To make:

1. Warm F-12, DMEM, FBS and G418 in water bath.
2. Add 3ml G418 and 59ml FBS to the bottle of DMEM and F-12.
3. Filter the solution to a new bottle.

### Fibroblast Culture Media:

Medium 106 (brand)

Low serum growth supplement (brand)

Gentamicin/Amphotericin-B (Invitrogen “Anti-Anti”)

To make:

1. Warm media and supplement in water bath.
2. Add 10ml (one container) supplement and 1ml (one vial) gentamicin to 500ml media (one full bottle)
3. Mix gently, avoiding bubbles.

MSC Media with  $\beta$ -glycerol phosphate

Note: this is the base media for osteoblast differentiation media (below)

Need:

$\beta$ -glycerol phosphate (Sigma, G-6251) – usually aliquoted in 15ml centrifuge tubes in -80°C freezer  
MSC culture media above

To mix  $\beta$ -glycerol phosphate, 54g is added to 250ml of DI water to make 1M concentration. Then filter with 0.2 $\mu$ m  
nalgene filter unit. Store 3ml aliquots of this in -80°C freezer.

When making MSC media with  $\beta$ -gly, add 3ml (1 aliquot from freezer) of  $\beta$ -gly solution above to 500ml of basic  
MSC culture media above.  $\beta$ -gly is stable in MSC Culture Media so can be added to in advance of differentiation  
media changes and stored in refrigerator.

For Osteoblast Differentiation Media

Need:

$\beta$ -gly media per above

Procedure – refer to separate *MSC Differentiation Media Change* protocol for details.

The basic mix concentration is as follows - for 2ml of media:

- 2 $\mu$ l of dexamethasone ( $10^{-5}$ M 1:1000 in media = effective  $10^{-8}$ M)
- 25 mg in 5ml of ascorbic acid (50 $\mu$ g/ml)
- 16ml of 1 M  $\beta$ -glycerol phosphate

## **12.12 MSC Differentiation (to Osteoblasts) Media Change**

D. Prawel

James Lab

June, 2010

Supplies/chemicals needed:

- 1 1 ml syringe with 22 gauge needle
- 1 10 ml syringe with 18 gauge needle
- 1 0.2  $\mu$ l syringe filter
- 1 50 ml centrifuge tube
- 1 15 ml centrifuge tube
- 1 5 ml pipette
- 1 25 ml pipette
- 1 epi-tube

Cell culture flask or additional 50 ml centrifuge tube, depending on quantity of media required for all cell wells.

Dexamethasone (D-8893, Sigma)

Ascorbic acid (powder) (255564, Sigma)

Cell culture media with  $\beta$ -glycerol phosphate (refer to *Making Cell Media* protocol)

Notes

This media must be made fresh as needed on the day cell media is changed.

Preparation & Procedure

Warm media (~20 minutes in water bath at 37°C).

Estimate amount of media needed, e.g. for 100 sample wells with 0.5ml per well, need 50ml of media. Add ~10% extra as safety factor.

Complete Steps A, B and C as follows:

A. Ascorbic Acid Solution

14. Weigh 25 mg Ascorbic Acid (powder) and put in 50 ml centrifuge tube.
15. Transfer 5 ml of MSC culture media (containing  $\beta$ -glycerol phosphate) to 50 ml centrifuge tube containing ascorbic acid.
16. Using a 10 ml syringe with an 18 ga needle, aspirate ascorbic acid/media solution repeatedly to mix until no ascorbic acid granules are visible.
17. Draw all ascorbic acid solution into 10 ml syringe. Replace needle with syringe filter.
18. Cover and set aside.

B. Dexamethasone (dex) Solution

1. Transfer 3 ml MSC culture media (containing  $\beta$ -glycerol phosphate) to 15 ml centrifuge tube.
2. Draw dexamethasone into 1 ml syringe with 22 ga needle until it fills base of needle.
3. Transfer dexamethasone to epi-tube. Then transfer 3  $\mu$ l of dexamethasone from the epi-tube to the 15 ml centrifuge tube from step 1 above. This results in approximately  $10^{-8}$ M solution.
4. Tip the centrifuge tube gently to mix.

C. Make Final Media

1. Transfer fresh differentiation media into either a cell culture flask or a 50 ml centrifuge tube, depending on how much media will be required for the media change.
2. Add 5-6 drops of ascorbic acid solution (from A above – NOT raw ascorbic acid) per 100 ml final differentiation media.
3. Add 1  $\mu$ l of dexamethasone solution (from B above – NOT raw dexamethasone) per 1 ml of final differentiation media.

### **12.13 MSC Harvest Protocol (rat)**

Prepare/plan to plate cells within a few hours of harvest. If seeding samples, sterilize control and test samples in advance.

#### **Materials for Harvest**

Rat

Surgical scissors

At least one scalpel blade per limb

At least two pairs of surgical gloves per person

50 mls PBS in 50 ml centrifuge tube  
Cold storage container for transport

### **Materials Needed in Lab**

50 ml centrifuge tube  
10 ml syringe with 18 g and 25 g needle (from 1 ml syringe)  
45 ml MSC culture media ( $\alpha$ -MEM with 10% fetal bovine serum (FBS, Sigma) and 1% penicillin/streptomycin (pen/strep, Sigma)) – see separate Making Culture Media protocol) – chilled to 20°C

### **Procedure**

#### **Harvest**

MSCs were collected from Wistar rats (*Rattus norvegicus*) supplied by Harlan Sprague Dawley, Inc. Limbs were aseptically removed from recently euthanized animals.

Femurs, ulnas, and humeri were isolated.

Scrape bones with scalpel blade to remove as much tissue as possible.

Store bones in cold PBS in a 50ml centrifuge tubes to prevent excessive dessication. Plan to flush marrow/cells immediately.

#### **In Lab**

Put about 45 mls of cold media in a 50 ml centrifuge tube.

Working in sterile hood.

Metaphyseal ends were removed from each bone to expose the bone marrow cavity.

Into a 50-ml centrifuge tube, flush marrow twice with cold culture media (from tube) using 10 ml syringes with 25 gauge needle, refilling each flush. Refill syringe and flush bones with same media using 18 gauge needle until no additional marrow material exudes. Keep tube with media on ice.

Dissociate clumps of marrow by drawing gently 4-6 times through 18 gauge needle. Filter suspension through a 70mm nylon strainer into clean tube.

Media containing cells was stored in incubator until used (within a few hours).

Count and seed the cells, using separate protocols.

## **12.14 MTT Assay Protocol**

D. Prawel

James Lab

April 2010

Cell viability will be measured after days 1 and 4 of culture (log phase growth) using a commercially available MTT assay kit (Sigma-Aldrich). Adhered cells are incubated at 37°C for 3 hr in a (3-[4,5-dimethylthiazol-2-yl]-2,5-diphenyl tetrazolium bromide (MTT) solution. Mitochondrial dehydrogenases of viable cells cleave the tetrazolium ring, yielding purple formazan crystals. Formazan crystals are then dissolved in the MTT solvent, which contains iso-propanol. The optical density (OD) of the solvent is proportional to the mitochondrial activity of the cells on the surface. OD is measured at 570 nm using a spectrophotometer (BMG Labtech?). Background absorbance at 690 nm is subtracted from the measured absorbance.

Wells kept covered to prevent evaporation, which can affect MTT results.

Cultures are prepared in multiwell plates. For best results, cell numbers should be determined during log growth stage. Each test should include a control sample and blank well, both containing complete culture medium without cells. Need to factor out affects from other than samples.

Sterile technique - Bacteria, mycoplasma and other microbial contaminants may also cleave the MTT tetrazolium ring; thus contaminated cultures should not be tested by this method.

MTT is phenotype specific, so to remove variability that may be caused by variances in cell types, and because MTT can be influenced by the physiological state of cells, it is sometimes advisable to create a standard calibration curve of cell counts vs. MTT OD.

Warm media and MTT solution in bath.

Remove cultures from incubator into laminar flow hood or other sterile working area.

Aseptically add MTT SOLUTION in an amount equal to 10% of the culture volume. (e.g. 100 µl per ml of solution on wells) in PBS. **Don't forget blank controls** – need to qualify MTT results from plate reader.

Incubate for 3 to 4 hours. Incubation times should be consistent when making comparisons.

During this time, **prepare MTT Solvent**. Need amounts equal to the culture volume, e.g. 1 ml per ml of solution in each well. However, 10% of the final solution should be Triton-X (to lyse cells). So, if need 10 mls of MTT Solvent, add 1 ml of Triton-X into 9 mls MTT solvent. Fluid densities vary, so these do not mix well. Need to vortex this mixture to disperse until no separation is visible. Then sterilize and store in hood until needed.

Vortex MTT Solvent mixture to disperse until no separation is visible.

Remove well plates from incubator and place into hood.

Aspirate off all media (containing MTT Solution) from each well.

Add 1 ml MTT Solvent to each well.

Gently agitate to completely dissolve any visible purple (formazan) crystals.

Plate out test solutions into 96 well plate(s).

**Plates should be read within one hour of adding MTT Solvent to samples.** Measure absorbance at a wavelength of 570, with a background of 690. Use the standard program on Ketul's plate reader, making sure to set cell locations and volume tested as 100 µl. Be sure to add extra wells containing MTT Solvent but no samples, and include blank wells.

### **12.15 Cell Staining and Immunofluorescence Protocol**

Osteocalcin & Osteopontin

D. Prawel (adapted from Josh Porter and Tim Ruckh)

This protocol is written for staining Osteocalcin, Osteopontin, and cell nuclei in MSCs.

Notes

The conjugated secondary antibodies (e.g. FITC/TRITC) are light sensitive, so avoid exposure to white light.

The OC and OPN stains are active for a maximum of 2 hours if kept in the dark. So check availability of fluorescent microscope in advance.

DAPI is extremely sensitive to light and will photobleach very quickly - in about ten minutes. Use very low exposure times on microscope (5 to 10 ms).

**Use the working dilution of the stains within 12 hours of reconstitution.**

Materials

Trypan blue stain

3.7 wt% Formaldehyde diluted in PBS (Sigma 252549)

Osteocalcin antibody (V-19 (goat), Santa Cruz Biotech sc-18319)

Osteopontin antibody (AKm2A1 (mouse), Santa Cruz Biotech sc-21742)

Fluorochrome (FITC – green)-conjugated secondary antibody (e.g. donkey anti-goat IgG, Santa Cruz Biotech sc-2024) (green)

Fluorochrome (TRITC (Texas Red))-conjugated secondary antibody (from any species other than FITC-derived, e.g. chicken anti-mouse IgG, Santa Cruz Biotech sc-2024)

Blocking serum for secondary antibody – Santa Cruz recommends matching secondary antibody species, e.g. donkey serum (Santa Cruz Biotech sc-2044), but Bovine Serum Albumin (BSA) works well and is much cheaper.

DAPI stain (Santa Cruz Biotech sc-3598) (blue nuclear stain) – if using Note: DAPI complicates this procedure because it must be imaged very quickly, and the immunofluorescent stains take a while to fluoresce. So there's a risk that while the immunofluorescent stains are cooking, the DAPI is expiring. Timing is critical – plan accordingly.

To carry to microscope: Tweezers, enough PBS in cent tube for rinsing samples, 1000 µg pipette with enough tips,

#### About Stock and Working Solutions

Estimate amount of working solutions needed for all test samples.

**Osteocalcin (OC) Antibody:** arrives as 200 µg in 1ml of PBS. It will be diluted 1:100 (to 2 µg/ml) in PBS - only the amount you will need. If other antibodies will be incubated simultaneously, e.g. OPN, will dilute 1:50 (to 4 µg/ml). *Do not count DAPI in this as it is a stain, not an antibody. This dilution is done during the procedure that follows.*

**Osteopontin (OPN) Antibody:** goat OPN antibody arrives as 200 µg in 1ml of PBS. It will be diluted 1:100 in PBS - only the amount you will need. As with OC, will dilute 1:50 if using two antibodies, e.g. OC, simultaneously). *Do not count DAPI in this as it is a stain, not an antibody. This dilution is done during the procedure that follows.*

**OC and OPN Labeled Secondary Antibodies:** e.g. Secondary antibodies arrive as 200 µg in 0.5 ml PBS. Dilute 1:200 in PBS. **This dilution is done during the procedure that follows.**

**Blocking Serum:** used to suppress non-specific binding of IgG. Dilute BSA 10% - 100 µg in 1 ml PBS (i.e. 1 ml in 10 ml). Add 40 µg/ml trypan blue to enhance images. In addition, also need to prepare 2% blocking serum, so dilute some of this 10% BSA 5x with PBS to get 2% BSA.

If using: **Nucleus Stain (DAPI)** arrives from Invitrogen as a powder (10mg). Dissolve all 10 mg of DAPI powder in 2 ml of DI water. This makes a 5 mg/ml stock solution of dihydrochloride and dilactate. On day of use, dilute the stock solution to 300nM in PBS - for 5ml of stain, add 105µl of the stock solution to 5ml PBS (300nM DAPI).

#### Excitation & Emission

FITC excites around 470-490 nm and has emission around 520 nm.

DAPI excites around 358 nm and has emission around 461 nm. DAPI is extremely sensitive to light and will photobleach very quickly - in about ten minutes. Use very low (5 to 10 ms) exposure times on fluorescent microscope.

#### Procedure

Need about 3 hours for this procedure, not counting imaging time.

**First, prepare primary antibodies per above.**

#### Fix Cells

Remove samples from media in new wells, rinse in PBS, then fix cells in 3.7 wt% paraformaldehyde/PBS for **15 minutes** at 37°C (e.g. for ten samples, need 10 ml of 3.7% paraformaldehyde. To make, need 3.7 gm paraformaldehyde in 10 ml PBS - refer to separate *Paraformaldehyde Fixing* protocol.

#### Permeabilize Cells

To permeabilize the cells, wash in PBS with 1 % triton-X for **5 minutes** at room temperature (e.g. for ten samples, need 10 ml of 1% Tritox-X).

Stain cells

1. After fixing and permeabilization, bath cells in 10% Blocking Serum in PBS (prepared in advance per above) for **30 minutes** to prevent nonspecific binding. (5 ml needed for 9 samples)
2. Rinse with PBS.
3. Bath samples in primary antibodies (e.g. against OC and OPN) and 2% blocking serum (assume total volume is 0.5 ml/well) for **1 hour** at room temperature. (e.g. for ten samples, each with 0.5 ml, need 5 ml of each) (need 5 ml of 2% block):
  - a. add 100  $\mu$ l of OC antibody solution and 100  $\mu$ l of blocking serum to 5 ml PBS
  - b. add 100  $\mu$ l of OPN antibody solution and 100  $\mu$ l of blocking serum to another 5 ml PBSTotal solution should be 10 ml. OC & OPN concentration is 50  $\mu$ l in 10 ml PBS = 40  $\mu$ g in 10 ml = 4  $\mu$ g/ml.
4. Wash 2-3X in PBS, 5 minutes each (total **20 minutes**)
5. Repeat blocking step: bath cells in 10% Blocking Serum in PBS (prepared in advance per above) for **30 minutes** (5 ml needed for 9 samples)
6. Wash 2-3X in PBS, 5 minutes each (total **20 minutes**)
7. **Turn lights off before add secondary antibodies (or use red/orange light).**
8. Bath samples in secondary antibodies and 2% blocking serum for **45 minutes** at room temperature. E.g. for ten samples (each with 0.5 ml) (need 5 ml of 2% block):
  - a. add 50  $\mu$ l of FITC secondary antibody solution and 200  $\mu$ l of blocking serum to 5 ml PBS
  - b. add 50  $\mu$ l of Texas Red secondary antibody solution and 200  $\mu$ l of associated blocking serum to another 5 ml PBS
  - c. Wrap in foil.

Go to microscope while the secondaries are cooking.

- 6) If using DAPI, add the DAPI stain at the microscope, about 10 minutes before other secondary antibodies finish. Plan accordingly. This is difficult to do with immunofluorescent stains. (see Live/Dead Staining Protocol for more details)
- 7) Rinse in PBS.
- 8) View on fluorescent microscope using FITC filter for green (OC) and Texas Red filter for red (OPN), DAPI filter for blue (nucleus). The non-specific proteins will initially appear, but will bleach out quickly, so be patient.

## 12.16 Seeding Cells

D. Prawel

James Lab

April 2010

Count Cells and dilute/concentrate to required cell numbers. (use protocol for Counting Cells)

Cells were seeded on all control and test surfaces in a 24-well plate at a density of 0.5 million/well ( $\sim 0.5 \times 10^6/\text{cm}^2$ ). Cells were cultured in the same media described elsewhere.

All control and test surfaces were briefly rinsed with warm DIH<sub>2</sub>O, then sterilized by exposing them to UV light for 1 hour. Then all samples briefly rinsed with warm PBS, followed a 5 minute exposure to UV, then a brief rinse with warm culture media and a final 5 minute exposure to UV.

Cultures were incubated at 37°C and 5% CO<sub>2</sub> for the duration of the study.

### **12.17 Cell Splitting/Freezing Protocols**

D. Prawel

James Lab

July, 2010

Making Media: see separate Making Cell Media protocol

Supplies/chemicals needed:

Cell culture grade water (ATCC, 30-2205)

Trypsin-EDTA (Fisher SV3003101)

Trypsin neutralizer (\_\_\_\_)

Sterile epi-tube

Hemocytometer with associated cover glass

Trypan blue stain

***All procedures done in the biosafety hood except as noted.***

Notes:

Cells are cultured at 37°C.

Suggested cell split ratio should be 1 to 4 (as detailed below).

For **fibroblasts** (they detach easily), Trypsin-EDTA must be diluted to 0.025%, and it comes as 0.05%, so must be 50% diluted in PBS. Make 20 vials at a time (in bio-hood), 4ml per vial, and freeze at -80C. Trypsin neutralizer is 0.5% FBS in PBS. Make 20 vials at a time (in bio-hood), 6ml per vial, using 119.4ml sterile PBS + 0.6ml FBS.

#### **Thawing cells:**

Need:

- 50ml centrifuge tube
- More than 25ml cell media (media type depends on cell type)
- 2 cell culture flasks
- 25ml pipette tube

19. Warm media (~20 minutes in water bath at 37°C).

20. Remove one vial of cells from freezer. Immediately submerge the vial up to the cap in a water bath at 37°C. Swirl around until all the ice is melted. Avoid getting bath water on cap.
21. Add 25ml of warm media to a 50ml centrifuge tube. Transfer 1 ml of cells from vial to tube. Gently invert to mix.
22. Transfer 13ml of media from tube into each of 2 cell culture flasks.
23. At this point, cell count should be approximately  $5 \times 10^5$  (assuming common practice).
24. Observe flasks in microscope to verify presence of cells.
25. Incubate at 37°C. Change media one day after thawing, and thereafter, as follows.

#### **Changing media:**

Change media one day after thawing or splitting of cells and every 2 days thereafter until they reach 50% confluence. Then change media every day. Cells should reach 80% to 90% confluence in approximately 1 week. Then they should be split and/or frozen.

**To change media:** Prepare sufficient media in advance. Aspirate old media and add 13ml of fresh media. Minimize disturbance of cells, e.g. touching the adherence surface, aspirating/adding media too quickly, etc.

#### **Splitting cells (e.g. when cells reach 80% to 90% confluence):**

Warm media, trypsin and trypsin neutralizer. Need at least 4ml of trypsin and 6ml of trypsin neutralizer for each flask (typically 4 flasks), and typically at least 52ml of media (13ml per flask).

If needed, Trypsin neutralizer is made as 0.5% FBS in PBS. Aliquots are made 6 ml/vial, so to make 20 vials:

$$120 \text{ ml total solution} = 119.4 \text{ ml PBS} + 0.6 \text{ ml FBS}$$

26. If splitting current cell culture flask, aspirate old media from the flask.
27. Add 1ml of trypsin into flask to rinse the bottom surface to remove remaining media. Quickly but gently rock to spread media over entire surface, then immediately but carefully aspirate trypsin from flask (from lower, front corner of flask, opposite cell adherent surface).
28. Add 3ml of trypsin to the flask, applying directly but gently on cell surface. This will lift the cells from the surface of flask and suspend them in the trypsin. Fibroblasts detach quickly, in a minute or two. Osteoblasts detach in about 3 minutes, MSCs in about 5-6 minutes, and Keratinocytes detach much slower (~25 to 30 minutes). If some time delay is required, put the flask back in incubator for this time.
29. Remove from bio-hood and rock gently until all cells are detached (confirm in microscope). Depending on cell type, after ~3minutes media becomes murky, and cells can be seen floating, sometimes as whitish skin on surface, and also can be seen as aggregates/clumps in the microscope.
30. Add 3ml trypsin neutralizer to flask, to stop the reaction. Mix gently. View flask on microscope. Some cells, e.g. MSCs, may need to be vortexed for a few minutes on high, to break up cell clumps. Do this in the following step.
31. Transfer all liquid from culture flask into 15ml centrifuge tube. Vortex if necessary. Confirm there is no appreciable clumping of cells by placing 50 $\mu$ l of cell solution onto glass slide and viewing on microscope.  
*Note: you can combine solutions if planning to freeze cells. Combine multiple flasks into a single 50ml centrifuge tube using this same procedure.*
32. Add additional 3ml of trypsin neutralizer to culture flask to collect all remaining cells.
33. Transfer all this solution into the centrifuge tube from previous step. Now have about 9ml of cell solution in the centrifuge tube. Gently invert a few times to mix.

34. Place this tube in the centrifuge and balance with another tube containing the same volume of water. Spin at 180G for 7 minutes. Gently remove tube from centrifuge and carefully aspirate off supernatant – VERY carefully so you don't suck up your cells). Only the cell pellet remains in centrifuge tube.
35. Add 5ml of media to the centrifuge tube and aspirate/mix to re-suspend.
36. Count cells (see separate Counting Cells protocol)
 

Example: 100 count from 5ml cell solution is  $200 \times 2 \times E^4 \times 5 = 20 \times E^6$  cells.

In splitting cells, one culture flask usually separates into about four additional flasks, depending on cell count.

*Note: Trypan Blue is highly toxic. Avoid all skin contact.*
37. Label flasks with cell type, passage (e.g. HDF<sub>n</sub><sup>+4</sup> is human fibroblasts, neonatal, 4<sup>th</sup> passage) and date.
38. Need 13ml media per cell culture flask, so four flasks need 47ml additional media (13 x 4 – 5 from above). Transfer all cell solution from cent tube into original flask. Add 47ml media to this flask. Then transfer 13ml of cell solution from this flask into each of 3 additional flasks (typically). View flasks in microscope to verify cells.
39. Place flasks in the incubator and change the media according to procedure above.

### **Freezing cells:**

1. Estimate number of vials. Pre-cool 10 (typical) cryo-vials per culture flask in refrigeration for 30mins.
2. Follow the splitting procedure above through and including step 10 (counting).
3. Place this tube in the centrifuge and balance with another tube containing the same volume of water. Spin at 180G for 7 minutes. Gently remove tube from centrifuge and carefully aspirate off supernatant – VERY carefully so you don't suck up your cells). Only the cell pellet remains in centrifuge tube.
4. During centrifugation, prepare freeze media. Will need 1ml per vial. Estimate number of cells in the culture flask. For 80% to 90% confluent fibroblasts, you typically get about 7 to 10 million cells per flask. Thus you typically need about 7 to 10 cryo-vials of freeze media, each containing 1 ml. 7-10ml of freeze media per culture flask, so you will usually be freezing cells from 3 culture flasks. Other cell types typically yield lower cell densities, so amounts vary.
 

To make freeze media: Add in tin-foil covered centrifuge tube appropriate amounts of the following to create 1xE6 cells per ml of freeze media. 72% (7.2ml for 10 ml freeze media) media, 20% (2ml) FBS and 8% (0.8ml) DMSO (as preservative). DMSO is light sensitive, so turn off room and hood light and use the red light.
5. After centrifugation carefully aspirate supernatant (media). Re-suspend cells in freeze media at a concentration of approximately 1 million cells per ml.
6. Place 1ml of freeze solution into each cryo-vial. Label all vials.
7. Place the vials in -80.
8. Put in liquid nitrogen (if available) after 24hrs.
9. Thaw one vial in few days to test their viability.

## 13 References

1. Popat, K.C., et al., *Decreased Staphylococcus epidermis adhesion and increased osteoblast functionality on antibiotic-loaded titania nanotubes*. *Biomaterials*, 2007. **28**(32): p. 4880-4888.
2. Ong, K.L., et. al., *Economic burden of revision hip and knee arthroplasty in Medicare enrollees*. *Clinical Orthopaedics and Related Research*, 2006(446): p. 22-28.
3. Soundrapandian, C., S. Datta, and B. Sa, *Drug-eluting implants for osteomyelitis*. *Critical Reviews in Therapeutic Drug Carrier Systems*, 2007. **24**(6): p. 493-545.
4. Rajaratnam, S.S., et al., *Long-term results of a hydroxyapatite-coated femoral component in total hip replacement*. *Journal of Bone and Joint Surgery-British Volume*, 2008. **90B**(1): p. 27-30.
5. Cuñé, J., et. al., *A Superficial Swab Culture is Useful for Microbiologic Diagnosis in Acute Prosthetic Joint Infections*. *Clin Orthop Relat Res*, 2009. **467**: p. 531-535.
6. Brett, D.M.e.a., *Foreign-Body Reaction Mimicking Postneurosurgical Infection after Cranioplasty*. *MILITARY MEDICINE*, 2008. **173**(7): p. 697-699.
7. Kummoona, R., *Posttraumatic Missile Injuries of the Orofacial Region*. *THE JOURNAL OF CRANIOFACIAL SURGERY / VOLUME 19, NUMBER 2 March 2008*, 2008. **19**(2): p. 300-305.
8. Grimer, R.J., et al., *Two-stage revision for infected endoprostheses used in tumor surgery*. *Clinical Orthopaedics and Related Research*, 2002(395): p. 193-203.
9. Price, J.S., et al., *Controlled release of antibiotics from coated orthopedic implants*. *Journal of Biomedical Materials Research*, 1996. **30**(3): p. 281-286.
10. Steflik, D.E., et al., *Ultrastructural analyses of the attachment (bonding) zone between bone and implanted biomaterials*. *Journal of Biomedical Materials Research*, 1998. **39**(4): p. 611-620.
11. Merolli, A., et al., *In vivo assessment of the osteointegrative potential of phosphatidylserine-based coatings*. *Journal of Materials Science: Materials in Medicine*, 2006. **17**(9): p. 789-794.
12. Lewis, G., *Hydroxyapatite-coated bioalloy surfaces: Current status and future challenges*. *Bio-Medical Materials and Engineering*, 2000. **10**(3-4): p. 157-188.
13. de Bruijn, J.D., C.A.v. Blitterswijk, and J.E. Davies, *Initial bone matrix formation at the hydroxyapatite interface <I>in vivo</I>*. *Journal of Biomedical Materials Research*, 1995. **29**(1): p. 89-99.
14. Goyenvalle, E., et al., *Osteointegration of femoral stem prostheses with a bilayered calcium phosphate coating*. *Biomaterials*, 2006. **27**(7): p. 1119-1128.
15. Frenkel, S.R., et al., *Osseointegration on metallic implant surfaces: Effects of microgeometry and growth factor treatment*. *Journal of Biomedical Materials Research*, 2002. **63**(6): p. 706-713.
16. Vasudev, D.V., et al., *In vivo evaluation of a biomimetic apatite coating grown on titanium surfaces*. *Journal of Biomedical Materials Research Part A*, 2004. **69A**(4): p. 629-636.
17. Wei, M.-H., et al., *Effects of Provider Patient Volume and Comorbidity on Clinical and Economic Outcomes for Total Knee Arthroplasty: A Population-Based Study*. *The Journal of arthroplasty*, 2010. **25**(6): p. 906-912.e1.

18. Sculo, T., *AAOS Instructional Course Lecture*, in *The economic impact of infected total joint arthroplasty*. 1993, American Academy of Orthopedic Surgeons.
19. Hoshi, K., H. Ozawa, *Matrix Vesicle Calcification in Bones of Adult Rats*. *Calcif Tissue Int*, 2000. **66**: p. 430–434.
20. Kirsch, T. and M. Pfaffle, *SELECTIVE BINDING OF ANCHORIN-CII (ANNEXIN-V) TO TYPE-II AND X-COLLAGEN AND TO CHONDROCALCIN (C-PROPEPTIDE OF TYPE-II COLLAGEN) - IMPLICATIONS FOR ANCHORING FUNCTION BETWEEN MATRIX VESICLES AND MATRIX PROTEINS*. *Febs Letters*, 1992. **310**(2): p. 143-147.
21. Merolli, A., et al., *In vivo assessment of the osteointegrative potential of phosphatidylserine-based coatings*. *Journal of Materials Science-Materials in Medicine*, 2006. **17**(9): p. 789-794.
22. Eanes, E.D., *MIXED PHOSPHOLIPID LIPOSOME CALCIFICATION*. *Bone and Mineral*, 1992. **17**: p. 269-272.
23. Santin, M.e.a., *Calcium-binding phospholipids as a coating material for implant osteointegration*. *J. R. Soc. Interface*, 2005. **3**: p. 277-281.
24. Hung, C.T., et al., *Intracellular Ca<sup>2+</sup> stores and extracellular Ca<sup>2+</sup> are required in the real-time Ca<sup>2+</sup> response of bone cells experiencing fluid flow*. *Journal of Biomechanics*, 1996. **29**(11): p. 1411-1417.
25. Pressl, D., C. Teichert, G. Hlawacek, H. Clemens, P. P. Iliev, A. Schuster, F. Feyerabend, R. Willumeit, *Characterization of Phospholipid Bilayers on Ti-6Al-4V and Ti-6Al-7Nb*. *Advanced Engineering Materials*, 2008. **10**(10): p. B47-B52.
26. Bosetti, M., Lloyd, A.W., Santin, M., Denyer, S.P. and Cannas, M., *Effects of phosphatidylserine coatings on titanium on inflammatory cells and cell-induced mineralisation in vitro*. *Biomaterials*, 2005. **26**: p. 7572-7578.
27. Eanes, E.D., *Biophysical aspects of lipid interaction with mineral: liposome model studies*. *Anat Rec*, 1989. **224**: p. 220-225.
28. Sela, J., et al., *Primary mineralization at the surfaces of implants*. *Critical Reviews in Oral Biology & Medicine*, 2000. **11**(4): p. 423-436.
29. Eanes, E.D. and A.W. Hailer, *CALCIUM-PHOSPHATE FORMATION IN AQUEOUS SUSPENSIONS OF PHOSPHATIDATE-CONTAINING LIPOSOMES*. *Journal of Dental Research*, 1987. **66**: p. 190-190.
30. Raggio, C.L., B.D. Boyan, and A.L. Boskey, *INVIVO HYDROXYAPATITE FORMATION INDUCED BY LIPIDS*. *Journal of Bone and Mineral Research*, 1986. **1**(5): p. 409-415.
31. Abrahamsson, I., et al., *Early bone formation adjacent to rough and turned endosseous implant surfaces - An experimental study in the dog*. *Clinical Oral Implants Research*, 2004. **15**(4): p. 381-392.
32. Wuthier, R.E., *Lipid composition of isolated epiphyseal cartilage cells, membranes and matrix vesicles*. *Biochimica et Biophysica Acta (BBA) - Lipids and Lipid Metabolism*, 1975. **409**(1): p. 128-143.
33. Camolezi, F.L., et al., *Construction of an alkaline phosphatase-liposome system: a tool for biomineralization study*. *International Journal of Biochemistry & Cell Biology*, 2002. **34**(9): p. 1091-1101.
34. Letellier, S.R., et al., *Oriented growth of calcium oxalate monohydrate crystals beneath phospholipid monolayers*. *Biochimica Et Biophysica Acta-General Subjects*, 1998. **1380**(1): p. 31-45.

35. Busscher, H.J. and R.B.H.C. Van Der Mei, *Initial microbial adhesion is a determinant for the strength of biofilm adhesion*. FEMS Microbiology Letters, 1995. **128**(3): p. 229-234.
36. Taylor, M.G., et al., *Structural studies of a phosphatidyl serine-amorphous calcium phosphate complex*. Cellular and Molecular Life Sciences, 1998. **54**(2): p. 196-202.
37. Poste, G. and A.C. Allison, *MEMBRANE-FUSION*. Biochimica Et Biophysica Acta, 1973. **300**(4): p. 421-465.
38. Boskey, A.L., and B.L. Dick, *The Effect of Phosphatidylserine on In Vitro Hydroxyapatite Growth and Proliferation*. CalcifTissue Int, 1991. **49**: p. 193-196.
39. Christoffersen, J. and W.J. Landis, *A contribution with review to the description of mineralization of bone and other calcified tissues in vivo*. The Anatomical Record, 1991. **230**(4): p. 435-450.
40. Papahadjopoulos, D., et al., *Studies on membrane fusion. III. The role of calcium-induced phase changes*. Biochimica et Biophysica Acta (BBA) - Biomembranes, 1977. **465**(3): p. 579-598.
41. Dluhy, R.A., et al., *FOURIER-TRANSFORM INFRARED SPECTROSCOPIC STUDIES OF THE EFFECT OF CALCIUM-IONS ON PHOSPHATIDYLSERINE*. Biochemistry, 1983. **22**(26): p. 6318-6325.
42. Hui, S.W., et al., *MEMBRANE-FUSION THROUGH POINT-DEFECTS IN BILAYERS*. Science, 1981. **212**(4497): p. 921-923.
43. Gomez-Fernandez, J., and J. Villalain, *The use of FT-IR for quantitative studies of the apparent pKa of lipid carboxyl groups and the dehydration degree of the phosphate group of phospholipids*. Chemistry and Physics of Lipids, 1998. **96**: p. 41-52.
44. Choi, S., Ware, W. et al., *Infrared Spectroscopic Studies on the Phosphatidylserine Bilayer Interacting with Calcium Ion: Effects of Cholesterol*. Biochemistry, 1991. **30**: p. 8563-8568.
45. Boskey, A.L., et al., *PHOSPHOLIPID CHANGES DURING FRACTURE-HEALING*. Proceedings of the Society for Experimental Biology and Medicine, 1980. **165**(2): p. 368-373.
46. Boskey, A.L.a.A.S.P., *Optimal Conditions for Ca-acidic Phospholipid-PO4 Formation*. Calcif Tissue Int, 1982. **34**: p. S1-S7 (Supplement).
47. Boskey, A.L. and A.S. Posner, *OPTIMAL CONDITIONS FOR CA-ACIDIC PHOSPHOLIPID-PO4 FORMATION*. Calcified Tissue International, 1982. **34**: p. S1-S7.
48. Liu, D. and L. Huang, *Role of cholesterol in the stability of pH-sensitive, large unilamellar liposomes prepared by the detergent-dialysis method*. Biochimica et Biophysica Acta (BBA) - Biomembranes, 1989. **981**(2): p. 254-260.
49. Grit, M. and D.J.A. Crommelin, *Chemical stability of liposomes: implications for their physical stability*. Chemistry and Physics of Lipids, 1993. **64**(1-3): p. 3-18.
50. Yu, G., J. Jian, J. Shen, *Synthesis and characterization of cholesterol-poly(ethylene glycol)-poly(D,L-lactic acid) copolymers for promoting osteoblast attachment and proliferation*. J Mater Sci: Mater Med, 2006. **17**: p. 899-909.
51. Edidin, M., *Lipid microdomains in cell surface membranes*. Current Opinion in Structural Biology, 1997. **7**(4): p. 528-532.
52. Schroeder, F., et al., *MEMBRANE CHOLESTEROL DYNAMICS - CHOLESTEROL DOMAINS AND KINETIC POOLS*. Proceedings of the Society for Experimental Biology and Medicine, 1991. **196**(3): p. 235-252.

53. Philippot, J., S. Mutaftschiev, and J.P. Liautard, *A very mild method allowing the encapsulation of very high amounts of macromolecules into very large (1000 nm) unilamellar liposomes*. *Biochimica et Biophysica Acta (BBA) - Biomembranes*, 1983. **734**(2): p. 137-143.
54. Gopalakrishna, P., et al., *Modulation of alpha 5 beta 1 integrin functions by the phospholipid and cholesterol contents of cell membranes*. *Journal of Cellular Biochemistry*, 2000. **77**(4): p. 517-528.
55. Julien, M., Tournier JF, Tocanne JF, *Differences in the transbilayer and lateral motion of fluorescent analogs of phosphatidyl choline and phosphatidyl ethanolamine in the apical plasma membrane of bovine endothelial cells*. *Exp Cell Res*, 1993. **208**: p. 387-397.
56. Ferraro, J.T., et al., *Depletion of plasma membrane cholesterol dampens hydrostatic pressure and shear stress-induced mechanotransduction pathways in osteoblast cultures*. *Am J Physiol Cell Physiol*, 2004. **286**(4): p. C831-839.
57. Simons, K. and E. Ikonen, *How Cells Handle Cholesterol*. *Science*, 2000. **290**(5497): p. 1721-1726.
58. Simons, K. and E. Ikonen, *Functional rafts in cell membranes*. *Nature*, 1997. **387**(6633): p. 569-572.
59. Eanes, E.D. and A.W. Hailer, *LIPOSOME-MEDIATED CALCIUM-PHOSPHATE FORMATION IN METASTABLE SOLUTIONS*. *Calcified Tissue International*, 1985. **37**(4): p. 390-394.
60. Skrtic, D. and E.D. Eanes, *Effect of different phospholipid-cholesterol membrane compositions on liposome-mediated formation of calcium phosphates*. *Calcified Tissue International*, 1992. **50**(3): p. 253-260.
61. Gristina, A.G., *Biomaterial-centered infection; microbial adhesion versus tissue integration*. *Science*, 1987. **237**.
62. Okazaki, Y., et al., *Corrosion resistance, mechanical properties, corrosion fatigue strength and cytocompatibility of new Ti alloys without Al and V*. *Biomaterials*, 1998. **19**(13): p. 1197-1215.
63. Khan, M.A., R.L. Williams, and D.F. Williams, *In-vitro corrosion and wear of titanium alloys in the biological environment*. *Biomaterials*, 1996. **17**(22): p. 2117-2126.
64. Kim, H.W., et al., *Hydroxyapatite and fluor-hydroxyapatite layered film on titanium processed by a sol-gel route for hard-tissue implants*. *Journal of Biomedical Materials Research Part B-Applied Biomaterials*, 2004. **71B**(1): p. 66-76.
65. Knabe, C., et al., *The effect of different titanium and hydroxyapatite-coated dental implant surfaces on phenotypic expression of human bone-derived cells*. *Journal of Biomedical Materials Research Part A*, 2004. **71A**(1): p. 98-107.
66. Yoshinari, M., et al., *Influence of surface modifications to titanium on antibacterial activity in vitro*. *Biomaterials*, 2001. **22**(14): p. 2043-2048.
67. Sundgren, J.E., P. Bodö, and I. Lundström, *Auger electron spectroscopic studies of the interface between human tissue and implants of titanium and stainless steel*. *Journal of Colloid and Interface Science*, 1986. **110**(1): p. 9-20.
68. Lausmaa, J., *Surface spectroscopic characterization of titanium implant materials*. *Journal of Electron Spectroscopy and Related Phenomena*, 1996. **81**(3): p. 343-361.
69. Lincks, J., et al., *Response of MG63 osteoblast-like cells to titanium and titanium alloy is dependent on surface roughness and composition*. *Biomaterials*, 1998. **19**(23): p. 2219-2232.

70. Larsson, C., et al., *Bone response to surface-modified titanium implants: studies on the early tissue response to machined and electropolished implants with different oxide thicknesses*. *Biomaterials*, 1996. **17**(6): p. 605-616.
71. Diebold, U., *The surface science of titanium dioxide*. *Surface Science Reports*, 2003(48): p. 53-229.
72. Bigi, A., et al., *In vitro culture of mesenchymal cells onto nanocrystalline hydroxyapatite-coated Ti13Nb13Zr alloy*. *Journal of Biomedical Materials Research Part A*, 2007. **82A**(1): p. 213-221.
73. ASTM, *Standard Guide for Descaling and Cleaning Titanium and Titanium Alloy Surfaces*, in *B 600-91*. 2006, ASTM International: West Conshohocken, PA, USA. p. 582-584.
74. Willumeit, R., et al., *In-vitro interactions of human chondrocytes and mesenchymal stem cells, and of mouse macrophages with phospholipid-covered metallic implant materials*. *European Cells & Materials*, 2007. **13**: p. 11-24.
75. Bigi, A., et al., *The response of bone to nanocrystalline hydroxyapatite-coated Ti13Nb11Zr alloy in an animal model*. *Biomaterials*, 2008. **29**(11): p. 1730-1736.
76. Ellingsen, J.E., *A study on the mechanism of protein adsorption to TiO2*. *Biomaterials*, 1991. **12**(6): p. 593-596.
77. Browne, M., P.J. Gregson, and R.H. West, *Characterization of titanium alloy implant surfaces with improved dissolution resistance*. *Journal of Materials Science-Materials in Medicine*, 1996. **7**(6): p. 323-329.
78. Albrektsson, T. and H.A. Hansson, *An ultrastructural characterization of the interface between bone and sputtered titanium or stainless steel surfaces*. *Biomaterials*, 1986. **7**(3): p. 201-205.
79. Rossetti, F.F., M. Bally, et. al., *Interactions between Titanium Dioxide and Phosphatidyl Serine-Containing Liposomes: Formation and Patterning of Supported Phospholipid Bilayers on the Surface of a Medically Relevant Material*. *Langmuir*, 2005. **21**: p. 6443-6450.
80. Branemark, P.I., et al., *OSSEO-INTEGRATED IMPLANTS IN TREATMENT OF EDENTULOUS JAW - EXPERIENCE FROM A 10-YEAR PERIOD*. *Scandinavian Journal of Plastic and Reconstructive Surgery and Hand Surgery*, 1977: p. 7-132.
81. Daculsi, G., R.Z. Legeros, and C. Deudon, *SCANNING AND TRANSMISSION ELECTRON-MICROSCOPY, AND ELECTRON-PROBE ANALYSIS OF THE INTERFACE BETWEEN IMPLANTS AND HOST BONE - OSSEO-COALESCENCE VERSUS OSSEOINTEGRATION*. *Scanning Microscopy*, 1990. **4**(2): p. 309-314.
82. Takatsuka, K., et al., *Bone-bonding behavior of titanium alloy evaluated mechanically with detaching failure load*. *Journal of Biomedical Materials Research*, 1995. **29**(2): p. 157-163.
83. Puelo, D.A., A. Nanci, *Understanding and controlling the bone-implant interface*. *Biomaterials*, 1999. **20**: p. 2311-2321.
84. Carlsson, L., et al., *OSSEOINTEGRATION OF TITANIUM IMPLANTS*. *Acta Orthopaedica Scandinavica*, 1986. **57**(4): p. 285-289.
85. de Lange, G.L. and K. Donath, *Interface between bone tissue and implants of solid hydroxyapatite or hydroxyapatite-coated titanium implants*. *Biomaterials*, 1989. **10**(2): p. 121-125.

86. Linder, L., et al., *Electron Microscopic Analysis of the Bone-Titanium Interface*. Acta Orthopaedica, 1983. **54**(1): p. 45-52.
87. Kasemo, B., *BIOCOMPATIBILITY OF TITANIUM IMPLANTS - SURFACE SCIENCE ASPECTS*. Journal of Prosthetic Dentistry, 1983. **49**(6): p. 832-837.
88. Frosch, K.H., et al., *Migration, Matrix Production and Lamellar Bone Formation of Human Osteoblast-Like Cells in Porous Titanium Implants*. Cells Tissues Organs, 2002. **170**(4): p. 214-227.
89. Jaffe, W.L. and D.F. Scott, *Total hip arthroplasty with hydroxyapatite-coated prostheses*. Journal of Bone and Joint Surgery-American Volume, 1996. **78A**(12): p. 1918-1934.
90. Labat, B., et al., *Interaction of a plasma-sprayed hydroxyapatite coating in contact with human osteoblasts and culture medium*. Journal of Biomedical Materials Research, 1999. **46**(3): p. 331-336.
91. Dorr, L.D., et al., *Bilateral total hip arthroplasty comparing hydroxyapatite coating to porous-coated fixation*. Journal of Arthroplasty, 1998. **13**(7): p. 729-736.
92. Sinha, R.K., et al., *SURFACE-COMPOSITION OF ORTHOPEDIC IMPLANT METALS REGULATES CELL ATTACHMENT, SPREADING, AND CYTOSKELETAL ORGANIZATION OF PRIMARY HUMAN OSTEOLASTS IN-VITRO*. Clinical Orthopaedics and Related Research, 1994(305): p. 258-272.
93. Kurachi, T., et al., *Effect of a titanium surface on bone marrow-derived osteoblastic cells in vitro*. Archives of Oral Biology, 1997. **42**(6): p. 465-468.
94. Brunette, D.M. and B. Chehroudi, *The effects of the surface topography of micromachined titanium substrata on cell behavior in vitro and in vivo*. Journal of Biomechanical Engineering-Transactions of the Asme, 1999. **121**(1): p. 49-57.
95. Piattelli, A., et al., *Histologic and histomorphometric analysis of the bone response to machined and sandblasted titanium implants: An experimental study in rabbits*. International Journal of Oral & Maxillofacial Implants, 1998. **13**(6): p. 805-810.
96. Hallab, N.J., et al., *Evaluation of Metallic and Polymeric Biomaterial Surface Energy and Surface Roughness Characteristics for Directed Cell Adhesion*. Tissue Engineering, 2001. **7**(1): p. 55-71.
97. Martin, J.Y., et al., *Effect of titanium surface roughness on proliferation, differentiation, and protein synthesis of human osteoblast-like cells (MG63)*. Journal of Biomedical Materials Research, 1995. **29**(3): p. 389-401.
98. Anselme, K., *Osteoblast adhesion on biomaterials*. Biomaterials, 2000. **21**(7): p. 667-681.
99. Buser, D., et al., *INFLUENCE OF SURFACE CHARACTERISTICS ON BONE INTEGRATION OF TITANIUM IMPLANTS - A HISTOMORPHOMETRIC STUDY IN MINIATURE PIGS*. Journal of Biomedical Materials Research, 1991. **25**(7): p. 889-902.
100. Tanahashi, M. and T. Matsuda, *Surface functional group dependence on apatite formation on self-assembled monolayers in a simulated body fluid*. Journal of Biomedical Materials Research, 1997. **34**(3): p. 305-315.
101. Viceconti, M., A. Toni, and A. Giunti, *Effects of some technological aspects on the fatigue strength of a cementless hip stem*. Journal of Biomedical Materials Research, 1995. **29**(7): p. 875-881.
102. Delecrin, J., et al., *SPECIFIC RESORBABLE CALCIUM-PHOSPHATE COATING TO ENHANCE OSTEOCONDUCTION*. Cells and Materials, 1994. **4**(1): p. 51-62.

103. Tanzer, M., et al., *The effect of adjuvant calcium phosphate coating on a porous-coated femoral stem*. Clinical Orthopaedics and Related Research, 2004(424): p. 153-160.
104. Nayab, S., L. Shinawi, J. Hobkirk, T.J. Tate, I. Olsen, F.H. Jones, *Adhesion of bone cells to ion-implanted titanium*. Journal of Material Science: Materials in Medicine, 2003. **14**: p. 991-997.
105. Nayab, S.N., F.H. Jones, and I. Olsen, *Effects of calcium ion implantation on human bone cell interaction with titanium*. Biomaterials, 2005. **26**(23): p. 4717-4727.
106. Ducheyne, P. and K.E. Healy, *THE EFFECT OF PLASMA-SPRAYED CALCIUM-PHOSPHATE CERAMIC COATINGS ON THE METAL-ION RELEASE FROM POROUS TITANIUM AND COBALT-CHROMIUM ALLOYS*. Journal of Biomedical Materials Research, 1988. **22**(12): p. 1137-1163.
107. Dekker, R.J., et al., *Bone tissue engineering on calcium phosphate-coated titanium plates utilizing cultured rat bone marrow cells: a preliminary study*. Journal of Materials Science: Materials in Medicine, 1998. **9**(12): p. 859-863.
108. Yang, Y., Kyo-Han Kim, Joo L Ong, *A review on calcium phosphate coatings produced using a sputtering process - an alternative to plasma spraying*. Biomaterials, 2005. **26**: p. 327-337.
109. Yunzhi Yang, K.-H.K., Joo L Ong, *A review on calcium phosphate coatings produced using a sputtering process - an alternative to plasma spraying*. Biomaterials, 2005(26): p. 327-337.
110. Daculsi, G., et al., *TRANSFORMATION OF BIPHASIC CALCIUM-PHOSPHATE CERAMICS INVIVO - ULTRASTRUCTURAL AND PHYSICOCHEMICAL CHARACTERIZATION*. Journal of Biomedical Materials Research, 1989. **23**(8): p. 883-894.
111. Tranquilli, P.L., et al., *Evaluation of different preparations of plasma-spray hydroxyapatite coating on titanium alloy and duplex stainless steel in the rabbit*. Journal of Materials Science: Materials in Medicine, 1994. **5**(6): p. 345-349.
112. Buma, P. and J.W.M. Gardeniers, *Tissue reactions around a hydroxyapatite-coated hip prosthesis: Case report of a retrieved specimen*. The Journal of arthroplasty, 1995. **10**(3): p. 389-395.
113. Vogely, H.C., et al., *Effects of hydroxyapatite coating on Ti-6Al-4V implant-site infection in a rabbit tibial model*. Journal of Orthopaedic Research, 2000. **18**(3): p. 485-493.
114. Moojen, D.J.F., et al., *Prophylaxis of Infection and Effects on Osseointegration Using a Tobramycin-Periapatite Coating on Titanium Implants-An Experimental Study in the Rabbit*. Journal of Orthopaedic Research, 2009. **27**(6): p. 710-716.
115. Yoshinari, M., et al., *Influence of surface modifications to titanium on oral bacterial adhesion in vitro*. Journal of Biomedical Materials Research, 2000. **52**(2): p. 388-394.
116. Rawlings, C.E., J.A. Persing, and J.M. Tew, *MODERN BONE SUBSTITUTES WITH EMPHASIS ON CALCIUM-PHOSPHATE CERAMICS AND OSTEOINDUCTORS*. Neurosurgery, 1993. **33**(5): p. 935-938.
117. Nanci, A., et. al., *Process for modification of implant surface with bioactive conjugates for Improved Integration*, USPTO, Editor. 1998, Univ. Montreal, Quebec, CANADA: USA.
118. Bhangu, A.A., et al., *Early distal femoral endoprosthesis survival: cemented stems versus the Compress (R) stop implant*. International Orthopaedics, 2006. **30**(6): p. 465-472.

119. Satsangi, A., et al., *Osteoblast response to phospholipid modified titanium surface*. *Biomaterials*, 2003. **24**(25): p. 4585-4589.
120. Satsangi, N., et al., *Osteoblast response and calcium deposition on phospholipid modified surfaces*. *Journal of Materials Science-Materials in Medicine*, 2004. **15**(6): p. 693-697.
121. Vogel, J.J. and B.D. Boyansaylers, *ACIDIC LIPIDS ASSOCIATED WITH LOCAL MECHANISM OF CALCIFICATION - REVIEW*. *Clinical Orthopaedics and Related Research*, 1976(118): p. 230-241.
122. Lloyd AW, S.M., et. al., *Phospholipid—coated implants*, USPTO, Editor. 1999: Great Britain.
123. Rossetti, F.F., M. Textor, and I. Reviakine, *Asymmetric distribution of phosphatidyl serine in supported phospholipid bilayers on titanium dioxide*. *Langmuir*, 2006. **22**(8): p. 3467-3473.
124. Shen, M.C. and T.A. Horbett, *The effects of surface chemistry and adsorbed proteins on monocyte/macrophage adhesion to chemically modified polystyrene surfaces*. *Journal of Biomedical Materials Research*, 2001. **57**(3): p. 336-345.
125. Parker, L.C., et al., *A Phosphatidylserine Species Inhibits a Range of TLR- but Not IL-1 $\beta$ -Induced Inflammatory Responses by Disruption of Membrane Microdomains*. *The Journal of Immunology*, 2008. **181**(8): p. 5606-5617.
126. Huynh, M.-L.N., V.A. Fadok, and P.M. Henson, *Phosphatidylserine-dependent ingestion of apoptotic cells promotes TGF- $\beta$ 1 secretion and the resolution of inflammation*. *Journal of Clinical Investigation*, 2002. **109**(1): p. 41.
127. Berkland, C., D.W. Pack, and K.K. Kim, *Controlling surface nano-structure using flow-limited field-injection electrostatic spraying (FFESS) of poly(-lactide-co-glycolide)*. *Biomaterials*, 2004. **25**(25): p. 5649-5658.
128. Grace, J.M. and J.C.M. Marijnissen, *A review of liquid atomization by electrical means*. *Journal of Aerosol Science*, 1994. **25**(6): p. 1005-1019.
129. Cloupeau, M. and B. Prunet-Foch, *Electrostatic spraying of liquids in cone-jet mode*. *Journal of Electrostatics*, 1989. **22**(2): p. 135-159.
130. Hohman, M.M., et al., *Electrospinning and electrically forced jets. II. Applications*. *Physics of Fluids*, 2001. **13**(8): p. 2221-2236.
131. Matthews, J.A., et al., *Electrospinning of Collagen Nanofibers*. *Biomacromolecules*, 2002. **3**(2): p. 232-238.
132. Jayasinghe, S.N. and A. Townsend-Nicholson, *Bio-electrosprays: The next generation of electrified jets*. *Biotechnology Journal*, 2006. **1**(9): p. 1018-1022.
133. Kumbar, S.G., et al., *A preliminary report on a novel electrospray technique for nanoparticle based biomedical implants coating: Precision electrospraying*. *Journal of Biomedical Materials Research Part B: Applied Biomaterials*, 2007. **81B**(1): p. 91-103.
134. Huang, Z.-M., et al., *A review on polymer nanofibers by electrospinning and their applications in nanocomposites*. *Composites Science and Technology*, 2003. **63**(15): p. 2223-2253.
135. Siefert, W., *Corona spray pyrolysis: A new coating technique with an extremely enhanced deposition efficiency*. *Thin Solid Films*, 1984. **120**(4): p. 267-274.
136. Chen, C.H., E.M. Kelder, and J. Schoonman, *Electrostatic sol-spray deposition (ESSD) and characterisation of nanostructured TiO<sub>2</sub> thin films*. *Thin Solid Films*, 1999. **342**(1-2): p. 35-41.

137. Hayati, I., A.I. Bailey, and T.F. Tadros, *Mechanism of stable jet formation in electrohydrodynamic atomization*. Nature, 1986. **319**(6048): p. 41-43.
138. Taylor, G., *Disintegration of Water Drops in an Electric Field*. Proceedings of the Royal Society of London A: Mathematical, Physical & Engineering Sciences, 1964. **280**: p. 383-397.
139. Shin, Y.M., et al., *Experimental characterization of electrospinning: the electrically forced jet and instabilities*. Polymer, 2001. **42**(25): p. 09955-09967.
140. Hohman, M.M., et al., *Electrospinning and electrically forced jets. I. Stability theory*. Physics of Fluids, 2001. **13**(8): p. 2201-2220.
141. Magarvey, R.H. and L.E. Outhouse, *NOTE ON THE BREAK-UP OF A CHARGED LIQUID JET*. Journal of Fluid Mechanics, 1962. **13**(1): p. 151-157.
142. Grace, J.M., & Dunn, P. F., *Droplet motion in an electrohydrodynamic fine spray*. Experiments in Fluids, 1996. **20**: p. 153-164.
143. Reneker, D.H., et al., *Bending instability of electrically charged liquid jets of polymer solutions in electrospinning*. Journal of Applied Physics, 2000. **87**(9): p. 4531-4547.
144. Zuo, W., et al., *Experimental study on relationship between jet instability and formation of beaded fibers during electrospinning*. Polymer Engineering & Science, 2005. **45**(5): p. 704-709.
145. Rayleigh, F., *On the equilibrium of liquid conducting masses charged with electricity*. Philos Mag, 1882. **14**: p. 184-186.
146. Taylor, G., *Electrically Driven Jets*. Proceedings of the Royal Society of London. Series A, Mathematical and Physical Sciences, 1969. **313**(1515): p. 453-475.
147. Inculet, I.I. and J.K. Fischer, *Electrostatic aerial spraying*. Industry Applications, IEEE Transactions on, 1989. **25**(3): p. 558-562.
148. Askeland, D.R., Pradeep P. Phule, *The Science and Engineering of Materials*. Fifth ed. 2006: pub: Thomson.
149. Gañán-Calvo, A.M., J. Davila, and A. Barrero, *Current and droplet size in the electro spraying of liquids. Scaling laws*. Journal of Aerosol Science, 1997. **28**(2): p. 249-275.
150. Moghadam, H., et al., *Electrospray modeling of highly viscous and non-Newtonian liquids*. Journal of Applied Polymer Science, 2010. **118**(3): p. 1288-1296.
151. Wilhelm, O., *Electrohydrodynamic spraying - Transport, mass and heat transfer of charged droplets and their application to the deposition of thin functional films*, in *Department of Physics*. 2004, Swiss Federal Institute of Technology: Zurich. p. 142.
152. Hartman, R.P.A., et al., *ELECTROHYDRODYNAMIC ATOMIZATION IN THE CONE-JET MODE PHYSICAL MODELING OF THE LIQUID CONE AND JET*. Journal of Aerosol Science, 1999. **30**(7): p. 823-849.
153. Kumbhar, S.G., et al., *Electrospun nanofiber scaffolds: engineering soft tissues*. Biomedical Materials, 2008. **3**(3).
154. Uematsu, I., et al., *Surface morphology and biological activity of protein thin films produced by electro spray deposition*. Journal of Colloid and Interface Science, 2004. **269**(2): p. 336-340.
155. Simpson, D.G.e.a., *Electroprocessed Collagen*, USPTO, Editor. 2002: USA.
156. Buchko, C.J., et al., *Processing and microstructural characterization of porous biocompatible protein polymer thin films*. Polymer, 1999. **40**(26): p. 7397-7407.

157. Deitzel, J.M., et al., *The effect of processing variables on the morphology of electrospun nanofibers and textiles*. Polymer, 2001. **42**(1): p. 261-272.
158. Lee, S.H., et al., *Infection after prosthetic reconstruction in limb salvage surgery*. International Orthopaedics, 2002. **26**(3): p. 179-184.
159. Monzón, M., F García-Álvarez, et. al., *Evaluation of four experimental osteomyelitis infection models by using precolonized implants and bacterial suspensions*. Acta Orthopaedica, 2002. **73**(1): p. 11 - 19.
160. Giulieri, S. and P.G.e. al., *Management of infection associated with total hip arthroplasty according to a treatment algorithm*. Infection, 2004. **32**: p. 222-228.
161. Moran, E., S. Masters, and e. al., *Guiding empirical antibiotic therapy in orthopaedics: The microbiology of prosthetic joint infection managed by debridement, irrigation and prosthesis retention*. Journal of Infection, 2007. **55**: p. 1-7s.
162. Gristina, A. and J. Costerton, *Bacterial adherence to biomaterials and tissue. The significance of its role in clinical sepsis*. J Bone Joint Surg Am, 1985. **67**(2): p. 264-273.
163. Gristina, A., et al., *Adherent Bacterial Colonization in the Pathogenesis of Osteomyelitis*. Science, 1985. **228**: p. 990-993.
164. An, Y.H. and R.J. Friedman, *Concise review of mechanisms of bacterial adhesion to biomaterial surfaces*. Journal of Biomedical Materials Research, 1998. **43**(3): p. 338-348.
165. Oosterbos, C.J.M., et al., *Osseointegration of hydroxyapatite-coated and noncoated Ti6Al4V implants in the presence of local infection: A comparative histomorphometrical study in rabbits*. Journal of Biomedical Materials Research, 2002. **60**(3): p. 339-347.
166. Zalavras, C.G., J.W. Costerton, ed. *Chapter 3: Biofilm, Biomaterials and Bacterial Adherence*. Orthopedic Knowledge Update: Musculoskeletal Infection, ed. A.A.o.O.S. (AAOS). Vol. Chapter 3. 2009, American Association of Orthopedic Surgeons (AAOS). 33-41.
167. Adams, C.S., et. al., *Controlled Release of Vancomycin from Thin Sol-Gel Films on Implant Surfaces Successfully Controls Osteomyelitis*. JOURNAL OF ORTHOPAEDIC RESEARCH, 2009. **27**: p. 701-709.
168. Forster, H., et al., *Bactericidal activity of antimicrobial coated polyurethane sleeves for external fixation pins*. Journal of Orthopaedic Research, 2004. **22**(3): p. 671-677.
169. McLaren, A.C., Gutierrez, F. N. et al, ed. *Chapter 9: Local Antibiotic Treatment*. Orthopedic Knowledge Update: Musculoskeletal Infection, ed. A.A.o.O.S. (AAOS). Vol. Chapter 9. 2009, American Academy of Orthopedic Surgeons (AAOS). 95-116.
170. Gottenbos, B., H.C.v.d. Mei, and H.J. Busscher, *Initial adhesion and surface growth of <I>Staphylococcus epidermidis</I> and <I>Pseudomonas aeruginosa</I> on biomedical polymers*. Journal of Biomedical Materials Research, 2000. **50**(2): p. 208-214.
171. Costerton, J.W., P.S. Stewart, and E.P. Greenberg, *Bacterial biofilms: A common cause of persistent infections*. Science, 1999. **284**(5418): p. 1318-1322.
172. Carmen, J., et. al., *Treatment of Biofilm Infections on Implants with Low-frequency Ultrasound and Antibiotics*. Am J Infect Control., 2005. **March**(33(2)): p. 78–82.
173. Miclau, T., L.E. Dahners, and R.W. Lindsey, *IN-VITRO PHARMACOKINETICS OF ANTIBIOTIC RELEASE FROM LOCALLY IMPLANTABLE MATERIALS*. Journal of Orthopaedic Research, 1993. **11**(5): p. 627-632.
174. Cornell, C.N. and J.M. Lane. *Current understanding of osteoconduction in bone regeneration*. 1998.

175. McLaren, A.C., et al., *The effect of glycine filler on the elution rate of gentamicin from acrylic bone cement - A pilot study*. Clinical Orthopaedics and Related Research, 2004(427): p. 25-27.
176. Lew, D.P. and F.A. Waldvogel, *Osteomyelitis*. Lancet, 2004. **364**: p. 369-379.
177. Goff, D.A., *Cost effective approaches to antimicrobial use in oncology patients*. Current Opinion in Infectious Diseases, 2002. **15**(6): p. 565-568.
178. Chang, H.I., et al., *Controlled release of an antibiotic, gentamicin sulphate, from gravity spun polycaprolactone fibers*. Journal of Biomedical Materials Research Part A, 2008. **84A**(1): p. 230-237.
179. Bryan, L.E. and S. Kwan, *Roles of ribosomal binding, membrane potential, and electron transport in bacterial uptake of streptomycin and gentamicin*. Antimicrob. Agents Chemother., 1983. **23**(6): p. 835-845.
180. Ruszczak, Z. and W. Friess, *Collagen as a carrier for on-site delivery of antibacterial drugs*. Advanced Drug Delivery Reviews, 2003. **55**(12): p. 1679-1698.
181. Rosenkrantz, B.E., Greco, J.R., Hoogerheide, J.G. and Oden, E.M., ed. *Gentamicin sulfate*. Analytical Profiles of Drug Substances, ed. K. Florey. Vol. 9. 1980, Academic Press: New York. 295-340.
182. Suller, M.T.E. and D. Lloyd, *The antibacterial activity of vancomycin towards *Staphylococcus aureus* under aerobic and anaerobic conditions*. Journal of Applied Microbiology, 2002. **92**(5): p. 866-872.
183. Powles, J.W., R. F. Spencer, A. M. Lovering, *Gentamicin release from old cement during revision hip arthroplasty*. J Bone Joint Surg Br, 1998. **80B**(4): p. 607-610.
184. NCCLS, *Performance standards for antimicrobial susceptibility testing, in Twelfth informational supplement M 100-S12*. 2002, National Committee for Clinical Laboratory Standards: Wayne, PA.
185. Lucke, M., et al., *A New Model of Implant-Related Osteomyelitis in Rats*. J Biomed Mater Res Part B: Appl Biomater, 2003. **67B**: p. 593-602.
186. Wahlig, H. and E. Dingeldein, *Antibiotics and Bone Cements: Experimental and Clinical Long-Term Observations*. Acta Orthopaedica, 1980. **51**(1-6): p. 49-56.
187. Lambert, R.J.W., *Susceptibility testing: inoculum size dependency of inhibition using the Colworth MIC technique*. Journal of Applied Microbiology, 2000. **89**(2): p. 275-279.
188. Henry, S.L. and K.P. Galloway, *LOCAL ANTIBACTERIAL THERAPY FOR THE MANAGEMENT OF ORTHOPEDIC INFECTIONS - PHARMACOKINETIC CONSIDERATIONS*. Clinical Pharmacokinetics, 1995. **29**(1): p. 36-45.
189. Sampath, S.S., K. Garvin, and D.H. Robinson, *PREPARATION AND CHARACTERIZATION OF BIODEGRADABLE POLY(L-LACTIC ACID) GENTAMICIN DELIVERY SYSTEMS*. International Journal of Pharmaceutics, 1992. **78**(2-3): p. 165-174.
190. Laurent, G., et al., *Mechanism of aminoglycoside-induced lysosomal phospholipidosis: In vitro and in vivo studies with Gentamicin and Amikacin*. Biochemical Pharmacology, 1982. **31**(23): p. 3861-3870.
191. Gracia, E., et al., *Application of a Rat Osteomyelitis Model to Compare in Vivo and in Vitro the Antibiotic Efficacy against Bacteria with High Capacity to Form Biofilms*. Journal of Surgical Research, 1998. **79**(2): p. 146-153.
192. Duran, L.W., *Preventing medical device related infections lise*. Vol. 11. 2000, Los Angeles, CA, ETATS-UNIS: Canon Communications LLC.

193. Smilack, J.D., W.H. Flittie, and T.W. Williams, Jr., *Bone Concentrations of Antimicrobial Agents After Parenteral Administration*. Antimicrob. Agents Chemother., 1976. **9**(1): p. 169-171.
194. van de Belt, H., et al., *Infection of orthopedic implants and the use of antibiotic-loaded bone cements - A review*. Acta Orthopaedica Scandinavica, 2001. **72**(6): p. 557-571.
195. Miclau, T., Edin ML, Lester GE, et al., *Bone toxicity of locally applied aminoglycosides*. J Orthop Trauma, 1995(9): p. 401-406.
196. Edin, M., Miclau T, Lester GE, et al., *Effect of cefazolin and vancomycin on osteoblasts in vitro*. Clin Orthop, 1996(333): p. 245-251.
197. Miclau, T., Edin ML, Lester GE, et al., *Effect of ciprofloxacin on the proliferation of osteoblast-like MG-63 human osteosarcoma cells in vitro*. J Orthop Res, 1998(16): p. 509-512.
198. McLaren, A.C., et al. *The effect of sampling method on the elution of tobramycin from calcium sulfate*. 2002.
199. Isefuku, S., C.J. Joyner, and A. Simpson, *Gentamicin may have an adverse effect on osteogenesis*. Journal of Orthopaedic Trauma, 2003. **17**(3): p. 212-216.
200. van de Belt, H., et al., *Gentamicin release from polymethylmethacrylate bone cements and Staphylococcus aureus biofilm formation*. Acta Orthopaedica Scandinavica, 2000. **71**(6): p. 625-629.
201. Claes, P.J., R. Busson, and H. Vanderhaeghe, *DETERMINATION OF THE COMPONENT RATIO OF COMMERCIAL GENTAMICINS BY HIGH-PERFORMANCE LIQUID-CHROMATOGRAPHY USING PRE-COLUMN DERIVATIZATION*. Journal of Chromatography, 1984. **298**(3): p. 445-457.
202. White, L.O., A. Lovering, and D.S. Reeves, *VARIATIONS IN GENTAMICIN-C1, GENTAMICIN-C1A, GENTAMICIN-C2, AND GENTAMICIN-C2A CONTENT OF SOME PREPARATIONS OF GENTAMICIN SULFATE USED CLINICALLY AS DETERMINED BY HIGH-PERFORMANCE LIQUID-CHROMATOGRAPHY*. Therapeutic Drug Monitoring, 1983. **5**(1): p. 123-126.
203. Silverman, L.D., et al., *Release of gentamicin from a tricalcium phosphate bone implant*. Journal of Orthopaedic Research, 2007. **25**(1): p. 23-29.
204. Cabanillas, P.F., et al., *Validation and in vitro characterization of antibiotic-loaded bone cement release*. International Journal of Pharmaceutics, 2000. **209**(1-2): p. 15-26.
205. Hendriks, J.G.E., et al., *The release of gentamicin from acrylic bone cements in a simulated prosthesis-related interfacial gap*. Journal of Biomedical Materials Research Part B-Applied Biomaterials, 2003. **64B**(1): p. 1-5.
206. Kanellakopoulou, K., et al. , *Carrier Systems for the Local Delivery of Antibiotics in Bone Infections*. Drugs, 2000. **59**(6): p. 1223-1232.
207. Hope, P.G., et al., *Deep infection of cemented total hip arthroplasties caused by coagulase negative staphylococci*. J Bone Joint Surg (Br), 1989(71): p. 851-4.
208. van de Belt, H., et al., *Staphylococcus aureus biofilm formation on different gentamicin-loaded polymethylmethacrylate bone cements*. Biomaterials, 2001. **22**(12): p. 1607-1611.
209. Kuechle, D.K., et al., *Elution of vancomycin, daptomycin and amikalin from acrylic bone cement*. Clin Orthop, 1991(264): p. 302-8.
210. Choi, J., et al., *Surface immobilization of biocompatible phospholipid polymer multilayered hydrogel on titanium alloy*. Colloids and Surfaces B: Biointerfaces, 2008. **67**(2): p. 216-223.

211. Morgan, J.R. and K.E. Williams, *Preparation and properties of liposome-associated gentamicin*. Antimicrob. Agents Chemother., 1980. **17**(4): p. 544-548.
212. Friess, W.F. and M. Schlapp, *Release mechanisms from gentamicin loaded poly(lactic-co-glycolic acid) (PLGA) microparticles*. Journal of Pharmaceutical Sciences, 2002. **91**(3): p. 845-855.
213. Zhang, X.C., et al., *BIODEGRADABLE CONTROLLED ANTIBIOTIC RELEASE DEVICES FOR OSTEOMYELITIS - OPTIMIZATION OF RELEASE PROPERTIES*. Journal of Pharmacy and Pharmacology, 1994. **46**(9): p. 718-724.
214. Cajal, Y., et. al., *Gentamicin Encapsulation in Liposomes: Factors Affecting the Efficiency*. Journal of Liposome Research, 1992. **2**(1): p. 11-22.
215. Lucke, M., et al., *Systemic versus local application of gentamicin in prophylaxis of implant-related osteomyelitis in a rat model*. Bone, 2005. **36**(5): p. 770-778.
216. Moghadam, H., et al., *Electro-spray of high viscous liquids for producing mono-sized spherical alginate beads*. Particuology, 2008. **6**(4): p. 271-275.
217. Liu, L., Y. Yang, and Y. Zhang, *A study on the electrical conductivity of multi-walled carbon nanotube aqueous solution*. Physica E: Low-dimensional Systems and Nanostructures, 2004. **24**(3-4): p. 343-348.
218. Fang, F., Y. F. Zhang, *DC electrical conductivity of Au nanoparticle/chloroform and toluene suspensions*. JOURNAL OF MATERIALS SCIENCE, 2005(40): p. 2979 – 2980.
219. Jendrasiak, G.L. and J.H. Hasty, *The electrical conductivity of hydrated phospholipids*. Biochimica et Biophysica Acta (BBA) - Lipids and Lipid Metabolism, 1974. **348**(1): p. 45-54.
220. Coyte, P.C., et al., *Economic evaluation of 2 treatments for pediatric femoral shaft fractures*. Clinical Orthopaedics and Related Research, 1997(336): p. 205-215.
221. Tengvall, P. and I. Lundström, *Physico-chemical considerations of titanium as a biomaterial*. Clinical Materials, 1992. **9**(2): p. 115-134.
222. Marini, J., *Dense  $\beta$ -tricalcium phosphate for use as a bioresorbable fixation screw: mechanical properties and in vitro degradation*, in *Mechanical Engineering*. 2006, Colorado State University: Ft. Collins.
223. Casal, H.L., Mantsch, H.H., Paltauf, F., Hauser, H., *Infrared and P-NMR studies of the effect of lithium and calcium ions on phosphatidylserines*. Biochim. Biophys. Acta Orthopaedica, 1987. **919**: p. 1275-1286.
224. Haines, T.H., *Do sterols reduce proton and sodium leaks through lipid bilayers?* Progress in Lipid Research, 2001. **40**(4): p. 299-324.
225. Sampath, S.S. and D.H. Robinson, *COMPARISON OF NEW AND EXISTING SPECTROPHOTOMETRIC METHODS FOR THE ANALYSIS OF TOBRAMYCIN AND OTHER AMINOGLYCOSIDES*. Journal of Pharmaceutical Sciences, 1990. **79**(5): p. 428-431.
226. Bernik, D.L., et al., *New kinetic model of drug release from swollen gels under non-sink conditions*. Colloids and Surfaces A: Physicochemical and Engineering Aspects, 2006. **273**(1-3): p. 165-173.
227. Siepmann, A., A. Gopferich, *Mathematical modeling of bioerodible, polymeric drug delivery systems*. Advanced Drug Delivery Reviews, 2001. **48**: p. 229–247.
228. Narasimhan, B., *Mathematical models describing polymer dissolution: consequences for drug delivery*. Advanced Drug Delivery Reviews, 2001. **48**: p. 195–210.

229. Haynesworth, S.E., M.A. Baber, and A.I. Caplan, *Cytokine expression by human marrow-derived mesenchymal progenitor cells in vitro: Effects of dexamethasone and IL-1 $\alpha$* . *Journal of Cellular Physiology*, 1996. **166**(3): p. 585-592.
230. Prockop, D.J., *Marrow Stromal Cells as Stem Cells for Nonhematopoietic Tissues*. *Science*, 1997. **276**(5309): p. 71-74.
231. Bianco, P., P.G. Robey, and P.J. Simmons, *Mesenchymal Stem Cells: Revisiting History, Concepts, and Assays*. *Cell Stem Cell*, 2008. **2**(4): p. 313-319.
232. Popat, K., Lara Leoni, Craig A. Grimes, Tejal A. Desai, *Influence of engineered titania nanotubular surfaces on bone cells*. *Biomaterials*, 2007. **28**: p. 3188–3197.
233. Morton, R.a.T.E., *Modification of the BCA Protein Assay to Eliminate Lipid Interference*. *ANALYTICAL BIOCHEMISTRY*, 1992. **204**: p. 332-334.
234. Mosmann, T., *Rapid colorimetric assay for cellular growth and survival: Application to proliferation and cytotoxicity assays*. *Journal of Immunological Methods*, 1983. **65**(1-2): p. 55-63.
235. Bosetti, M., et al., *Cell behaviour on phospholipids-coated surfaces*. *Journal of Materials Science: Materials in Medicine*, 2007. **18**(4): p. 611-617.
236. Smith, P.K., et al., *Measurement of protein using bicinchoninic acid*. *Analytical Biochemistry*, 1985. **150**(1): p. 76-85.
237. Eaton, R., *Plasma alkaline phosphatase assay: interconversion of results by two methods*. *Clin Chem*, 1977. **23**(11): p. 2148-2150.
238. Anderson, H.C., *Molecular Biology of Matrix Vesicles*. *Clinical Orthopaedics and Related Research*, 1995. **314**: p. 266-280.
239. Shin, M., Yoshimoto H, and V. JP, *In vivo bone tissue engineering using mesenchymal stem cells on a novel electrospun nanofibrous scaffold*. *Tissue Engineering*, 2004. **10**: p. 33-38.
240. Cali, J.P., G.N. Bowers, Jr., and D.S. Young, *A Referee Method for the Determination of Total Calcium in Serum*. *Clin Chem*, 1973. **19**(10): p. 1208-1213.
241. Ueno, H., et al., *Skin autofluorescence, a marker for advanced glycation end product accumulation, is associated with arterial stiffness in patients with end-stage renal disease*. *Metabolism*, 2008. **57**(10): p. 1452-1457.
242. Marcu, L., WS Grundfest, and J. Maarek, *Photobleaching of Arterial Fluorescent Compounds: Characterization of Elastin, Collagen and Cholesterol Time-resolved Spectra during Prolonged Ultraviolet Irradiation*. *Photochemistry and Photobiology*, 1999. **69**(6): p. 713-721.
243. Lutgers, H.L., et al., *Skin Autofluorescence as a Noninvasive Marker of Vascular Damage in Patients With Type 2 Diabetes*. *Diabetes Care*, 2006. **29**(12): p. 2654-2659.
244. Le, T.T., et al., *Label-free molecular imaging of atherosclerotic lesions using multimodal nonlinear optical microscopy*. *Journal of Biomedical Optics*, 2007. **12**(5): p. 054007.
245. Georgakoudi, I., et al., *NAD(P)H and Collagen as in Vivo Quantitative Fluorescent Biomarkers of Epithelial Precancerous Changes*. *Cancer Research*, 2002. **62**(3): p. 682-687.
246. Fujimoto, D., K.-y. Akiba, and N. Nakamura, *Isolation and characterization of a fluorescent material in bovine achilles tendon collagen*. *Biochemical and Biophysical Research Communications*, 1977. **76**(4): p. 1124-1129.
247. Baginski, E.S., et al., *Direct microdetermination of serum calcium*. *Clinica Chimica Acta*, 1973. **46**(1): p. 46-54.

248. Chenu, C., et al., *Osteocalcin induces chemotaxis, secretion of matrix proteins, and calcium-mediated intracellular signaling in human osteoclast-like cells*. *J. Cell Biol.*, 1994. **127**(4): p. 1149-1158.
249. Choi, S.T., et al., *Osteopontin might be involved in bone remodelling rather than in inflammation in ankylosing spondylitis*. *Rheumatology*, 2008. **47**(12): p. 1775-1779.
250. Denhardt, D. and X. Guo, *Osteopontin: a protein with diverse functions*. *FASEB J.*, 1993. **7**(15): p. 1475-1482.
251. Colford, J., D. Sailer, and C. Langman, *Five Osteocalcin Assays Compared: Tracer Specificity, Fragment Interference, and Calibration*. *Clin Chem*, 1997. **43**(7): p. 1240-1241.
252. Porter, J.R., A. Henson, and K.C. Popat, *Biodegradable poly([var epsilon]-caprolactone) nanowires for bone tissue engineering applications*. *Biomaterials*, 2009. **30**(5): p. 780-788.
253. Bonucci, E., *LOCUS OF INITIAL CALCIFICATION IN CARTILAGE AND BONE*. *Clinical Orthopaedics and Related Research*, 1971(78): p. 108-&.
254. Lee, J.Y., et al., *Assembly of collagen-binding peptide with collagen as a bioactive scaffold for osteogenesis in vitro and in vivo*. *Biomaterials*, 2007. **28**(29): p. 4257-4267.
255. Murphy, W.L. and P.B. Messersmith, *Compartmental control of mineral formation: adaptation of a biomineralization strategy for biomedical use*. *Polyhedron*, 2000. **19**(3): p. 357-363.
256. Chusuei, C., et al., *Calcium Phosphate Phase Identification Using XPS and Time-of-Flight Cluster SIMS*. *Analytical Chemistry*, 1999. **71**: p. 149-153.
257. Murphy, W.L., et al., *Effects of a bone-like mineral film on phenotype of adult human mesenchymal stem cells in vitro*. *Biomaterials*, 2005. **26**(3): p. 303-310.
258. Kubinova, S., et al., *Cholesterol-modified superporous poly(2-hydroxyethyl methacrylate) scaffolds for tissue engineering*. *Biomaterials*, 2009. **30**: p. 4601-4609.
259. Xu, J., J Ji, JC Shen, *The Effect of a Cholesterol Liquid Crystalline Structure on Osteoblast Cell Behavior*. *Biomedical Materials*, 2009. **4**(2).
260. Skrtic, D. and E.D. Eanes, *EFFECT OF MEMBRANE CHOLESTEROL ON CALCIUM-PHOSPHATE FORMATION IN AQUEOUS SUSPENSIONS OF ANIONIC LIPOSOMES*. *Calcified Tissue International*, 1992. **50**(1): p. 55-60.
261. Hwang, J.J., et al., *Self-assembling biomaterials: Liquid crystal phases of cholesteryl oligo(L-lactic acid) and their interactions with cells*. *Proceedings of the National Academy of Sciences of the United States of America*, 2002. **99**(15): p. 9662-9667.
262. O'Brien, F.J., et al., *The effect of pore size on cell adhesion in collagen-GAG scaffolds*. *Biomaterials*, 2005. **26**(4): p. 433-441.